2017

Charge Transfer Dissociation Mass Spectrometry of Biomolecules

Pengfei Li

Charge Transfer Dissociation Mass Spectrometry of Biomolecules

Pengfei Li

Dissertation submitted
to the Eberly College of Arts and Sciences
at West Virginia University

in partial fulfillment of the requirements for the degree of

Doctor of Philosophy in
Chemistry

Glen P. Jackson, Ph. D., Chair
Stephen J. Valentine, Ph. D.
Suzanne C. Bell, Ph.D.
Patrick S. Callery, Ph.D.
Peng Li, Ph. D.

Department of Chemistry

Morgantown, West Virginia
2017

Keywords: Charge Transfer Dissociation, CTD, Ion Activation Technique, Peptides, Insulin, Lipids, Oligosaccharides, HDX

ABSTRACT

Charge Transfer Dissociation Mass Spectrometry of Biomolecules

Pengfei Li

Recent advances in many biological disciplines are closely related to the development and application of new mass spectrometry techniques. The investigation of gas-phase ion activation techniques is one of the active research fields. Although researchers have developed a variety of ion activation techniques, they all suffer from certain intrinsic limitations—either limited in the types of fragment ions, or limited by the inefficiency with low charge-state precursor ions. Most of the ion activation techniques are not commercially available, and are at their developing stages.

As an attempt to explore new possibilities of fragmenting a gas-phase ion, charge transfer dissociation (CTD) was developed by the Jackson group. CTD is not only workable with low charge state precursor ions (1+ and 2+), but also is workable with highly charged precursor ions (4+, 5+, and 6+). For peptide analysis, CTD produces extensive backbone fragment ions, including *a/x*, *b/y*, and *c/z* ions. Additionally, CTD generates characteristic amino acid side-chain losses, which can complement the sequence information from backbone fragments. An interesting phenomenon of CTD reaction is that the type of predominant fragment ions shifts from *a/x* to *c/z* as the precursor charge state increases from 1+ to 3+, or more.

For intact insulin analysis, CTD enables the oxidation through a one-electron (dominant) or two-electron (minor) oxidation pathway, which increased the charge state of the intact protein by 1 or 2, respectively. Direct CTD produces a few fragment ions outside the loop defined by disulfide linkages together with charge-increased/charge-decreased species. The MS^3-level CID fragmentation of the charge-increased species shows the capability of breaking disulfide linkages, thus provides enhanced structural information. Making use of the ability of being workable with 1+ precursor ions, CTD was employed to fragment phospholipids with various degree of unsaturation. CTD extensively fragments the C-C single bonds within lipid acyl chain, and provides information regarding C=C double bond location. For lipids with various head groups, CTD shows the capability of fragmenting the acyl chains to some extent, but the efficiencies are not suitable for on-line HPLC experiments at this time. CTD was also applied to structural characterization of a methylated linear oligosaccharide, generating both extensive between-ring and cross-ring cleavages. Given the similarity in radical nature between CTD and ETD, CTD was integrated into a HDX workflow to probe the gas-phase conformation of ubiquitin. CTD shows comparable performance to ETD, which demonstrated the potential of CTD in pinpointing the secondary structural elements of gas-phase proteins/peptides.

In addition to the exploration to CTD technique, some efforts were devoted to examine the fragmentation behavior of radical cations generated from metastable atom-activated dissociation (MAD) reactions. ESI-generated protonated, sodiated and potassiated POPC ions were firstly subjected to MAD reactions, and then the resulting

$[POPC]^{+\bullet}$ ions were further mass-selected and subjected to MS^3-level CID reactions respectively. The resulting mass spectra are almost identical—independent of the first generation adducting species. Moreover, the MS^3 CID experiment produced extensive fragmentation along the lipid acyl chain, providing valuable structural information associated with C=C double bond positioning.

DEDICATION

Dedicated to my parents, whose constant love and support made this work possible.

ACKNOWLEDGEMENTS

First of all, I would like to thank my advisor, Dr. Glen Jackson, for devoting his time and efforts to help me on the "journey" to my doctoral degree. He spent a great amount of time in my course discussions, research proposal discussions, analytical seminar rehearsals, research paper preparation and doctoral dissertation preparation. I benefited a lot from his wide range of knowledge—from basic concepts in analytical chemistry, to the hands-on experience of various instruments, to the deep insights into dissociation mechanisms from the physical chemistry perspective. I cannot remember how many times I got inspired from his vivid drawing of instrument schematics or electron-push mechanisms on blackboards, which makes difficult theoretical topics so easy and straightforward and helps me build my own knowledge base. I not only learned the knowledge itself, but also learned the art of mastering knowledge—how to break down difficult concepts and integrate pieces of knowledge into a compact network.

Next, I would like to thank Dr. Robert (Bobby) Deimler and Dr. William (Billy) Hoffmann. They were the senior graduate student and postdoc at the time when I joined the group. They spent a great amount time in passing on their experience to me, from the basic steps of operating instruments, to the working principles of a single instrumental unit, as well as important concepts in analytical discipline. They acted like "big brothers" to me: every time I encountered issues in my experiments, they are the first ones I would go to for help. They showed great patience and willingness to coach me. Even if it was a simple calculation formula, they did not mind helping me check each step to fix the error.

I would like to thank my other lab mates: Dr. Yan An, Dr. Feng Jin, Kateryna Konstantynova, BohuiLv, Mayara P. V. De Matos, Taylor Krivenki, Ashley Cochran,

Tyler Davidson, Korina Menking-Hoggatt, Zachary Sasiene, Halle Edwards, and Mario Balapuwaduge Mendis, as well as "short-term" members in our laboratory—Heather Birks, Clayton Johnson, Tyler Williams, Iris Kreft and Dr. David Ropartz. All the group members have made contributions in creating a positive and collaborative laboratory atmosphere, in which the lab members help each other in both research work and daily life. All these leave me with fond and valuable memories for my graduate experience.

I also would like to thank the members of my dissertation committee—Dr. Stephen Valentine, Dr. Peng Li, Dr. Suzanne Bell and Dr. Patrick Callery. They spent a lot of time reading through my proposal and dissertation, and offered me valuable suggestions to improve both the written and oral work. I would also like to acknowledge the National Institutes of Health (NIH) for the financial support over the course of this work through funding provided by 1R01GM114494-01.

Last but not least, I would also like to thank three collaborators—Dr. Gregory Donohoe, Iris Kreft and Dr. David Ropartz. Dr. Gregory Donohoe came up with the idea of coupling CTD technique with on-line HDX workflow, and then we carried this experiment out together on our Bruker amaZon ETD mass spectrometer. His enthusiasm and expertise in peptide and protein chemistry left a strong impression on me. Iris Kreft made a significant contribution to our insulin manuscript by conducting CTD experiments upon insulin and processing data afterwards. It was quite an enjoyable experience to work with her during her six-month stay in our group. Dr. David Ropartz travelled from France to our laboratory in pursuit of a suitable fragmentation technique for fragmenting oligosaccharides. He taught me a lot of fundamentals in sugar chemistry and made it less complicated for me. He showed an impressive ability in arranging and

documenting experiments in a well-organized way. His passion and dedication to sugar chemistry was very impressive to me, and I really enjoyed working with him.

Table of Contents

LIST OF TABLES

LIST OF FIGURES

LIST OF SCHEMES

LIST OF ABBREVIATIONS

3D	Three-Dimensional
API	Atmospheric Pressure Ionization
CTD	Charge Transfer Dissociation
CR	Charge-Reduction
ECD	Electron Capture Dissociation
EDD	Electronic Detachment Dissociation
EED	Electronic Excitation Dissociation
EI	Electron Ionization
EID	Electron Ionization/Induced Dissociation
EIEIO	Electron Impact Excitation of Ions from Organics
ESI	Electrospray Ionization
ETD	Electron Transfer Dissociation
ExD	Electron Transfer/Capture Dissociation
fs-LID	Femtosecond Laser-Induced Ionization/Dissociation
FAB	Fast Atom Bombardment
FT-ICR	Fourier Transform Ion Cyclotron Resonance
GPA	Glycerophosphatidic Acid
GPC	Glycerophosphocholine
GPE	Glycerophosphoethanolamine
HDX	Hydrogen-Deuterium Exchange
HE-CID	High-Energy Collision-Induced Dissociation

He-CTD	Helium Charge Transfer Dissociation
IRMPD	Infrared Multiphoton Dissociation
KeV	Kilo-electronvolts
LE-CID	Low-Energy Collision-Induced Dissociation
LIT	Linear Ion Trap
LMCO	Low Mass Cut-Off
MALDI	Matrix-Assisted Laser Desorption Ionization
MAD	Metastable Atom-Activated Dissociation
MIDI	Metastable-Induced Dissociation of Ions
MS	Mass Spectrometry
MS^n	Tandem Mass Spectrometry
MS^2	MS/MS
NETD	Negative Electron Transfer Dissociation
niECD	Negative Ion Electron Capture Dissociation
OzESI	Ozone-Induced ESI
OzID	Ozone-Induced Dissociation
PA	Phosphatidic Acid
PC	Phosphatidylcholine
PG	Phosphatidylglycerol
PI	Phosphatidylinositol
PSD	Post-Source Decay
PTMs	Post-Translational Modifications
QIT	Quadrupole Ion Trap

RDD	Radical-Directed Dissociation
TOF	Time of Flight
S/N	Signal-to-Noise Ratio
SID	Surface-Induced Dissociation
SM	Sphingomyelin
UVPD	Ultraviolet Photodissociation
XUVPD	Extreme Ultraviolet Photodissociation

CHAPTER 1: INTRODUCTION

1.1 Goals of the Project

The overall goal of this project was to develop a novel tandem mass spectrometry (MS/MS) fragmentation technique—charge transfer dissociation (CTD)—that could be implemented on a commercial quadrupole ion trap (QIT). We wanted to characterize the application of CTD to the structural analysis of biomolecules such as peptides, lipids and oligosaccharides, and to reveal the pros and cons of CTD by comparing the results with current/state-of-the-art MS/MS fragmentation techniques. The dissociation of biomolecules has been an active research field in which a variety of MS/MS techniques have been employed, including kinetic-based, electron-based and photon-based methods. This comparison provided some information about the fragmentation behavior of CTD—the types of bonds that can be cleaved in biomolecules. In addition, we wanted to provide some mechanistic insight into the possible dissociation channels of CTD. The behavior and mechanistic understanding of this technique should facilitate the interpretation of CTD spectra in the future, expand the scope of CTD applications, and enrich the knowledge base of tandem mass spectrometry.

Collision-induced dissociation (CID) is the most common method for fragmenting biomolecules in tandem mass spectrometers. CID is a slow-heating process, which tends to break the weakest bond of a gas-phase biomolecule, such as amide bonds of peptides and glycerol backbone bonds of lipids. Given the high initial kinetic energy and high potential energy involved in CTD process, we expected CTD to adopt high-energy fragmentation pathway that could provide unique fragment ion information to complement the results from CID experiments. Because of the radical-directed high-

energy pathways, CTD experiments were expected to exhibit similar dissociation features that are often observed in other high-energy fragmentation techniques, such as high-energy collision-induced dissociation (HE-CID), electron ionization dissociation (EID) and 193nm ultraviolet photodissociation (UVPD). CTD was therefore expected to induce multiple cleavages in a more variety of bonds in biomolecules, such as C_α-C bond, C-N bond, N-C_α bond in peptides, or C-C bonds within acyl chains of lipids.

One significant feature of the aforementioned high-energy dissociation techniques is that they typically produce characteristic amino acid side-chain losses from the target peptide. These side-chain losses are of diagnostic value because they can provide secondary confirmation of the presence of some amino acids, which can complement/verify the sequence information from the backbone fragments. Side-chain cleavages are typically not obtainable via CID because it tends to generate meaningless small losses (e.g. water and ammonia). For this reason, another goal of this research was to investigate whether or not CTD is capable of producing such amino acid-specific side-chain losses, and if so, determine the extent of this capability compared to existing high-energy dissociation techniques.

As a novel fragmentation technique, it is important to understand the mechanism/dissociation channels of CTD. The type of bonds that can be cleaved during CTD and the type of side-chain losses that could be generated via CTD were carefully compared with the kinetic-based, electron-based and photon-based dissociation techniques, as well as high-energy and low-energy dissociation techniques. These comparisons were taken into account together with the experimental setup of CTD in order to carry out a comprehensive assessment of the mechanism of this technique—what

dissociation channels are involved in CTD and which category CTD falls into. On one hand, the clarification of these questions would provide superior insight into the correlation between mass spectral peaks and biomolecule structures. On the other hand, this would help explore the possibility of using CTD to solve the existing bioanalytical problems, such as the differentiation of leucine/isoleucine, the localization of labile modifications, the determination of C=C double bond location(s) in lipid acyl chains.

1.2 Project Overview

The project began by implementing CTD onto a Bruker amaZon three-dimensional quadrupole ion trap mass spectrometer, which is detailed in the experimental section in Chapter 2. The first report of CTD in our group was conducted by Drs. Hoffmann and Jackson and was carried on a Thermo dual pressure linear ion trap instrument, so moving the helium source to the 3D trap was not a trivial undertaking. The fact that CTD capability can be readily transferred between different instrument platforms is a demonstration of its robustness and potential for future upgrade.

The next step was to optimize CTD for the structural analysis of substance P and bradykinin at charge states of 1+, 2+ and 3+. This is an extension of our first CTD publication, which was centered on the analysis of 1+ substance P. Substance P and bradykinin are considered “benchmark” peptides for the performance assessment of a variety of MS/MS techniques at their developing stages. The setup facilitated the follow-up comparison between CTD and current MS/MS techniques. Both backbone and side-chain fragmentations were observed in this CTD study, the details of which are summarized in Chapter 2.

The next step was to integrate CTD into a "top-down" proteomic workflow. A relatively small-sized protein—bovine insulin—was subjected to CTD fragmentation. CTD of intact bovine insulin produced some fragments around the disulfide linkage-protected regions. Moreover, the CTD-generated single insulin chain cations were further isolated and subjected to MS^3 CID. This combination produced more structural information compared to MS^2-level experiments. The relevant results are summarized in Chapter 3.

The fourth step was to utilize CTD for structural analysis of lipids with varying acyl chain length (16 to 20 carbons), varying degree of unsaturation (0 to 4 C=C double bonds) and varying head groups. The structural investigation of phospholipids is summarized in Chapter 4. The analysis of lipids with alternative head groups is included in the first part of Chapter 6.

In addition to the investigation of CTD fragmentation, we also compared and contrasted the new CTD results with metastable atom-activated dissociation (MAD). In this study we investigated CTD, MAD and CID of protonated, sodiated, and potassiated adducts of POPC. We also investigated the ability to collisionally activate an abundant un-fragmented product ion of CTD, $[POPC]^{+\bullet}$. The oxidized product ions $[POPC]^{+\bullet}$ were subjected to collisional activation at the MS^3 level. The MS^3 CID spectra from different adducting lipids showed enormous fragmentation features in common between CID and MAD, which are summarized in Chapter 5.

In addition to showing additional CTD data of lipids, Chapter 6 also shows CTD mass spectra of a methylated oligosaccharide. Moreover, the third par of Chapter 6 describes the attempt of integrating CTD into an HDX workflow of the interrogation of

gas-phase conformation of a ubiquitin ion—a collaborative project with Dr. Stephen Valentine's group in the department of chemistry at WVU.

1.3 Quadrupole Ion Trap Mass Spectrometry

1.3.1 Instrument Construction

The three-dimensional (3D) quadrupole ion trap (QIT) was co-invented by Wolfgang Paul and Hans Georg Dehmelt. Due to the remarkable contribution of quadrupole theory, and it's application to physical and chemical measurements of quadrupole devices, Paul and Dehmelt shared half of the 1989 Nobel Prize in Physics [1]. The QIT generally performs two functions: (1) it can serve as an ion storage device that confines gas-phase ions for a certain amount of time, during which manipulations such as mass-selection, fragmentation, photoactivation of chemical reaction can be carried out; (2) it can serve as a mass analyzer by scanning ions out of the trap to a detector during a mass instability scan. QITs are comprised of three electrodes—two end-cap electrodes sandwiching one ring electrode in the middle, as shown in Figure 1.1. The two end-cap electrodes look quite similar, but they sometimes differ in the number of small apertures that let the ions in or out. For example, the Bruker amazon has one ~3 mm hole in the entrance end cap and seven ~1.5 mm ion apertures in the exit end cap.

Trapping of ions is accomplished by applying a radiofrequency voltage on the order of 1 MHz and 200-10,000 V to the ring electrode, while grounding the end-cap electrodes. By increasing the rf amplitude or decreasing the rf frequency, ions become help with less and less force, and eventually become unstable. The holes in the exit end-cap enable the ions to pass through the end-cap instead of neutralizing on its surface.

Figure 1.1. Exhibition of three electrodes: one ring electrode being sandwiched by two end-cap electrodes. Reproduced from reference [1] with permission.

Figure 1.2 shows a cutaway schematic of QIT. The asymptotes originating from the geometry of the ion trap form an angle of 53°34′ with respect to the cylindrical axis (z-axis) of the ion trap. For an ideal QIT, r_0 and z_0 obeys the following relationship:

$$r_0^2 = 2z_0^2 \qquad (1)$$

where, z_0 is dependent on r_0 according to equation (1). For most commercial QIT instruments on the market, r_0 is either 1.00 cm or 0.707 cm [1]. This 'stretching' ensures that ions always exit the trap axially, towards the detector, and vastly improves the detection efficiency.

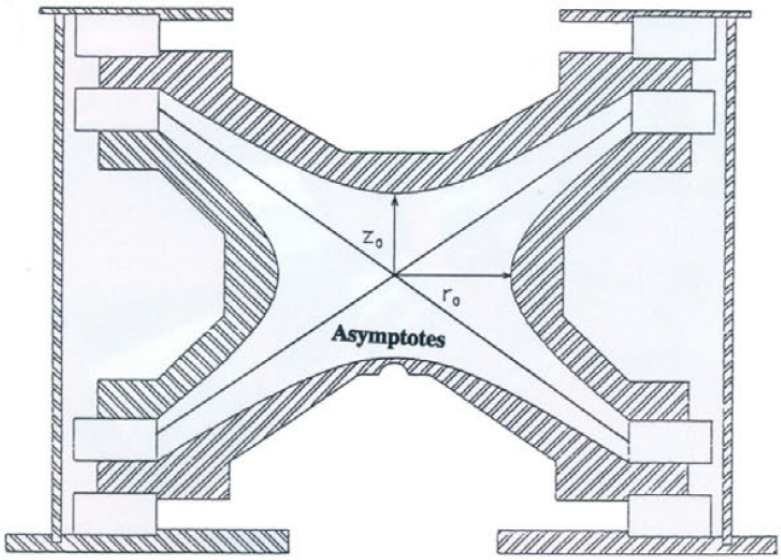

Figure 1.2. Cutaway schematic of a 3D ion trap device. Reproduced from reference [1] with permission.

1.3.2 Quadrupole Theory

To facilitate the mathematical deduction, we will start from a linear quadrupole mass analyzer, as shown in Figure 1.3.

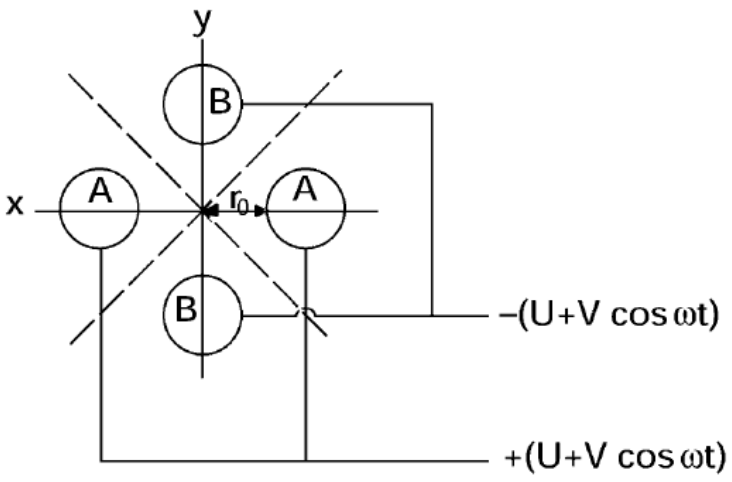

Figure 1.3. Cutaway schematic of a linear quadrupole. Reproduced from reference [2] with permission.

The electric potential (ϕ) at any given point (x, y, z) is given by:

$$\phi = A(\lambda x^2 + \sigma y^2 + \gamma z^2) + C \quad (2)$$

where, A = rf + dc potential, and C is a constant. The terms λ, σ and γ are weighting constants. The first derivative of the electric potential (ϕ) with respect to x, y, and z provides the electric in each dimension, and the second derivative provides the electric force in each dimension, which is given by the following second derivatives:

$$\frac{\partial^2\phi}{\partial x^2} = 2\lambda A \quad \frac{\partial^2\phi}{\partial y^2} = 2\sigma A \quad \frac{\partial^2\phi}{\partial z^2} = 2\gamma A \quad (3)$$

To satisfy Laplace condition ($\nabla^2\phi = 0$):

$$\nabla^2\phi = 2A(\lambda + \sigma + \gamma) = 0 \quad (4)$$

Since A cannot be zero:

$$\lambda + \sigma + \gamma = 0 \quad (5)$$

For a 2D mass filter and linear ion trap:

$$\lambda = -\sigma = 1, \gamma = 0 \quad (6)$$

For a 3D ion trap:

$$\lambda = \sigma = 1, \gamma = -2 \quad (7)$$

According to equation (2), we can obtain:

$$\phi = A(x^2 + y^2 - 2z^2) + C \quad (8)$$

Due to equation (8), the electric potentials for x pair and y pair can be derived respectively:

$$\phi_{x\,pair} = A(r_0^2) + C \quad (9)$$

$$\phi_{y\,pair} = A(-r_0^2) + C \quad (10)$$

ϕ_0 is the electric potential difference between x pair and y pair:

$$\phi_0 = \phi_{x\,pair} - \phi_{y\,pair} = 2Ar_0^2 \quad (11)$$

Since $\phi_0 = 2[U+V\cos(\Omega t)]$:

$$A = \frac{U+V\cos\Omega t}{r_0^2} \qquad (12)$$

Due to equation (8), we know:

$$\phi_{x,y} = A(x^2 - y^2) + C \qquad (13)$$

At zero potential, C=0, so:

$$\phi_{x,y} = \frac{U+V\cos\Omega t}{r_0^2}(x^2 - y^2) \quad (14)$$

In the quadrupole, the ion experiences the force, F:

$$F = ma = m\frac{d^2x}{dt^2} \qquad (15)$$

$$F = Eq = -e\frac{\partial\phi}{\partial x} \qquad (16)$$

Substituting equation (15) into equation (16), we get:

$$m\frac{d^2x}{dt^2} = -e\frac{\partial\phi}{\partial x} \qquad (17)$$

Firstly, let's consider the field in the x-direction:

From equation (14), we have:

$$\phi_x = \frac{U+V\cos\Omega t}{r_0^2}(x^2) \qquad (18)$$

$$\frac{d^2x}{dt^2} = (-x)(\frac{2eU}{mr_0^2} + \frac{2eV\cos\Omega t}{mr_0^2}) \qquad (19)$$

Likewise, in the y-direction we should have:

$$\frac{d^2y}{dt^2} = (y)(\frac{2eU}{mr_0^2} + \frac{2eV\cos\Omega t}{mr_0^2}) \qquad (20)$$

While confined in a quadrupole field, the movement of ions can be mathematically described by the solutions to the Mathieu equation [3]:

$$\frac{d^2u}{d\xi^2} + (a_u - 2q_u\cos 2\xi)u = 0 \qquad (21)$$

In the x-direction, equation (19) can be converted into:

$$\frac{d^2x}{dt^2} + x\left(\frac{2eU}{mr_0^2} + \frac{2eV\cos\Omega t}{mr_0^2}\right) = 0 \qquad (22)$$

Provided that $\cos\Omega t = \cos 2\xi$, compare equation (21) with equation (22), we obtain the trapping parameters:

$$a_z = \frac{-8eU}{mr_0^2\Omega^2}; \quad q_z = \frac{4eV}{mr_0^2\Omega^2} \qquad (23)$$

For a 'stretched' ion trap, the trapping parameters are as follows:

$$a_z = \frac{-8eU}{m(r_0^2+2z_0^2)\Omega^2}; \qquad q_z = \frac{4eV}{m(r_0^2+2z_0^2)\Omega^2} \qquad (24)$$

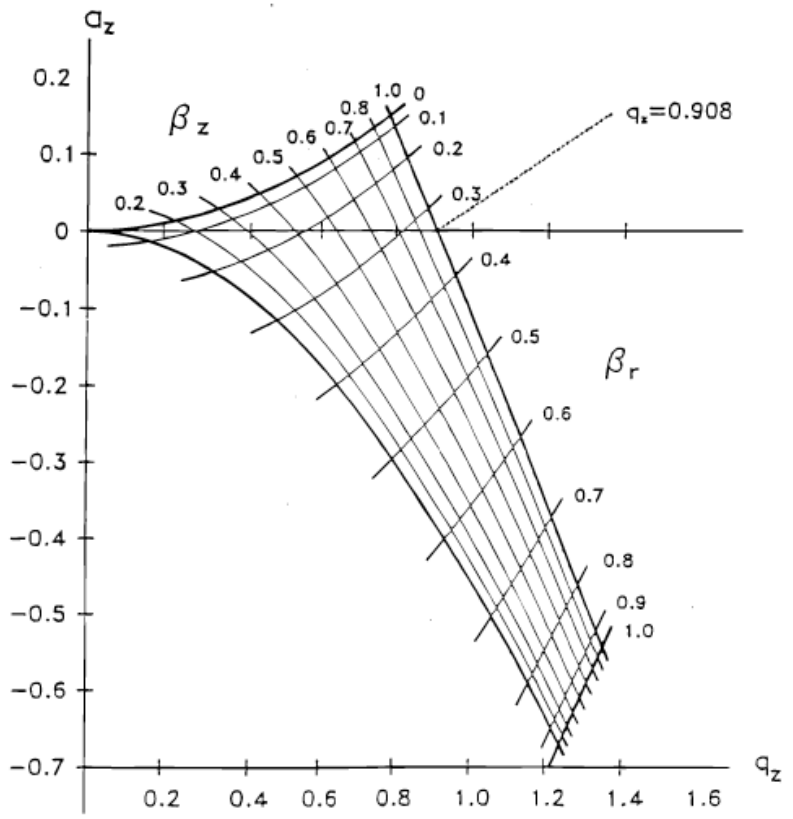

Figure 1.4. Mathieu stability diagram regulating the stability of an ion in the quadrupole field. Reproduced from reference [1] with permission.

Figure 1.4 shows the diagram indicating a stable trajectory versus an unstable trajectory in the quadrupole field. In quadruple ion traps, we typically do not use dc potentials at all, the stability parameter a=0 and the ions can only move along the q_z axis.

The stability boundary intersects with the q_z axis at q_z=0.908. All the ions with a q_z value between 0 and 0.908 maintain a stable trajectory in the quadrupole field, i.e. are stored in the field. Ions with a q_z value outside this range possess an unstable trajectory, i.e. are ejected from the quadrupole field. An ion with a stability parameter q_z=0.908 is the one with the lowest *m/z* value that could be confined in the quadrupole field, thus this special working point is called low mass cut-off (LMCO).

1.3.3 Ion Storage and Ejection

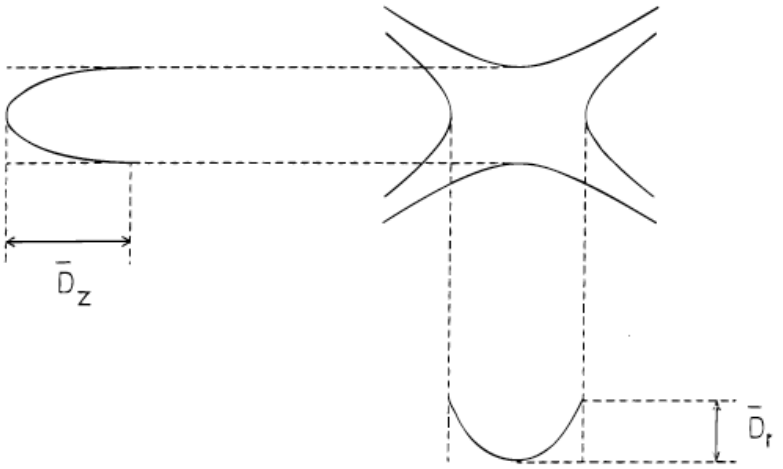

Figure 1.5. Illustration of depths of trapping potential well. Reproduced from reference [1] with permission.

In a quadrupolar field, the electric field increases linearly as one approaches an electrode and the relative stability of the ions can be thought of as a trapping potential well inside a trapping device—aka the Dehmelt pseudo-potential well, $\bar{D}$--shown in Figure 1.5. The ions maintaining a stable trajectory are stored in the ion trap, but they are not equally stable. For ions with different q_z values, it takes different amount of energy to kick them out.

Figure 1.6 shows the relative "residing point" of an ion with a given *m/z* value on the q_z axis. The ions with greater *m/z* value reside closer to q_z=0 side, while the ions with smaller *m/z* value reside closer to q_z=0.908 side. The ion with q_z≈0.67 reside at the deepest point of the trapping potential well, thus it is the one with the greatest "stability" in the trapping device, i.e. it takes the most amount of energy to remove this ion from the trapping device.

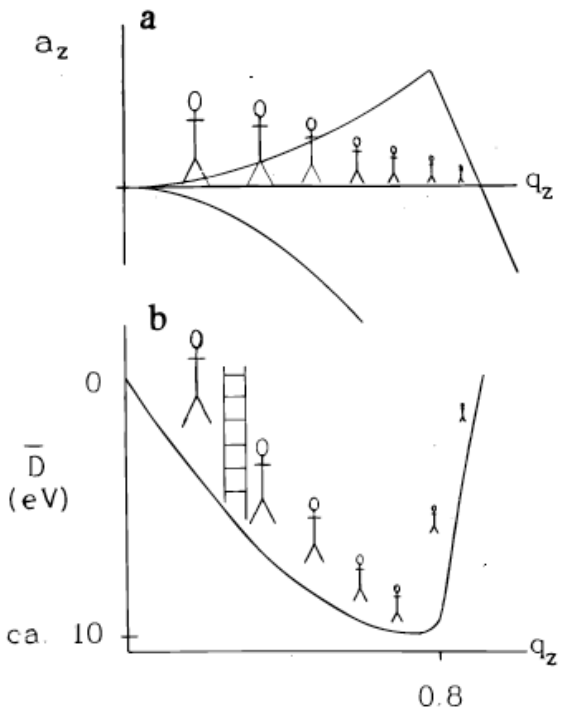

Figure 1.6. (a) Representation of working points in the stability diagram for a series of ions stored in the trap. (b) The corresponding depth of each ion in the trapping well; the ladder indicates the relative stability of ions with different *m/z* values. Reproduced from reference [1] with permission.

The successive ejection of the ions confined in the trapping device is called analytical scan, as shown in the "scan" segment in Figure 1.7. The quadrupole field is ramped up linearly, causing the elevation of q_z values of all the trapped ions. As the q_z values of each ion exceed 0.908, they will be progressively ejected through the exit end-

cap to the detector. Ions at different q_z values have difference frequencies of oscillation in the trap, typically between 50-Ω/2, where Ω is the drive (rf) frequency on the ring electrode. Holding an ion at a fixed q_z value provides the ion with a unique oscillatory frequency. One can then apply a matching supplementary frequency to the end-cap electrodes to resonantly excite the ion of interest. Resonantly exciting ions at low amplitudes (e.g. ~1-2 V)—i.e. "tickling" them—causes the ions to accelerate, collide with the helium bath gas, transfer kinetic to internal energy, and increase their vibrational energy.

With enough "tickling", precursor ions can be selectively fragmented in this manner. With larger amplitudes of resonance excitation (e.g. >3 V), ions can be resonantly ejected from the trap. This capability can easily be used to isolate a desired precursor ion from a wide mixture of ions, subject the precursor to resonance excitation, and then scan the products out the trap for mass analysis. This process is termed collisional activation, which is one of the corner stones of tandem mass spectrometry [4].

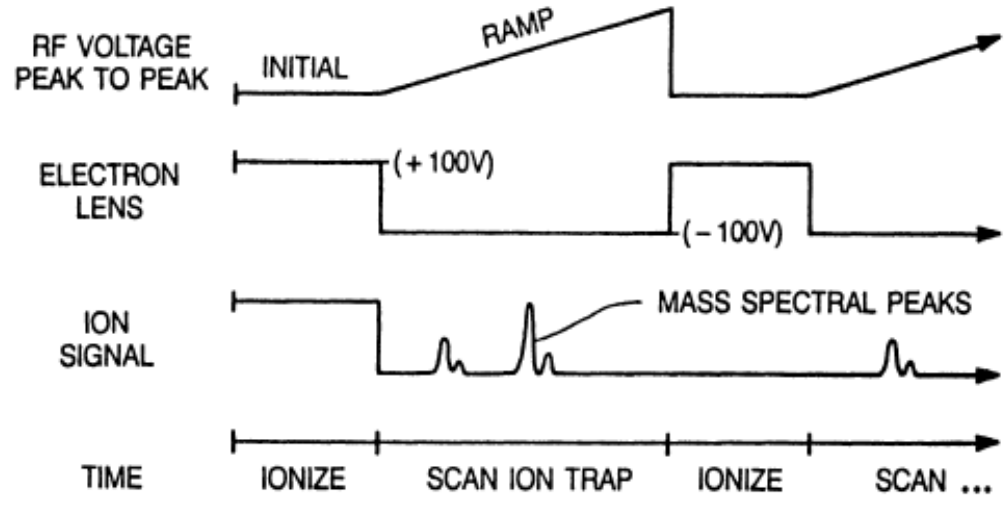

Figure 1.7. The scan functions of mass-selective instability mode for an ion trap mass spectrometer. Reproduced from reference [2] with permission.

1.4 Mass Spectrometric Techniques for Peptides

1.4.1 Introduction to Tandem Mass Spectrometry

Mass spectrometry (MS) has become an indispensible tool for the study of biomolecules. Mass spectrometric analysis of biomolecules is started with electron ionization mass spectrometry (EI-MS) [3]. In an EI source, the analyte molecule is bombarded with an electron at ~70 electron volts (eV). This bombardment results in both ionization and fragmentation—the formation of molecular ion and the formation fragment ions [5]. However, the molecular ions are oftentimes absent in the resulting EI spectrum, making it difficult to obtain the molecular weight information. The advent of matrix-assisted laser desorption ionization (MALDI) [6] and electrospray ionization (ESI) [7] in 1990s offers a solution to circumvent this problem. On one hand, these soft ionization techniques preserve intact molecular ions to a much greater extent, so that the molecular weight information is obtainable. On the other hand, they do not produce fragment ions, thus no useful structural information. To enhance the obtainable structural information, tandem mass spectrometry (MS^n) experiments are often conducted. In an MS^2 experiment, the analyte precursor ions are first generated from MALDI or ESI source. Then, the target ion is mass-selected and subjected to an ion activation technique (i.e. MS/MS fragmentation technique). A certain amount of potential energy will be imparted into the precursor ion, causing it to break apart into small fragments. Then, all the ions are mass analyzed. The MS^2 experiment seems to be more complicated than a single stage MS experiment, but it can provide both molecular weight and fragment ion information, the combination of which can greatly facilitate the structural identification of the target molecule.

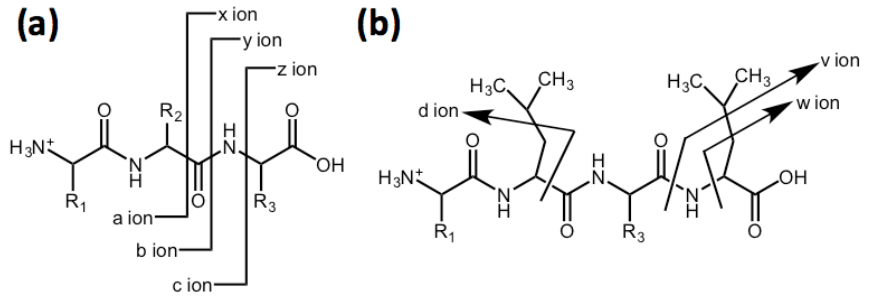

Figure 1.8. Nomenclature of peptide fragment ions: (a) *a/x*, *b/y,* and *c/z* ions; (b) *d*, *v,* and *w* ions.

Figure 1.8 illustrates the widely accepted nomenclature for peptide fragment ion fragmentation in tandem mass spectrometry [8]. Figure 1.8a shows the fragment ions resulting from backbone cleavages: C_α-C bond cleavage generates *a/x* ions; C-N bond cleavage generates *b/y* ions; N-C_α bond cleavage generates *c/z* ions. Figure 1.8b illustrates the fragment ions resulting from the simultaneous cleavage of both backbone and side-chain: *d* ion originates from the side-chain loss from the *a* ion; *v* ion from the *y* ion; w ion from the *z* ion.

1.4.2 Collision-Based Dissociation

Collision-induced dissociation (CID) is the most widely used MS/MS fragmentation technique [7]. CID activates a selected ion through collisions with a buffer bath gas (e.g. He, Ar, N_2, etc). The collision energy can range from several eV in triple quadrupole instruments or trapping instruments, to kilo-eV (keV) in sector instruments or tandem time of flight (TOF) instruments [9]. The former is called low energy collision-induced dissociation (LE-CID), while the latter is called high-energy collision-induced dissociation (HE-CID).

LE-CID is commonly classified as a "slow-heating" process [11], in which tens or hundreds of collisions happen at pressures of ~10^{-3} Torr, with relative long intervals (hundreds of microseconds) between successive collisions. In this context, dissociation and isomerization chemistry can happen in between collisions. A significant attribute of LE-CID is that after the kinetic energy is converted into internal energy, the internal energy has time to redistribute over all vibrational degree of freedom of the target molecule. Because of this redistribution, the fragment ions have enough time to isomerize/rearrange before fragmenting, which sometimes make spectral interpretation more challenging.

Due to the wide involvement in bioanlytical studies, the mechanism of LE-CID has been widely studied on a near-exhaustive array of precursor molecules. One popular mechanism for peptides is shown in Scheme 1.1. LE-CID is extensively described in the "mobile proton model" [12] wherein a protonated peptide generated from the ESI source starts with a finite number of ionizing protons that initially reside on the most basic sites, i.e. N-terminus, side-chain of histindine, lysine or arginine. Upon collisional activation,

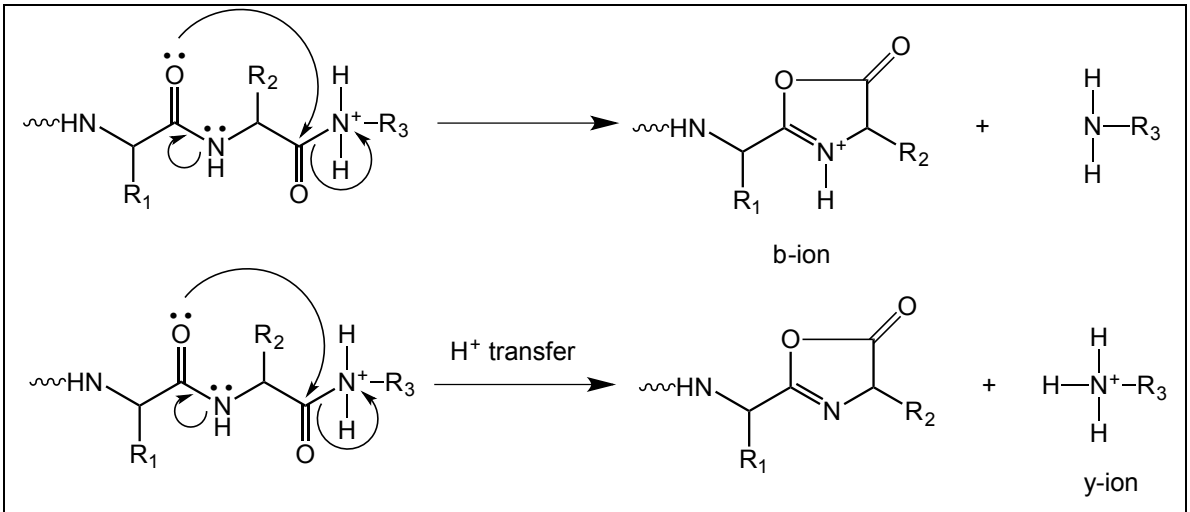

Scheme 1.1. Proposed mechanism for the formation of *b/y* ions [10].

these protons can relocate to less basic sites, as shown in Figure 1.9. The dissociation will eventually occur in the vicinity of the charge-side, which is often referred to as charge-site directed dissociation.

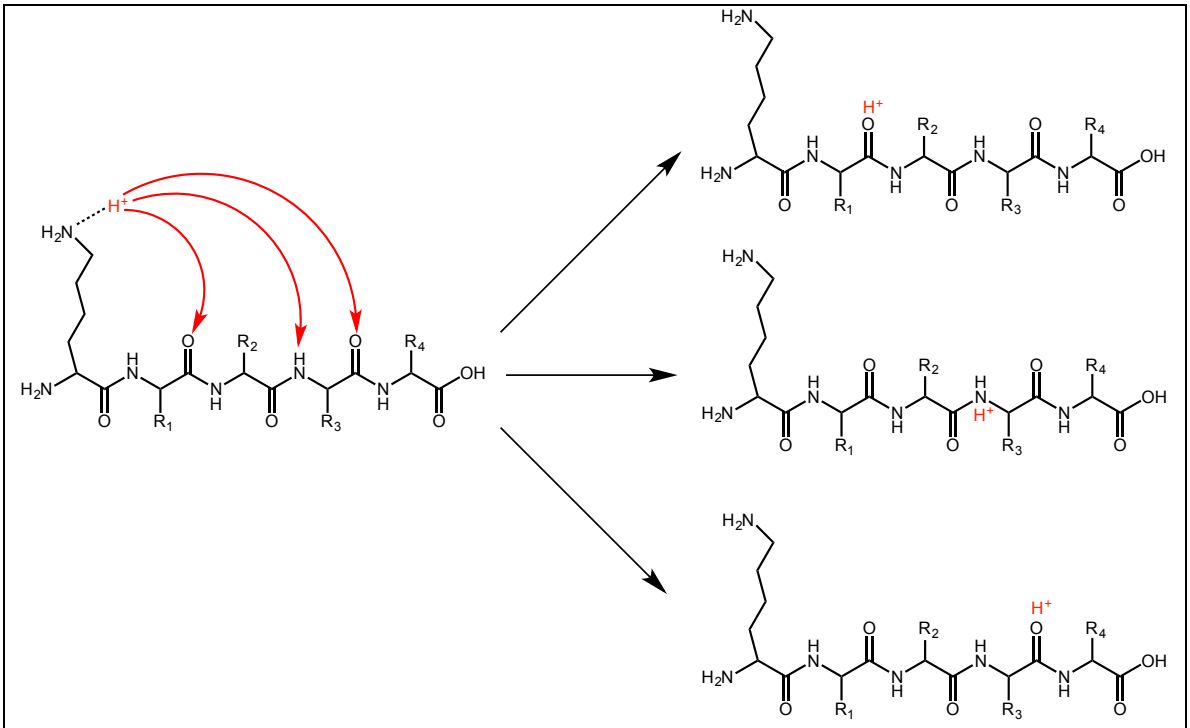

Figure 1.9. Proton relocating to less basic sites during slow heating, LE-CID [12].

In contrast to LE-CID, HE-CID is a "fast" process [11], in which only a few (N < 5) collisions happen in the pressure range of ~10^{-6} Torr. The activation time scale of HE-CID can be as short as an order of a few microseconds. In HE-CID, considerably higher internal energies are imparted into the target molecule, and in a much shorter time scale. As a result, multiple reaction channels can be activated in HE-CID, such as high-energy dissociation channels, low energy dissociation channels as well as sequential dissociation channels. In HE-CID spectra, in addition to *b/y* ions that are commonly seen in LE-CID spectrum, abundant side-chain cleavage ions (*d*, *v*, *w* ions) and immonium ions (originates from sequential dissociation) are often observed [11].

Surface-induced dissociation (SID) is another type of collision-based dissociation. In SID, precursor ions are accelerated to smash into a surface to induce fragmentation [13]. The surfaces are typically fluorinated self-assembled monolayers on gold to provide a relatively immovable surface as the collision target. For this reason, the amount of energy deposited by SID is far greater than by any form of CID. Another difference is that SID is a fast, single-step activation process, whereas LE-CID involves multiple steps of collisional activation. As an energetic activation technique, SID is widely employed to study the behavior of gas-phase protein complexes, which, because of their massive number of degrees of freedom, are impervious to fragmentation via CID.

1.4.3 Electron-Based Dissociations

Electron capture dissociation (ECD) was developed by McLafferty and coworkers in 1998 [14]. ECD is mostly carried out on a Fourier transform ion cyclotron resonance mass spectrometers (FT-ICR MS). Electrons are generated from a heated filament installed outside of the ICR cell. The filament is carefully regulated to ensure the resulting electrons are of low electron energy (< 0.2 eV), which in turn guarantees the occurrence of an effective ECD reaction [2]. ECD is very effective in fragmenting multiply charged peptides and even proteins. With the excellent mass resolving power and mass accuracy of FT-ICR platform, ECD is widely adopted in top-down proteomic workflows.

However, FT-ICRs are incredibly expensive (>$ 1M) and are high-maintenance, which significantly limits the availability of ECD to most research laboratories. To combat this issue, electron transfer dissociation (ETD) was introduced by Hunt and coworkers [15] in 2004. In ETD, a singly charged reagent radical anion transfers an

electron to a multiply charged precursor cation, causing an ECD-like fragmentation. The fragmentation pattern and the adopted pathway highly resemble ECD, but ETD can be carried out on a relatively low-cost instrument platform, such as a 3D quadrupole ion trap (QIT) or linear ion trap (LIT). The ability to achieve ECD-like performance on a cheaper mass spectrometer accounts for the more widespread utilization of ETD. ECD/ETD reactions primarily cleaves N-C_α bond of peptide backbone, while keeping labile post-translational modifications (PTMs) intact to a greater extent than traditional CID technique [16].

Several mechanisms have been proposed to account for the fundamentals of ETD/ECD reactions. Scheme 1.2 illustrates the critical steps in the Cornell mechanism proposed by McLafferty et al. The Utah-Washington mechanism is another popular suggestion about the pathways of ETD/ECD reactions, which has been well presented in

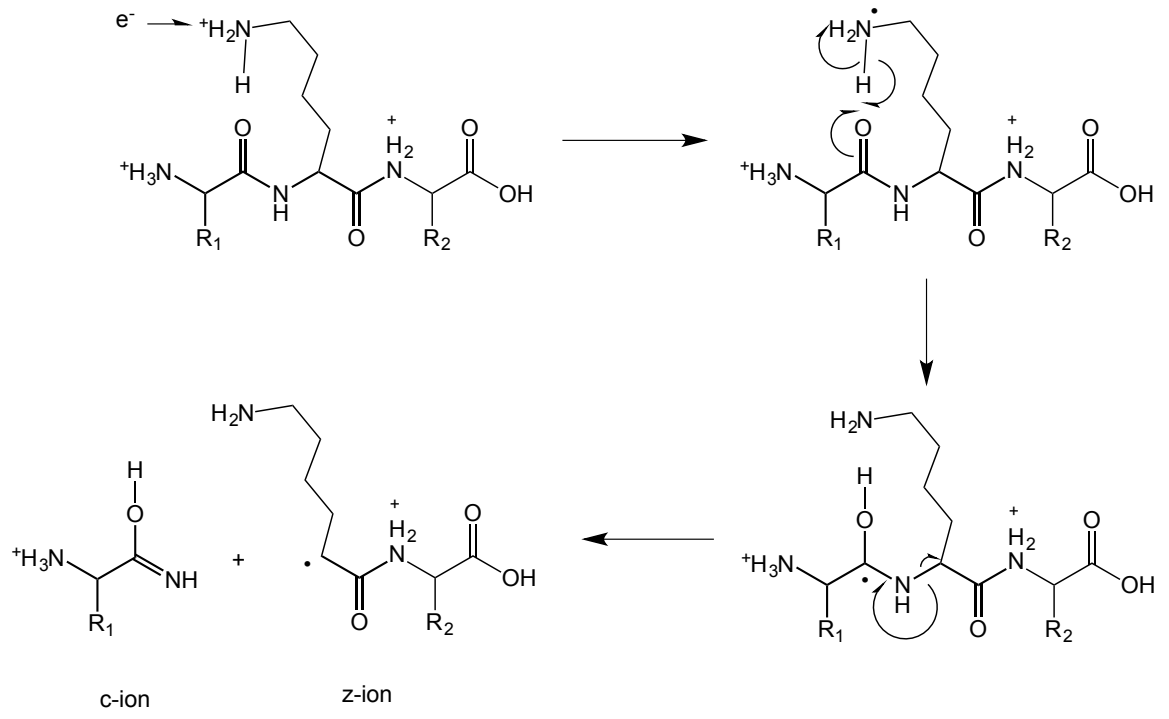

Scheme 1.2. Proposed fragmentation pathway for ETD/ECD [15].

reference [16]. Despite the broad utilization and commercial implementation of ETD and ECD, a significant drawback is that the performance of ETD and ECD shows strong dependence on precursor charge state [17]. ETD and ECD decrease the charge state of the precursor ion by 1, so they cannot work with 1+ precursor ions. For 2+ precursor ions, their performance is greatly compromised compared to that of 3+ precursor ions. Additional details and example experimental results and discussions are provided in Chapter 2.

Electronic excitation dissociation (EED) was developed by Zubarev and coworkers in 2003 [18]. MALDI-generated singly protonated peptide was irradiated by electrons that were accelerated to 17-21 eV, which produced ionized species ($[M+H]^{2+\bullet}$). The ionized species then captured a low-energy electron to form an electronically excited species ($[M+H]^{+}$*). The electronically excited species can further dissociate into *a* and *c′* ions. Substance P and bombesin were both tested using EED [18]. In addition to the said backbone cleavages, some side-chain cleavages were also observed.

In an extension of the idea of using energetic electrons to fragment peptides, Zubarev's group also developed electron ionization dissociation (EID) [19]. In EID electrons with kinetic energies on the order of 20~80 eV are used to irradiate peptide cations. The irradiation results in extensive fragmentation along the peptide backbone, with singly ionized species, doubly ionized species as well as a variety of amino acid side-chain losses. As with other electron-based methods (ECD/EED), EID is almost exclusively limited to FT-ICR mass spectrometers, which puts the instrument out of the range of most academic and analytical labs.

1.4.4 Photon-Based Dissociations

Infrared multiphoton dissociation (IRMPD) is a photon-based ion activation technique that is also traditionally conducted on FT-ICR platforms. Similar to LE-CID, IRMPD falls within the "slow-heating technique" family. Tens or hundreds of infrared photons (~0.1 eV) have to be absorbed to raise the internal energy of a precursor ion above it's threshold for dissociation [20]. Due to the stepwise energy deposition, energy redistribution is as common in IRMPD as it is in LE-CID. Analogous to LE-CID, IRMPD primarily breaks amide bonds in peptides, generating *b* and *y* fragment ions.

Different from IRMPD, ultraviolet photodissociation (UVPD) relies on the absorption of UV photons [21]. Absorption of a single UV photon can offer much greater energies (e.g. 193 nm=6.4 eV), so high-energy fragmentation pathways can be activated in UVPD experiments. As a result, extensive *a/x* ions from peptide backbone can be seen in UVPD results [22].

Femtosecond laser-induced ionization/dissociation (fs-LID) employs ultrashort (<35 fsec) laser pulses for energy deposition and fragmentation [23]. Different from IRMPD and UVPD, fs-LID does not require a suitable chromophore for photon absorption. The energetic activation nature of fs-LID results in the production of charge-increased odd-electron species ($[M+H]^{2+\bullet}$) as well as extensive backbone fragment ions, from which a greater sequence coverage can be obtained than LE-CID.

The idea of irradiating precursor ions with tunable photon energy is the domain of action spectroscopy, which is often carried out by coupling a linear ion trap mass spectrometer to the synchrotron radiation beamline facilities [24]. The photon energy can from range 5.2 eV (238 nm) to 20 eV (62 nm), which allows a continuous covering of all

major wavelengths of interest. For 1+ substance P, the photon-dissociation mainly produces *a* ions. As the photon energy increases from 7.8 eV to 18 eV, increased odd-electron species ($[M+H]^{2+\bullet}$) and amino acid side-chain losses begin to show up. The fragmentation patterns provide insight into the thresholds for the appearance of certain fragments, and provide very useful sequence information.

1.4.5 Ion/Neutral Reactions

The idea of fragmenting peptide cations/anions with a beam of metastable atoms was firstly introduced by Zubarev and coworkers in 2005 [25]. This fragmentation technique was firstly carried out in a modified QIT platform, and then implemented on a modified linear ion trap-TOF mass spectrometer by Berkout and coworkers in 2006 [26-28]. A few years later, the Jackson research group implemented this technique on a 3D QIT instrument platform, and they devoted significant efforts to the mechanistic investigation and further application of this ion activation technique [29-33].

This fragmentation technique is termed metastable-induced dissociation of ions (MIDI) or metastable atom-activated dissociation (MAD). The metastable atoms are produced from a fast atom bombardment (FAB) gun and introduced into a trapping device to interact with the selected precursor ions. For 1+ and 2+ substance P or bradykinin, extensive backbone fragmentation with all the six types of fragment ions (*a, b, c, x, y* and *z* ions) was observed. Moreover, for precursor ions with charge state $\geq 2+$, MAD produces both charge-increased and charge-decreased species. The former is believed to originate from Penning ionization (PI) process, while the latter originates from charge-reduction (CR) process (similar to ETD/ECD) [30]. These two pathways correspond to the possible competing dissociation channels occurring during MAD. A

third possible channel could be a kinetic-based dissociation pathway, which can account for the generation of significant amount of *b/y* fragment ions.

To date, MAD has been carried out in a variety of studies associated with biomolecular structures, including multiply charged peptide cations and anions, 1+ peptide and lipid cations, phosphorylated peptide cations, disulfide bonds and cleaving the amide ring structure of proline [29-33]. MAD shows intriguing features: extensive cleavages on peptides and phospholipids, capability of working with 1+ and negative precursor ions, remarkable preservation of the PTMs and the capability of differentiating leucine/isoleucine residues in the modified peptides. More results concerning MAD fragmentation of phospholipids are presented in Chapter 4.

1.5 Mass Spectrometric Techniques for Lipids

Lipids are important biomolecules that perform critical functions in the biochemistry of living organisms [34]. Phospholipids are an important sub-class of lipids ; they not only builds up cellular membranes, but also play crucial roles in signal transduction, intercellular adhesion, and energy storage in biological systems [118, 119]. The structure of glycerophospholipids is shown in Figure 1.10. The fatty acyl/fatty ether/fatty vinyl ether substitute connected to sn-1 position is called R_1 chain; the fatty acyl substitute connected to sn-2 position is called R_2 chain; the head group resides on the sn-3 position of the glycerol backbone.

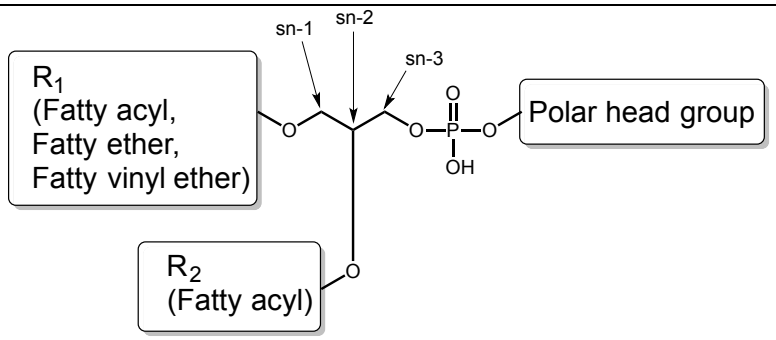

Figure 1.10. Structural illustration of a glycerophospholipid [34].

1.5.1 Collision-Based Dissociations of Lipids

As the most widely used ion activation technique, CID has been extensively performed on phospholipids. In a typical phospholipid CID spectrum, the most abundant fragment peak is at *m/z* 184.0, which corresponds to the phosphocholine head group. Several less abundant fragment peaks are associated with the loss of entire acyl chains. Figure 1.11 shows the typical cleavages induced by LE-CID.

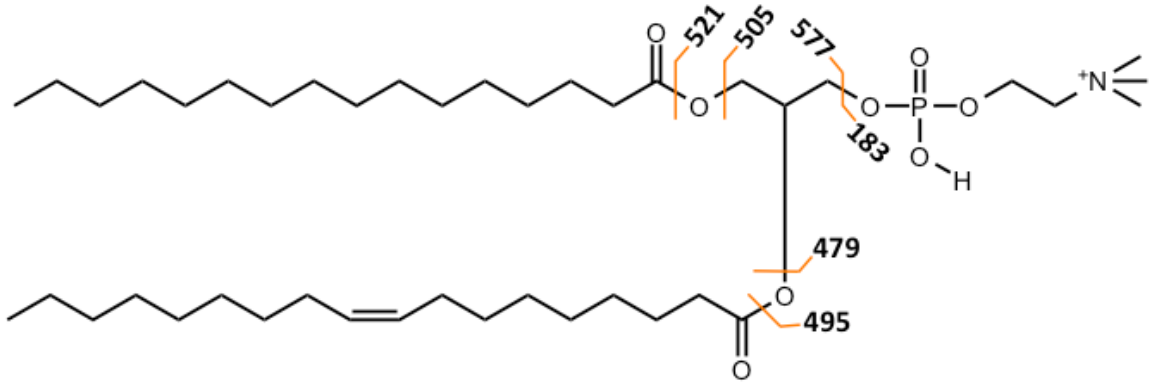

Figure 1.11. Fragment ion map for ion trap CID of POPC (PC, 16:0/18:1(9Z)).

The amount of structural information obtained via LE-CID is so limited that researchers have spent substantial effort in enhancing the structural information. Hsu and Turk used adduction with various alkali (Li, Na, K) salts to study the effect of different metal adducting ions on the behavior of CID [35]. They found that α-hydrogens at sn-2

acyl chain are more labile than those at sn-1 acyl chain, which accounts for the general preference for sn-2 elimination in LE-CID experiments. They have also conducted multistage mass spectrometry (MS^n) upon lithiated lipid adduct ions as an attempt to maximize the structural information obtainable via CID [36]. When they performed $MS^{3(or\ 4)}$-level experiments, they could obtain the fragment ion pairs that reveal the location of C=C double bond.

1.5.2 Electron-Based Dissociations of Lipids

ETD and ECD decrease the charge state of the precursor ion. It is quite challenging to ETD/ECD experiments on lipids because electrospray source primarily forms singly charged lipid adduct ions. McLuckey and coworker lowered the ESI interface voltage gradient and produced doubly charged (sodiated) lipid ions [37]. These lipid ions were exposed to azobenzene radical anions to effect ETD reaction. In the resulting spectrum, they observed product ions associated with both sodium-transfer and electron-transfer processes. This ETD reaction only produced fragments corresponding to entire acyl chain losses, thus provide limited structural information, but it is nonetheless an interesting attempt for assessing ETD performance on lipids.

Electron impact excitation of ions from organics (EIEIO) employs energetic electrons (~10 eV) for the irradiation of precursor ions. Campbell and Baba reported the structural characterization of phospholipids using EIEIO [38]. EIEIO not only produced a near-complete fragmentation pattern on phospholipids, but also produced diagnostic fragment ions that reveal unique structural features. The fragment associated with the cleavage of C1-C2 glycerol bond can be used to differentiate sn-1/sn-2 positional isomers. The differential cleavage efficiency on the C=C double bond and neighboring C-C single

bond leads to a “V” shape dent on the EIEIO spectrum, which indicates the C=C double bond location.

Electron-induced dissociation (EID) is another electron-based technique introduced for lipid characterization [39]. Similar to EIEIO fragmentation, EID cleaves most C-C and C-O bonds on the precursor lipid, including glycerol backbone and two acyl chains. Such an extensive fragmentation provides enriched structural information, on top of which C=C double bond location and acyl chain positioning information could be provided as well.

1.5.3 Photon-Based Dissociations of Lipids

Unlike ETD/ECD reactions, IRMPD and UVPD do not have a precursor charge-state barrier. Phosphatidylinositol phosphate species were fragmented using IRMPD [40]. The major fragments observed are related to the cleavages around the phosphate group. Brodbelt and coworkers carried out the dissociation of a serious of lipid A species using 193 nm UVPD [41]. Compared with CID results, 193 nm UVPD exhibited a better efficiency in cleaving C-C bond between the amine and carbonyl groups.

1.5.4 Ion/Ion (Neutral) Reactions

McLuckey and coworkers reported a gas-phase ion/ion reaction for structural characterization of phospholipids, which is also named charge inversion reaction [42]. On a modified triple-quadrupole/linear ion trap mass spectrometer, lipid cations and 1,4-phenylenedipropionic acid anions are alternately introduced into the ion trap. Followed by a mutual confinement of 1000 ms, the two types of ions reacted via proton/methyl group transfer. The result is that the lipid cations were converted into anion species. A

further collisional activation of this anion species produced considerably more structural information than a direct CID experiment.

Blanksby and coworkers recently implemented ozone oxidation into MS/MS experiment for structural determination of phospholipids [43]. Ozone was introduced into the ESI chamber to interact with the charged lipid species exiting the spray needle, and then the whole mixture was sampled into a triple quadrupole mass spectrometer. In the resulting OzESI (ozone-induced ESI) spectrum, the pairs of product ions separated by 48 Da localize the C=C double bond. OzESI shows great performance for the analysis a pure lipid molecule, but the spectrum gets too complicated with a multiple lipid-containing mixture.

To overcome this issue, Blanksby and coworkers further developed this method into OzID (ozone-induced dissociation), which was conducted on a linear ion trap instrument (Thermo LTQ) [44]. In OzID, the ESI-generated lipid ions are firstly mass-selected in the ion trap, and then exposed to an ozone vapor to effect a gas-phase ion-molecule reaction, which can generate the aforesaid diagnostic fragment pairs. OzID can be further combined with trap CID reaction, either in parallel or in tandem. Such a combination can further increase the extent of cleavages, thus enhance the obtainable structural information.

1.6 Charge Transfer Dissociation Mass Spectrometry

1.6.1 Background

As discussed in the previous part, in the field of gas-phase ion activation (MS/MS fragmentation), the way to impart energy into a selected ion is either via collision with gas molecule (CID)/surface (SID), or interaction with electron (ECD, EED,

EID)/electron-donating reagent (ETD), or interaction with photon (IRMPD, UVPD, fs-LID, action spectroscopy). For negative ion mode experiments, ion activation can be realized via electron detachment dissociation (EDD) [45] and negative electron transfer dissociation (NETD) [46]. For the ion activation techniques relying on the interaction with electron/electron-donating reagent/electron-accepting reagent (NETD), they share the common feature—all effected via the interaction of two oppositely charged species—if one positive then the other one must be negative. Then there is an interesting argument worth thinking: is it feasible to effect ion activation via the interaction between two homo-polarity species.

Hakansson and coworkers first reported a gas-phase ion activation technique employing electrons with energy ~3.5-6.5 eV to interact with peptide anions to induce fragmentation, which is termed negative-ion electron capture dissociation (niECD) [47]. Due to the capture of an electron by a negative ion, charge-increased odd-electron species ($[M-H]^{2-\bullet}$) were observed, along with a series of *c/z* fragment ions. This proves the feasibility of effecting the ion activation via negative-negative interaction. Then what about positive-positive interaction?

Zubarev and coworkers were apparently the first to obtain reasonable quality data in positive ion mode; they reported the pioneering work of fragmenting peptide cations via the activation with a beam of high-energy cations [48]. A microwave plasma gun was employed for the production of the cation beam, which is introduced into the HCD cell of an Orbitrap mass spectrometer (Thermo Scientific Q Exactive). The trapped peptide cations were first exposed to a beam of air plasma cations, and then dissociated into *a/x*, *b/y* and *c/z* fragment ions. Compared to the results from a conventional CID experiment,

the results of this work are more structurally informative. However, this experimental setup is not flawless. There are non-negligible flaws that need to be solved. As the authors mentioned in their publication, the composition of the air plasma is very complicated and it includes positive, negative and neutral species—electrons, metastables, radicals and clusters. Due to the complex nature of plasma, it is hard to define the potential energy brought about by such an interaction. What's more, it is almost impossible to sort out the origin of the resulting fragments. Does this fragment originate from an intermediate or directly from the precursor? Does this fragment come from an electron-transfer process, proton-transfer process or positive-positive interaction? It is also possible that some fragments may originate from oxygen atom or OH radical attachment/detachment that will lead to spectral misinterpretation. Zubarev's group does not appear to be pursuing this research at this time, so answers to these questions will likely go unanswered.

1.6.2 Previous Research in the Jackson Group

At the same time that Zubarev's group published on the possibility of cation-cation reactions, the Jackson research group was also looking into similar novel gas-phase ion activation techniques. Dr. William Hoffmann (former postdoc) and Dr. Jackson were attempting to use helium ions to abstract an electron from precursor cations, to induce gas-phase ion chemistry and provide high activation energies. Because the proposed mechanism involves the transfer of charge from a precursor ion to a reagent cation, they termed the technique charge transfer dissection (CTD) [49]. Instead of the complex microwave air plasma used by Zubarev's group, Drs. Hoffmann and Jackson used a beam of pure helium cations, and instead of the Orbitrap platform, they used a

relatively low-cost linear ion trap (LIT) mass spectrometer. With the installation of a saddle field fast ion/fast atom source (ion gun), helium cations with kinetic energy of more than 6 keV were produced and introduced into the ion trap to fragment the selected ions. The keV-level initial kinetic energy is more than sufficient to overcome the Coulombic repulsion between the two cationic species. The helium cation has an electron affinity (EA) of 24.6 eV, which far exceeds the ionization energy (IE ≈ 10.6 eV) of 1+ substance P [50]. Aside from the kinetic energy required to overcome the activation barrier, the excess energy (>13 eV) should be more enough to break any bonds along peptide backbone (Bond Dissociation Energy: C_α-C≈3.6 eV, C-N & N-C_α≈3.2 eV). The reaction between the 1+ precursor and helium cation is summarized as follows [49]:

$$[M + H]^+ + He^+ \rightarrow [M + H]^{2+\cdot *} + He^0 \rightarrow \text{Fragments} \qquad (21)$$

In their first demonstration of the technique, helium cation irradiation of 1+ substance P produced charge-increased odd-electron species ($[M+H]^{2+\bullet}$) along with an extensive backbone fragmentation pattern [49]. As shown in Figure 1.12, the backbone fragments nearly covered the whole peptide sequence. A series of *a* ion predominates the product ion spectrum. This pattern showed great consistency with the results from 193 nm UVPD, action spectroscopy and fs-LID experiments. This is a strong indicator that CTD process adopts high-energy fragmentation channels analogous to the said techniques [49].

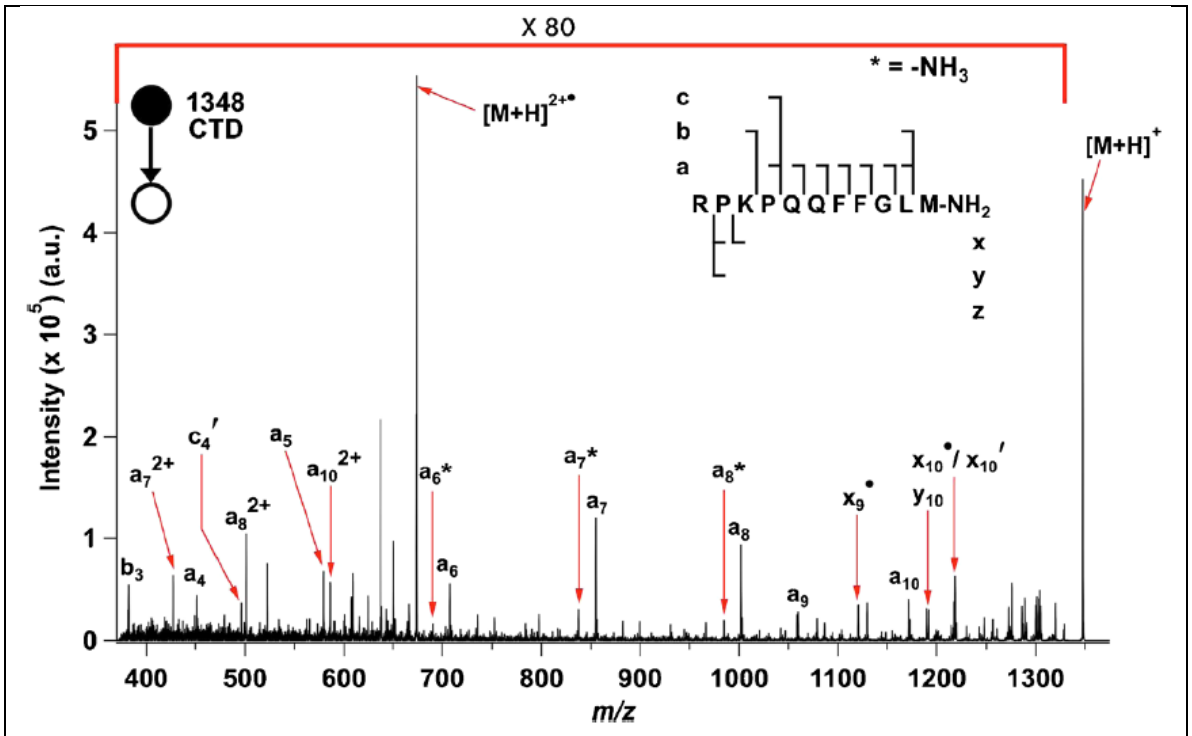

Figure 1.12 CTD spectrum of [substance P+H]$^+$. Reproduced from reference [49] with permission.

CHAPTER 2: CHARGE TRANSFER DISSOCIATION (CTD) MASS SPECTROMETRYOF PEPTIDE CATIONS: CHARGE STATE DEPENDENCE AND SIDE-CHAIN LOSSES

Reproduced in part with permission from Pengfei Li, Glen P. Jackson*, J. Am. Mass Spectrom.* 2017, DOI : 10.1007/s13361-016-1574-y

2.1 Introduction

In recent years, mass spectrometry (MS) has become an indispensable tool for the study of biological molecules such as lipids [51], oligosaccharides [52], peptides [53, 54], proteins [55], and DNA [56]. With the development of soft ionization methods such as fast atom bombardment (FAB), matrix-assisted laser desorption/ionization (MALDI) and electrospray ionization (ESI), single-stage MS plays an important role in the molecular weight determination of an intact molecule of interest [9]. However, interrogation of detailed structural information of a gas-phase molecule usually requires multiple stages of MS or tandem mass spectrometry (MS/MS) [57].

A variety of MS/MS fragmentation methods have been developed and implemented on modern mass spectrometric instruments, the most common of which is collision-induced dissociation (CID) [58]. Collisional activation tends to break the weakest bonds of gas-phase peptides and proteins—such as amide bonds—and produces *b/y* ions for the deduction of peptide sequence information. However, CID can also result in the loss of weakly bound post-translational modifications (PTMs), which has been shown to limit its usefulness [30, 59].

Electron capture and electron transfer dissociation (ECD/ETD or ExD) are two alternative MS/MS techniques that can overcome the aforementioned limitations [16]. Unlike CID, ExD cleaves peptide backbone N–Cα bonds to produce *c/z* ions with a more

extensive peptide/protein sequence coverage than CID [47]. In addition, ExD retains PTMs to a much greater extent than CID, which facilitates the elucidation of PTMs site information [16]. However, the fact that ExD relies on charge reduction makes it incompatible with 1+ precursor ions, and its performance is compromised for 2+ precursor ions [17]. The inefficiency with peptide dications can be problematic for implementing ExD with enzymatic digestion workflows, because many tryptically digested peptides are doubly charged [60].

To combat these issues, significant interest has been placed in the development of new ion activation methods, such as electronic excitation dissociation (EED) [18], electron ionization dissociation (EID) [61], ultraviolet photodissociation (UVPD) [62, 63], femtosecond laser-induced ionization/dissociation (fs-LID) [23], action spectroscopy (synchrotron radiation) [24], and metastable atom-activated dissociation (MAD) [26, 64]. These fragmentation methods all possess a common feature—the capability of dissociating low charge state (1+ & 2+) precursor ions, thus providing complementary structural information to ETD/ECD. Some methods (e.g. EID) even show almost equal fragmentation efficiency and sequence coverage between the dissociation of 1+, 2+and multiply-charged precursor ions [61], which makes them promising for a proteomic workflow.

Charge transfer dissociation (CTD) is another alternative ion activation method for MS/MS experiments [65]. Contrary to the common ion/ion dissociation methods, CTD utilizes the interaction between homo-polarity ions such as peptide cations and helium cations, which, in the case of 1+ substance P, results in a dominant series of *a* ions. It has been widely reported that the fragmentation pattern of MS/MS techniques

shows certain dependence on the charge state of precursor ions and the type of mass analyzer [17, 63, 66]. To investigate this dependence, CTD fragmentation of substance P and bradykinin at different charge states (1+, 2+ and 3+) was carried out in a 3D ion trap mass spectrometer. Various types of cleavages were observed—including backbone and side-chain cleavages—which provide mechanistic insight into the fragmentation channels involved in CTD process. Although our preliminary studies were conducted on a 2D ion trap [65], the current work was accomplished on a 3D ion trap, which shows some subtle differences in the resulting fragmentation patterns. The somewhat improved capabilities of the current 3D trap configuration probably stem from the closer proximity between the helium ion gun and the trapping volume.

2.2 Experimental

2.2.1 Instrumentation

Helium CTD (He-CTD) fragmentations of substance P and bradykinin were carried out using a modified Bruker amaZon ETD mass spectrometer (Bruker Daltronics, Bremen, Germany). A saddle field ion/fast atom source (VSW/Atomtech, Maccles field, UK) installed with the ion gun anode lens was interfaced onto the top cover of 3D ion trap via a home-built metal cover [65]. The source installation, connection between electronic components and the working principle are similar to our previous instrumental setup on LTQ Velos Pro and experimental setup of MAD-MS [58, 65].

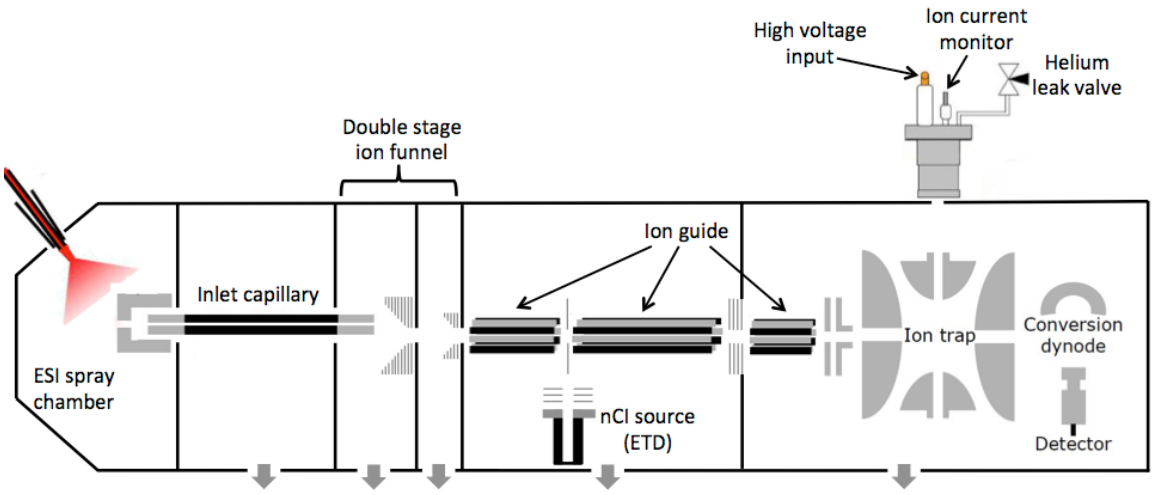

Figure 2.1. Schematic of installation of saddle field ion source onto Bruker amaZon ETD mass spectrometer.

2.2.2 Materials

Substance P and bradykinin were purchased from Sigma-Aldrich (St Louis, MO) and used without further purification. The peptides were reconstituted into a water/ methanol/acetic acid mixture (49.5:49.5:1 v/v/v), aiming for a final concentration of 60 μM and were electrosprayed using a standard Bruker Apollo source [58].

2.2.3 Method

Experiments were performed in the MS/MS mode on the 3D ion trap instrument, and the saddle field ion source was switched on during the section of scan function that is typically reserved for CID. The peptide solutions were infused using an electronic syringe pump (#1725, Hamilton Company Reno, Nevada, NV) at a flow rate of 160 μL/h. Precursor ions were isolated using an isolation window of 2 Da, after which they were irradiated with the helium cation beam. The low mass cut-off (LMCO) value was typically set to be *m/z* 150 for the removal of ionized pump oil fragments. A +6 kV

square wave with a pulse width of 25 ms was supplied to the saddle field ion source anode for the generation of reagent helium cations. The helium gas flow was controlled via a variable leak valve and the pressure read-out was obtained from the ion trap gauge in the main vacuum region. Using this indirect measurement, the helium gas supply was adjusted to provide a main vacuum pressure of ~1.20×10^{-5} mbar for all the experiments, which is only slightly above the base pressure around 8 x 10^{-6} mbar. All the CTD mass spectra presented in this work were time-averaged for 0.5-2 minutes to improve the signal-to-noise ratio (S/N).

For section 2.3.5, the ESI source was switched to negative mode, so the detector only picks up signals from possible product anions. The ESI voltages were set to be +800 V and – 500 V. All the following mass spectra were collected under "enhanced resolution mode". The LMCO value was set to be *m/z* 70. The saddle field ion source conditions and data acquisition times are the same as previous section.

2.3 Results and discussion

2.3.1 Substance P: 1+, 2+, and 3+ Charge States

He-CTD was performed on singly, doubly and triply protonated substance P respectively, as shown in Figure 2.2. Upon the interaction with helium cations, the 1+, 2+, and 3+ precursors of substance P gave oxidized product ions (charge-increased species) at *m/z* 673.9, *m/z* 450.4 and *m/z* 337.8, corresponding to product ions $[M+H]^{2+\bullet}$, $[M+2H]^{3+\bullet}$, and $[M+3H]^{4+\bullet}$ respectively. Gas-phase oxidation, or increasing the charge state of gas-phase ions has been observed in a variety of fragmentation methods, including He-MAD [48, 58], EID and EED [18, 61], and photon-based dissociation methods [23, 24].

Charge-increased species mainly originate from the electron detachment of precursor ions, i.e. charge transfer. Helium cations have an electron affinity of ~24.6 eV, and given that they are generated from a 6 kV saddle field ion source, there is more than enough energy to overcome the Coulombic repulsion barrier to enable charge transfer to occur [24, 48, 50, 57, 65]. In addition to charge-increased species, charge-reduced product ions were observed in He-CTD spectra of 2+ and 3+ substance P cations. These hydrogen-rich charge-reduced species correspond to *m/z* 1349.8 ($[M+2H]^{+\bullet}$) and *m/z* 675.0 ($[M+3H]^{2+\bullet}$) respectively, which are commonly observed in electron-based methods (e.g., ECD/ETD). It seems unreasonable for He^{+} to serve as an electron transfer reagent for such charge reduction reactions, so we performed several experiments to investigate the source of the electron-donating reagents.

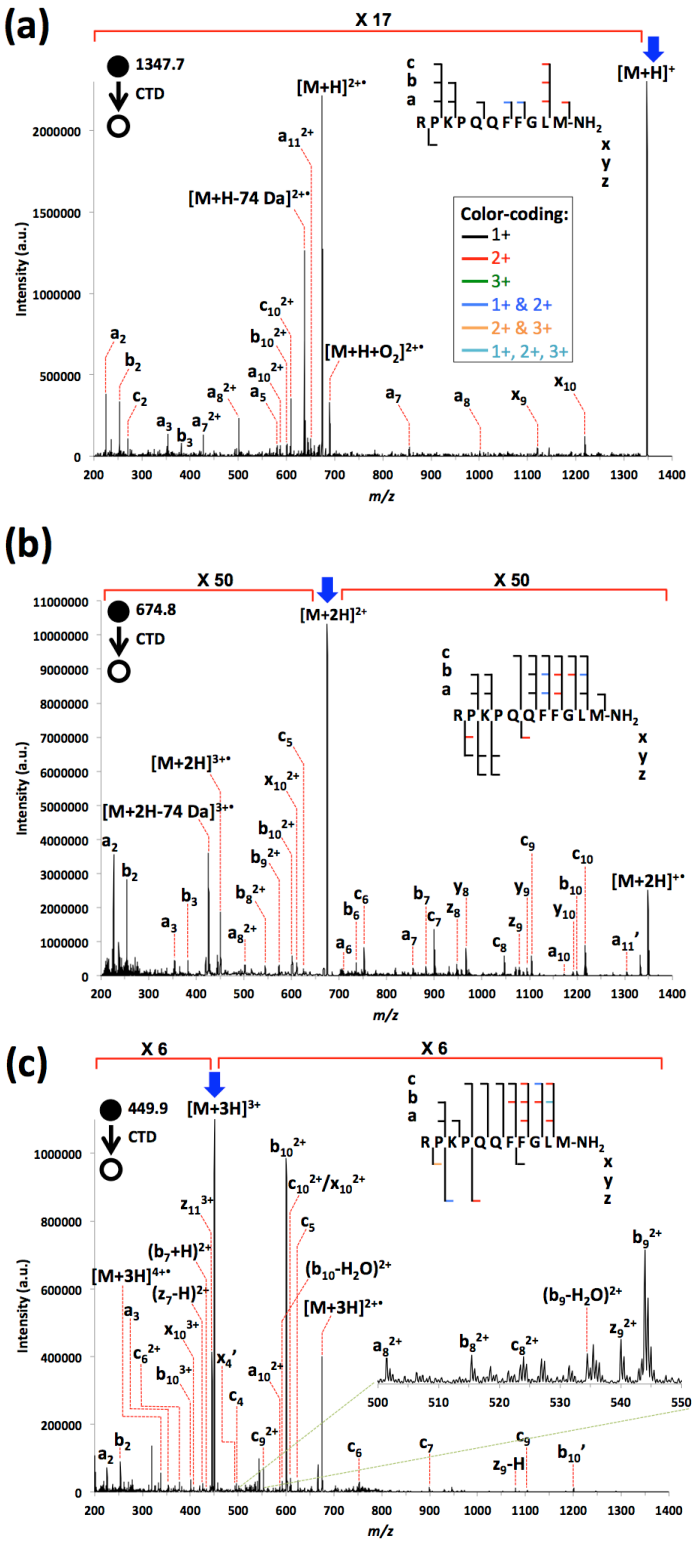

Figure 2.2. He-CTD spectrum of (a) singly, (b) doubly and (c) triply protonated substance P. The *m/z* ranges of interested have been multiplied by factors of 17, 50 and 6, respectively, for clarity. Precursor ions are indicated by blue arrows. The inset in panel (a) shows the color-coding scheme of peptide sequencing used throughout this work.

Despite the fact that the CTD source is designed to operate as an efficient cation source, a wide range of negative ions are observed in the background CTD spectrum when the trap is operated in negative ion mode (vide infra). Although we are unsure of the exact mechanism(s) of negative ion formation, the CTD source is apparently able to form negative ions from background impurities in the trap, and these anions can be trapped and used as reagent anions for ETD. One of the more abundant background ions has a mass-to-charge ratio of 184 (see Figure 2.8, for example), does not fragment using CID and reacts with residual oxygen to form adducts at M+16 (*m/z* 200) and M+32 (*m/z* 216). CID of the M+16 and M+32 adducts re-forms the original reagent anion at *m/z* 184, indicating that the reagent is probably polycyclic/aromatic and almost certainly a radical (vide infra) [67-69].

Figure 2.2c shows that these reagent anions are reasonably effective at forming *c* and *z* ions from the 3+ precursor of substance P. Fortunately, this charge reduction mechanism can be minimized by raising the LMCO during CTD activation to prevent the co-accumulation of reagent anion, with the caveat that increasing the LMCO also limits the observable range of product ions for CTD. The same CTD experiment with an elevated LMCO is shown in Figure 2.11. The intensity of charge-reduced species, $[M+2H]^{+\bullet}$, decreased dramatically with increasing LMCO, with no significant change in the intensity of other product ions.

A series of *a* ions was observed in the He-CTD spectrum of singly protonated substance P, which is consistent with our previous experimental results on a 2D ion trap [65]. The current work shows additional low-mass fragment ions (e.g. a_2, b_2 and c_2) that were not observed on the 2D ion trap, but weaker signal-to-noise (S/N) for fragments in

the range from *m/z* 700 to *m/z* 1300. Reilly et al. [63] have reported that the fragmentation of ions observed in UV photodissociation can be affected by the type of mass analyzer, and we suspect that the observed differences between the 2D trap results and 3D trap results are cause by experimental differences. These differences could be minimized by raising the LMCO value and increasing the CTD time on the 3D ion trap to make the conditions more similar to the experiments on the 2D ion trap.

Similar to electron-based fragmentation methods [17, 66], CTD of substance P also shows certain charge state-dependence on fragmentation. Product ion spectra of He-CTD of 2+ and 3+ substance P produced more than twice the number of fragment ions than the 1+ precursor, mainly because of the addition of *c* and *z* ions. Additional doubly- and triply-charged fragment ions were also observed from the higher charge state precursor ions. For example, the He-CTD spectrum of 2+ substance P (Figure 2.2b) is dominated by both *a* and *b* ions, with a few *c, y* and *z* ions, but the He-CTD spectrum of 3+ substance P is dominated by *c* ions. The near-complete series of *a* ions for the 1+ precursor is commonly observed in high-energy dissociation methods, and suggests the involvement of a high-energy fragmentation channel [65]. The existence of *b/y* and *c/z* fragment ion series mainly originates from vibrational excitation (e.g. CID) and charge-reduction processes, respectively, which clearly become more dominant than oxidation as the charge state of the precursor increases.

To probe the relationship between CTD and ETD, ETD fragmentation of 2+ and 3+ substance P was conducted on the same instrument. Results are in Figure 2.3. ETD of 2+ substance P produced only six *c* ions, covering half of the peptide sequence. In

contrast, ETD of 3+ substance P produced almost complete sequence coverage of *c* ions, along with some *a, b* and *z* ions.

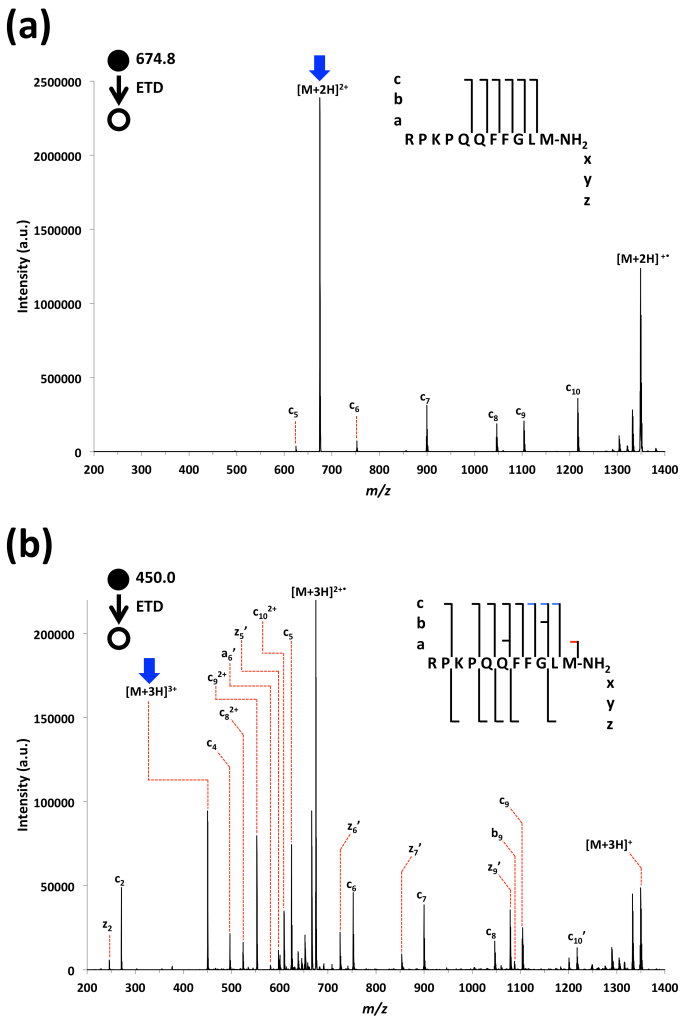

Figure 2.3. ETD spectra of (a) doubly and (b) triply protonated substance P.

2.3.2 Side-Chain Losses from Substance P

In addition to the aforementioned backbone fragmentation, side-chain cleavages were observed for substance P, as shown in Figures 2.4 and 2.5. Amino acid side-chain losses have been well-noted and referred to as ($M^{\bullet}$ - X) regions in variety of tandem MS

approaches, including UVPD [62, 63], action spectroscopy [24], fs-LID [23], EID [61], EED [18], ECD [14, 70-76], ETD [77], CID [78] and MAD [58].

Figure 2.4 provides zoomed-in regions of the same spectra from Figure 2.2 to show more clearly the side-chain losses from the ionized product ions. The oxidized cations are often referred to as hydrogen-deficient species in other studies [61]. For the He-CTD spectrum of 1+ substance P, diagnostic side-chain losses from $[M+H]^{2+\bullet}$ were observed, including even-electron rearrangements and radical losses. These observations are consistent with commonly-observed neutral losses from $[M+H]^{2+\bullet}$, including: 1 Da ($^{\bullet}H$) [61], 15 Da ($^{\bullet}CH_3$from Met) [24], 47 Da ($^{\bullet}SCH_3$ from Met) [24], 58 Da ($^{\bullet}CH_2CONH_2$ from Glu) [24, 78], 61 Da ($^{\bullet}CH_2SCH_3$ from Met) [57], 71 Da (CH_2=$CHCONH_2$from Gln) [78], and 74 Da (CH_2=$CHSCH_3$ from Met) [18, 57].

An interesting ion at *m/z* 689.9 was also observed and is tentatively assigned as an oxygen adduct of the oxidized product ion, i.e. $[M+H+O_2]^{2+\bullet}$. This ion is accompanied by an ion 44 Da less at *m/z* 667.8, which probably corresponds to $[M+H+O_2-CO_2]^{2+\bullet}$ probably forms from the oxidation of the $[M+H-CO_2]^{2+\bullet}$ product [57, 61]. Radical ions have been observed to react with residual oxygen during their confinement in electrodynamic ion traps, which was also noted for the ETD-generated $z^{\bullet}$ ions [67, 68] and MAD-generated $[POPC]^{+\bullet}$ radical ions [69].

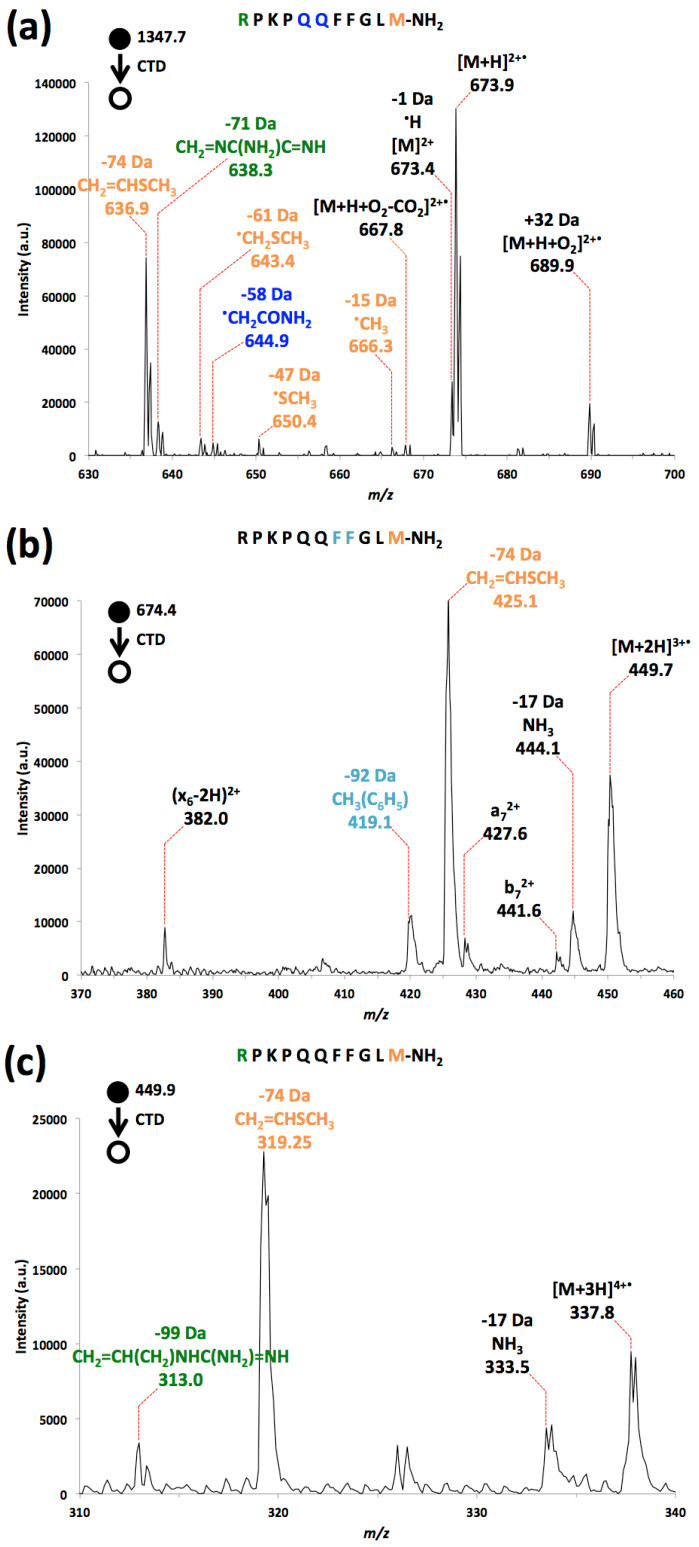

Figure 2.4. Zoomed-in He-CTD spectra of (a) 1+, (b) 2+, and (c) 3+ precursor ions of substance P, showing *m/z* ranges corresponding to the (M• - X) ranges of oxidized (charge-increased) product ions.

When the charge state of substance P precursor increases to 2+ and 3+, fewer side-chain losses from ionized species were observed. Observed losses include: 17 Da (NH_3) [24], 74 Da (CH_2=$CHSCH_3$ from Met) [18] and 92 Da ($CH_3(C_6H_5)$ from Phe) [24] were lost from $[M+2H]^{3+\bullet}$. 17 Da (NH_3) [24], 74 Da (CH_2=$CHSCH_3$ from Met) [18] and 99 Da (CH_2=$CH(CH_2)NHC(CH_2)$=NH from Arg) [78] were lost from $[M+3H]^{4+\bullet}$.

Figure 2.4a shows CTD of the 1+ precursor ion. In this spectrum, the product ion at m/z 673.4 ($[M]^{2+}$) likely results from an $H^{\bullet}$ loss from the oxidized product ion, $[M+H]^{2+\bullet}$. Whereas the loss of 1 Da neutrals ($^{\bullet}H$) from charge increased (oxidized) products likely involves the loss of H radicals, the same loss of 1 Da from charge-reduced species, such as in Figure 2.5a, most likely originates from a competitive proton transfer processes during the reactions.

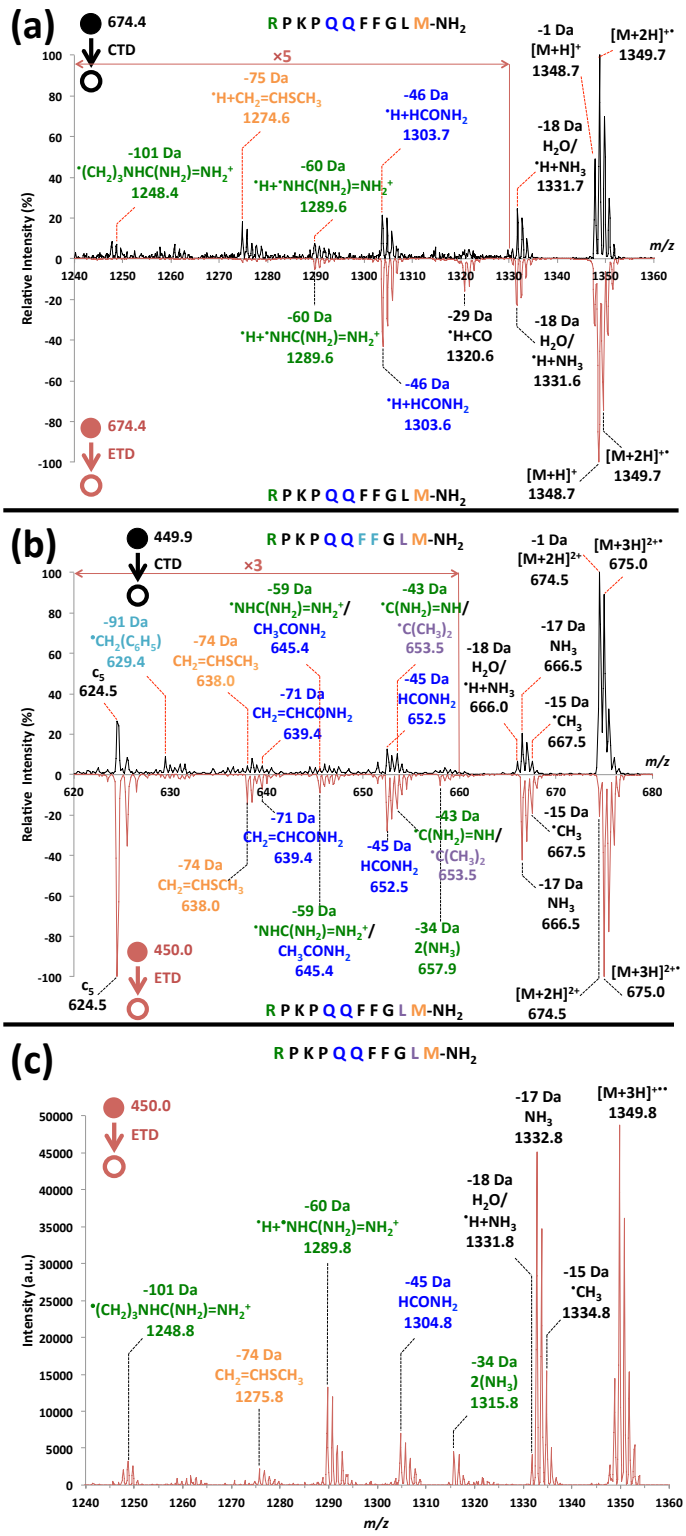

Figure 2.5. Head-to-tail zoomed-in spectra of reduced (charge-decreased) product ions of: (a) He-CTD versus ETD of 2+ substance P, (b) He-CTD versus ETD of 3+ substance P, and (c) 1+ product ions from ETD of 3+ substance P. Each spectrum is normalized to the tallest peak within the (M• - X) range of charge-reduced product ions.

Zoomed-in *m/z* regions of charge-reduced species from He-CTD spectra of 2+ and 3+ substance P precursors are shown in top panels of Figure 4a and 4b. ETD spectra of 2+ and 3+ substance P are magnified to show the ($M^{\bullet}$ - X) regions, which are listed as bottom panels in Figure 2.5a, 2.5b and an individual panel in Figure 2.5c.

The CTD spectrum in top panel of Figure 2.5a shows several neutral losses from $[M+2H]^{+\bullet}$, including 18 Da (H_2O or $^{\bullet}H+NH_3$) [61, 79-81], 46 Da ($^{\bullet}H+HCONH_2$ from Gln) [79, 80], 60 Da ($^{\bullet}H+^{\bullet}NHC(NH_2)=NH_2^+$ from Arg) [14, 79-81], 75 Da ($^{\bullet}H+CH_2=CHSCH_3$ from Met) [72, 81] and 101 Da ($^{\bullet}(CH_2)_3NHC(NH_2)=NH_2^+$from Arg) [72]. Similar neutral losses from the ETD product $[M+2H]^{+\bullet}$ are also observed [77]. Two exceptions are the 75 Da side-chain loss, which is unique to CTD, and the 29 Da loss, which is only observed in the ETD product ion spectrum. In the absence of high mass accuracy, the 29 Da loss is tentatively assigned as $^{\bullet}H+CO$ [79].

Compared to the low abundance and small neutral losses from the $[M+2H]^{+\bullet}$ product ion, neutral losses from the $[M+3H]^{2+\bullet}$ product ion are more abundant for both CTD and ETD. Moreover, the types of neutral losses from the radical dication $[M+3H]^{2+\bullet}$ are also different from that of $[M+2H]^{+\bullet}$. The observed neutral losses in the CTD spectrum and their tentative assignments are: 15 Da ($^{\bullet}CH_3$) [81], 18 Da (H_2O or $^{\bullet}H+NH_3$)[61, 79, 81], 43 Da ($^{\bullet}C(NH_2)=NH$ from Arg or $^{\bullet}C(CH_3)_2$ from Leu) [61, 78], 45 Da ($^{\bullet}H+HCONH_2$ from Gln) [79, 80], 59 Da ($^{\bullet}NHC(NH_2)=NH_2^+$ from Arg or CH_3CONH_2 from Gln) [14, 79-81], 71 Da ($CH_2=CHCONH_2$ from Gln) [78, 81], 74 Da ($CH_2=CHSCH_3$ from Met) [78, 81] and 91 Da ($^{\bullet}CH_2(C_6H_5)$) [24]. Interestingly, the CTD spectrum has a unique small loss of 91 Da, and the ETD spectrum has a unique loss of 34 Da ($2(NH_3)$ from Arg) [77].

Unlike CTD, ETD of 3+ substance P precursor also produced the singly charged ETnoD product ($[M+3H]^{+\bullet\bullet}$), whose ($M^{\bullet}$ - X) region shows the same small losses as those observed for $[M+2H]^{+\bullet}$ and $[M+3H]^{2+\bullet}$. Similar neutral losses have also been observed in ECD experiments [79].

In general, the CTD and ETD spectra show many similarities in the ($M^{\bullet}$ - X) regions of both $[M+2H]^{+\bullet}$ and $[M+3H]^{2+\bullet}$. The similar neutral losses between the two activation methods are indicative of similar fragmentation mechanism, which adds more confidence of our previous hypothesis that electron-based fragmentation mainly accounts for the fragments located in the high mass end of CTD spectrum. The similarity in CTD and ETD spectra of multiply charged precursor ions suggests that the ExD-like fragments in CTD experiments originate from the interaction with ETD-like reagent anions, such as negative ions derived from vacuum pump oil or other common contaminants.

By operating the trap in negative ion mode, the CTD source and trap conditions can be shown to produce multiple anions in the region *m/z* 180-220 (see Section 2.3.5). One particularly abundant anion exists at *m/z* 184. Isolation of this abundant background anion showed two interesting properties: 1) the anion could reversibly add O and O_2, which indicates the anion is a radical; and 2) the anion is resistant to collisional activation, which indicates it may contain fused ring systems. Section 2.3.5 will provide more details about the interrogation of the background anion in CTD. Background anions generated by the CTD gun are present at most *m/z* values below m/z 200, and they can be easily excluded from the trap to prevent electron transfer reactions by raising the LMCO value >220 Da. Charge reduction (e.g. ETD-like activation) is still observed, even when the co-storage of anions and cations is minimized, which indicates that a second

mechanism must also exist to explain the charge reduction of multiply-protonated peptide cations. It is possible that the He cation beam contains a fraction of helium metastable atoms, which have relatively low ionization potentials and could serve as an electron transfer reagents.

2.3.3 Bradykinin:1+, 2+ and 3+ Charge States

He-CTD was also conducted on 1+, 2+, and 3+ bradykinin cations, and the results are shown in Figure 2.6. Upon irradiation with helium cations, charge-increased product ions were observed for all the three charge states. Charge-reduced product ions could only be observed for 2+ and 3+ precursors of bradykinin, as expected. These observations are in good agreement with the observations for CTD of substance P [65], and the previous study by Zubarev and coworkers [48]. Unlike CTD of 1+ substance P, CTD of 1+ bradykinin produces an abundant series of *x* ions in addition to the previously observed *a* ions. CTD of 1+ bradykinin also produces more *b*, *y*, *c* and *z* ions. The coexistence of *a/x* ion pairs provides greater confidence in sequencing and more confidence that the *a* ions are formed via direct C-CO cleavage and not from CO losses from intermediate *b* ions.

Consistent with He-CTD results of 2+ and 3+ substance P, fewer *a/x* ions and more *b/y* and *c/z* ions are observed for 2+ and 3+ bradykinin. And similar to CTD of 3+ substance P, the product ion spectrum for CTD of 3+ of bradykinin is dominated by *c/z* ions. The abundant *c/z* ions again point to the domination of an ETD-like mechanism for the higher charge state precursors in CTD.

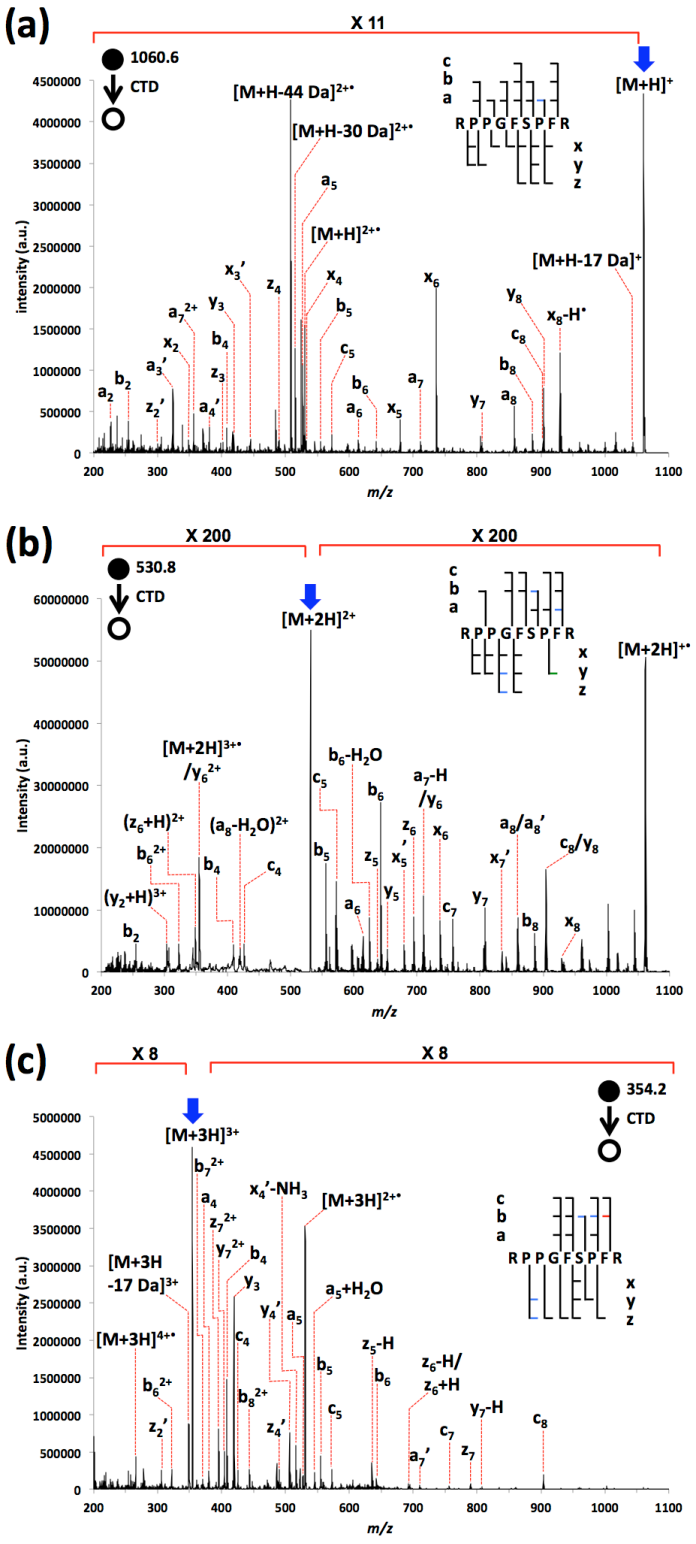

Figure 2.6. He-CTD spectrum of (a) singly, (b) doubly and (c) triply protonated bradykinin. Different *m/z* ranges of interested have been multiplied by a factor of 11, 200 and 8, respectively, for clarity.

2.3.4 Side-Chain Losses from Bradykinin

As shown in Figure 2.7a, He-CTD of 1+ bradykinin precursor produced five significant fragments corresponding to small neutral losses from $[M+H]^{2+\bullet}$. Similar to the ($M^{\bullet}$ - X) regions of substance P, an oxygen adduct ion at *m/z* 546.3 as well as an accompanying ion at *m/z* 524.3 (formed through CO_2 loss) are observed.

As might be expected, significant differences in small neutral losses of bradykinin and substance P are observed. For example, bradykinin in Figure 2.7a shows four different small losses: 30 Da (HCHO) [61], 44 Da ($^{\bullet}C(NH_2)=NH_2^+$ from Arg) [24], 62 Da ($^{\bullet}C(NH_2)=NH_2^+ + H_2O$) [24] and 91 Da ($^{\bullet}CH_2(C_6H_5)$ from Phe) [24], two of which are of significantly higher intensity compared to that in CTD experiment of 1+ substance P. The appearance of fragments corresponding to side-chain losses from Phenylalanine and Arginine in the ($M^{\bullet}$ - X) region of $[M+H]^{2+\bullet}$ is consistent with the fact that bradykinin possesses twice the amount of phenylalanine and arginine residues, and that these residues are at or adjacent to the C-terminus in bradykinin.

He-CTD of 2+ bradykinin cations produced many small losses within the ($M^{\bullet}$ - X) region of $[M+2H]^{+\bullet}$ (Figure 2.7b), and a few small losses within the ($M^{\bullet}$ - X) region of $[M+3H]^{2+\bullet}$ (Figure 2.7c). Most of the small losses for bradykinin are similar to those observed in the same ($M^{\bullet}$ - X) region of charge-reduced species from CTD of 2+ and 3+ of substance P. The similar neutral losses include: 16 Da ($^{\bullet}H+^{\bullet}CH_3$), 17 Da ($NH_3$), 18 Da ($H_2O$ or $^{\bullet}H+NH_3$), 28 Da (CO), 43 Da ($^{\bullet}C(NH_2)=NH$ from Arg), 59 Da ($^{\bullet}NHC(NH_2)=NH_2^+$ from Arg), 101 Da ($^{\bullet}(CH_2)_3NHC(NH_2)=NH_2^+$from Arg). Different small losses are observed as well. For example, bradykinin shows losses corresponding to: 19 Da ($^{\bullet}H+H_2O$) [81], 31 Da ($^{\bullet}H+HCHO$) [61], 44 Da ($^{\bullet}C(NH_2)=NH_2^+$ from Arg) [81],

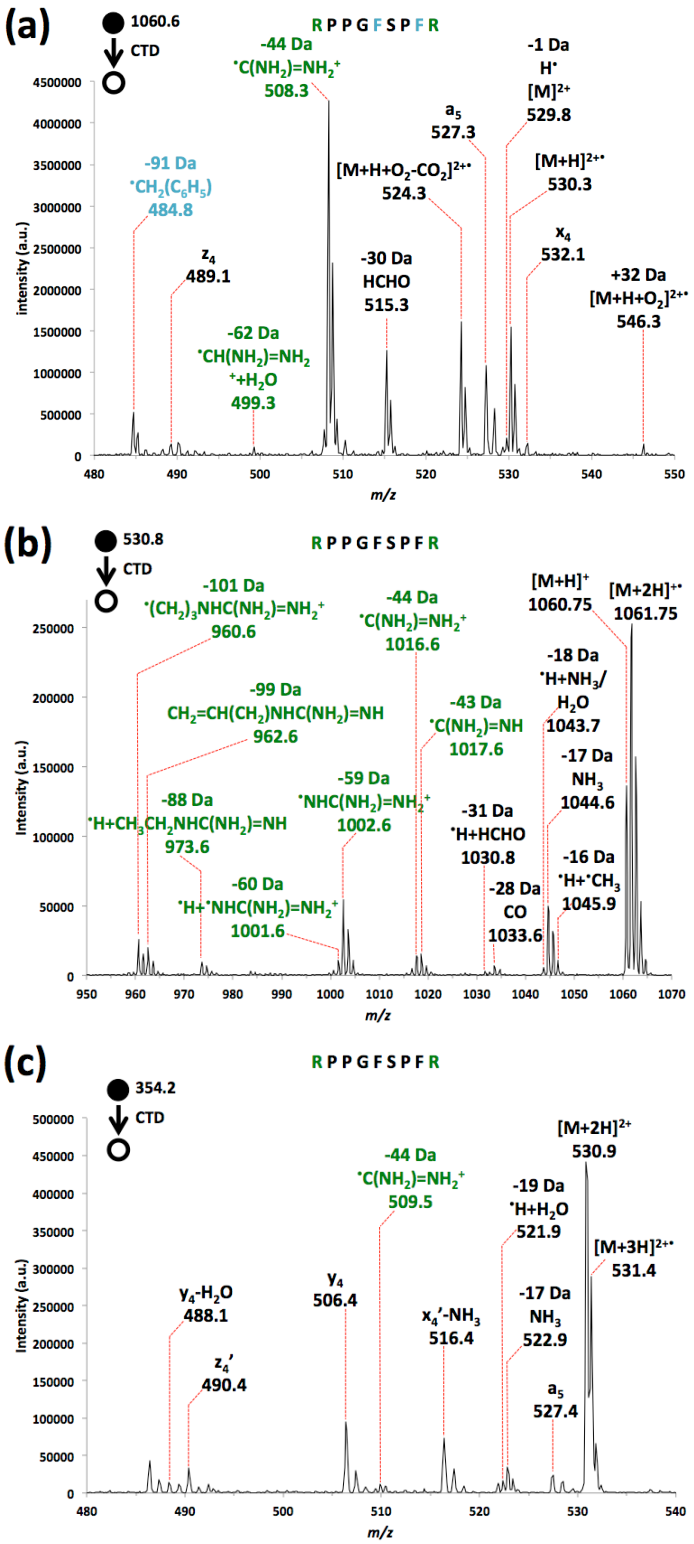

Figure 2.7. Zoomed-in He-CTD spectra of (a) singly protonated bradykinin showing ($M^{\bullet}$-X) regions of $[M+H]^{2+\bullet}$ (oxidized product ion), (b) doubly and (c) triply protonated bradykinin showing ($M^{\bullet}$ - X) regions of $[M+2H]^{+\bullet}$ and $[M+3H]^{2+\bullet}$ (charge-reduced product ions) respectively.

60 Da ($^{\bullet}H+^{\bullet}NHC(NH_2)=NH_2^+$ from Arg) [77], 88 Da ($^{\bullet}H+CH_3CH_2NHC(NH_2)=NH$ from Arg) [81] and 99 Da ($CH_2=CH(CH_2)NHC(NH_2)=NH$ from Arg) [79]. Compared to substance P (RPKPQQFFGLM), bradykinin (RPPGFSPFR) has a higher composition of arginine residues, which could possibly account for the more frequent observation of arginine side-chain losses in bradykinin. A similar observation was observed in the ECD study of bradykinin methyl ester ($RPPGFSPFROCH_3$) [79]. Upon ECD, bradykinin with a C-terminal methyl ester showed a predominance of arginine-specific losses in the ($M^{\bullet}$ - X) region of $[M+2H]^{+\bullet}$.

2.3.5 Origin of Charge-Reduced Species

With the ESI source off, saddle field ion source was turned on, so the "empty" eletrodynamic quadrupole ion trap was irradiated with helium cations. Aside from the generation of helium cations, a high flux of electrons was also produced in the saddle field ion source. Hypothetically, the "un-removed" electron beam sputters on the pump oil deposited on the inside surface of the quadrupole ion trap, which would then undergo a desorption process, generating aromatic anions. As electron carriers, these aromatic anions would transfer electrons to the isolated precursor cations to generate ETD-like product ions.

Figure 2.8c shows the oxygen (O_2) attachment to the ion at *m/z* 184. Upon collisional activation, a reverse process—oxygen (O_2) detachment was observed in Figure 2.8e. This "reversible" process proves the occurrence of oxygen attachment, which indicates the radical nature of the ion at *m/z* 184 (i.e. $[M]^{-\bullet}$). Accordingly,

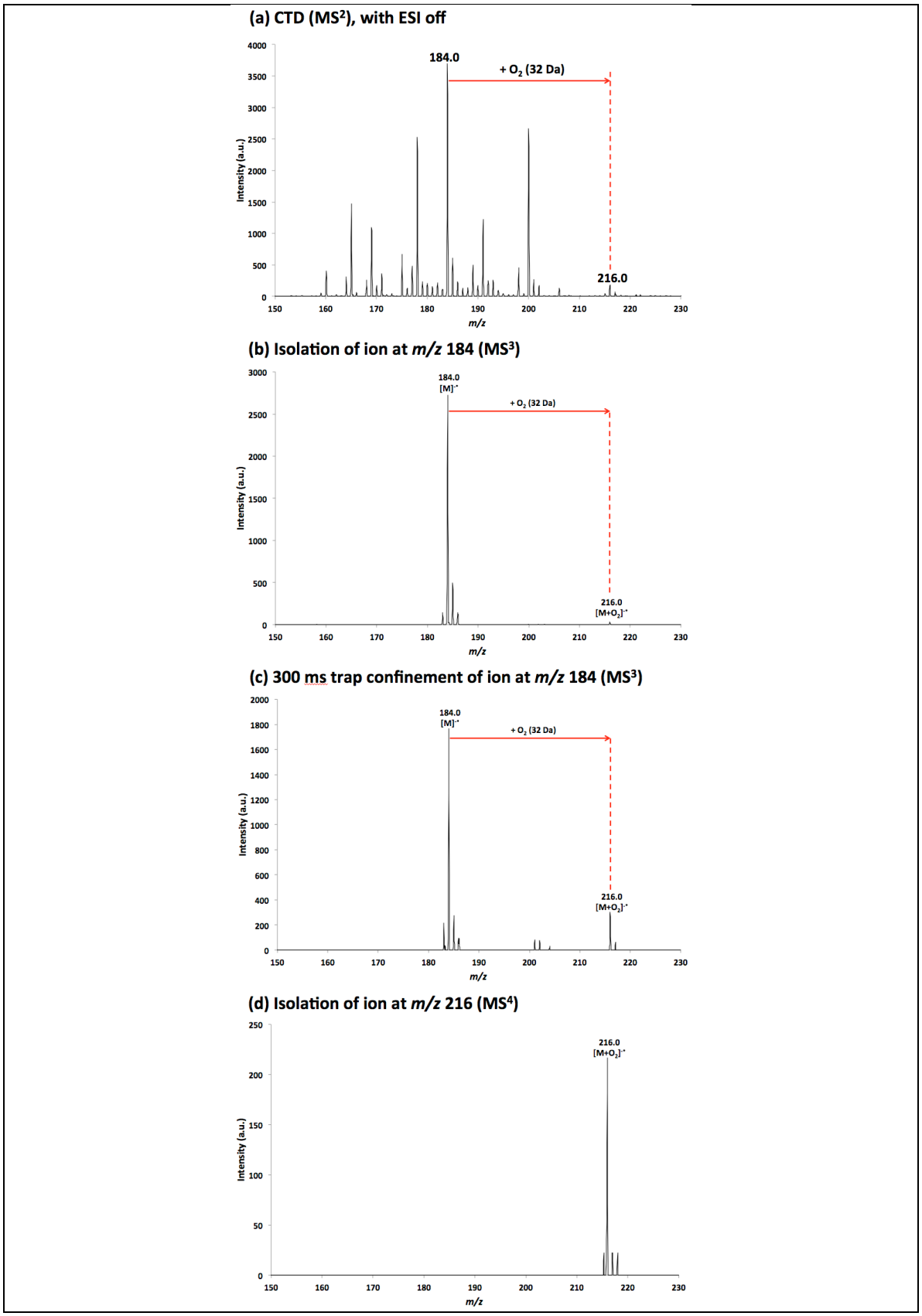
(a) CTD (MS²), with ESI off
184.0
+ O2 (32 Da)
216.0
Intensity (a.u.)
m/z
(b) Isolation of ion at m/z 184 (MS³)
184.0
[M]·+
+ O2 (32 Da)
216.0
[M+O2]·+
Intensity (a.u.)
m/z
(c) 300 ms trap confinement of ion at m/z 184 (MS³)
184.0
[M]·+
+ O2 (32 Da)
216.0
[M+O2]·+
Intensity (a.u.)
m/z
(d) Isolation of ion at m/z 216 (MS⁴)
216.0
[M+O2]·+
Intensity (a.u.)
m/z

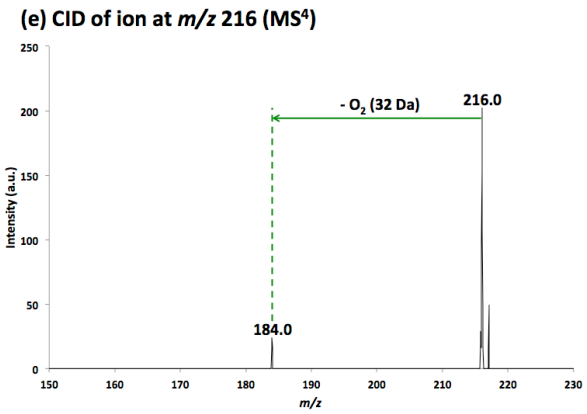

Figure 2.8. (a) CTD spectrum of pump oil residue at MS^2. (b) Isolation spectrum of ion at *m/z* 184 at MS^3. (c) Product ion spectrum after 300 ms trap confinement at MS^3. (d) Isolation spectrum of ion at *m/z* 216 at MS^4. (e) CID spectrum of ion at *m/z* 216 at MS^4 with an activation voltage of ~0.5 V.

the ion at *m/z* 216 was assigned to be $[M+O_2]^{-\bullet}$. To explore the identity/chemical composition of M (*m/z* 184), this ion was further isolated and subjected to collisional activation (vide infra).

In Figure 2.9b, the ion at *m/z* 184 ($[M]^{-\bullet}$) was subjected to a CID activation voltage of ~1.0 V, but it still didn't fragment. This fact further suggests the highly stable structure of M, which could be a polycyclic/aromatic hydrocarbon.

With limited structural details could be drawn from the above experimental data, the most likely candidate at present is a naphthalene derivative at *m/z* 184 ($[M]^{-\bullet}$). Vacuum pump oil contains a large proportion of saturated hydrocarbons, but because hydrodreated paraffinic oils are derived from medium/heavy petroleum distillates, they also contain polycyclic and aromatic constituents. The ion at *m/z* 184 seems to have eight double bond equivalents, so could be a negatively charged substituted naphthalene radical, $[C_{14}H_{16}]^{-\bullet}$, as shown in Figure 2.10. This structure would be consistent with the apparent resistance to collisional activation. Based on the expected elemental

composition of the precursor anion at m/z 184, it must have fewer double-bond equivalents than the popular reagent anion fluoranthene.

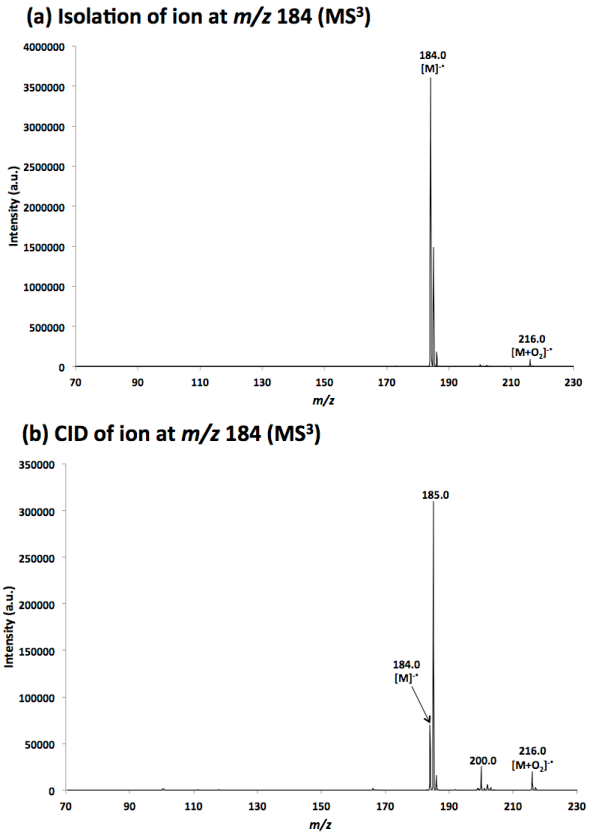

Figure 2.9. (a) Isolation spectrum of ion at *m/z* 184 at MS^3. (b) CID spectrum of ion at *m/z* 184 at MS^3 with an activation voltage of ~1.0 V.

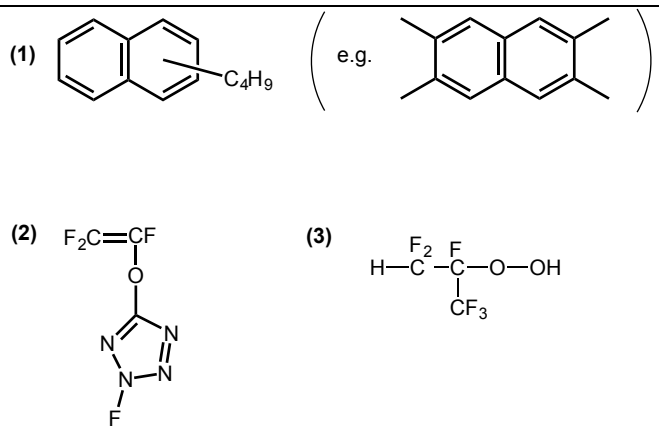

Figure 2.10. The proposed possible structures of the ion at *m/z* 184.

Another, less likely possibility, is that the background anions are fluorinated compounds. Fluorinated compounds could originate from the decomposition of fluoroelastomer from Viton, which is used in most LC systems in the pumps. Scheme S1 shows hypothetical chemical structure of the ion at *m/z* 184; (2), derived from reference [82], or; (3), derived from reference [83]. However, we expect that thee fluorinated compounds would provide some observable product ions under collisional activation, but none were observed.

The formation of adducts with O_2 has been well noted for polyaromatics [84, 85] and halogenated compounds [86]. And a resonance electron capture mechanism was proposed for the generation of such adducts [85].

He-CTD of $[\text{bradykinin}+2\text{H}]^{2+}$ was carried out at various low mass cut-off (LMCO) values: *m/z* 150, *m/z* 200, *m/z* 250, *m/z* 300, , *m/z* 350 and *m/z* 400. The rest of the experimental parameters were the same as described in the "Experimental" part. Relative intensity of each product ion (i.e. b_4, $(a_8\text{-}H_2O)^{2+}$, c_5, z_6, x_6, y_8, $[M+H]^+$, $[M+2H]^{+\bullet}$) is calculated as follows:

$$\text{Relative Intensity} = \frac{\text{Intensity of one product ion}}{\sum \text{Precursor ion(leftover)} + \sum \text{All product ions}}$$

The plot of relative intensity versus LMCO is shown in Figure 2.11.

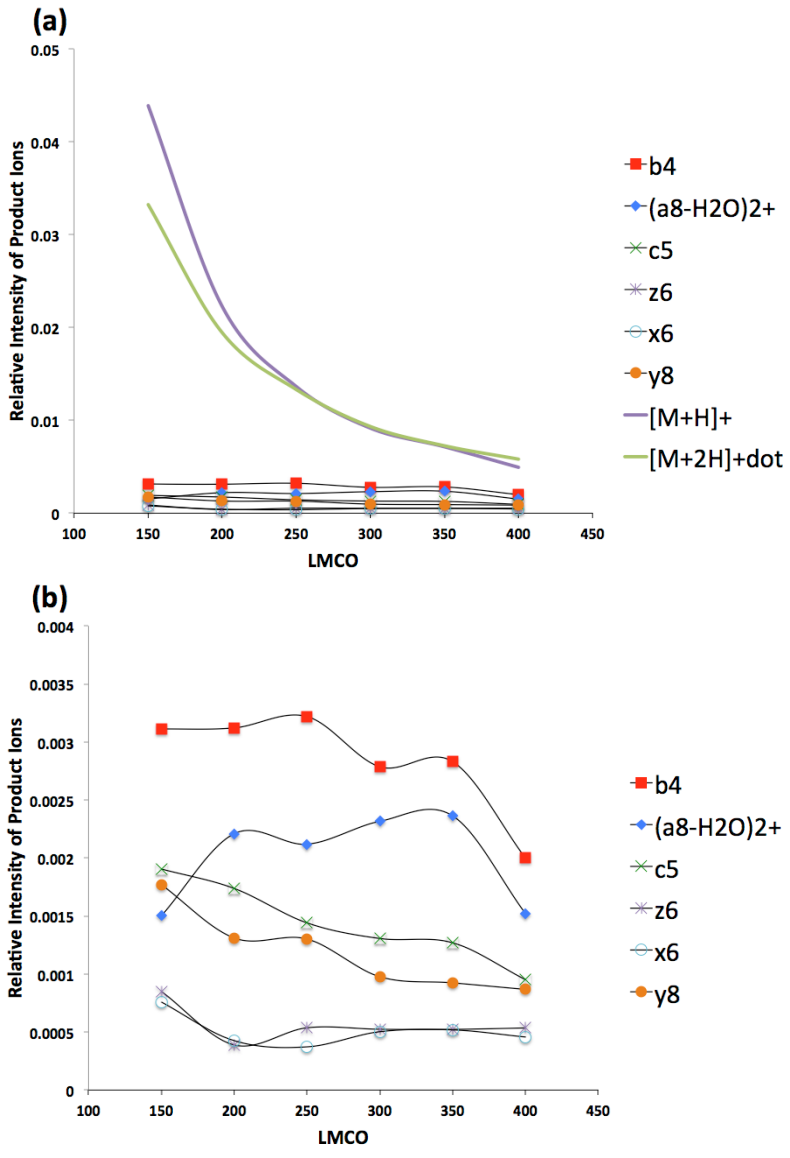

Figure 2.11. Relative intensity of product ions from He-CTD of $[\text{bradykinin+2H}]^{2+}$ is plotted versus LMCO. (a) Plot for b_4, $(a_8\text{-H}_2\text{O})^{2+}$, c_5, z_6, x_6, y_8, $[\text{M+H}]^+$, $[\text{M+2H}]^{+\bullet}$ product ions. (b) "Zoomed-in" plot for b_4, $(a_8\text{-H}_2\text{O})^{2+}$, c_5, z_6, x_6, y_8 product ions.

2.4 Conclusions

Charge transfer dissociation of singly, doubly and triply protonated substance P and bradykinin was conducted in a 3D ion trap mass spectrometer. The charge state of the precursor ions significantly impacted the number and the types of ions produced—*a/x* versus *c/z*—correlates with the relative contributions of oxidative versus reductive mechanisms, respectively. Consistent with our previous experimental results, CTD of singly charged precursors produces an abundance of *a/x* fragments, and the distribution of charge between complementary *a/x* ion pairs is dependent on the relative basicity of the peptide termini. CTD of doubly and triply charged precursors produced additional *b/y* ions and *c/z* ions. The type of fragment ions provides helpful hints on possible fragmentation channels that CTD adopts: high-energy, and ETD-like (i.e. radical) pathways. Accompanying side-chain losses were also observed in CTD spectra, which are in good agreement with the previous results from photo-activated, collisionally activated, and electron-based dissociation experiments. The side chain losses can provide valuable diagnostic information about amino acid composition to support the backbone-sequencing ions. The enriched structural information obtainable via CTD, along with the relative low-cost of 3D ion instrument platform, makes this approach a promising tool for the interrogation of gas-phase biomolecules.

CHAPTER 3: TOP-DOWN CHARGE TRANSFER DISSOCIATION (CTD) OF GAS-PHASE INSULIN: EVIDENCE OF A ONE STEP, TWO-ELECTRON OXIDATION MECHANISM

Reproduced in part with permission from Pengfei Li, Iris, Kreft, Glen P. Jackson*, J. Am. Mass Spectrom.*in submission.

3.1 Introduction

B-cells in Langerhans of the pancreas produces insulin, which not only maintains the blood glucose levels from getting too high or too low, but also regulates the amino acid uptake and inhibits the breakdown of glycogen, protein and fat [87]. Analogous to many polypeptide species, insulin contains multiple disulfide linkages for stabilizing its three-dimensional structure, and these disulfide bonds ensure the correct biological function. The multiple disulfide linkages form a cyclic structure in insulin, the presence of which inhibits the structural analysis of insulin via tandem mass spectrometry approaches. To retrieve the primary sequence information within the cyclic structure in these molecules, certain techniques have been employed to disrupt disulfide linkages.

Mass spectrometry (MS) shows high selectivity and sensitivity, and the capability of performing a variety of experiments, which makes it an appealing technique for analyzing biological molecules [16]. Due to the advent of soft ionization methods such as electrospray ionization (ESI) [88] or matrix-assisted laser desorption ionization (MALDI) [89], biomolecules can be formed intact for the purposes of molecular weight determination. The development of tandem mass spectrometry (MS/MS or MS^2) has greatly advanced the application of MS to the structural characterization of biomolecules [57].

Disulfide linkage-containing polypeptides have been extensively examined during the past few decades using various MS/MS techniques, including collision-induced

dissociation (CID) [90-93], post-source decay (PSD) [89], electron capture dissociation (ECD) [94-96], electron transfer dissociation (ETD) [93, 97-101], electron induced dissociation (EID) [102], electron detachment dissociation (EDD) [103], infrared multiphoton dissociation (IRMPD) [103] and ultraviolet photodissociation (UVPD) [104-108]. As the most widely used ion activation technique [11], CID makes use of ion/molecule collisions to convert kinetic energy to internal energy for the purpose of fragmenting the target ion. For peptides, CID mainly gives rise to *b* and *y* fragment ions from backbone amide bond cleavages. Insulin, at various charge states of 1+, 2+, 3+, 4+ and 5+ has investigated with CID, and the fragmentation efficiency is strongly dependent on the precursor charge state [92]. One particular limitation of CID is that little or limited sequence information within the cyclic structure could be retrieved [92]. Electron-based ion activation methods, like ECD, has shown the capability to cleave disulfide bonds, but ECD exhibited a relatively low dissociation efficiency [109]. Julian and coworkers combined UV activation with ECD to fragment insulin, which broke all three-disulfide bonds of insulin and exhibited a more extensive backbone fragmentation than ECD alone [108]. In other work, Loo and coworkers employed sulfolane as the supercharging reagent in protein solution, and the resulting supercharged protein ions exhibited elevated ECD efficiency and S-S bond dissociation efficiency [110].

Charge transfer dissociation (CTD) using helium is an alternative MS/MS technique developed by the Jackson research group [65], and is very similar in energy and mechanism to metastable atom-activated dissociation (MAD) [27-29, 59, 111-113]. CTD employs helium cations with kiloelectronvolt kinetic energies to bombard the target peptide cations, which can produce a nearly complete set of *a* ions from 1+ substance P

[65] and also promotes radical ion fragmentation of peptides and oligosaccharides [114, 115]. In the present work, we explore the possibility of integrating CTD into a top-down workflow for small proteins by fragmenting the 4+, 5+ and 6+ charge states of bovine insulin with CTD. Whereas the resulting fragmentation pattern is very similar to ETD fragmentation demonstrated by others, we demonstrate the occurrence of an unexpected one-step, two-electron oxidation pathway, which highlights the unprecedented high energy that is available through CTD. We also characterize the difference between radical fragmentation pathways and even electron pathways for hydrogen deficient and hydrogen rich radical cations.

3.2 Experimental

3.2.1 Instrumentation

All experiments were performed on a modified Bruker (Bruker Daltonics, Bremen, Germany) equipped with a saddle field fast ion gun installed on the top of ring electrode [58, 65]. Briefly, a 2-mm hole was drilled in the ring electrode for the permission of helium cations into the trap. The Saddle field fast ion was used as the helium source. The ion source was installed onto a three-dimensional quadrupole ion trap (QIT) mass. The instrument modification is described in detail elsewhere [114].

3.2.2 Materials

Bovine insulin was purchased from Sigma-Aldrich (St. Louis, MO) and used without further purification. The insulin solution was prepared with a final concentration of approximately 20 μM in 49.5/49.5/1 (v/v/v) methanol/water/glacial acetic. Methanol (HPLC-grade) and glacial acetic acid were purchased from Fisher Scientific (Waltham,

MA). Water was obtained from an in-house Milli-Q purification system with >18 MΩ salt content.

3.2.3 Methods

Mass spectrometry measurement

All mass spectra were collected in positive mode with an ESI voltage of 4.5 kV, capillary voltage of 8 V, capillary temperature of 250°C, and a heated ESI source temperature of 60°C. The helium trap pressure, as measured in the main vacuum chamber, was 1.2 $x10^{-5}$ mbar. Full mass spectra were collected at different operating *m/z* ranges depending on the precursor ion.

Collision-induced dissociation measurements

The precursor ion of interest was isolated using a selection window of ±4 Da relative to the selected centroid *m/z* value. The ion current control (ICC) module was deactivated and the accumulation time (injection time) was typically 1.0 ms. The low mass cutoff (LMCO) was typically set to be approximately ~¼ of the precursor mass. E.g., for 5+ insulin (*m/z* 1148.0), the LMCO was set to be *m/z* 300. The CID amplitude was set to be ~0.30 V and "SmartFrag" mode was disabled. A typical CID experiment used 1.5-minutes of averaging spectra.

Charge transfer dissociation measurements

CTD experiments were conducted similarly to CID experiments, except that the QIT injection time was set to be 50 ms. A variable leak-valve was used to control the flow of the helium (1.20 x 10^{-5} mbar) through the ion gun. CTD was performed by the introduction of helium cations into the three-dimensional quadrupole ion trap. A waveform generator was synchronized with the period reserved for CID fragmentation.

The waveform generator was triggered by a TTL signal from the mass spectrometer, the details of which are provided elsewhere [65]. A typical CTD experiment consists of a 2.5-minute period of product ion accumulation spectra and a 2.0 min-period of background accumulation spectra (i.e. helium beam on but ESI off). The time-averaged background spectrum was subtracted from the time-averaged product ion spectrum. In the MS^3 CID experiments, CTD-generated product ions were isolated and subjected to a CID amplitude of 0.25 V at the MS^3 level. The follow-up isolation/ion storage experiments (MS^4 level) were carried out using a similar procedure. At the MS^4 stage, the isolation window was 10 Da and the LMCO was 500.

Resonance Ejection

Resonance ejection experiments were conducted for the investigation of dissociation pathways. The precursor ions of interest were isolated and subjected to helium irradiation at the MS^2 level. A particular product ion could then be resonantly ejected during the CTD reaction through the application of a relatively large CID amplitude (~2.5 V) at a frequency that corresponded to the desired intermediate. The experiment was repeated three times, and all the product ion spectra were averaged for final analysis. The experiment was repeated with the CID amplitude set to 0 V to ensure that the factor of scattering losses due to prolonged storage was independent of the factor of resonance ejection.

3.3 Results and Discussion

3.3.1 Insulin: 4+, 5+ and 6+ Charge States

CTD spectra of $[insulin+4H]^{4+}$, $[insulin+5H]^{5+}$, and $[insulin+6H]^{6+}$ are shown in Figure 3.1. In Figure 3.1a, when the 4+ insulin precursor ion was subjected to helium

cation irradiation, two types of radical cations are generated; [insulin+4H]$^{5+\bullet}$, the charge-increased or oxidized product ion (CTnoD); and [insulin+4H]$^{3+\bullet}$, the charge-decreased or reduced product ion (ETnoD). The proposed pathway of [insulin+4H]$^{5+\bullet}$ formation is shown in Equation (1):

$$[M + 4H]^{4+} + He^{+}{}_{(fast)} \rightarrow [M + 4H]^{5+\bullet} + He^{0}{}_{(fast)} \qquad (1)$$

Similar charge-increased product ions were also observed in the CTD spectra of insulin 5+ and 6+ charge states. The formations of the two charge-increased species are proposed in Equation (2) and (3).

$$[M + 5H]^{5+} + He^{+}{}_{(fast)} \rightarrow [M + 5H]^{6+\bullet} + He^{0}{}_{(fast)} \qquad (2)$$

$$[M + 6H]^{6+} + He^{+}{}_{(fast)} \rightarrow [M + 6H]^{7+\bullet} + He^{0}{}_{(fast)} \qquad (3)$$

The presence of charge-reduced product ions indicates that a side channel of ETD-like behavior is occurring. We recently described an attempt to characterize the potential reagent anions [115], which showed that the reagent anions originate from background contamination, are radical anions and are highly unsaturated. The reagent negatives ions appear to comprise a homologous series, which maximizes in abundance around *m/z* 184-220. The CTD activation of large mass precursor like insulin permitted the LMCO to be raised to *m/z* 300 to prevent the co-accumulation of the background reagent anions, and thereby reduce the extent of ETD. The benefit of operating with an elevated LMCO is that the ETD pathway is minimized and the oxidized products of insulin are generally more abundant than the charge-reduced product ions, as shown in Figure 3.1a.

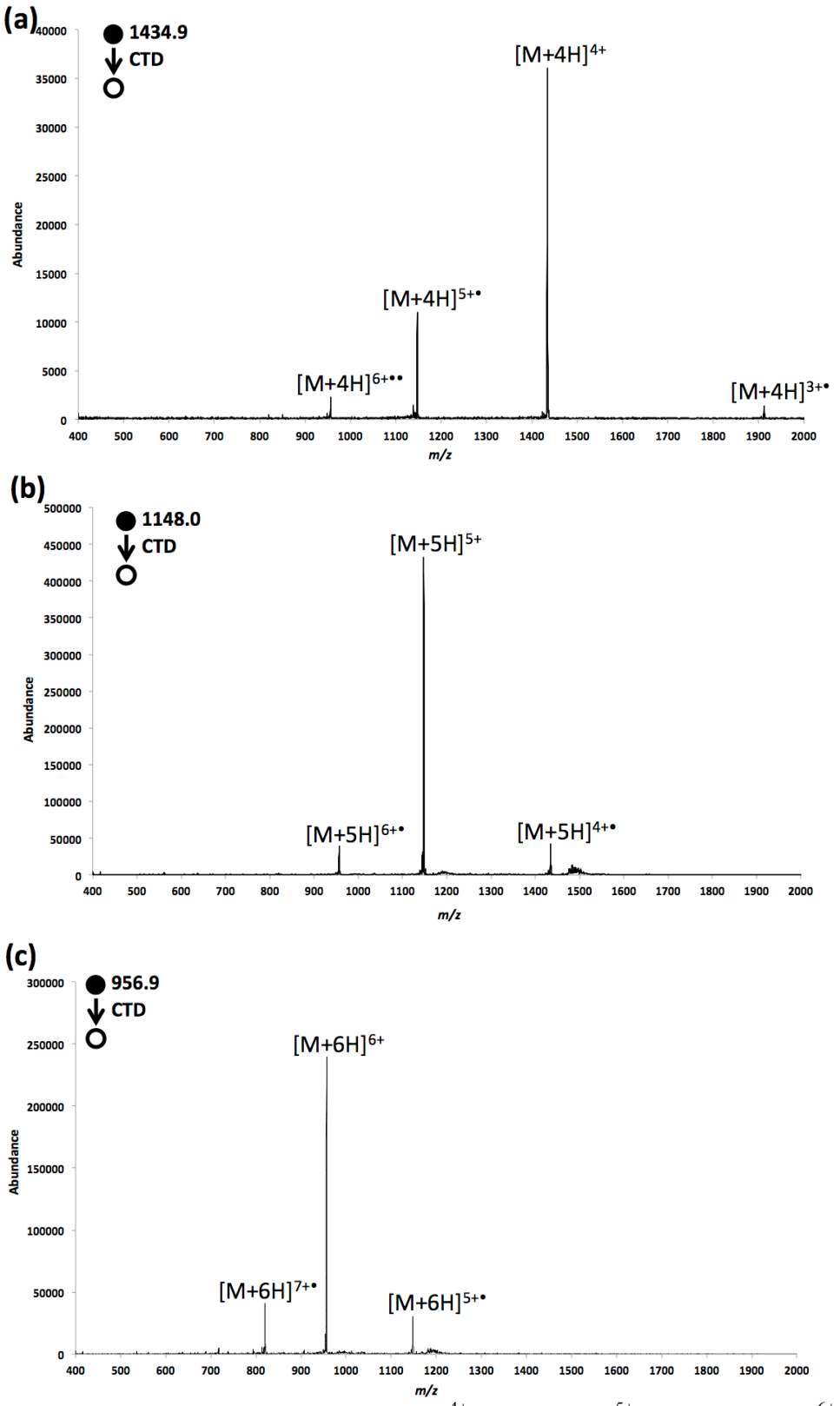

Figure 3.1. CTD spectra of isolated (a) $[M+4H]^{4+}$, (b) $[M+5H]^{5+}$ and (c) $[M+6H]^{6+}$ ions derived from bovine insulin.

The close-ups of Figure 3.1a, Figure 3.1b and Figure 3.1c are shown in Figure 3.2, Figure 3.4 and Figure 3.5, respectively. The identified fragments are annotated on the protein structure in Scheme 3.1. As shown in Figure 3.2, only a few fragments were induced from CTD of 4+ insulin, and these included two low-intensity fragment ions (By_6 and By_{11}^{2+}) arising from the cleavage on the C-terminus of chain B. No evidence for separation of the two chains was observed in the CTD spectrum of 4+ insulin. One possible cause of the limited number of observed fragmentation products is the limited signal-to-noise (S/N) ratio of the precursor; the 4+ charge state is simply a low abundance charge state and it is difficult to obtain a large precursor ion signal (ESI spectrum of insulin is given in Figure 3.3).

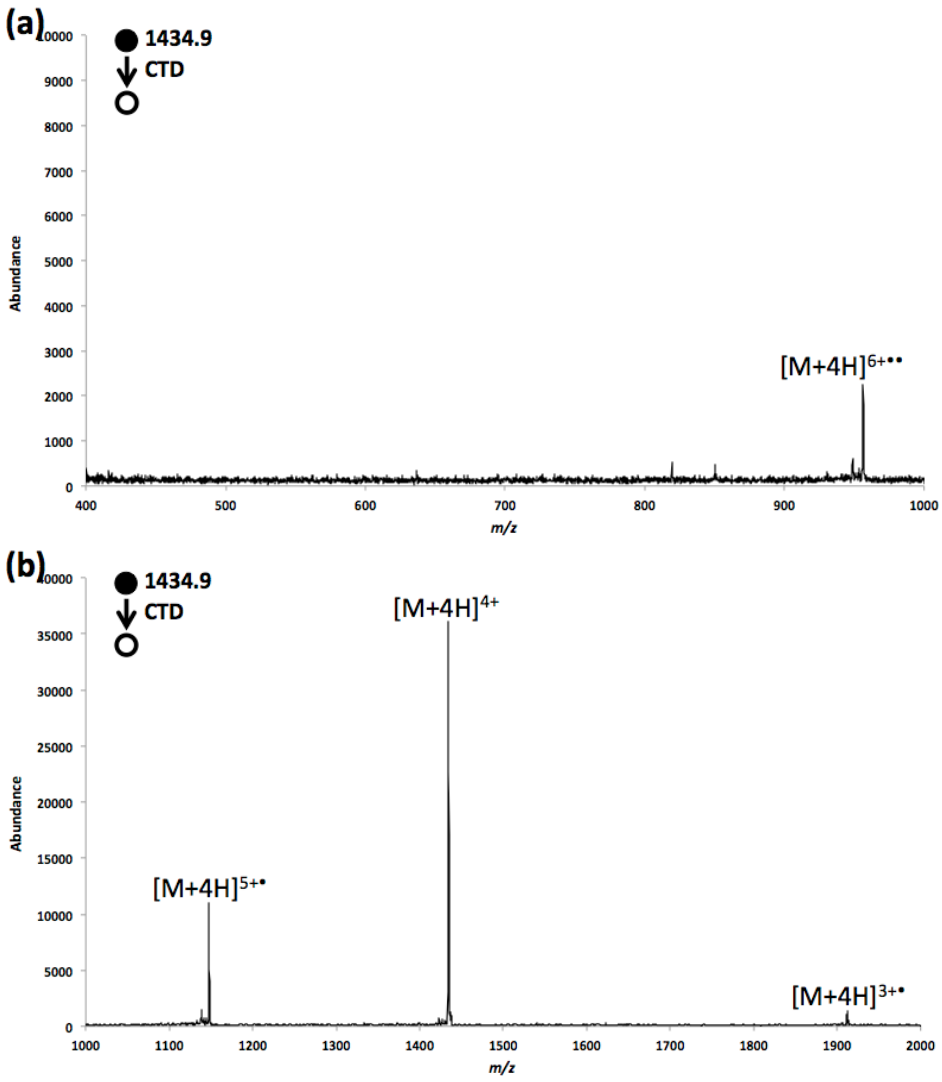

Figure 3.2. CTD spectrum of insulin 4+ ranging from (a) *m/z* 400-1000, and (b) *m/z* 1000-2000.

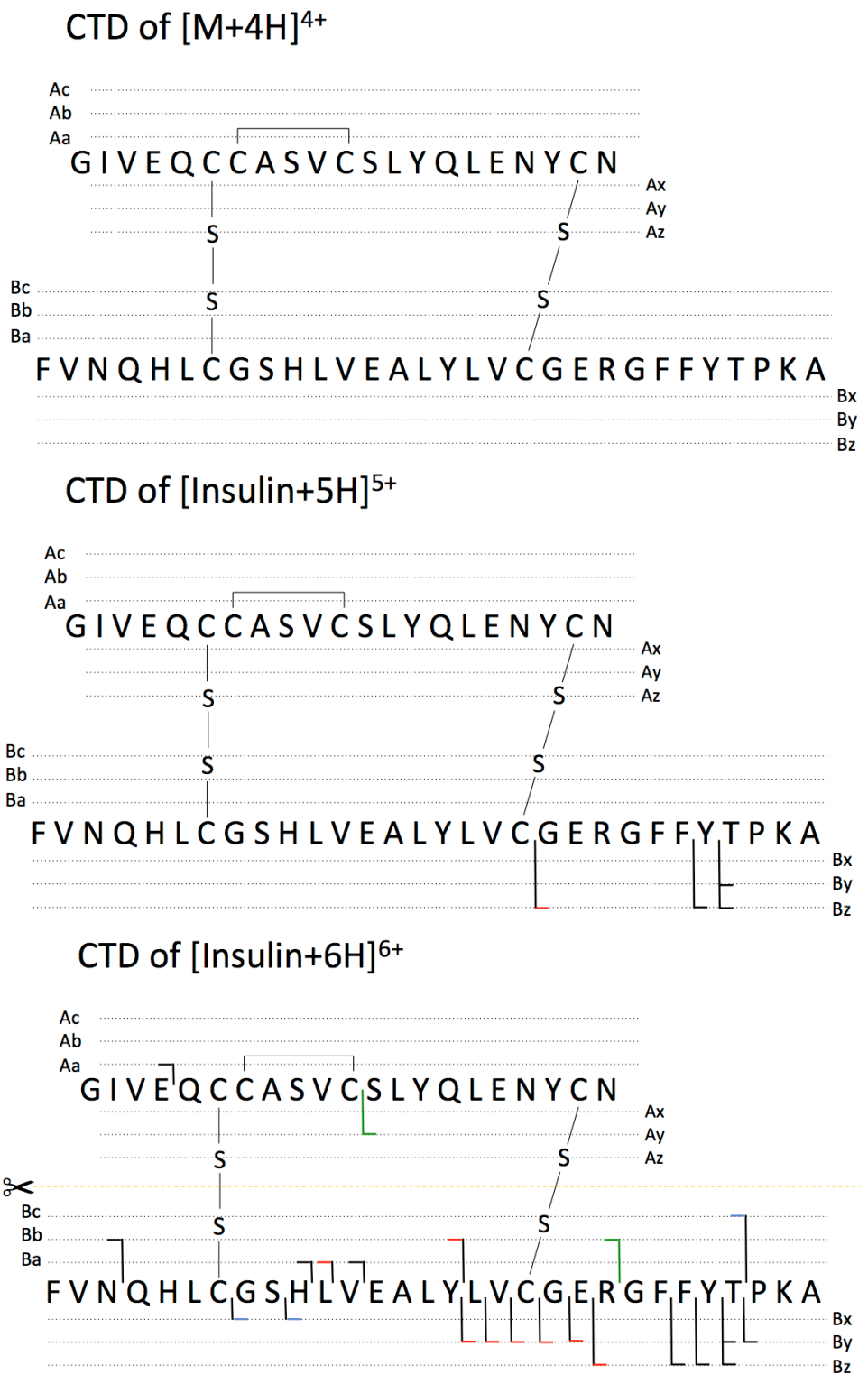

Scheme 3.1. Dissociation channels observed in CTD of insulin at charge states of 4+, 5+ and 6+. Key for peptide sequencing: black line, product ions observed in charge state 1+; red line, product ions observed in charge state 2+; blue line observed in charge state 3+; fragment ion with another chain attached are marked with a green line.

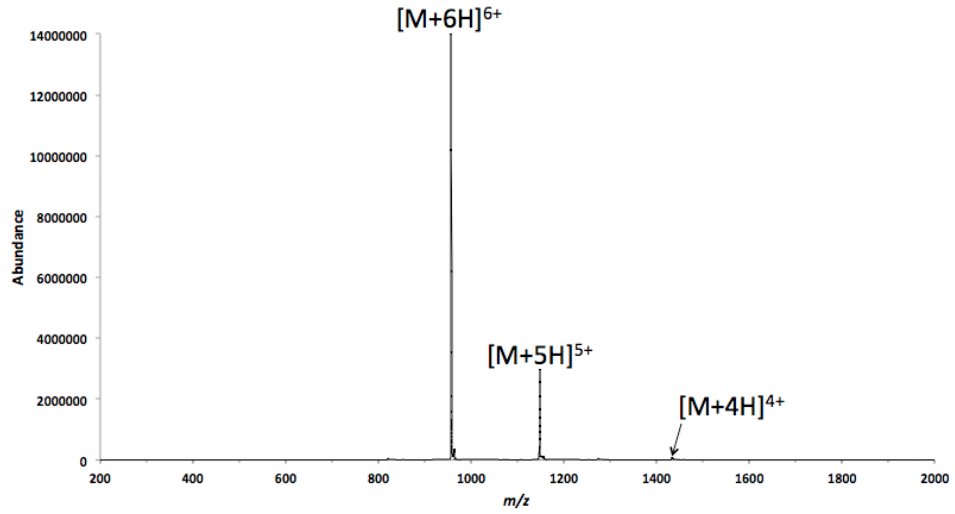

Figure 3.3. ESI spectrum of insulin.

Figure 3.4 shows an expanded CTD spectrum of 5+ insulin. Only four fragment ions were identified, all of which originated from the cleavage of the C-terminus of chain B, outside the cyclic structure defined by the disulfide linkages. No cleavages inside the cyclic structure were observed. Similar to the 4+ insulin spectrum, there is no evidence for the separation of the two chains.

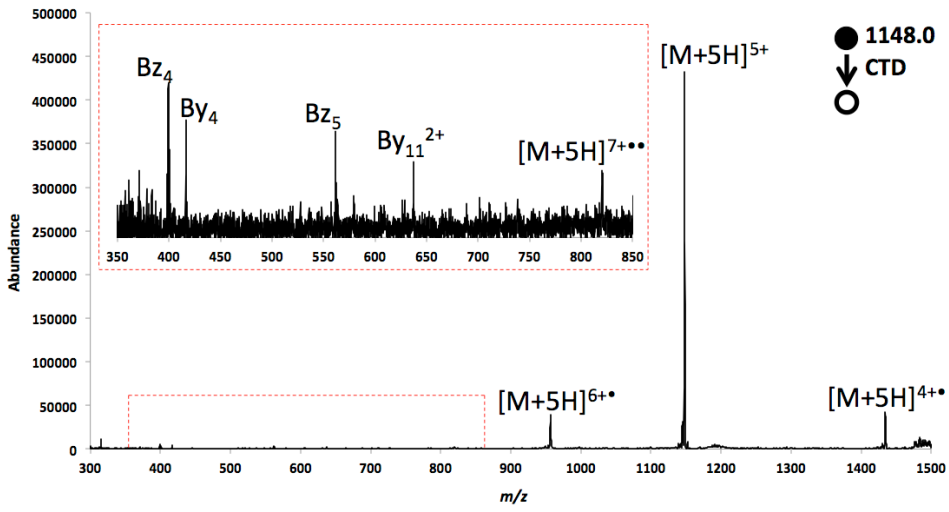

Figure 3.4. CTD spectrum of 5+ insulin.

Compared with the results from 4+ and 5+ insulin, CTD of 6+ insulin produced many more fragment ions, as shown in Figure 3.5. In contrast to CID [91], ETD [98] and ECD [94], CTD of 6+ insulin produced a set of contiguous *z* ions; i.e. Bz_4, Bz_5 and Bz_6 (in red font). Similar to the CTD results of 5+ insulin, these fragments arise from the cleavage of C-terminus of chain B and outside the cyclic region. One fragmentation product of chain A was observed (Aa_4), which originates from the cleavage of the N-terminus of chain A: again, outside the cyclic region.

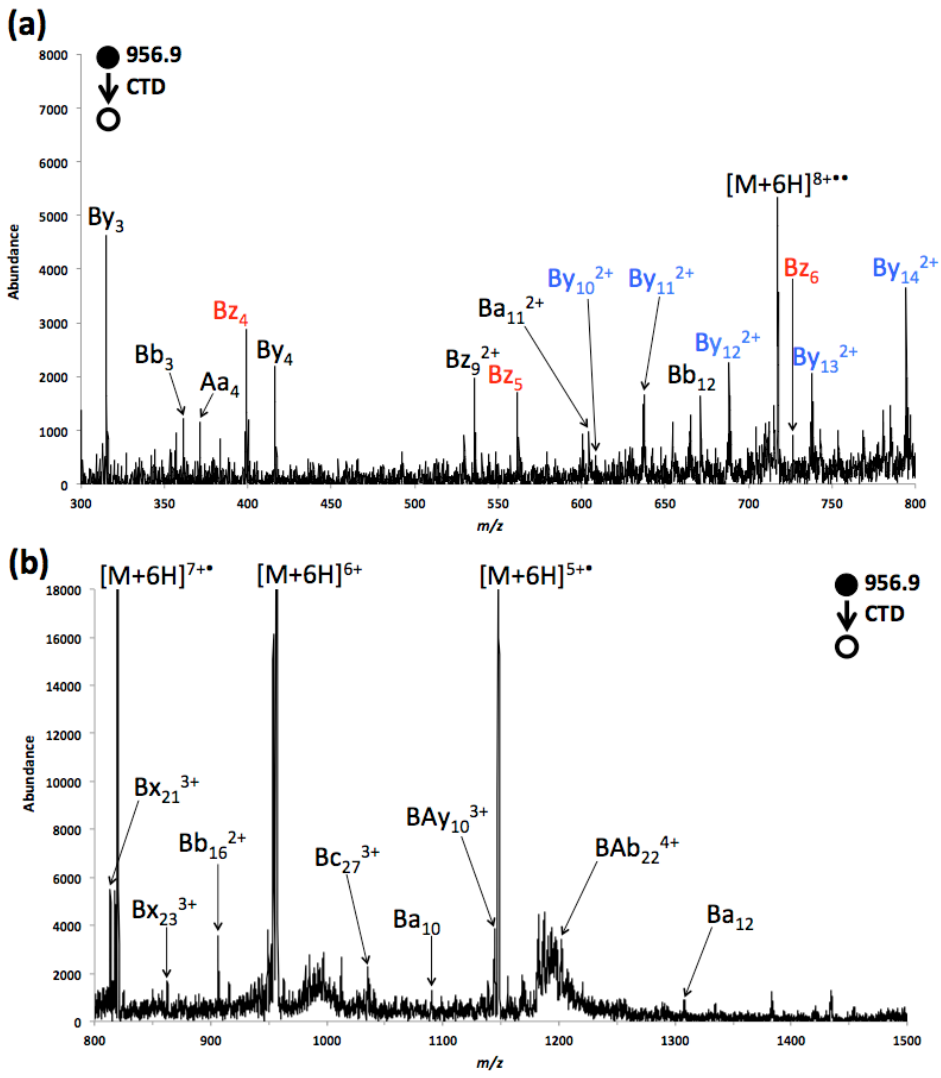

Figure 3.5. Zoomed in CTD spectra of 6+ insulin ranging from (a) *m/z* 300-800, and (b) *m/z* 800–1500.

A set of doubly charged contiguous *y* ions from chain B; i.e. By_{10}^{2+}, By_{11}^{2+}, By_{12}^{2+},By_{13}^{2+} and By_{14}^{2+} (blue font), was also observed from the 6+ precursor. Fragmentation in these region appears rather unique to CTD, since most techniques (CID [91, 92], ETD [98], ECD/AI ECD [108]) struggle to induce fragmentation in this region. The By_{10}^{2+} and By_{11}^{2+} fragments are be formed from the cleavage of C-terminus of chain B, outside the cyclic region, but the formation of By_{12}^{2+},By_{13}^{2+} and By_{14}^{2+} requires breakage of both inter-chain disulfide linkages in addition to the backbone cleavage. Similarly, the ions Ba_{10}, Ba_{11}^{2+} and Ba_{12} also require the cleavage of both disulfide linkages. Additionally, this set of internal-fragment ions are also distinguishes CTD from the other techniques, despite the otherwise remarkable similarity between CTD and ETD [98] for exocyclic cleavages. All the above observations indicate that CTD can directly cleave backbone and disulfide linkages in a single activation step, and is thereby capable of providing some primary sequence information within the cyclic structure.

The above CTD results have also show a dependence of CTD behavior on the charge state of the precursor ions. The dependence of CTD behavior upon low precursor charge states (1+, 2+ and 3+) of smaller peptides has been studied in our previous work [115]. In this study, as the precursor charge state increases from 4+ to 6+, an increase in the number of fragment ions was observed. This means more bonds and a greater variety of bonds were cleaved at higher precursor charge states, which is consistent with previous studies using ETD [98]. However, unlike ETD, CTD is not expected to become more efficient or more exothermic as the charge state of the precursor increases. In fact, one would expect the efficiency and efficacy of cation-cation reactions in CTD to decrease as the charge sate of the precursor ion increases. It therefore seems possible that the

improvement in product ions observed through CTD of the 6+ precursor could in fact be due to unwanted ETD side reactions. Another possibility is that the increase in charge state of the 6+ precursor enhances the extent of protein unfolding, thus making the protein more susceptible to fragmentation when interacting with helium cations.

The backbone cleavages preferentially occur near the C-terminus of chain B—which is consistent with the ECD and ETD work of others [92, 94, 98, 108]—and in regions close to aromatic residues, like tyrosine, which also has been noted by others [109]. Compared to ETD, CTD does not produce as many fragment ions near the N-terminus of chain B for 6+ insulin precursor. ETD excels in retrieving primary sequence information outside the cyclic structure, but only occasionally provides backbone information within the cyclic structure [98, 109]. In CID experiments of 5+ insulin [90, 92], all the cleavages occur in regions external to the disulfide bonds and no structurally informative fragments were obtained from within the cyclic region. To increase the sequence coverage and probe the fragmentation mechanism, we therefore used supplemental collisional activation to fragment the primary product ions that underwent oxidation with dissociation; i.e. the CTnoD product ions.

3.3.2 MS^3 CTD/CID Experiments upon Insulin

Figure 3.6 shows the MS^3 CID spectrum of the CTnoD product ion $[Insulin+6H]^{7+\bullet}$ derived from CTD of $[Insulin+6H]^{6+}$. The MS^3 CID spectrum is dominated by a wide range of *y* ions derived from the cleavage of chain B and the separation of chain A. In the low mass range (*m/z* 400-1000), one set of doubly charged contiguous *y* ions were observed, namely By_{11}^{2+}, By_{12}^{2+} and By_{13}^{2+} (in red font). In the high mass range (*m/z* 1000-1400), fragment ions originating from the cleavages of chain

B with the entire chain A attached (i.e. ABb_{22}^{4+}, ABb_{24}^{4+},ABc_{28}^{4+} and ABz_{24}^{4+} in blue font) were observed.

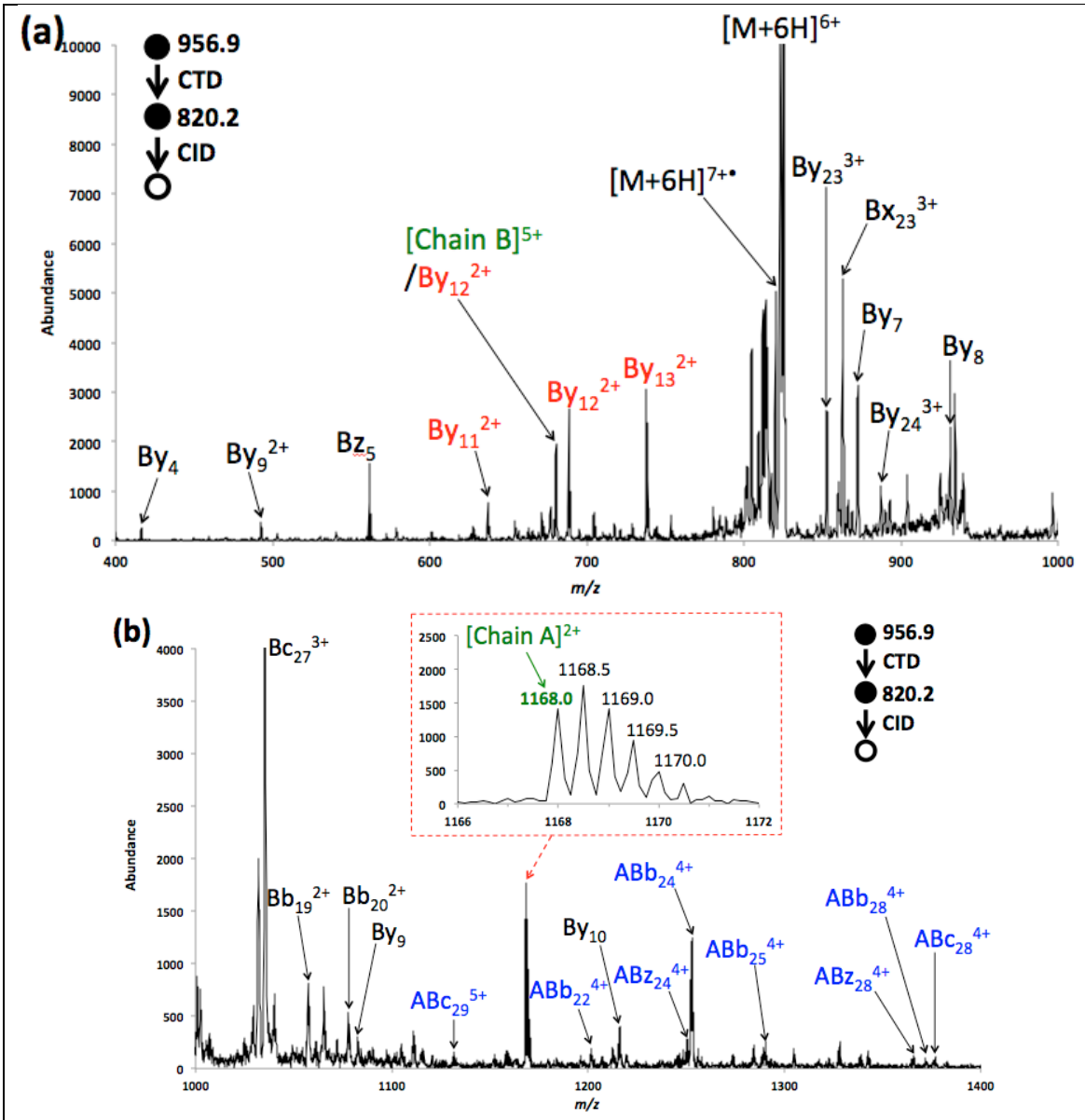

Figure 3.6. MS^3 CID spectrum of [Insulin+6H]$^{7+\bullet}$ ranging from (a) *m/z* 400-1000, and (b) *m/z* 1000-1400.

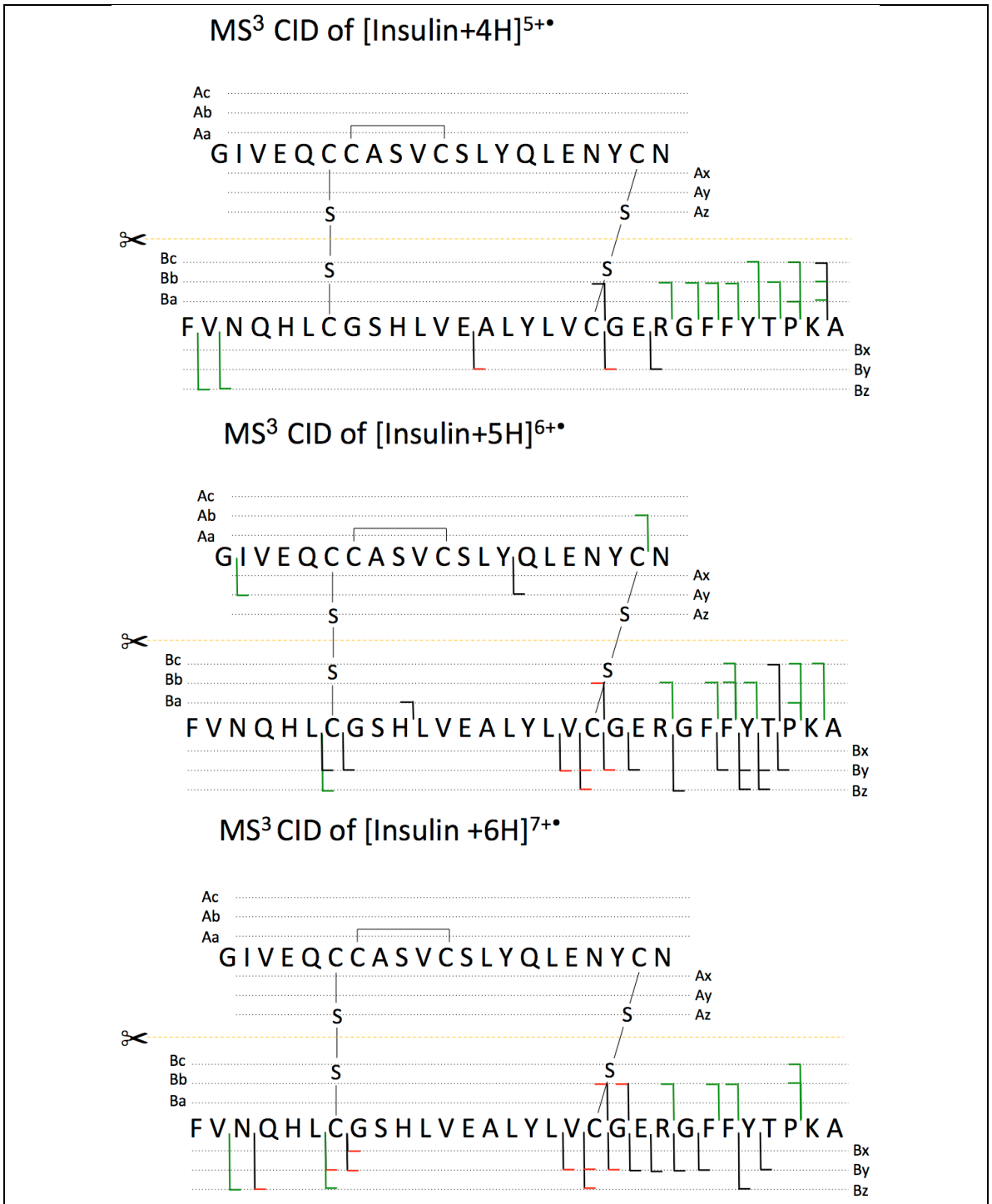

Scheme 3.2. Dissociation channels observed in (a) MS^3 CID of $[Insulin+4H]^{5+\bullet}$ derived from CTD $[Insulin+4H]^{4+}$, (b) MS^3 CID of $[Insulin+5H]^{6+\bullet}$ derived from CTD $[Insulin+5H]^{5+}$ and (c) MS^3 CID of $[Insulin+6H]^{7+\bullet}$derived from CTD $[Insulin+6H]^{6+}$. Key for peptide sequencing: black line, product ions observed in charge state 1+; red line, product ions observed in charge state 2+; fragment ion with another chain attached are marked with a green line.

Figure 3.6a shows a fragment ion at *m/z* 680.2, corresponding in mass to the 5+ Chain B product ion ([Chain B]$^{5+}$, green font). The complementary 2+ Chain A product ion shows up at *m/z* 1168.0 ([Chain A]$^{2+}$, inset in Figure 4b, green font). The [Chain A]$^{2+}$ fragment is rarely observed in regular CID experiments [92], but it is more often observed in radical activation methods [108]. As shown in the fragment map for MS^3 CTD/CID (the bottom panel in Scheme 2), the formation of [Chain A]$^{2+}$ requires the cleavage of both disulfide bonds. One mechanism for the cleavage of a disulfide bond is proposed in Scheme 3.3. It is also reasonable to assume that the disulfide bond(s) cleaves after the amino acid backbone cleavage through previously described hydrogen or radical transfers [94, 108]. Cleavage of two inter-chain disulfide bonds was also observed in MS^3 CTD/CID experiments of [Insulin+4H]$^{5+\bullet}$ and [Insulin+5H]$^{6+\bullet}$, shown below.

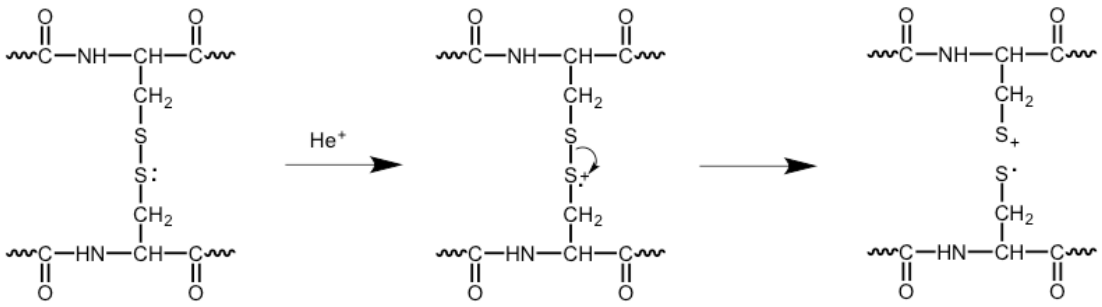

Scheme 3.3. Proposed mechanism for the cleavage of S-S bond.

The CID spectrum of the CTnoD product [Insulin+4H]$^{5+\bullet}$ derived from CTD of [Insulin+4H]$^{4+}$ is shown in Figure 3.7. In the low mass range (*m/z* 400-1000), only three low-abundance fragments were generated. In the high mass range (*m/z* 1000-1400), more fragment ions with higher abundances were produced. Most of the fragments were in the 4+ charge state, originating from the cleavage of the B-chain, outside the cyclic structure, with the A-chain still attached. A few 5+ fragment ions were observed (vide infra),

including $(AB b_{29}\text{-}NH_3)^{5+}$ and $(AB a_{29}\text{-}NH_3)^{5+}$, and a dominant ammonia loss from an intact insulin ion, $(Insulin\text{-}NH_3)^{5+}$, which is rarely observed in common MS/MS experiments. Two contiguous ion sets ($AB b_{22}^{4+}$, $AB b_{23}^{4+}$, $AB b_{24}^{4+}$ and $AB b_{25}^{4+}$ (in red font)) and ($AB b_{23}^{3+}$, $AB b_{24}^{3+}$ and $AB b_{25}^{3+}$ (in blue font)) were also observed.

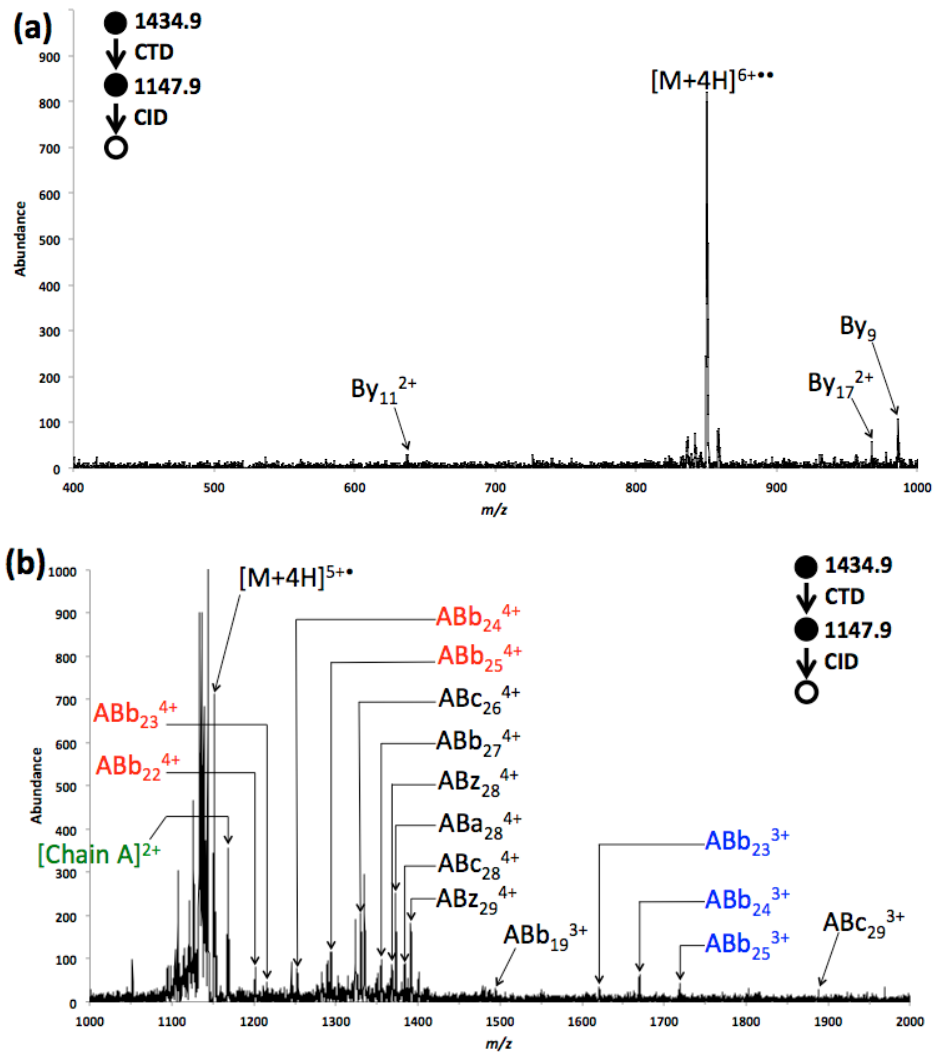

Figure 3.7. MS^3 CID spectrum of $[Insulin+4H]^{5+\bullet}$ ranging from (a) *m/z* 400-1000 and (b) *m/z* 1000-2000.

To examine the congested area in Figure 3.7, a narrow region of the spectrum (*m/z* 1110-1180) is expanded in Figure 3.8. Analogous to MS^3 CTD/CID experiment of $[Insulin+6H]^{7+\bullet}$, a complementary chain adduct ion pair—$[Chain\ A]^{2+}$ and $[Chain\ B]^{3+}$—was also observed for $[Insulin+4H]^{5+\bullet}$. It is noteworthy that intact Chain A is always formed in the 2+ charge state, regardless of the precursor charge sate undergoing CTD. Moreover, the sum of the charge states of the two individual chain adduct ions equals that of the precursor insulin adduct ion. The distribution of product ion charge states agrees closely with the results from CID reaction of gold-cationized insulin [91]. In the gold-adducted insulin studies, McLuckey and coworkers also observed complementary chain adduct pairs ($(B\text{-chain})^{4+}/(A\text{-chain})^{1+}$ and $(B\text{-chain})^{3+}/(A\text{-chain})^{2+}$) in their MS^3 ETD/CID experiment of $[insulin+5H]^{5+}/[insulin+6H]^{5+\bullet}$ [98]. They reasoned that the radical nature of $[M+6H]^{5+\bullet}$ could account for the insulin chain separation in this MS^3 experiments [98]. The analogous charge-state split of precursor ions—asymmetric pattern—has also been widely reported in low-energy CID experiments of other protein complex ions [13, 116].

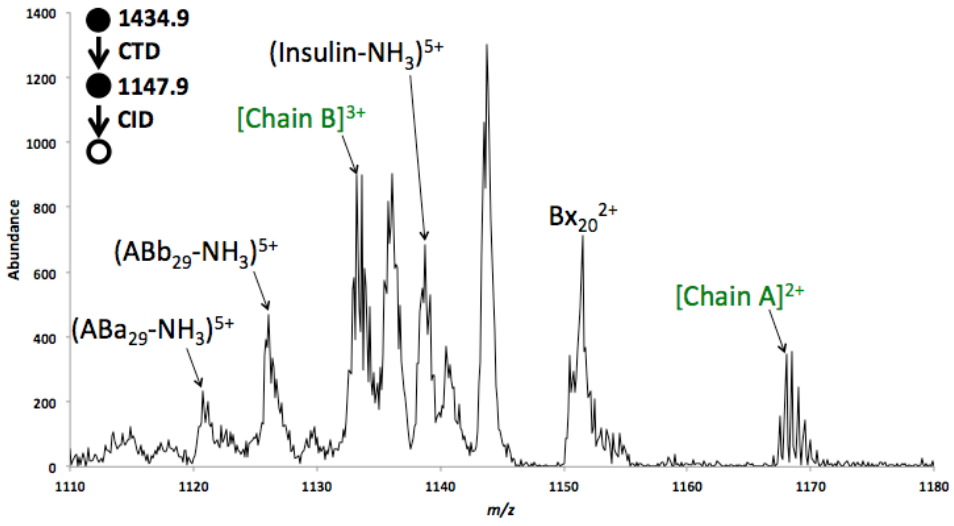

Figure 3.8. MS^3 CID of $[insulin+4H]^{5+\bullet}$ derived from CTD of $[insulin+4H]^{4+}$.

To determine whether the individual chain adduct ions ($[Chain\ A]^{2+}$ and $[Chain\ B]^{3+}$) are radical species or even-electron species, each of them was isolated at MS^4-level and stored in the ion trap for 200 ms to react with background oxygen (Figure 3.9 and 3.10). It has been reported that when the radical species are stored in the electrodynamic ion trap at room temperature, they often react with residual oxygen. The addition of O or O_2 to distonic radical cations has been observed in ETD [67], fs-LID [68], He-MAD [117], and He-CTD [115]. However, oxygen-attachment was not observed for either $[Chain\ A]^{2+}$ or $[Chain\ B]^{3+}$, indicating that the two types of individual chain adduct ions are more likely to be even-electron species, or that the radical resides on the sulfur atoms and does not undergo the typical oxygen addition.

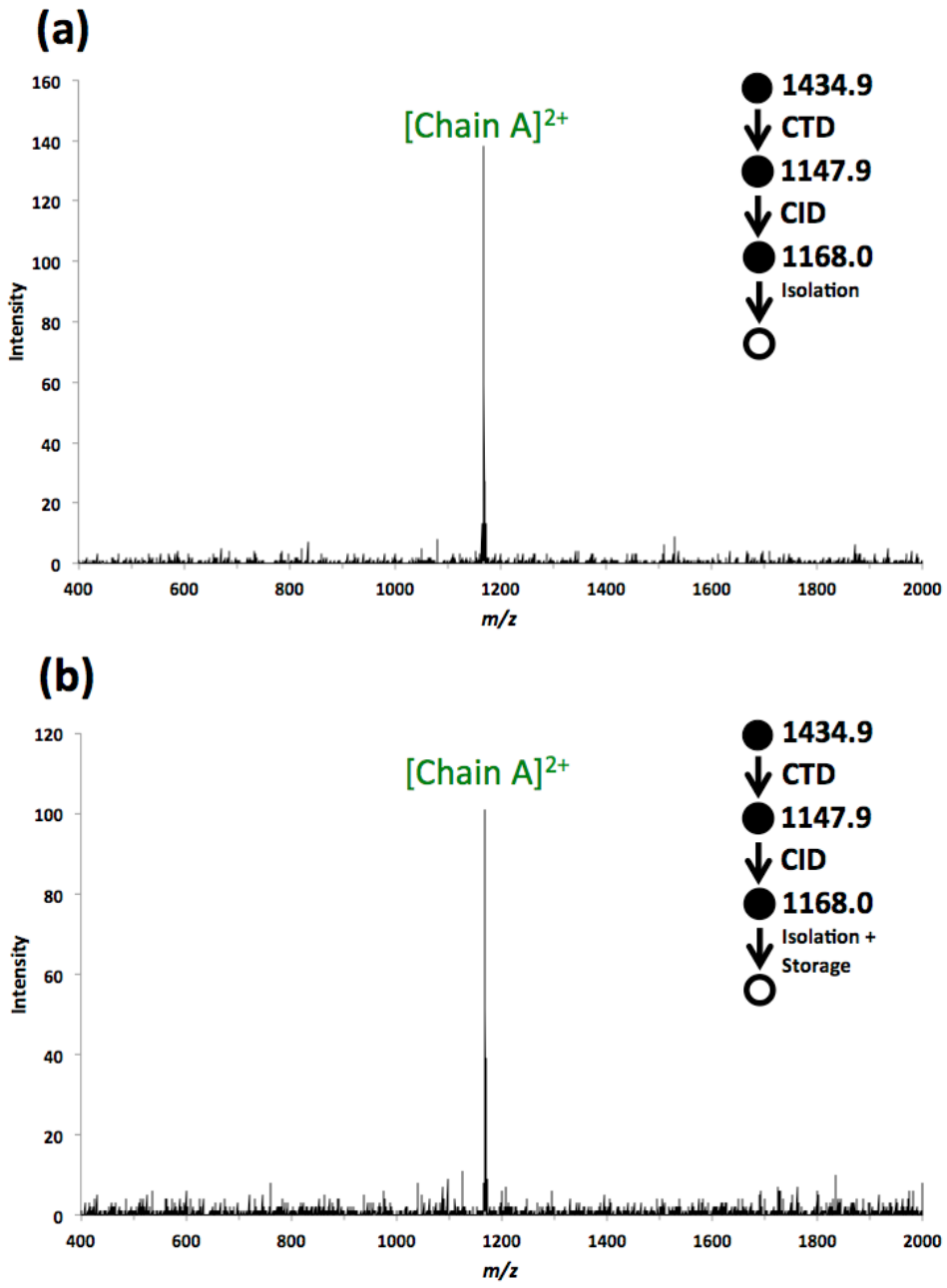

Figure 3.9. (a) Isolation spectrum of $[Chain A]^{2+}$ at MS^4 level, following MS^3 CID of $[M+4H]^{5+\bullet}$ derived from MS^2 CTD of $[M+4H]^{4+}$. (b) The same condition as (a) except an extra ion storage time of 200 ms.

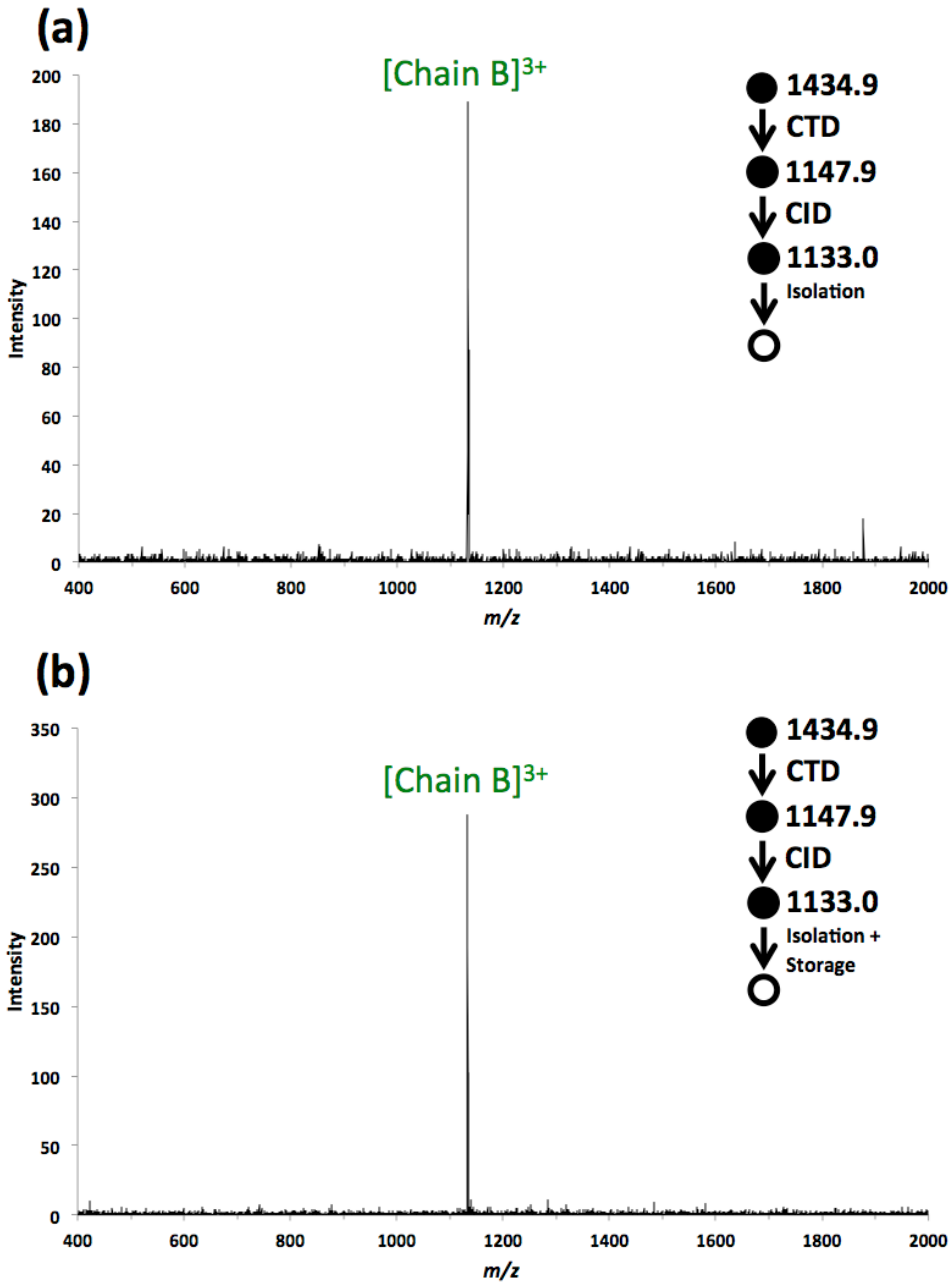

Figure 3.10. (a) Isolation spectrum of $[Chain\ B]^{2+}$ at MS^4 level, following MS^3 CID of $[M+4H]^{5+\bullet}$ derived from MS^2 CTD of $[M+4H]^{4+}$. (b) The same condition as (a) except an extra ion storage time of 200 ms.

The fragmentation behavior of the individual chain adduct ions have been well documented in literature. For example, Zubarev and coworkers observed doubly charged peptide monomers due to the cleavage of an S-S bond in UVPD experiments [104]. In

similar work, Wongkongkathepa et al [108] showed that ESI-generated 6+ insulin could be mass-selected and irradiated by 266 nm UV laser to provide the individual Chain A/B fragments. McLafferty and coworkers have reported singly charged peptide monomers corresponding to the breakage of an S-S bond in ECD experiments [94].

Different from ETD/ECD, which are dominated by charge-reduction and hydrogen rich radical cations, CTD is dominated by charge increased and hydrogen deficient radical cations, with a smaller contribution of charge-decreased products [115]. Given the previous discussions on the charge-increased product $[Insulin+4H]^{5+\bullet}$, MS^3 CID spectrum of the charge-decreased product $[Insulin+6H]^{5+\bullet}$ derived from CTD of $[Insulin+6H]^{6+}$ was collected as well (Figure 3.11). Analogous to MS^3 CID experiment for charge-increased species ($[Insulin+4H]^{5+\bullet}$), complementary chain adduct ion pair—$[Chain\ A]^{2+}$ and $[Chain\ B]^{3+}$—was also observed from CID of the charge-reduced species ($[Insulin+6H]^{5+\bullet}$). This observation is consistent with the aforementioned McLuckey and coworkers' publication [98], which involved ETD as the source for generating of $[Insulin+6H]^{5+\bullet}$. The consistency indicates a robust similarity between the radical intermediates that seems independent of a hydrogen transfer mechanism.

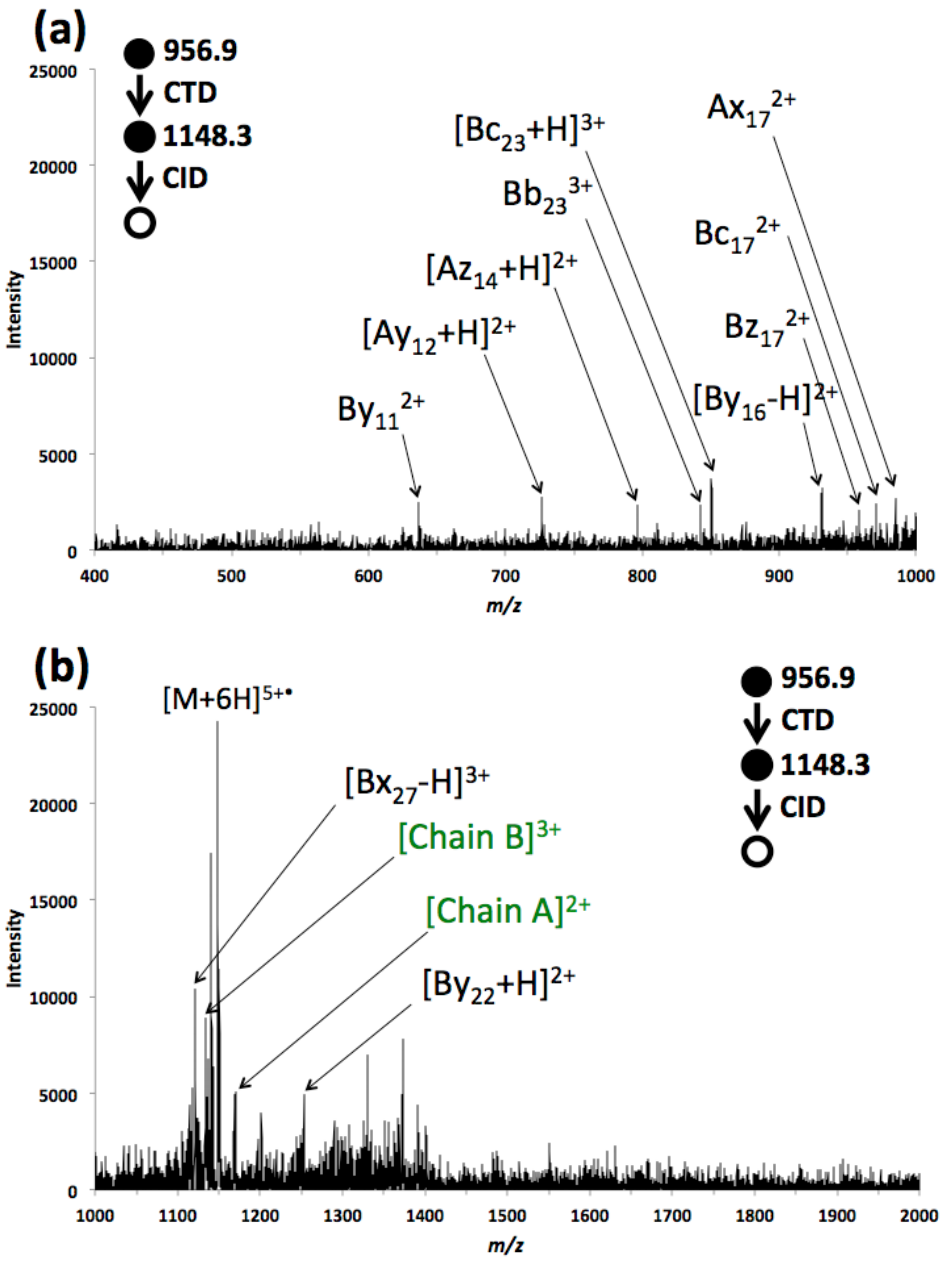

Figure 3.11. MS^3 CID spectrum of $[insulin+6H]^{5+\bullet}$ from (a) *m/z* 400 - 1000. (b) *m/z* 1000 – 2000 (CID amplitude = 0.3 V).

The CTD-generated $[Insulin+5H]^{6+\bullet}$ was also isolated and subjected to collisional activation. The resulting MS^3 CID spectrum (Figure 3.12) provided greater fragmentation efficiency and better signal-to-noise (S/N) ratio than $[Insulin+4H]^{5+\bullet}$. CID of $[Insulin+5H]^{6+\bullet}$ produced more *y* ions outside the cyclic structure on the C-terminus of

chain B. Consistent with the above CID results of the CTnoD products, CID of [Insulin+5H]$^{6+\bullet}$ also produced individual chain adduct ion pair: [Chain A]$^{2+}$ and [Chain B]$^{4+\bullet}$.

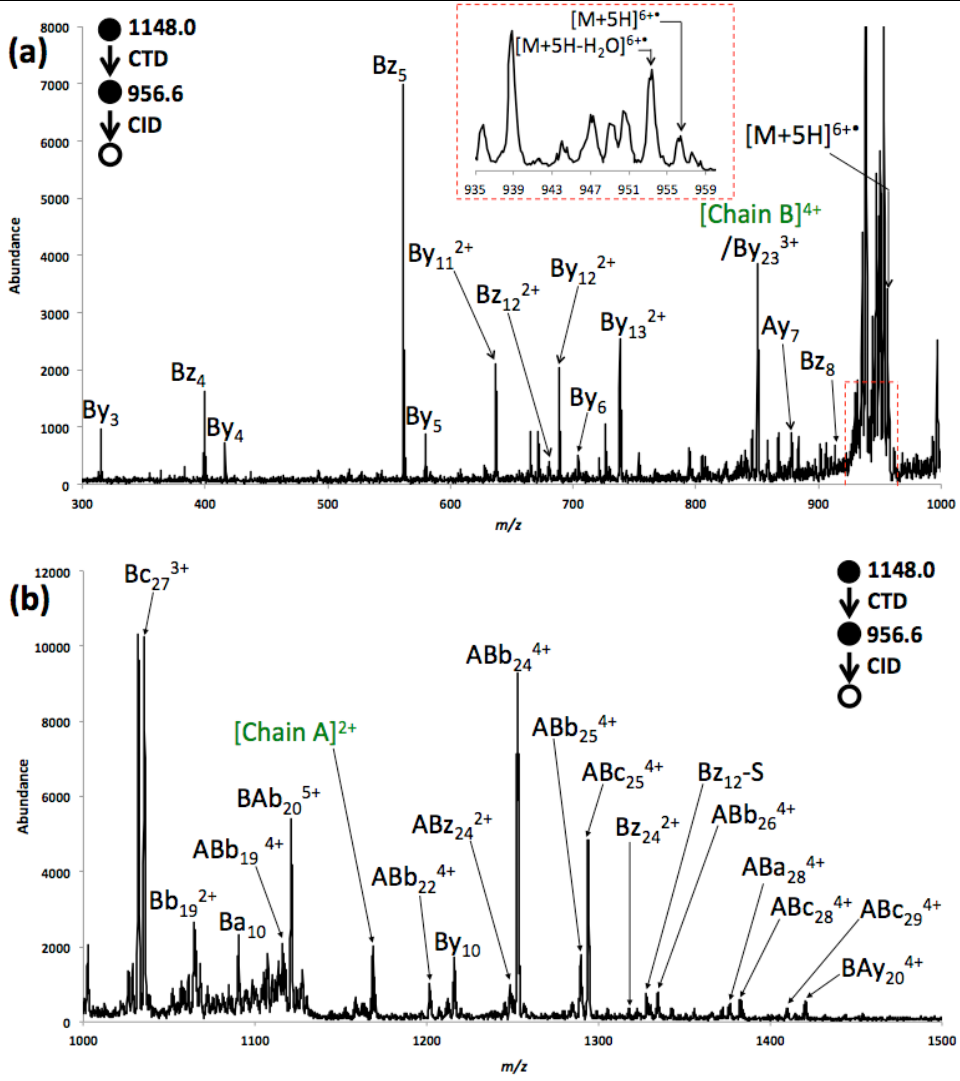

Figure 3.12. MS^3 CID (amplitude = 0.25) spectrum of [Insulin+5H]$^{6+\bullet}$ ranging from (a) *m/z* 300-1000 and (b) *m/z* 1000-1500.

3.3.3 Resonance Ejection Experiments upon Insulin

Figure 3.13 shows an expanded region of the same spectrum in Figure 3.1b for CTD of the precursor $[M+5H]^{5+}$. Figure 3.13a shows straightforward CTD and 6b shows the same experiment, but with concurrent resonant ejection on the primary product, and possible intermediate, $[M+5H]^{6+\bullet}$. This resonance ejection experiment was conducted to investigate the mechanism of formation of the doubly ionized species $[M+5H]^{7+\bullet\bullet}$, which can form via two possible pathways: (1) directly from the precursor ion (Pathway A) via a one step, two electron oxidation mechanism; or (2) through two consecutive reactions (Pathway B) involving the generation of an intermediate ($[M+5H]^{6+\bullet}$), from which the product ion $[M+5H]^{7+\bullet\bullet}$ is formed from a second helium cation.

A. $[M+5H]^{5+} + He^{+} \rightarrow \ [M+5H]^{7+\cdot\cdot} + e^{-} + He$ (4)

B. $[M+5H]^{5+} + He^{+} \rightarrow He + \langle [M+5H]^{6+\cdot} \rangle$

$$\langle [M+5H]^{6+\cdot} \rangle + He^{+} \rightarrow [M+5H]^{7+\cdot\cdot} + 2e^{-} \quad (5)$$

Figure 3.13a shows a regular CTD spectrum of the $[M+5H]^{5+}$, in which both $[M+5H]^{6+\bullet}$ and $[M+5H]^{7+\bullet\bullet}$ were present. In Figure 3.13b, the first-generation product ion, and possible intermediate, $[M+5H]^{6+\bullet}$ was resonantly ejected during CTD. Figure 3.13b clearly shows that even in the presence of simultaneous ejection of $[M+5H]^{6+\bullet}$, the product ion $[M+5H]^{7+\bullet\bullet}$ is still readily observable. Quantitation of the peak heights using three sets of alternating spectra of CTD with and without resonance ejection (supplemental Figure 3.15) showed no significant decrease in the product ion abundance. These results clearly demonstrate that the formation of $[M+5H]^{7+\bullet\bullet}$ is not affected by the immediate removal of $[M+5H]^{6+\bullet}$ and that $[M+5H]^{7+\bullet\bullet}$ is therefore a direct product of the two-electron oxidation pathway provided pathway A (eqn. 4).

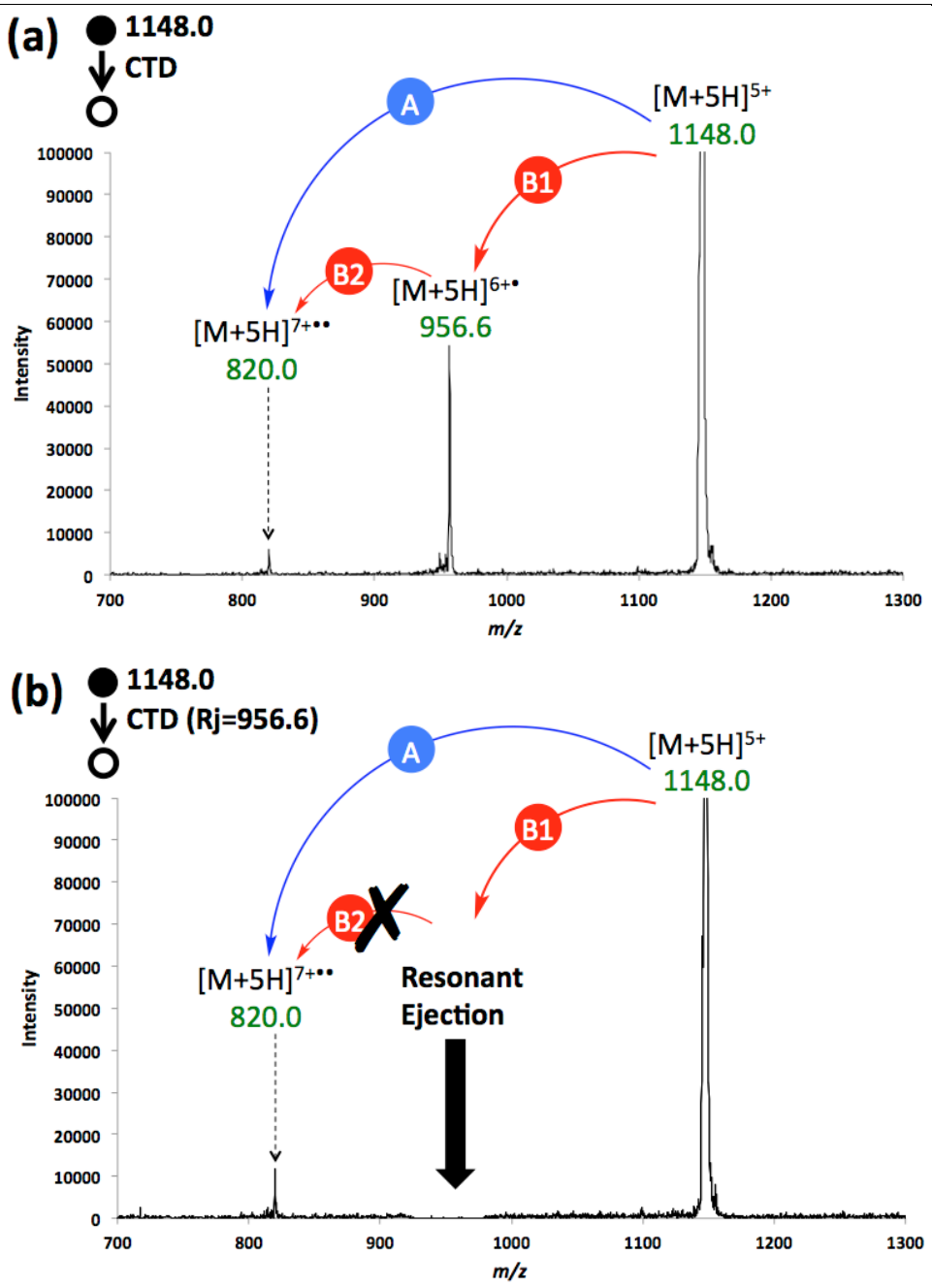

Figure 3.13. (a) CTD spectrum of 5+ insulin, (b) CTD spectrum of 5+ insulin, with resonance ejection on the possible intermediate $[M+5H]^{6+\bullet}$.

To confirm the result, a similar experiment was repeated using the $[M+6H]^{6+}$ precursor and resonantly ejecting the $[M+6H]^{7+\bullet}$ product ion (Figure 3.14). The relevant reactions in this case are:

A. $[M+6H]^{6+} + He^{+} \rightarrow [M+6H]^{8+\cdot\cdot} + e^{-} + He$ (6)

B. $[M+6H]^{6+} + He^{+} \rightarrow He + \langle [M+6H]^{7+\cdot} \rangle$

$\langle [M+6H]^{7+\cdot} \rangle + He^{+} \rightarrow [M+6H]^{8+\cdot\cdot} + 2e^{-}$ (7)

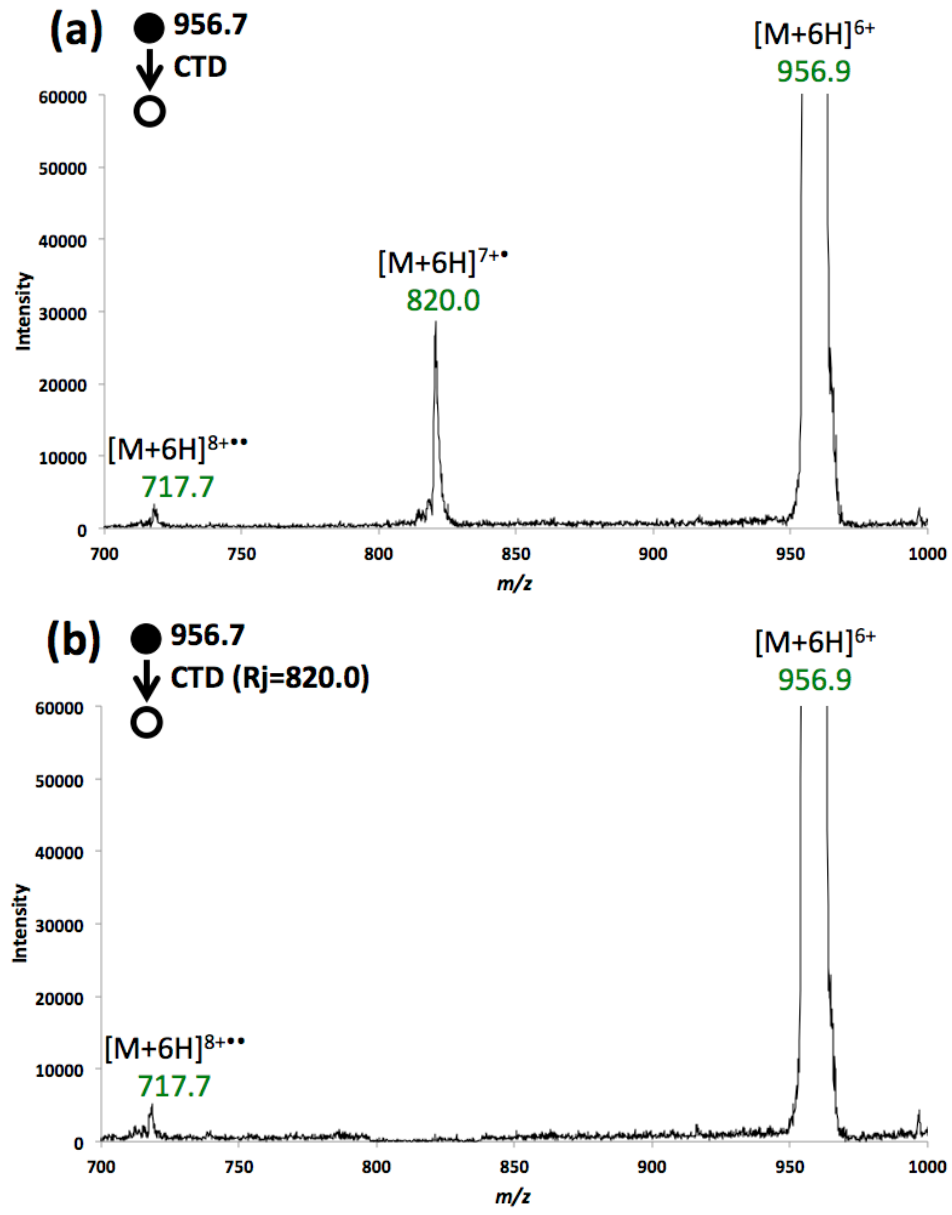

Figure 3.14. The statistic calculation is given in supporting information (a) CTD spectrum of insulin 6+, (b) the same experiment with $[M+6H]^{7+\bullet}$ is being resonantly ejected.

Consistent with the previous result, when $[M+6H]^{7+\bullet}$ was resonantly ejected during CTD of $[M+6H]^{6+}$, the intensity of two-electron oxidation product $[M+6H]^{8+\bullet\bullet}$ was also unaffected by the removal of the potential intermediate (Figure 3.14). These resonance ejection experiments verify that the doubly ionized ion is formed directly from the protonated precursor ion via a one-step two-electron process. The changes in the peak intensities in Figure 6 and Figure 3.14 are statistically verified in Table 3.1, Table 3.2 and Figure 3.15.

Table 3.1. Intensities and relevant calculations of fragment ions at *m/z* 820.0, *m/z* 956.6 and *m/z* 1148.0, during CTD of $[insulin+5H]^{5+}$.

m/z	820.0 $[M+5H]^{7+\bullet\bullet}$	956.6 $[M+5H]^{6+\bullet}$	1148.0 $[M+5H]^{5+}$
Intensity of #1	36877	165540	633618
Intensity of #2	21596	90570	546083
Intensity of #3	23369	130784	576564
Average	27280.67	128964.67	585422
Standard deviation	8357.82	37518.10	44434.65

Table 3.2. Intensities and relevant calculations of fragment ions at 820.0, *m/z* 956.6 and *m/z* 1148.0, during CTD of $[insulin+5H]^{5+}$, while **resonantly ejecting *m/z* 856.6 $[Insulin+5H]^{6+\bullet}$**.

m/z	820.0 $[M+5H]^{7+\bullet\bullet}$	**956.6 $[M+5H]^{6+\bullet}$(Ej)**	1148.0 $[M+5H]^{5+}$
Intensity of #1	16627	**49**	483226
Intensity of #2	19495	**69**	611897
Intensity of #3	14300	**40**	746016
Average	16807.33	**52.67**	613713
Standard deviation	2602.19	**14.84**	131404.4
T-Test	0.107>0.05		0.396>0.05

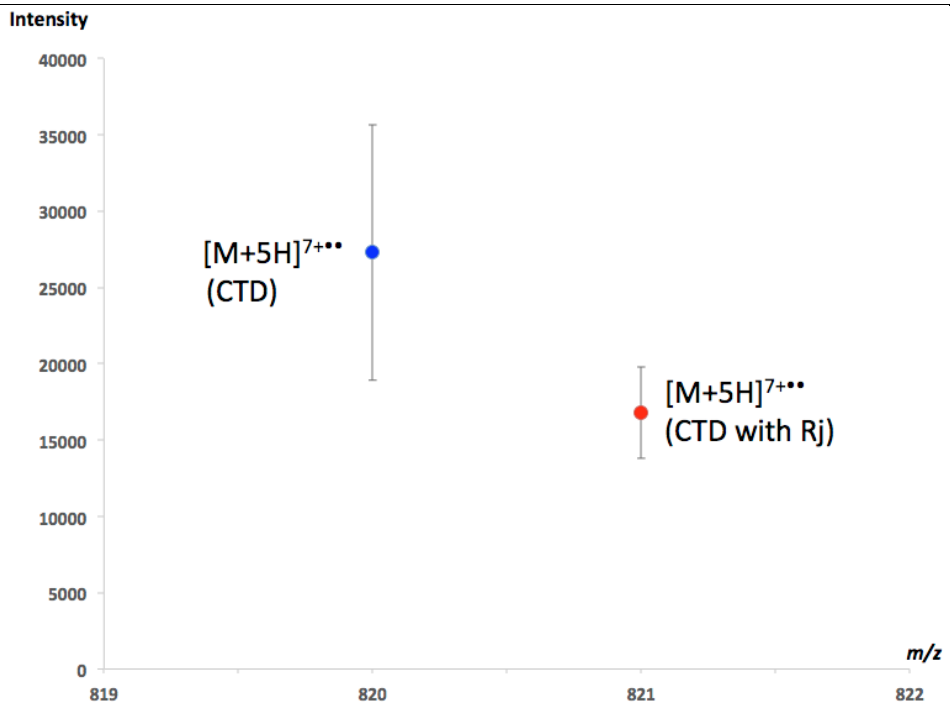

Figure 3.15. The averaged intensity of [insulin+5H]$^{7+\bullet\bullet}$ with error bar. The blue dot: regular CTD experiment; red dot: CTD experiment with resonant ejection of possible intermediate [insulin+5H]$^{6+\bullet}$.

The ability to perform a one-step removal of two electrons (double ionization) has been reported once before by Zubarev and coworkers in their electron ionization dissociation (EID) experiments [19] in an FT-ICR. Zubarev et al were able to produce doubly ionized species, $[M+nH]^{(n+2)+}$, by bombarding peptide cations ($[M+nH]^{n+}$, n≥1) with ≥ 40 eV electrons. However, these species from 1+ and 2+ precursors were hard to discern in the FT-ICR than ≥ 3+ precursors because of their overlap with the third and second parasitic harmonics of the precursors. To our knowledge, such high-energy activation (≥ 40 eV) barriers have only been reported in the high-energy EID experiments on a FT-ICR platform, which makes it all the more unusual to replicate the capability on a low-cost QIT mass spectrometer.

To further probe the behavior of the doubly ionized species, two follow-up experiments were conducted. Firstly, $[insulin+5H]^{7+\bullet\bullet}$ (or $[insulin+6H]^{8+\bullet\bullet}$) generated from CTD of $[insulin+5H]^{5+}$ (or $[insulin+6H]^{6+}$) was isolated at the MS^3 level and confined in the ion trap for an extra 200 ms to see if it would react with residual oxygen in a manner that distonic radical cations are prone. The isolation spectra are shown in Figure 3.16a and 3.17a, respectively, and show the successful mass-selection at MS^3 level. However, with the addition of a 200 ms reaction period between $[insulin+5H]^{7+\bullet\bullet}$ or $[insulin+6H]^{8+\bullet\bullet}$ with residual oxygen, neither charge state resulted in any oxygen attachment. As discussed in the previous sections, oxygen attachment is commonly observed for certain radical cations. But the absence of oxygen attachment could not exclude the possibility of $[insulin+5H]^{7+\bullet\bullet}$ and $[insulin+6H]^{8+\bullet\bullet}$ being radical cations. We reasoned that there is a slight possibility that these doubly ionized species are radical cations, but their structure/configuration somehow prevent them from reacting with residual oxygen in the electrodynamic ion trap.

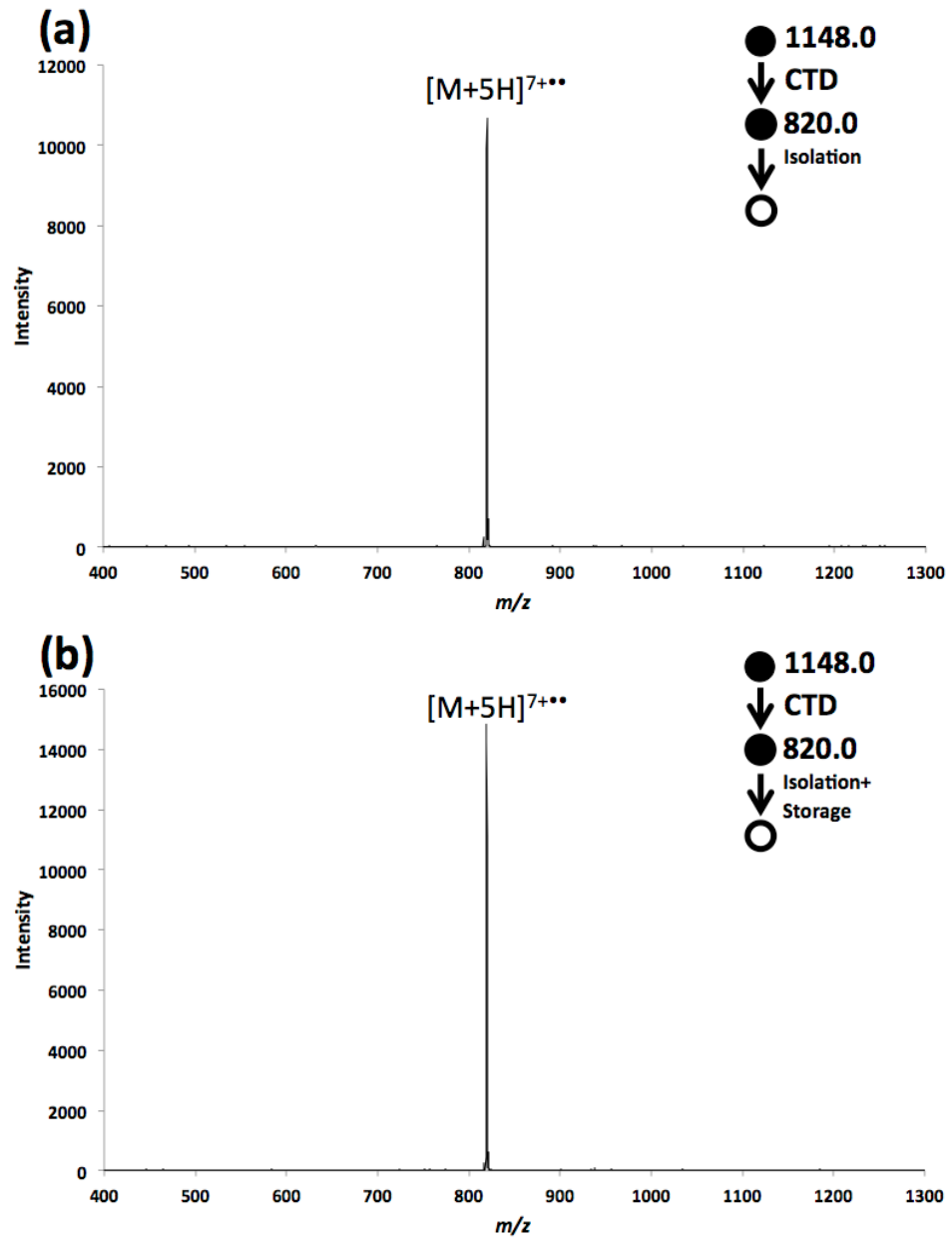

Figure 3.16. (a) Isolation spectrum of $[insulin+5H]^{7+\bullet\bullet}$ at MS^3 level. (b) 200 ms ion storage of $[insulin+5H]^{7+\bullet\bullet}$ following isolation at MS^3 level.

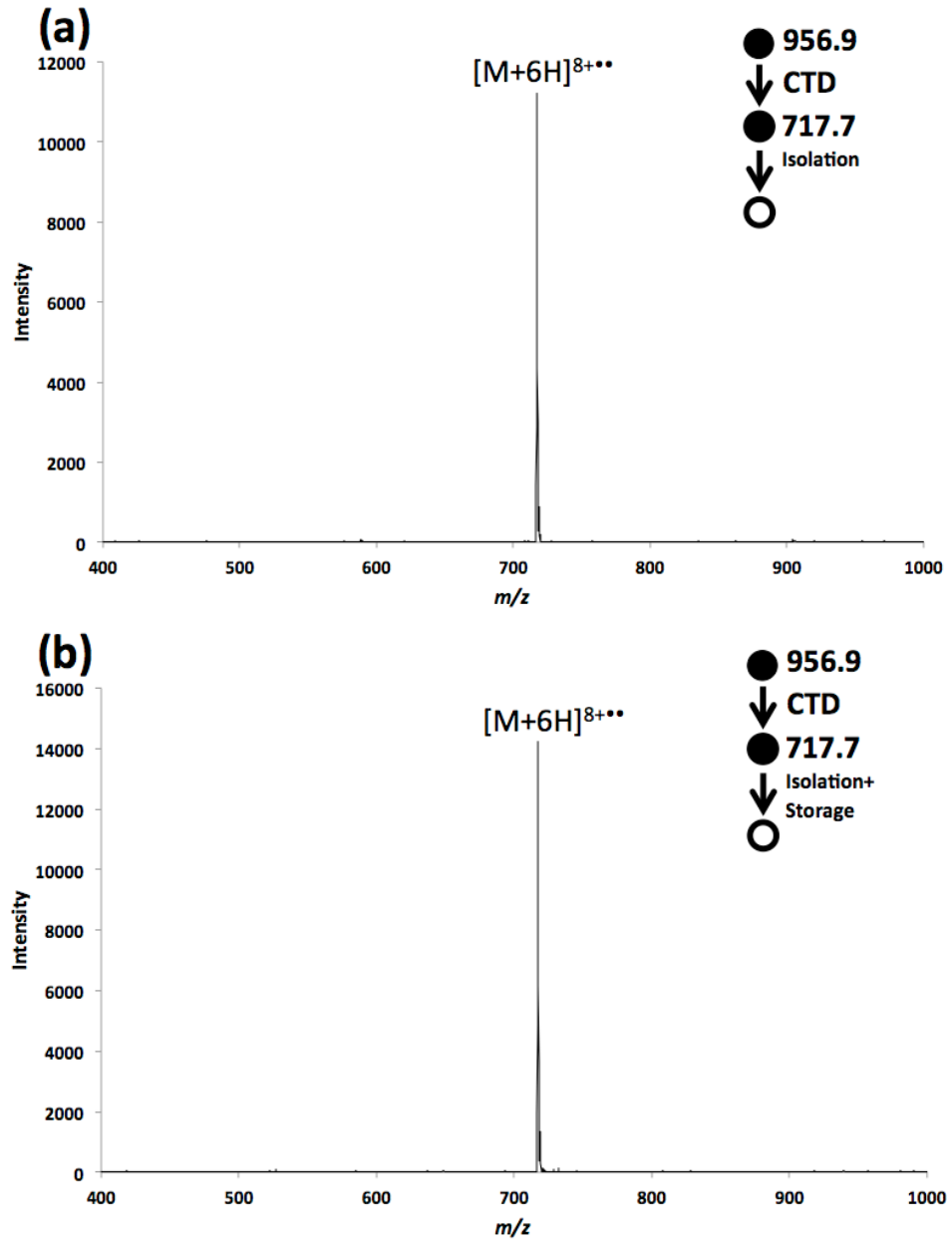

Figure 3.17. (a) Isolation spectrum of $[insulin+6H]^{8+\bullet\bullet}$ at MS^3 level. (b) 200 ms ion storage of $[insulin+6H]^{8+\bullet\bullet}$ following isolation at MS^3 level.

Secondly, $[insulin+5H]^{7+\bullet\bullet}$ was mass-selected in the same way as shown in Figure 3.16a. Instead of ion storage, $[insulin+5H]^{7+\bullet\bullet}$ was fragmented with a CID amplitude of 0.3 V at MS^3 level (Figure 3.18). Seven fragment ions were observed, most of which originate from the cleavage of B-chain. Only one fragment ion originates from the

cleavage of A-chain. For comparison purpose, CID spectrum of ESI-generated [insulin+7H]$^{7+}$ was collected as well (Figure 3.19). Thirteen B-chain fragment ions were observed, among which a contiguous ion set (By_3, By_4, By_5) was generated. Similar to MS^3 CTD/CID spectrum, only one A-chain fragment ion was observed. The fragment map comparison of the above experiments is shown in Scheme 3.4. Although MS^3 CID of the doubly ionized species ([insulin+5H]$^{7+\bullet\bullet}$) produced fewer fragment ions and higher noise level, it interesting to attempt an interrogation of this rarely reported species.

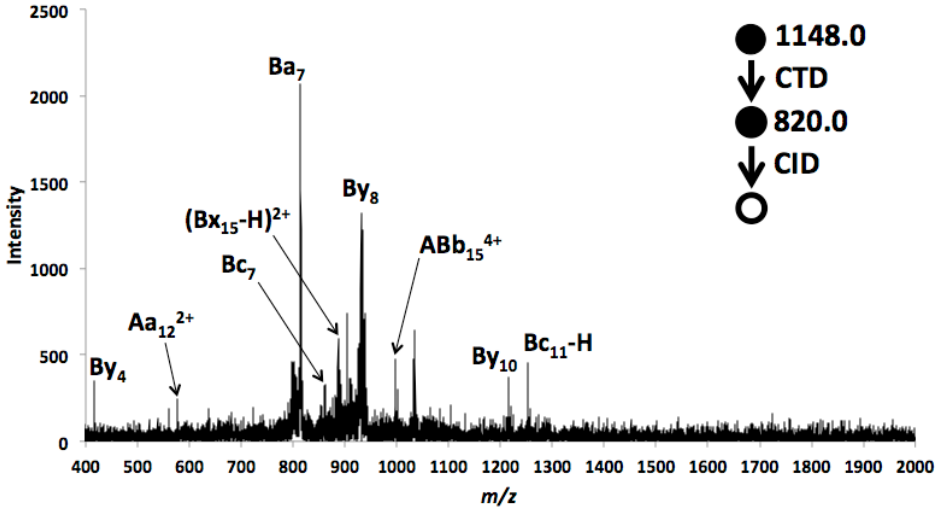

Figure 3.18. MS^3 CID spectrum of [insulin+5H] $^{7+\bullet\bullet}$ derived from CTD of [insulin+5H]$^{5+}$ (CID amplitude = 0.30 V).

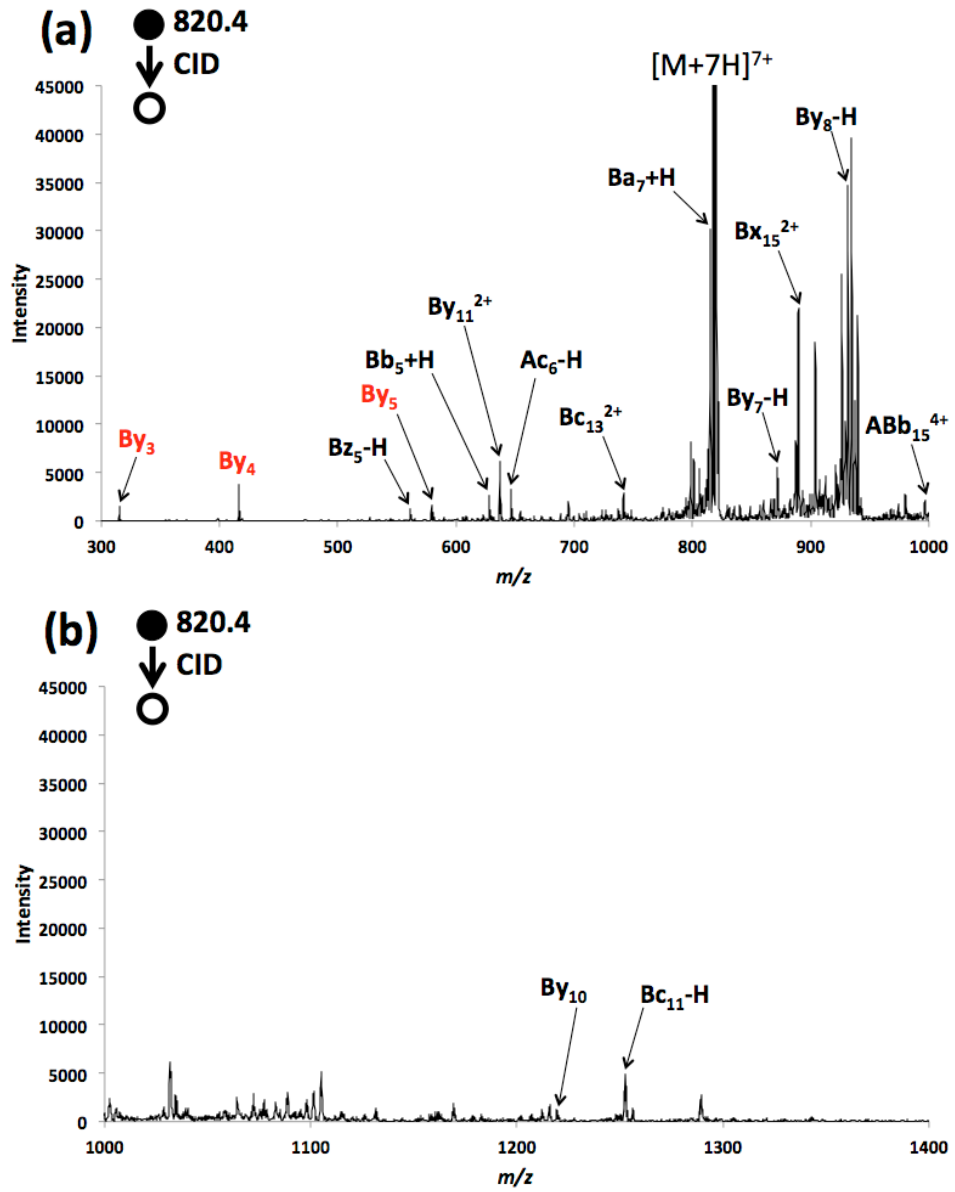

Figure 3.19. Zoomed-in CID spectrum of $[insulin+7H]^{7+}$ from (a) *m/z* 300 - 1000. (b) *m/z* 1000 – 1400 (CID amplitude = 0.3 V).

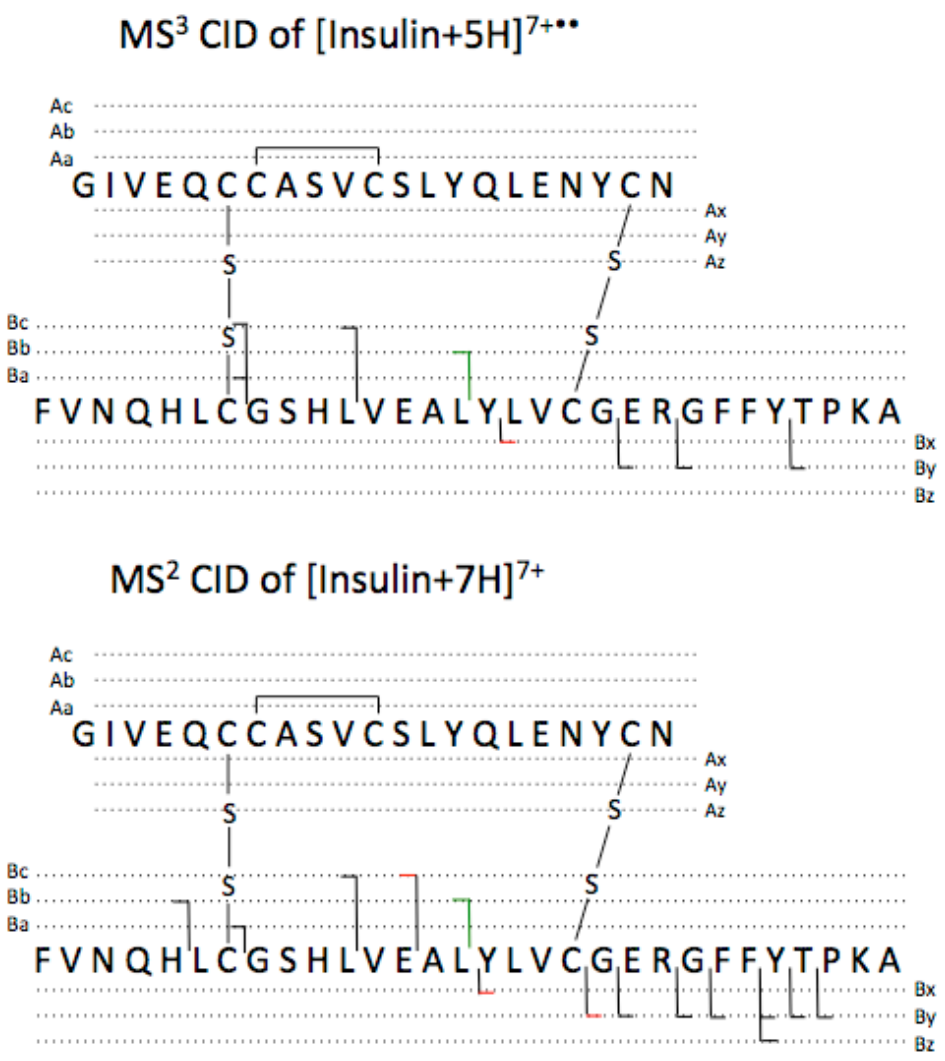

Scheme 3.4. Fragment map of (a) MS^3 CID of $[insulin+5H]^{7+\bullet\bullet}$, (b) CID of $[insulin+7H]^{7+}$.

3.4 Conclusions

ESI-generated insulin cations (at charge states of 4+, 5+ and 6+) were subjected to helium-cation irradiation, producing both charge-increased species and charge-decreased species. These species are accompanied by a few fragment ions, the number and relative abundances of which are highly dependent on the precursor charge state. 6+ insulin produced the maximum number of fragment ions, most of which originates from the cleavages of B-chain outside the cyclic structure defined by the disulfide linkages. The charge-increased product ions from CTD process were further mass-selected and subjected to CID reaction at MS^3 level. This approach effectively broke disulfide linkages, showing the capability of producing more fragment ions than a single CTD experiment. Resonance ejection experiments were conducted during CTD experiments to prevent consecutive CTD reactions. Instead of the commonly observed one-electron oxidation pathways, an interesting one-step two-electron oxidation pathway for the formation of $[M+nH]^{(n+2)+\bullet\bullet}$ was revealed, which has an activation barrier of at least 20 eV. The di-radical nature of the doubly oxidized product could not be confirmed through reaction with residual oxygen or by CID. The above results, along with the low-cost instrument platform, indicate that CTD is an intriguing high-energy fragmentation method for the structural interrogation of gas-phase biomolecules.

CHAPTER 4: CHARGETRANSFER DISSOCIATION (CTD) OF PHOSPHOCHOLINES: GAS-PHASE ION/ION REACTIONS BETWEEN HELIUM CATIONS AND PHOSPHOLIPID CATIONS

Reproduced in part with permission from Pengfei Li, Glen P. Jackson*, J. Mass Spectrom.* in revision.

4.1 Introduction

Lipids are essential components of cellular membranes in living cells [118, 119]. In addition to serving as a "container" for the cell, lipids also show remarkable involvement in a range of lipid-lipid and lipid-protein interactions, thus acting as key players with distinctive biochemical roles and biophysical properties [3]. A detailed description of all lipids and their functions at the cellular level would greatly facilitate the understanding of signaling, lipid metabolism, and membrane vesicle trafficking. However, the full structural characterization and quantitation of all lipids in a given system remains a formidable challenge to biochemists [34].

Mass spectrometry (MS) has emerged as an indispensable analytical tool for the structural characterization of lipids. Soft ionization techniques, such as electrospray ionization (ESI) [34] and matrix-assisted laser desorption/ionization (MALDI) [120], help ionize lipids in their native states, without requiring derivatization and without causing decomposition, thereby enabling the unequivocal determination of molecular weights. These soft ionization techniques are typically used in conjunction with tandem mass spectrometry (MS/MS) to provide structural detail and to help resolve constitutional isomers. Low energy collision-induced dissociation (CID) is the most prevalent MS/MS technique, and it has been employed for the structural analysis of a wide variety of lipid classes, including sphingomyelin (SM) [7], phosphatidylglycerol (PG)

[121],glycerophosphoethanolamine (GPE) [122], glycerophosphocholine (GPC) [35], and glycerophosphatidic acid (GPA) [36].

Low-energy collisional activation of lipids mainly produces fragments corresponding to the loss of entire fatty acyl substituents, like neutral ketenes and fatty acids, and is thus not informative enough for full structure characterization [123]. To enhance the amount of obtainable structural information, a variety of MS/MS techniques have been explored as the alternative for the structural interrogation of lipids, including high-energy (HE) CID [124, 125], ion/molecule reactions such as Paternò-Büchi reactions [126], OzESI/OzID [44, 127-131]), ion/ion reactions [42, 132], ion/photon reactions(e.g. UVPD [41], IRMPD [40]), electron-based reactions(e.g. ETD [37], EIEIO [38], EID [39, 133]) and radical-directed dissociation (RDD) [134, 135].

In OzESI/OzID, the exposure of unsaturated lipids to ozone molecules results in an ozonide, which then dissociates into fragment ion pair(s) with diagnostic mass separation that enables an unambiguous identification of sites of unsaturation [44, 128]. McLuckey, Blanksby and coworkers have shown that gas-phase ion/ion reactions can be used to convert lipid cations into their anion form, thereby providing incredible selectivity toward certain lipid classes [42, 132]. When combined with low energy CID, ion/ion reactions could provide enhanced structural information, such as acyl chain lengths and degrees of unsaturation [42, 132]. Whereas the current state of the art in tandem mass spectrometry has a variety of approaches to target certain functional groups and chemistries, the communities interested in lipid characterization and lipidomics would stand to benefit from additional, complementary or more-universal approaches to tandem mass spectrometry.

Charge transfer dissociation (CTD) is a possible alternative to the aforementioned MS/MS techniques, and it proceeds via exposure of gas-phase precursor cations to a kiloelectronvolt beam of helium cations [49]. Upon the interaction with helium cations, peptide cations decompose via radical-driven pathways that are significantly different from low energy CID, but analogous to other high-energy fragmentation methods [49]. CTD has the ability to increase the number of positive charges on a precursor ion and is workable with singly charged precursor ions, unlike ETD and ECD. The activation energy in CTD is determined by both the electron affinity of the helium cation (~24.6 eV) and kinetic energy, and can drive reactions with appearance potentials greater than 24 eV [49, 136].

In this study, we demonstrate the utility of CTD as a means of structural characterization for phosphatidylcholines. Helium-cation irradiation of protonated lipids produces highly extensive cleavage along lipid acyl chains (i.e. POPC, PSPC) and charge-increased ion series for lipids containing multiply carbon-carbon (CC) double bonds (i.e. 9E- and 9Z-DOPC). The 12-Da peak spacing feature and ratio change in fragment ion intensity in the vicinity of the C=C double bond are closely related to the position and geometry of C=C double bond(s), which leads toward a near-complete characterization of lipid structures.

4.2 Experimental

4.2.1 Instrumentation

All mass spectra (CID, CTD and MAD) were collected on a Bruker amaZon ETD mass spectrometer (Bruker Daltronics, Bremen, Germany), which has been modified to perform lipid cation/helium cation or lipid cation/metastable atom reactions. Installation

of saddle field fast ion/fast atom source (VSW/Atomtech, Macclesfield, UK), connection between electronic components and working principle are highly analogous to those described for Thermo Fisher LTQ Velos Pro instrument [49] and experimental setup of MAD-MS [137].

4.2.2 Materials

All the lipids used in this experiment were purchased from Avanti Polar Lipids (Alabaster, AL). The involved lipids and their shorthand designations are as follows: 1-hexadecanoyl-2-octadecanoyl-sn-glycero-3-phosphocholine (PSPC, 16:0/18:0), 1-hexadecanoyl-2-(9Z-octadecenoyl)-sn-glycero-3-phosphocholine (POPC, 16:0/18:1(9Z)), 1,2-di-(9E-octadecenoyl)-sn-glycero-3-phosphocholine (9E-DOPC, 18:1/18:1(9E,9E)), 1,2-di-(9Z-octadecenoyl)-sn-glycero-3-phosphocholine (9Z-DOPC, 18:1/18:1(9Z, 9Z)), 1,2-di-(5Z,8Z, 11Z,14Z-eicosatetraenoyl)-sn-glycero-3-phosphocholine (DAPC, 20:4/20:4), and sphingomyelin (SM, d18:1/18:0). Lipid analytes were prepared at a concentration of ~60 μM in a solution of 49.5/49.5/1 (v/v/v) methanol/water/acetic acid prior to positive electrospray ionization (ESI).

4.2.3 Method

Each lipid solution was continuously infused into the ESI source with an electronic syringe pump (#1725, Hamilton Company Reno, Nevada, NV) at a flow rate of 160 μL/h. The skimmer was at ground potential and the electrospray needle was set at 4.5 kV. The temperature of the heated capillary was 220°C. The $[M+H]^+$ or $[M+Na]^+$ ions were mass-selected using an isolation window of 1.0 or 4.0 Da depending on the need for isotope information. The saddle field ion source was only switched on during an MS^2 scan function in which the isolated ions were stored at a desired low mass cut-off (e.g.

150) with the excitation amplitude for CID set to zero volts. A 6 kV square wave with a pulse width of 25 ms was applied to the saddle field ion source for the generation of reagent helium cations. The helium flow was controlled via a variable leak valve, and the pressure read-out was obtained from pressure monitor of the ion trap gauge in the main vacuum region. Using this indirect measurement, the helium gas supply was adjusted to provide a reading of ~1.20×10^{-5} mbar for all the experiments, which was barely above the base pressure of ~8×10^{-6} mbar in the main vacuum chamber. A typical low mass cut off (LMCO) value of *m/z* 150 was used for the removal of ionized residual background compounds. All the mass spectra (CID, CTD and MAD) were accumulated in the profile mode, with up to 4 minutes of averaging to improve the signal-to-noise ratio (S/N).

4.3 Results and Discussion

4.3.1 Protonated POPC: CTD vs. MAD vs. CID

Helium irradiation of protonated POPC results in a range of fragments, as shown in Figure 4.1a. The CTD spectrum looks generally similar to the MAD spectrum (Figure 4.1b), but both differ greatly from traditional CID (Figure 4.1c) [123] or electron ionization (EI) spectra [138, 139]. All fragmentation methods give a dominant fragment ion at *m/z* 184.0, which is a diagnostic fragment of the phosphocholine head group [140, 141]. The CTD spectrum also shows a doubly charged fragment at *m/z* 380.4, which corresponds to the charge-increased product $[POPC+H]^{2+\bullet}$, which is similar to the Penning ionized product ion observed in MAD [141]. CTD shows three major fragments at *m/z* 478.4, *m/z* 496.4 and *m/z* 521.4, which are associated with entire acyl chain losses. These fragments resemble closely the MAD fragmentation pattern, but greatly differ from

that of CID. Helium-CTD also shows an extensive dissociation along two acyl chains ranging from *m/z* 550 to *m/z* 732, which is also similar to MAD.

Helium-CTD of sodiated POPC produces a fragmentation pattern that highly resembles that of MAD spectrum of $[POPC+Na]^+$, as shown in Figure 4.2. In addition to the phosphocholine head group fragment at *m/z* 184.0 and the ionized species $[M+Na]^{2+\bullet}$ at *m/z* 391.5, CTD produced a variety of fragments related to cleavages of the glycerol backbone and its vicinity. Examples include the loss of trimethylamine ($N(CH_3)_3$) at *m/z* 723.5, the entire head group at *m/z* 599.5, sn-1/sn-2 acyl chains at *m/z* 526.5 and *m/z* 500.5, and simultaneous loss of two units, such as at *m/z* 441.4 and *m/z* 467.5. The cleavage of the C1-C2 bond within the glycerol backbone at *m/z* 513.5 was observed, which is observed in CTD and MAD spectra, but not CID. The CTD spectra of protonated POPC and sodiated POPC show different product ion distributions, as has been observed in low energy CID [7, 35, 123] and post source decay (PSD) experiments [120]. The distinction in PSD spectra for the two adduct forms is attributed to the different binding of H^+ and Na^+ to lipid head group [120].

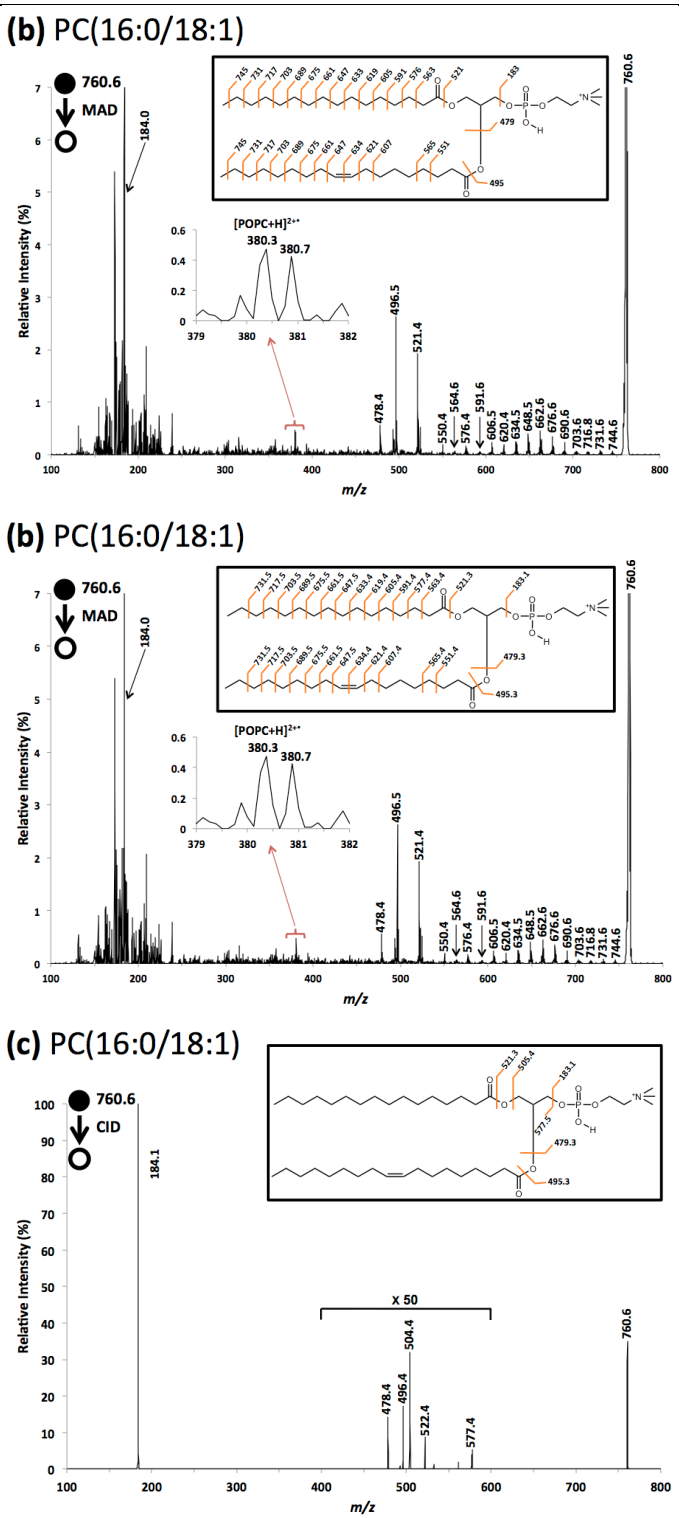

Figure 4.1. (a) CTD spectrum of $[POPC+H]^+$ (16:0/18:1). (b) MAD spectrum of $[POPC+H]^+$(16:0/18:1). (c) CID spectrum of $[POPC+H]^+$(16:0/18:1). The diagram insets show possible cleavages and theoretical masses for fragmentations without hydrogen rearrangements.

The results in Figure 4.1.and 4.2 indicate that the CTD process involves both CID-like even-electron fragmentation pathways and MAD-like radical-induced fragmentation pathways [141]. Ionization of 1+ precursor ions by Penning ionization or charge transfer are expected to be different in energy by the ionization potential of a helium metastable atom, which is about 4.77 eV [142]. Although this difference seems significant, He metastable atoms and He cations are both more than 19.8 eV above the ground state, so both have more than enough energy to ionize most 1+ precursor ions, which typically have ionization energies of around 10 eV [50].

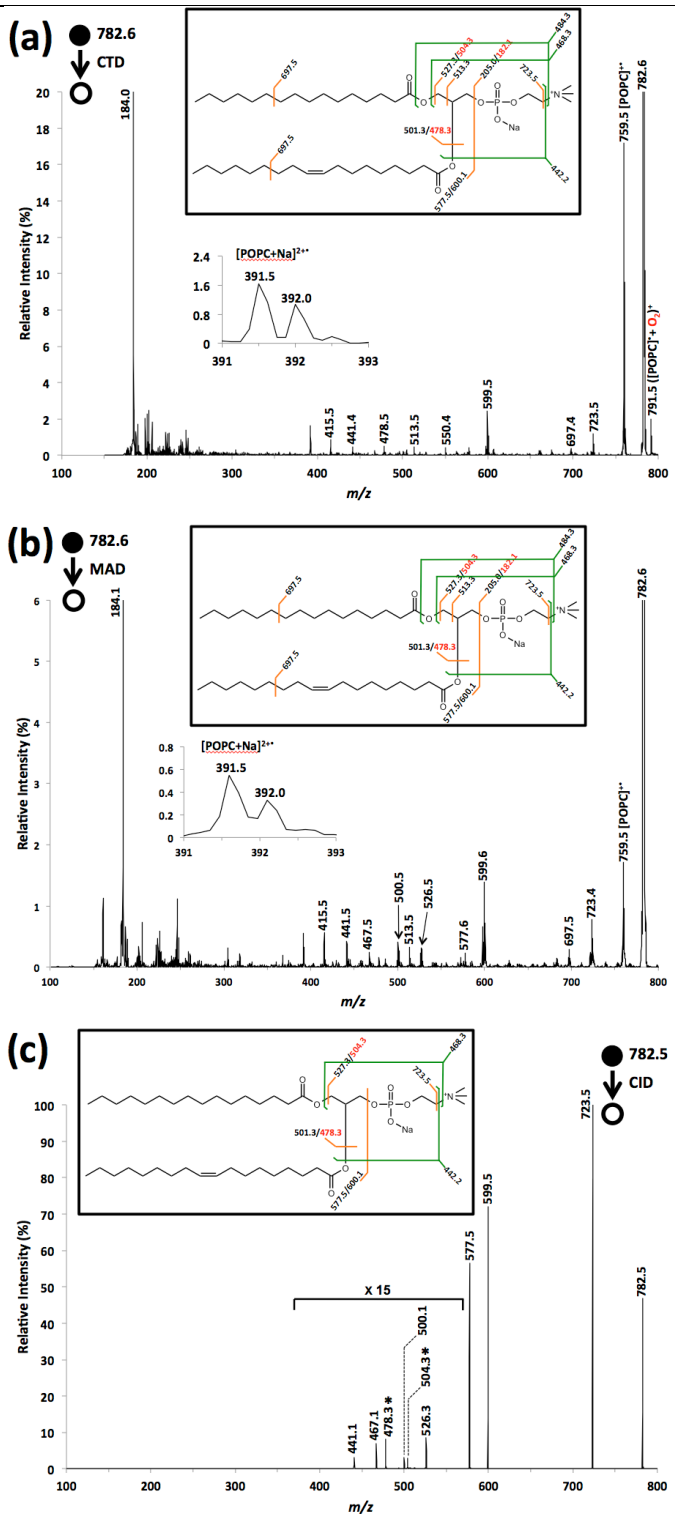

Figure 4.2. (a) CTD spectrum of $[POPC+Na]^+$ (16:0/18:1). (b) MAD spectrum of $[POPC+ Na]^+$ (16:0/18:1). (c) CID spectrum of $[POPC+ Na]^+$ (16:0/18:1).

A more detailed comparison between CTD and MAD spectra of $[POPC+H]^+$ is given using the zoomed-ins in Figure 4.3a and 4.3b, and Figure 4.5a and 4.5b.

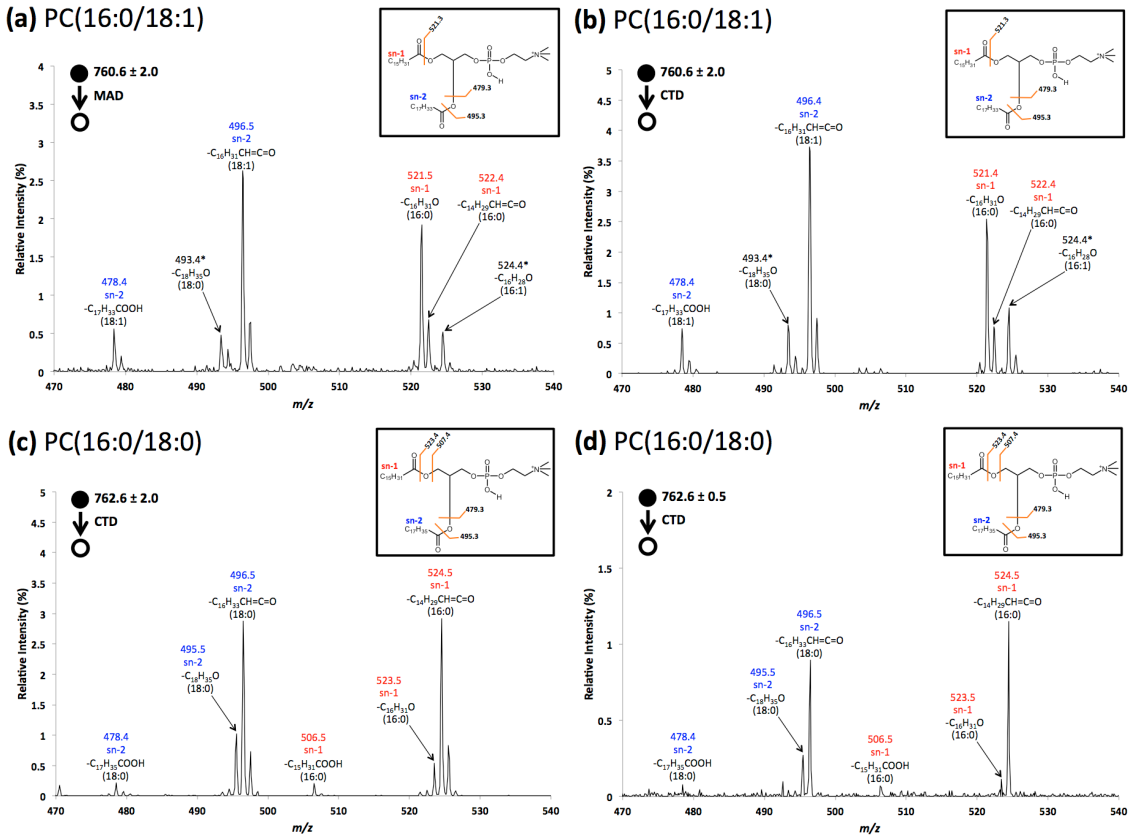

Figure 4.3. Zoomed-in regions from *m/z* 470-540: (a) MAD spectrum of $[POPC+H]^+$ (16:0/18:1); (b) CTD spectrum of $[POPC+H]^+$ (16:0/18:1); (c) CTD spectrum of $[PSPC+H]^+$ (16:0/18:0) with a precursor isolation window width=4.0; (d) CTD spectrum of $[PSPC+H]^+$ (16:0/18:0) with a precursor isolation window width=1.0.

The CTD spectrum of $[POPC+H]^+$ shows strong similarity to the MAD spectrum in the region from *m/z* 470-540 (Figure 4.3a and 4.3b). The common features include neutral ketene losses at *m/z* 522 (sn-1) and *m/z* 496 (sn-2), as well as elimination of sn-2 fatty acid at *m/z* 478 [141]. Because the same batch of purchased POPC sample was used for both MAD and CTD experiments, the same set of contamination peaks at *m/z* 493.4 (loss of C(18:0) chain) and *m/z* 524.4 (loss of C(16:1) chain) were observed [141], possibly originating from the isomerization of POPC during its synthesis process [38,

143]. The spectrum in Figure 4.3d is a replicate experiment of Figure 2c, but with a much narrower isolation window (width = 1.0 Da). The exclusion of the ^{13}C contribution in Figure 2d helps to confirm the peak assignments in Figure 4.3c.

Different from the CID spectrum of PSPC (Figure 4.4), the CTD spectrum in Figure 2c shows two sets of fragments associated with sn-1/sn-2 ketene losses: odd-electron fragments at *m/z* 495.5 and *m/z* 523.5, and even-electron fragments at *m/z* 496.5 and *m/z* 524.5. For both POPC and PSPC, the CTD spectra show preferential neutral ketene loss over neutral fatty acid loss, which resembles radical-induced EID [39] but significantly differs from even-electron CID (Figure 4.4).

As for the even-electron fragments in Figure 4.3c, CTD does not show a distinctive preference in the formation of *m/z* 496 (sn-2 ketene loss) or *m/z* 522/524 (sn-1 ketene loss), which compromises its ability to differentiate between the sn-1 and sn-2 ketene losses. In this regard, CTD is slightly less informative than CID, which preferentially produces sn-2 ketene loss over sn-1 ketene loss (*m/z* 496 >*m/z* 522 or 524) (Figure 4.4) [35, 39, 140]. In contrast to this general preference for sn-2 ketene loss over sn-1 ketene loss, Ho and Huang show no such preference for sn-2 ketene loss in LE-CID experiments in a quadrupole ion trap [123] and Jones et al. observed a slight preference for sn-1 ketene loss over sn-2 ketene loss in the EID fragmentation of phospholipids [39].

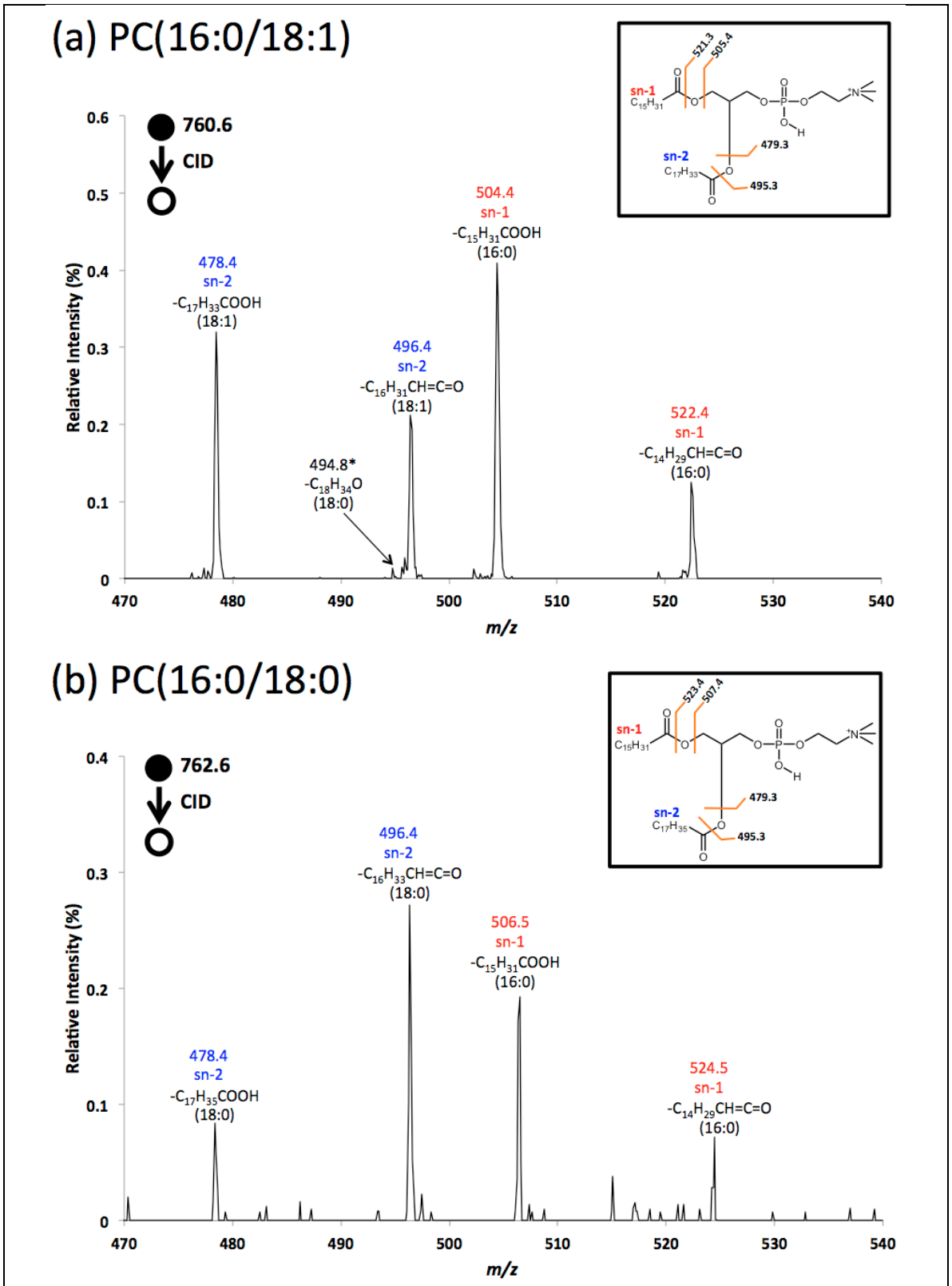

Figure 4.4. Zoomed-in regions from *m/z* 470-540 of CID spectra of (a) $[POPC+H]^+$ (16:0/18:1) and (b) $[PSPC+H]^+$ (16:0/18:0).

The odd-electron fragments in Figure 4.3c were also observed in MAD [141] and EID [39] spectra of the same lipid, which suggests analogous fragmentation pathways among CTD, MAD and EID. The odd-electron fragments must be generated via the introduction of radical species during the fragmentation process, indicating the involvement of radical cleavages in CTD [141]. Interestingly, the fragment at *m/z* 495.5 (sn-2 position) is more abundant than the one at *m/z* 523.5 (sn-1 position). This trend agrees with that from the said EID results: the more favorable formation of radical cation associated with sn-2 position [39]. This coincidence, along with the more favorable neutral ketene loss over fatty acid loss in CTD, is indicative of high resemblance of CTD in its mechanistic nature to that of EID.

4.3.2 CTD: POPC vs. PSPC

For ease of discussion, the two spectra in Figure 4.5a and 4.5b are labeled in three sections. The section labeled "I" shows the acyl cleavages close to the ω-end of the lipid chains. The CTD spectrum of $[POPC+H]^+$ (Figure 3b) shows extensive fragmentation along the two acyl chains in this region, such as the even-electron fragments at *m/z* 730.5, *m/z* 716.5, *m/z* 702.5, *m/z* 688.5, *m/z* 676.5 and *m/z* 662.5, which correspond to the neutral loss of C_nH_{2n+2} molecules. In the same region, odd-electron fragments at *m/z* 731.5, *m/z* 717.5, *m/z* 703.5, *m/z* 689.5, *m/z* 675.5 and *m/z* 661.5 were observed (green font), which corresponding to neutral loss of $C_nH_{2n+1}^{\bullet}$ alkyl radicals. Almost the same even-/odd-electron fragment series were observed in both MAD (Figure 3a) and EID spectra reported elsewhere [39].

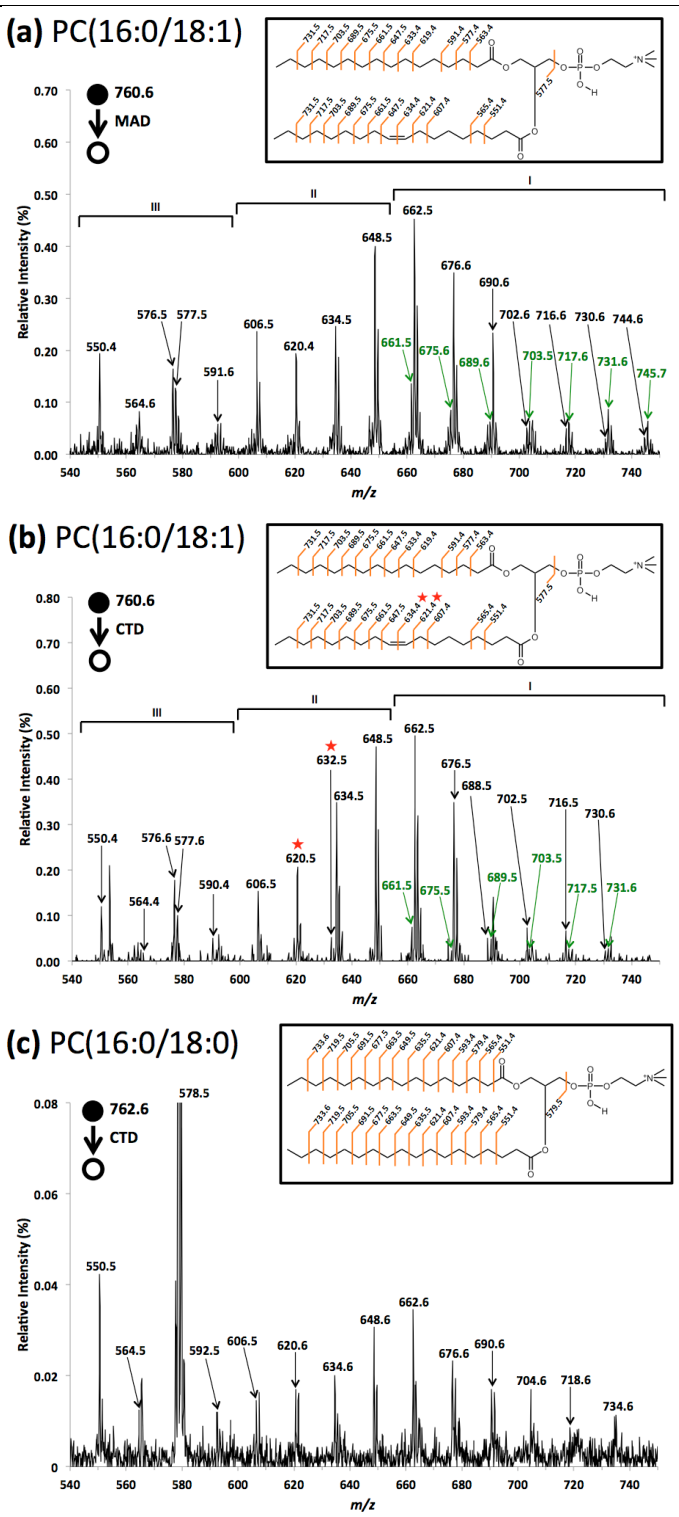

Figure 4.5. Zoomed-in regions from *m/z* 540-750: (a) MAD spectrum of $[POPC+H]^+$ (16:0/18:1); CTD spectra of (b) $[POPC+H]^+$ (16:0/18:1) and (c) $[PSPC+H]^+$ (16:0/18:0). The green font shows the $C_nH_{2n+1}^{\bullet}$-type losses.

4.3.3 9E/9Z-DOPC: CID vs. CTD

The ladder-like patterns of even-electron fragments are separated by 14.0 Da units, which is a commonly observed pattern in EI [138, 139] and HE-CID [144] as well as the recently reported electron-based MS/MS experiments on lipids, EIEIO [38] and EID [39]. The accompanying odd-electron fragments associated with the losses of alkyl radicals were also reported in other high-energy MS/MS experiments [38, 39, 144]. Others have proposed that the serial neutral loss of C_nH_{2n+2}could either be the neutral loss of an alkane or be the neutral loss of an alkene+H_2 (i.e. 1,4-cyclic elimination) [39, 145]. In most general respects, CTD fragmentation can therefore be rationalized through radical mechanisms proposed by others [144, 146].

In section II, the vinyl bond vicinity, CTD-generated fragments exhibit identical nominal masses to that of MAD, but distinctive differences were also observed between MAD and CTD. For example, MAD shows reduced intensities at the CC double bond site along with the elevated ion intensity corresponding to distal allyl cleavages—the most prevalent dissociation pattern of unsaturated acyl chains, which has been widely reported in FAB [147], HE-CID [146], EIEIO [38] and EID [39] experiments. In CTD, this vicinity looks slightly different and contains a distinctive pair of peaks at *m/z* 620.5 and *m/z* 632.5, whose spacing is a diagnostic 12 Da. This characteristic peak spacing has been well studied and documented as the diagnostic value for localization of CC double bonds. Mass spectrometric experiments involving EI [148], HE-CID [149], RDD [134, 135], MAD-MS^3 CID [69] have made use of this diagnostic feature for the determination of double bond positioning in unsaturated fatty acid derivatives and phospholipids.

Similar to MAD, CTD only produces a few fragments in section III, the α-end of the acyl chain, including contributions from both sn-1 and sn-2 acyl chain cleavages. It is generally rare to observe dissociation in this region of the lipid, but the fragments observed for CTD are analogous to EID results of $[POPC+H]^+$ [39]. The fragment at *m/z* 577.6 could possibly be attributed to cleavage related to head group loss.

Consistent with CTD results of POPC, CTD of PSPC (Figure 4.5c) also produces extensive dissociation along two acyl chains, with an even greater extent of fragmentation. PSPC is structurally different from POPC in that it contains two fully saturated acyl chains (16:0/18:0). Consequently, a more extensive ladder-like dissociation pattern can be seen from *m/z* 718.6 to *m/z* 550.5, which corresponds to the mutual contribution of sn-1 and sn-2 acyl chains. Moreover, the fragment ion intensities appear to be more uniform along the entire saturated acyl chains [38]. It is worth noting that the nominal masses from *m/z* 592.5 to *m/z* 718.6 are in one-to-one correspondence with those in EID of PSPC [39]. A difference between POPC and PSPC is that CTD of PSPC does not produce the aforementioned odd-electron fragment series. The lack of odd-electron fragments in PSPC is analogous to EID experiments [39]. A very abundant peak at *m/z* 578.5, which corresponds to cleavage of C3-C4 bond, was observed in the CTD spectrum of PSPC, which could originate from either the C3-C4 bond on C(16:0) acyl chain or the C5-C6 bond on C(18:0) acyl chain [39].

4.3.3 9E/9Z-DOPC: CID vs. CTD

CID and CTD spectra of protonated 9E-DOPC (18:1/18:1) are shown in Figure 4.6a and 4.6b. Collisional activation of this lipid only produces three fragments, as we reported before [141]. But CTD of the same lipid produces a much more extensive fragmentation coverage, which includes head group losses at *m/z* 184.0, *m/z* 521 for the sn-1/sn-2 alkyl ketene loss and *m/z* 505 for the sn-1/sn-2 fatty acid loss. CTD also produces charge-increased, or oxidized, product ions such as $[9E\text{-}DOPC+H]^{2+\bullet}$ at *m/z* 393.5, $[9E\text{-}DOPC+H\text{-}C_9H_{19}]^{2+\bullet}$ at *m/z* 330.5, and acyl chain cleavages spanning the CC double bond. This pattern is almost identical to a previously reported MAD spectrum of $[9E\text{-}DOPC+H]^{+}$ (18:1/18:1) [141]. The close similarity of the two ion activation methods suggests a similar mechanistic nature in them, which can help evidence mechanistic hypothesis in the fragmentation pathway of CTD.

The middle panels (c and d) of Figure 4.6 compare the range *m/z* 500-530 for CID and CTD results of 9E-DOPC. The bottom panels (e and f) show CID and CTD spectra of 9Z-DOPC. In CTD, the peak patterns around *m/z* 521 and *m/z* 505 resemble MAD [141], but vastly differ from that of CID. CID mainly proceeds through even-electron rearrangements, yielding even-electron fragments. The zoomed-in CTD spectrum of cis-double bond lipid (9Z-DOPC) looks very similar to that of trans-double bond lipid (9E-DOPC), which agrees with the reported difficulty in differentiating cis- and trans-geometry of double bonds [150]. For CTD of both 9E- and 9Z-DOPC, the preference in ketene loss (*m/z* 522.5) over fatty acid loss (*m/z* 506.5) is in contrast to CID spectra. This preferential ketene loss in CTD is consistent with the aforesaid trend for POPC and PSPC. The reproducible feature across lipids with different acyl chain combinations further

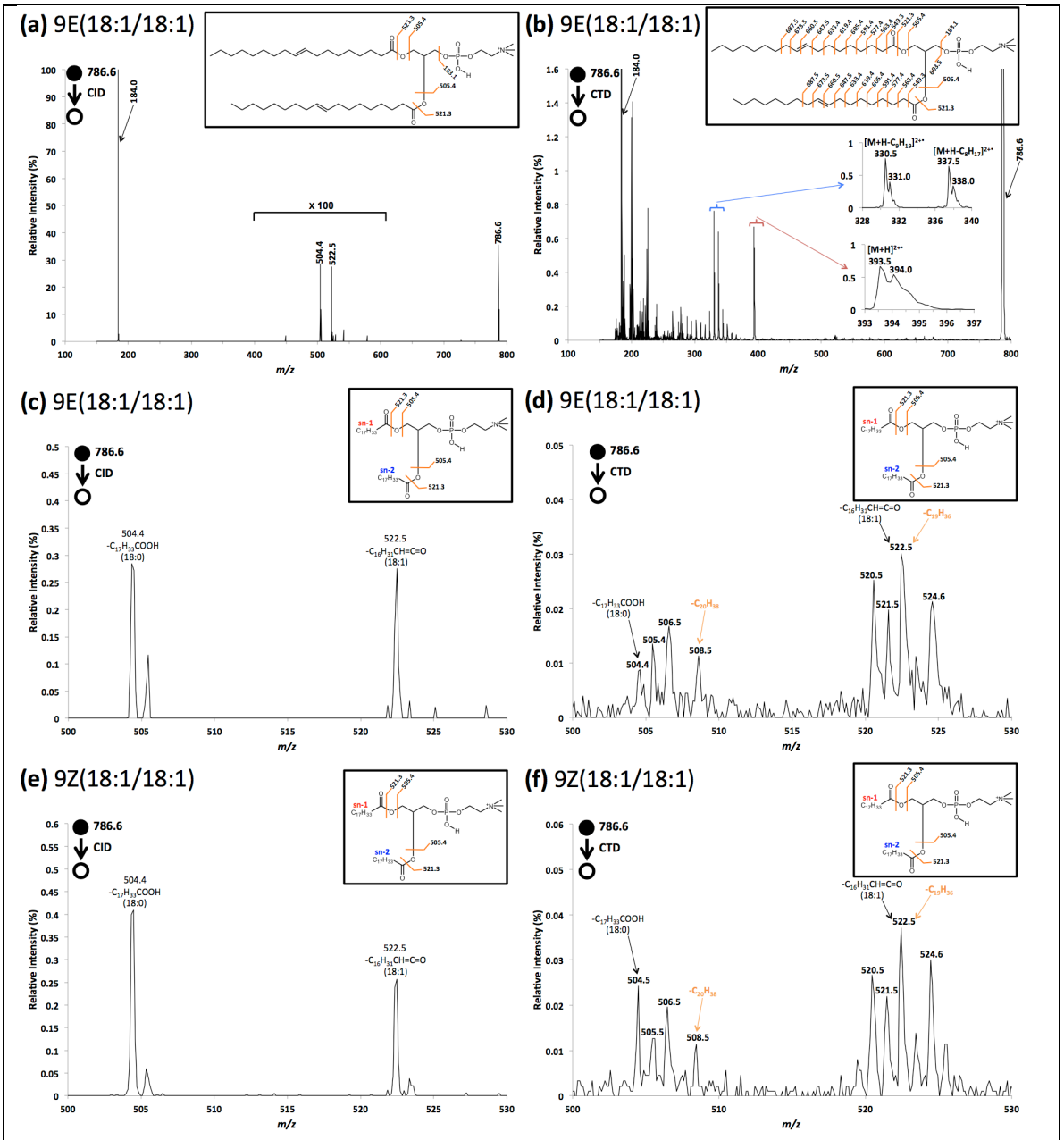

Figure 4.6. (a) CID spectrum of $[9E\text{-}DOPC+H]^+$ (18:1/18:1). (b) CTD spectrum of $[9E\text{-}DOPC+H]^+$ (18:1/18:1). Zoomed-in regions from *m/z* 500-530: (c) CID spectrum of $[9E\text{-}DOPC+H]^+$ (18:1/18:1); (d) CTD spectrum of $[9E\text{-}DOPC+H]^+$ (18:1/18:1); (e) CID spectrum of $[9Z\text{-}DOPC+H]^+$ (18:1/18:1); (f) CTD spectrum of $[9Z\text{-}DOPC+H]^+$ (18:1/18:1). The orange font in panel (d) and (f) shows the C_nH_{2n-2}-type losses and their tentative assignments.

confirms the distinctive mechanistic nature of CTD, which should be different from that of even-electron CID, but is close to radical dissociation feature of MAD, EIEIO and EID.

Figure 4.7a and 4.7b show magnified CTD spectra of $[9E\text{-}DOPC+H]^+$and $[9Z\text{-}DOPC+H]^+$ from *m/z* 530-750. In contrast to PSPC, which has two saturated acyl chains, 9E- and 9Z-DOPC both contain two unsaturated acyl chains. Consistent with CTD results of POPC and PSPC, a ladder-like fragmentation pattern was observed in CTD spectra of both 9E- and 9Z-DOPC. Different from the CTD results of POPC and PSPC, fewer fragments were observed for 9E- and 9Z-DOPC. The lack of C-C singly bonds cleavages closer to ω-end was also seen in EID spectra of 9Z- and 6Z-DOPC [39]. It seems that the presence of multiple CC double bonds obstructs the propensity of fragmentation in CTD and other radical-induced approaches.

Consistent with the CTD results of POPC, the diagnostic peak spacing of 12 Da was also observed in the double bond region for both 9E- and 9Z-DOPC, which offers an unambiguous localization of CC double bonds in both lipids. The consistency in this 12 Da spacing demonstrates the reproducibility of CTD in producing this double bond-specific feature. These results also indicates the promising potential of CTD for the diagnosis or differentiation of sites of unsaturation in lipids, or further possible extension into other biomolecules with unsaturated olefinic chains, such as fatty acids methyl esters (FAMEs).

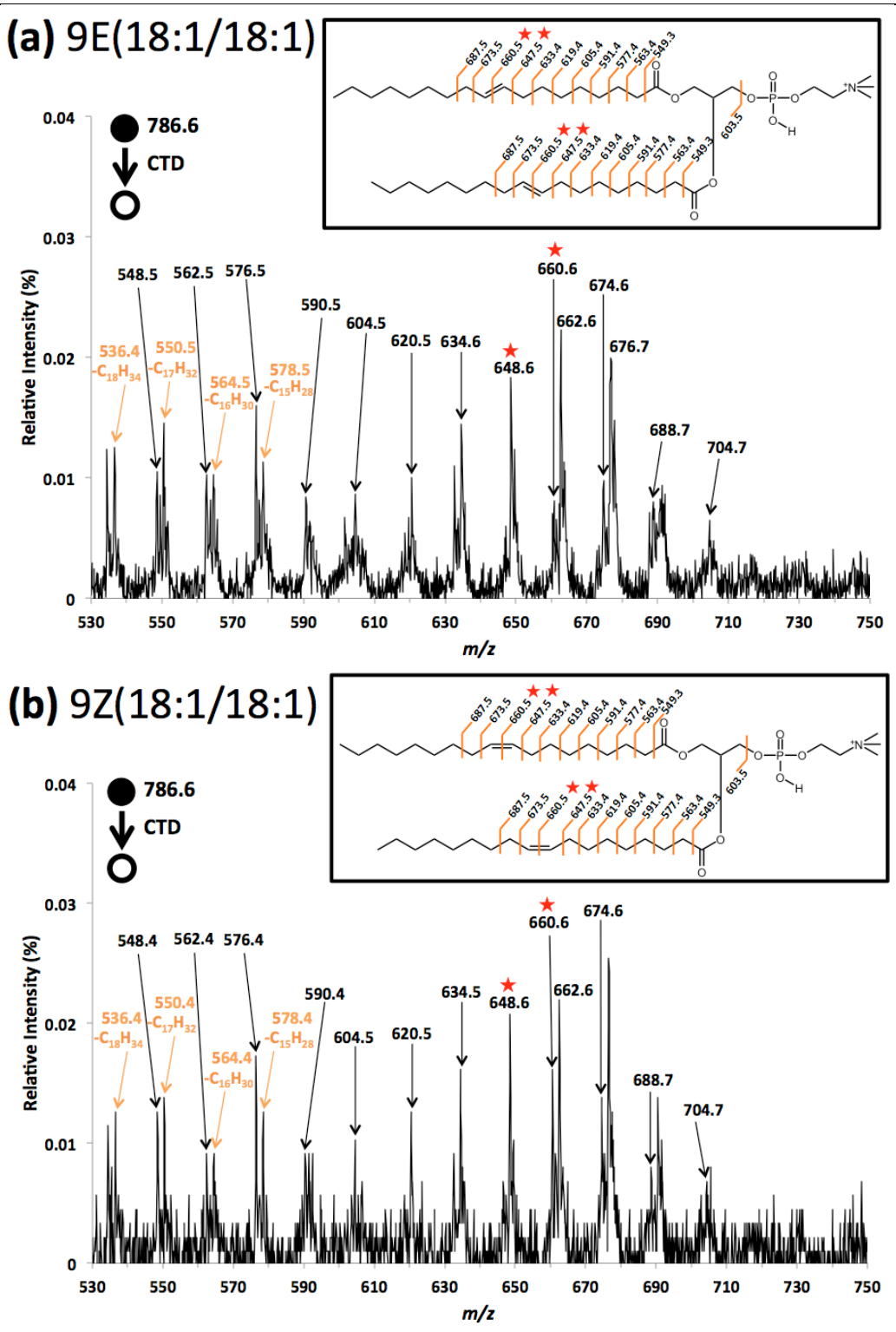

Figure 4.7. Zoomed-in regions from *m/z* 530-750 of CTD spectra of (a) $[9E\text{-DOPC+H}]^+$ (18:1/18:1); (b) $[9Z\text{-DOPC+H}]^+$ (18:1/18:1). The orange font shows the C_nH_{2n-2}-type losses and their tentative assignments.

In contrast to the CTD spectra of POPC and PSPC, CTD spectra of 9E- and 9Z-DOPC show a unique neutral losses, including: *m/z* 508 ($-C_{20}H_{38}$), *m/z* 522 ($-C_{19}H_{36}$), *m/z* 536 ($-C_{18}H_{34}$), *m/z* 550 ($-C_{17}H_{32}$), *m/z* 564 ($-C_{16}H_{30}$) and *m/z* 578 ($-C_{15}H_{28}$) (orange font in Figure 4c, 4d, 5a and 5b). The tentative assignments are shown in parentheses, above. This type of C_nH_{2n-2} neutral loss is consistent with the observation in EID experiments, which could be attributed to the mutual cleavages of both unsaturated acyl chains [39].

Figure 4.8 compares the unique doubly charged ion series in CTD of [9E-DOPC+H]$^+$and [9Z-DOPC+H]$^+$, which shows a peak spacing of 7.0 Da instead of 14.0 Da. To our best knowledge, this 7.0 Da-ladder pattern was rarely reported in gas-phase ion activation experiments. Nevertheless, this pattern was also observed in MAD spectra of 9E- and 9Z-DOPC [141], again suggesting a significant mechanistic similarity between CTD and MAD. The doubly charged ion series almost covers the entire acyl chain. 9E- and 9Z-DOPC spectra not only exhibit a similar extent of chain cleavage, but also show a similar fragment ion intensity distribution. Noticeably, the most abundant peaks are at *m/z* 330 and *m/z* 337 corresponding to cleavages at or next to the site of unsaturation in both lipids.

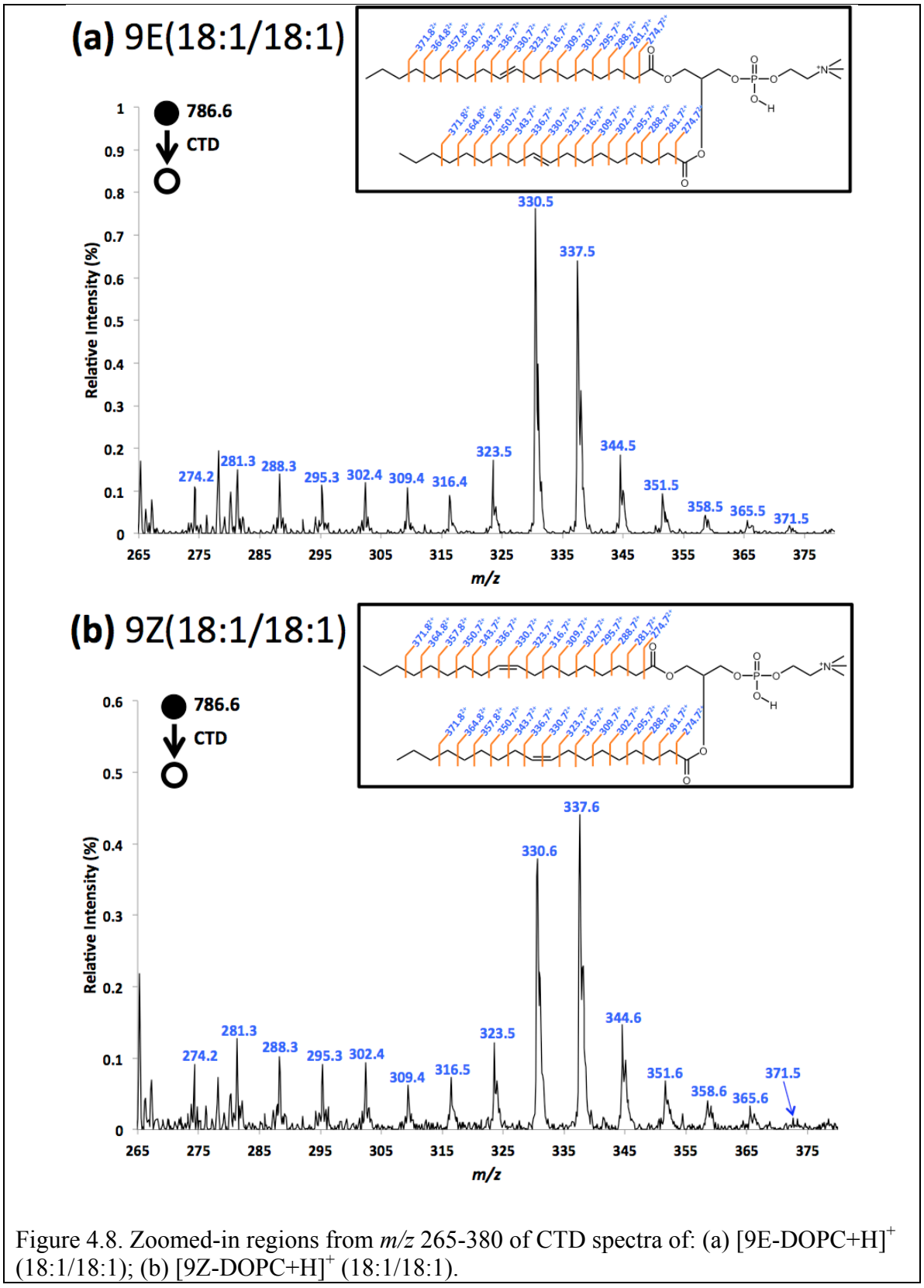

Figure 4.8. Zoomed-in regions from *m/z* 265-380 of CTD spectra of: (a) $[9E\text{-}DOPC+H]^+$ (18:1/18:1); (b) $[9Z\text{-}DOPC+H]^+$ (18:1/18:1).

In the spectrum for 9E-DOPC (Figure 4.8a), the peak at *m/z* 330 is more abundant than *m/z* 337; while in 9Z-DOPC spectrum, the trend appears to be reversed. The variation in fragment ion intensities seems to be sensitive to the geometry of double bond. Since 9E- and 9Z-DOPC only differ in double bond geometry, identical fragments are generated for both lipids. Given the similar dissociation pattern and lack of diagnostic fragments, the most common way to discriminate them is to track the changes in relative abundances of certain fragments. This concept has been reported and utilized in the differentiation of geometrical isomers of FAMEs using low-energy electron ionization mass spectrometry [150].

4.3.4 CTD: Sphingomyelin and DAPC

Figure 4.9 shows the comparison between CTD and CID spectra of protonated sphingomyelin. Collisional activation of sphingomyelin produces very few fragments: *m/z* 184.0, associated with phosphocholine head group loss, and *m/z* 713.6, associated with a neutral water loss [141]. The inefficiency of CID in producing structurally informative fragments is consistent with literature reports [7, 147, 151].

However, CTD of the same precursor of sphingomyelin is capable of producing a few additional fragments, including a characteristic charge-increased product ion ($[M+H]^{2+\bullet}$) at *m/z* 365.9 and two fragments at *m/z* 447.4 and *m/z* 491.4 corresponding to the entire acyl chain losses. These distinctive product ions are only observed in CTD and not observed in MAD of the same species [141]. Sphingomyelin is structurally different from the other tested phospholipids: one fatty acyl group is alkylated to the lipid backbone, with the other fatty acyl group being connected to sphingosine via an amide

bond [147]. The absence of the two ester-connections could possibly make a less "fragile" molecule, resulting in a less efficient dissociation pattern of MS/MS techniques.

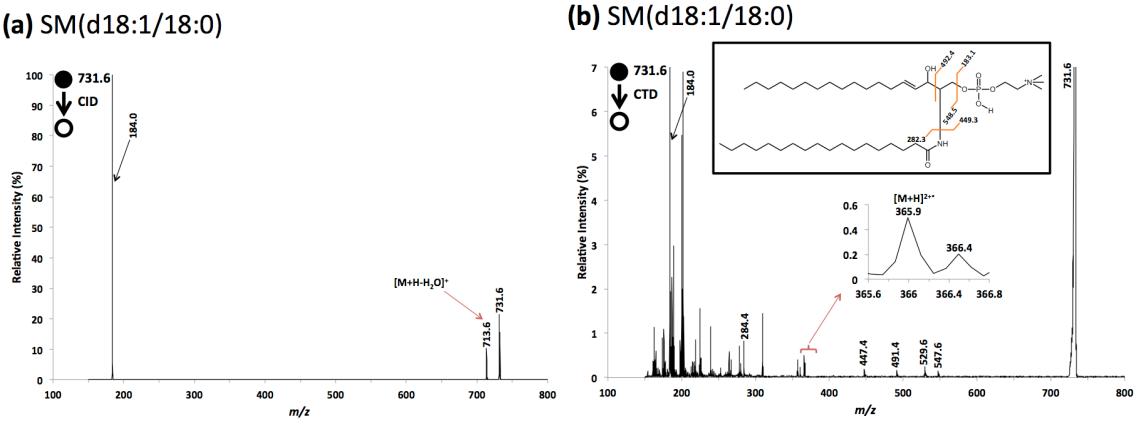

Figure 4.9. (a) CID spectrum of $[SM+H]^+$ (d18:1/18:0). (b) CTD spectrum of $[SM+H]^+$ (d18:1/18:0).

CID and CTD spectra of $[DAPC+H]^+$ are shown in Figure 4.10. Upon collisional activation, $[DAPC+H]^+$mainly produces fragments corresponding to head group loss, sn-1/sn-2 fatty acid and alkyl ketene losses, which is quite similar to the pattern of CID of $[9E-/9Z-DOPC+H]^+$. CTD of DAPC produces the same cleavages, but also produces 1+ and 2+ fragments in the vicinity of the four double bonds. The charge-increased product ion $[M+H]^{2+\bullet}$at *m/z* 415.4 was generated, as was the case for all the examined phospholipids. The zoomed-in region from *m/z* 500 to 850 shows a relatively poor S/N ratio, which is inferior to that of MAD spectrum [141]. Consistent with MAD of DAPC, CTD of DAPC also produces quite limited cleavages. The rationale offered in MAD experiment [141] could possibly account for this inefficient fragmentation of CTD too.

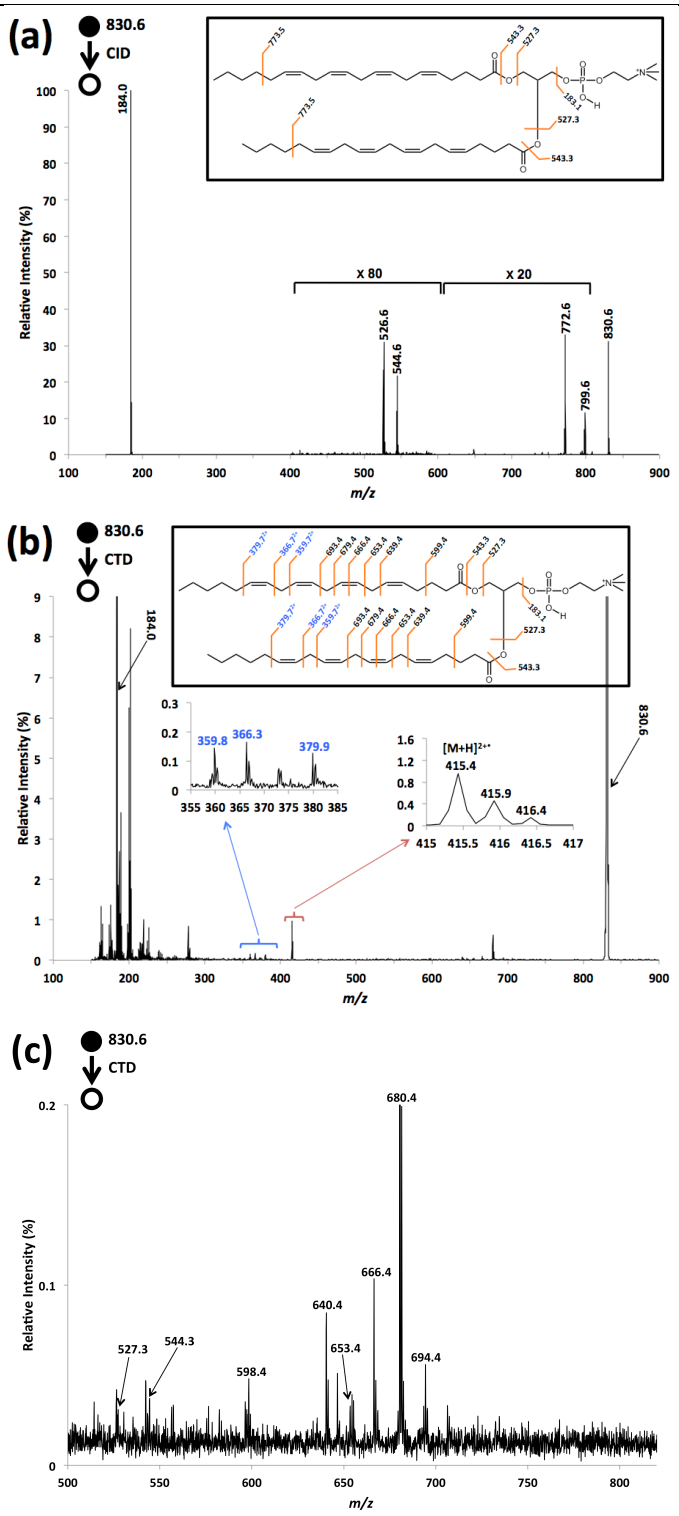

Figure 4.10. (a) CID spectrum of $[DAPC+H]^+$ (20:4/20:4). (b) CTD spectrum of $[DAPC+H]^+$ (20:4/20:4). (c) Zoomed-in region of CTD spectrum of $[DAPC+H]^+$ (20:4/20:4).

4.4 Conclusions

Charge transfer dissociation mass spectrometry (CTD-MS) has previously been shown as a promising alternative for structure interrogation of gas-phase peptide ions and complex carbohydrates [136]. Herein, we report CTD-MS on a different set of biomolecules—phospholipids, gives rise to helpful CID-like fragments, but also produces extensive dissociation within lipid acyl chains, which provides information that is not achievable through CID. The additional structural information includes the CC double bond positioning, and possible the stereochemistry. Importantly, the diagnostic spacing of ion pairs is preserved across a range of lipids with varying acyl chain lengths and number of CC double bonds. If tested on a larger pool of lipids, CTD could be exploited to probe the structure of other classes of lipids or to the gas phase chemistry of other biomolecules. The quite poor signal to noise and spectral complexity make CTD less appealing than OzID or other radical-induced methods, but improvements in efficiency and signal to noise could make CTD more appealing for lipid analysis in the future.

CHAPTER 5: MULTISTAGE MASS SPECTROMETRYOF PHOSPHOLIPIDS USING COLLISION-INDUCED DISSOCIATION (CID) IN TANDEMWITH METASTABLE ATOM-ACTIVATED DISSOCIATION (MAD)

Reproduced in part with permission from Pengfei Li, William D. Hoffmann, Glen P. Jackson*, Int. J. Mass Spectrom.* 2016, 403, 1 – 7.

5.1 Introduction

Lipids are the major building blocks of cellular membranes and possess crucial relevance in signal transduction and the storage of energy in biological systems [88]. Changes in lipid profiles and distribution are found to be closely related to many pathological conditions such as Alzheimer's disease, Down syndrome, and diabetes [6]. Because of the biological relevance of lipids in organisms, substantial efforts have been devoted to the study of lipids or lipidomics [3, 152].

Mass spectrometry is a powerful method that has become an indispensable tool in the study of biomolecules. Mass spectrometric applications in lipid analysis started with electron ionization mass spectrometry (EI-MS) [153, 154]and fast atom bombardment mass spectrometry (FAB-MS) [155], before matrix-assisted laser desorption ionization mass spectrometry (MALDI-MS) and electrospray ionization mass spectrometry (ESI-MS) became available in the 1990s [6, 156]. Being soft ionization techniques, MALDI and ESI analysis of phospholipids exhibits a sensitivity 2 to 3 orders of magnitude greater than that achieved by FAB-MS [156].

The aforementioned soft ionization techniques excel in preserving intact molecular ions, at the expense of useful structural information, i.e. molecular ions but no fragment ions. To enhance the structural information, tandem mass spectrometry (MS^n) experiments are often performed. As the most widely used tandem MS method, collision-

induced dissociation (CID) has been widely used in structural elucidation of lipids[121, 156-159]. CID-based mass spectra of phospholipids are typically dependent on the adduct form of precursor ion: i.e. the CID spectrum of protonated adducts are dominated by a phosphocholine ion at *m/z* 184, whereas CID of alkali metal-adducted ions produces several fragment ions that allow elucidation of the identities and positions of fatty acid substituents [157]. CID of proton bound dimers has recently been shown to distinguish cis and trans isomers of double bonds, in addition to their position in the acyl chains [160].

In addition to CID, other methods of tandem mass spectrometry—such as post source decay (PSD) [161], ozone induced dissociation (OzID) [43, 44, 128, 130, 162, 163]—have also been applied in lipid analysis. In OzID, mass-selected lipid cations are exposed to ozone vapor to initiate the gas-phase ion-molecule reaction. Ozonolysis results in diagnostic fragment ions that can unambiguously identify C=C double bond location(s). Radical-involved fragmentation methods, such as infrared multiphoton dissociation (IRMPD) [40], ultraviolet photodissociation (UVPD) [164], electron transfer dissociation (ETD) [165] and electron impact excitation of ions from organics (EIEIO) [38] were also recently employed in the characterization of glycerolipids. These high energy and radical-based methods typically activate more pathways than even electron, low energy rearrangements, so provide complementary fragments to conventional CID [166].

Metastable-atom activated dissociation (MAD) is another developing tandem MS fragmentation method [25, 28, 31, 32, 137, 167, 168]. To date, MAD has been used in a variety of studies concerning peptide structures, including multiply charged cations and

anions, 1+ cations, phosphorylated cations, disulfide bonds, to cleave the amide ring structure of proline and to differentiate isoleucine from leucine [31, 32, 137]. In addition to fragmenting peptides, MAD has recently been carried out on lipid cations [169]. In contrast to CID, which exclusively proceeds through even-electron mechanism, MAD produces both even-electron and odd-electron fragments.

To explore the unique features of MAD, we herein demonstrate the ability to acquire CID spectra of radical cations that are independent of the charging adduct ions. Isolated, even-electron adduct ions ($[M+H]^+$, $[M+Na]^+$, $[M+K]^+$) are first converted to odd-electron molecular ions $[M]^{+\bullet}$ through MAD. Low-energy collisional activation of the isolated radical cations ions then induces extensive fragmentation along the acyl chains of the lipids through mechanisms that are not achievable from CID of even-electron precursor ions. Distinctive radical fragments are also observed and described, which illustrate the potential utility of this type of gas-phase ion manipulation.

5.2 Experimental

5.2.1 Instrumentation

All experiments were performed on a modified Bruker amaZon ETD mass spectrometer (Bruker Daltonics, Bremen, Germany). The modification method, the connection between electronic components and the working principle are described elsewhere[137, 169].

5.2.2 Materials

The lipid used in this study was 1-hexadecanoyl-2-(9Z-octadecenoyl)-sn-glycero-3-phosphocholine PC(16:0/18:1(9Z)), which is abbreviated as POPC. POPC was diluted to a final concentration of 60 μM using a 9:1 (v/v) mixture of methanol to water

containing 1% (v/v) acetic acid for protonated form or 0.05 M NaCl (or KCl) for metal-adducted form. Ultra high purity helium (Airgas, Parkersburg, WV) was used with the FAB gun and further purified using a noble gas purifier (HP2, VICI, Houston, TX).

5.2.3 Method

Singly charged lipid precursor ions were generated through electrospray ionization (ESI) using an electronic syringe pump (#1725, Hamilton Company Reno, Nevada, NV) with a flow rate of 160 μL/h. The ion of interest was isolated using an isolation window of 4 Da before exposing them to the helium metastable beam. The low mass cut off (LMCO) during MAD was typically *m/z* 155 to prevent the accumulation of Penning ionized pump oil. The metastable beam was pulsed on for 30ms at an anode voltage of 7 kV. The FAB gun is attached to the main vacuum chamber lid, so the FAB gas pressure is indirectly measured by reading on the pressure monitor of the ion trap gauge in the main vacuum region. In all the experiments, the FAB gas supply was adjusted to provide a reading of ~1.20×10^{-5} mbar.

A typical MS^2 MAD experiment included 0.5 minutes of isolation of precursor ion, 2 minutes of He-MAD of the precursor ion and 0.5 minutes of He-MAD background signal (ESI source off while MAD source on). A typical MS^3MAD/CID experiment consisted of an additional 0.5 minutes of isolation of precursor ion at MS^3 stage and 4 minutes of CID reaction at MS^3 stage with an amplitude of 0.35V. AnMS^2 CID experiment included 0.5 minutes of isolation of precursor ion and 4 minutes of CID reaction. All the mass spectra collected during the isolation period or fragmentation period were averaged to improve the signal to noise ratio (S/N). The averaged

fragmentation spectra additionally underwent background subtraction for the removal of unwanted background noise.

5.3 Results and Discussion

5.3.1 MAD of POPC in Protonated, Sodiated and Potassiated Forms

Figure 5.1 shows the Helium MAD (He-MAD) spectra of the protonated, sodiated and potassiated forms of POPC. Upon the interaction with metastable helium atoms, the protonated form of POPC produces a variety of cleavages along the acyl chains. The 14 Da increments resemble high-energy CID (HE-CID) spectra, which suggests that a charge-remote-like mechanism is taking place in this process [169-171]. Conversely, MAD of the metal-adducted forms rarely cleaves the acyl chains, but instead forms abundant fragment ions arising from the glycerol backbone and head group. These results show how the adducting species of the precursor ion has a significant influence on the MAD fragmentation patterns, as has been observed qualitatively for CID of phosphocholines [158, 159]. Relative to the protonated precursor, the presence of metal adducts (i.e. Na^+ or K^+) appears to restrict the number of fragments within the acyl chains (i.e. in the region *m/z* 550-750).

He-MAD spectra of all the three forms show a predominant peak at *m/z* 184.0 (or 184.1), corresponding to the formation of the low-energy phosphocholine ion [159]. Distinctive peaks at *m/z* 380.2 and 391.5 are observed from both protonated and sodiated forms of POPC, respectively, which are the characteristic 2+ Penning ionized product ions [137, 169]. The 2+ Penning ionized product is not observed in the He-MAD spectrum of potassiated POPC.

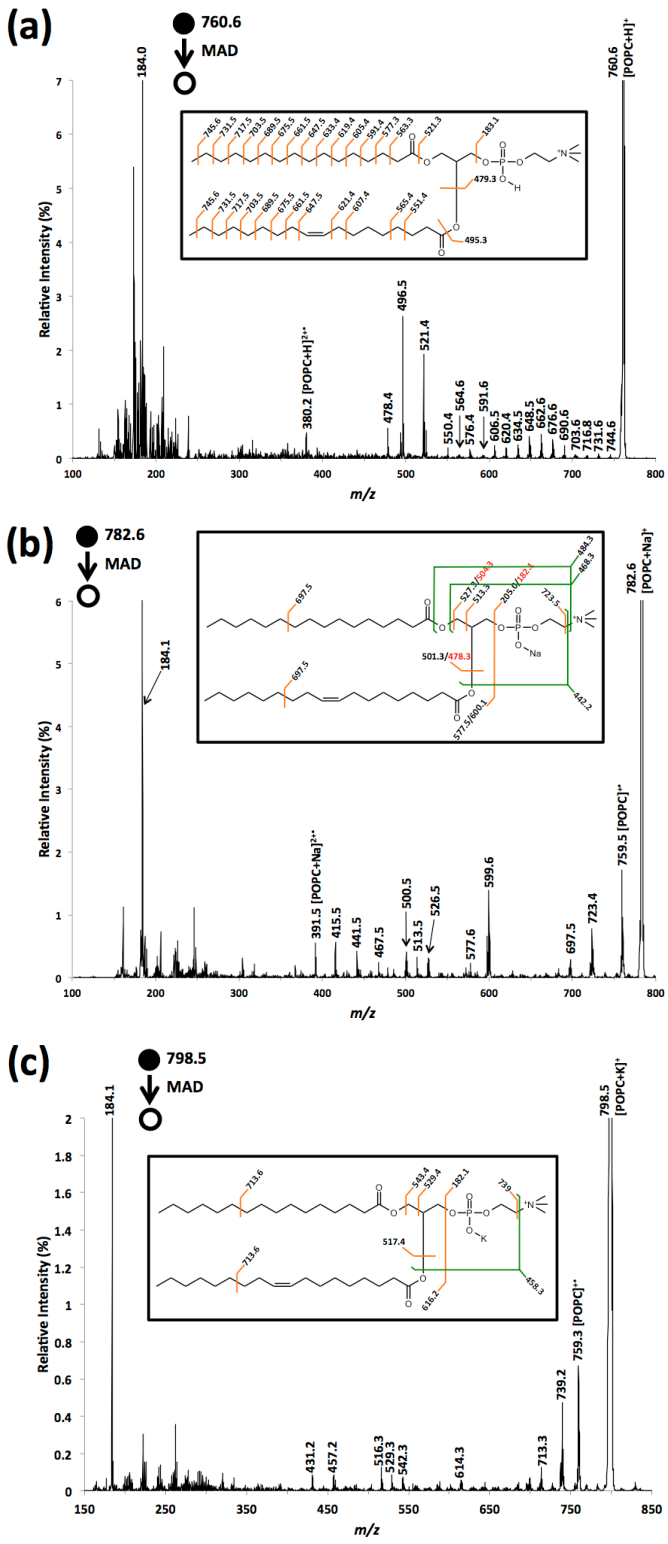

Figure 5.1. He-MAD spectra of (a) protonated form of POPC, (b) sodiated form of POPC, (c) potassiated form of POPC. Insets show possible cleavages and theoretical masses for fragmentations without hydrogen rearrangements.

In the He-MAD spectrum of protonated POPC, ions at *m/z* 478.4, 496.5 and 521.4 are also observed, which correspond to the loss of the sn-2 fatty acid (18:1, -282 Da) as well as the loss of acyl chains as ketenes from sn-2 (18:1, -264 Da) and sn-1 (16:0, -239Da) positions, respectively. These fragments are commonly observed in low energy CID experiments [159], but also observed in the lipidomic analysis using a LC-MS^E approach [172]. He-MAD of metal-adducted POPC produces similar sn-1 and sn-2 cleavages as well. In addition, MAD product ions corresponding to two covalent cleavages are also observed, such as the simultaneous loss of the sn-2 acyl chain and either trimethylamine ($N(CH_3)_3$) or phosphocholine head group for both sodiated and potassiated POPC.

He-MAD of the sodiated and potassiated precursors of POPC both give strong molecular ions at *m/z* 759.6. The $[POPC]^{+\bullet}$ molecular ion is not readily observable in the product ion spectrum of the protonated precursor, which could be due to several reasons: 1) the mass resolution is compromised because of the space charge effects of the abundant precursor ion at *m/z* 760.6 [1], and 2) the loss of a hydrogen is far less favorable than the loss of sodium or potassium. Although the product at *m/z* 759.6 ($[POPC]^{+\bullet}$) is obscured by the more-dominant ($[POPC+H]^+$) at *m/z* 760.6 in the He-MAD spectrum of $[POPC+H]^+$, the product ion at *m/z* 759.6 could be effectively isolated using the standard isolation procedure of the Bruker ion trap. Mass isolation uses slower scan speeds than mass acquisition, so achieves superior mass resolution. Evidence for the formation of $[POPC]^{+\bullet}$ from $[POPC+H]^+$, via the loss of $H^\bullet$, is presented in Figure 5.2a. The reaction presumably proceeds via the following mechanism:

$$He^M + [POPC + X^+]^+ \rightarrow He^0 + [POPC^{+\cdot} + X^\cdot]^{+\cdots} \rightarrow POPC^{+\cdot} + X^\cdot \qquad (1)$$

where X = H, Na or K; He^M is the helium metastable atom and He^0 is the helium ground state atom. In reaction 1, the electron released from Penning ionization of the lipid is effectively captured by the charging cation, which subsequently dissociates because of the significantly reduced bond strength.

Reaction (1) is also in competition with straightforward Penning ionization product shown in reaction (2):

$$He^M + [POPC + X^+]^+ \rightarrow He^0 + [POPC^{+\cdot} + X^+]^{2+\cdot} + e^- \qquad (2)$$

The 2+ product ions of reaction (2) are a prominent feature in the He-MAD spectra when X = H^+ and Na^+, but is not observed when X = K^+. The preference for reaction (1) vs. reaction (2) is probably dependent on the combined effects of electron affinity, electron capture cross section and bonding energy. The potassiated adduct clearly favors internal electron capture through reaction (1), despite the fact that it has the lowest electron affinity of the three cations. At present, we can only speculate that the binding energy of the cations is a dominant factor in these reactions [173] and conformational differences being a possible secondary factor [174]. Potassium has the lowest binding affinity for POPC of the three cations and is most readily lost [173].

Isolation and collisional activation of $[POPC^{+\cdot} + Na^+]^{2+\cdot}$ at *m/z* 391.5 resulted in charge separation and a dominant radical molecular ion of $[POPC]^{+\bullet}$ at *m/z* 759.6, as shown in reaction (3).

$$[POPC^{+\cdot} + Na^+]^{2+\cdot} \xrightarrow{CID} POPC^{+\cdot} + Na^+ \qquad (3)$$

Collisional activation of the protonated radical dication at *m/z* 380.2 yielded many abundant fragments, but did not provide the radical molecular ion through reaction (3). These observations indicate that a variety of competing reactions occur during He-MAD,

and the adducting cations show evidence of both capturing and not capturing the free electron from Penning ionization of the lipid. Potassium seems to have the largest electron capture cross section despite its smallest electron affinity.

5.3.2 MAD-MS^3 CID of POPC in Protonated, Sodiated and Potassiated forms

Figure 5.2a shows the isolated $[POPC]^{+\bullet}$ product peak at *m/z* 759.6 following He-MAD of $[POPC+H]^+$. The observation of a "companion" product ion at *m/z* 791.5 in the isolation spectrum of $[POPC]^{+\bullet}$ is evidence for the oxidation of the radical cation with background oxygen in the trap. McLuckey and coworkers have documented the enhanced reactivity of radical peptide cations towards oxidation with residual oxygen [175]. The observation of $([POPC]^{\bullet}+O_2)^+$ ion is indicative of a distonic radical ion structure for a certain population of $[POPC]^{+\bullet}$, in which the radical is distributed among a variety of locations that are "far" away from the charge site. Scheme 1 shows 4 examples of the possible isomeric structures of $[POPC]^{+\bullet}$ ion. Blanksby and coworkers [135, 166] have reported the study of lipids and fatty acid derivatives using radical-directed dissociation (RDD), in which a variety of radical sites were proposed to rationalize various fragments arising from radical-directed processes, e.g. isomeric structure (1) rationalizes the formation of the fragment at *m/z*537.5; isomeric structure (2) rationalizes the fragment at *m/z* 550.5; (3) and (4) are consistent with the formation of fragment ion pair at *m/z* 632.5 (α-allylic H-abstraction pathway) and *m/z*634.4 (ω-allylic H-abstraction pathway), vide infra [135, 166].

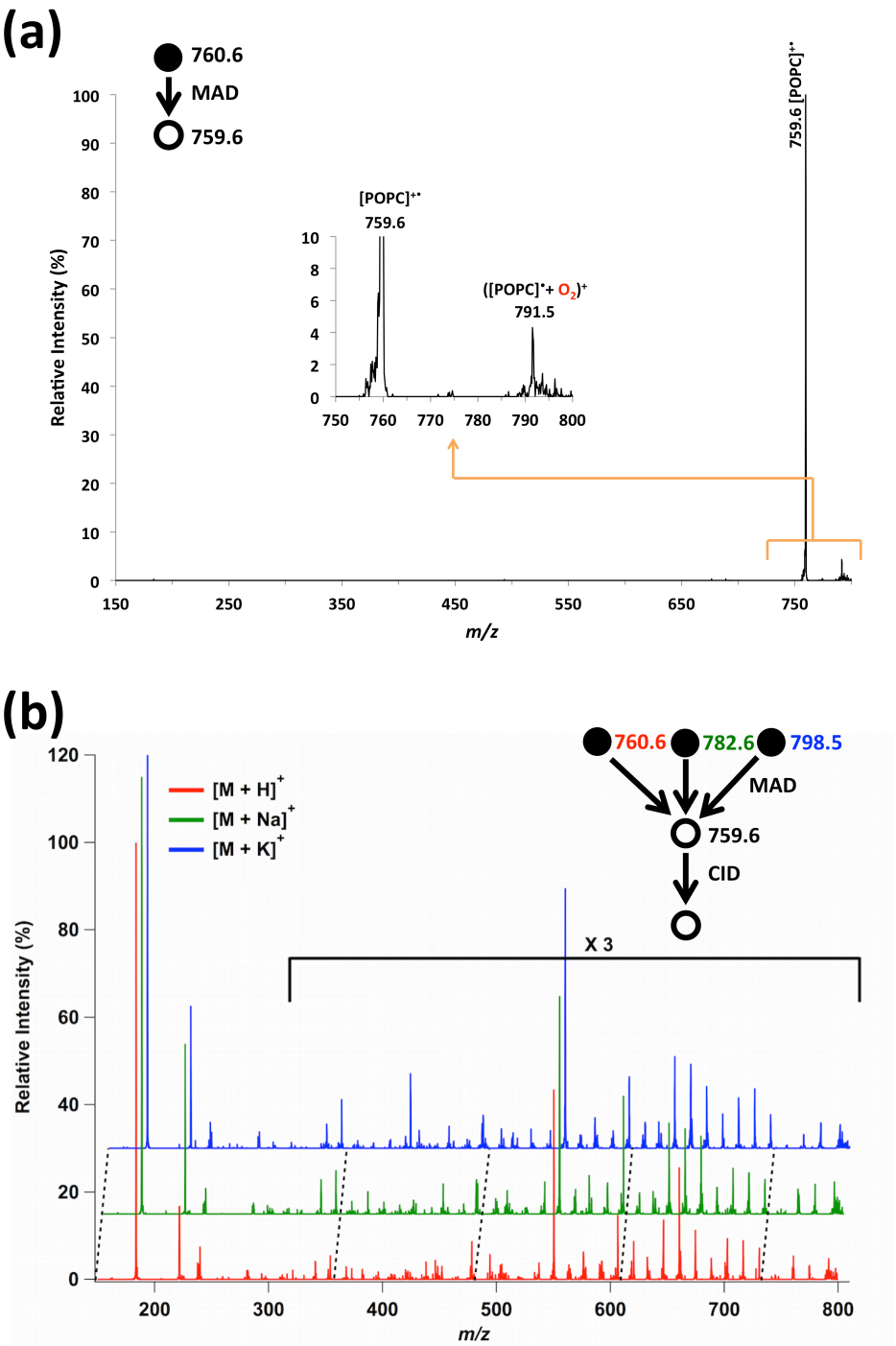

Figure 5.2. Panel (a): Example of an isolation spectrum for the $[POPC]^{+\bullet}$ cation at *m/z* 759.6 from He-MAD of protonated form of POPC. Inset in panel (a) shows the magnified spectrum of the *m/z* range of interest. Panel (b): Waterfall plot to show the similarities of the MS^3 CID spectra of the same intermediate in panel a from the protonated, sodiated and potassiated forms of POPC.

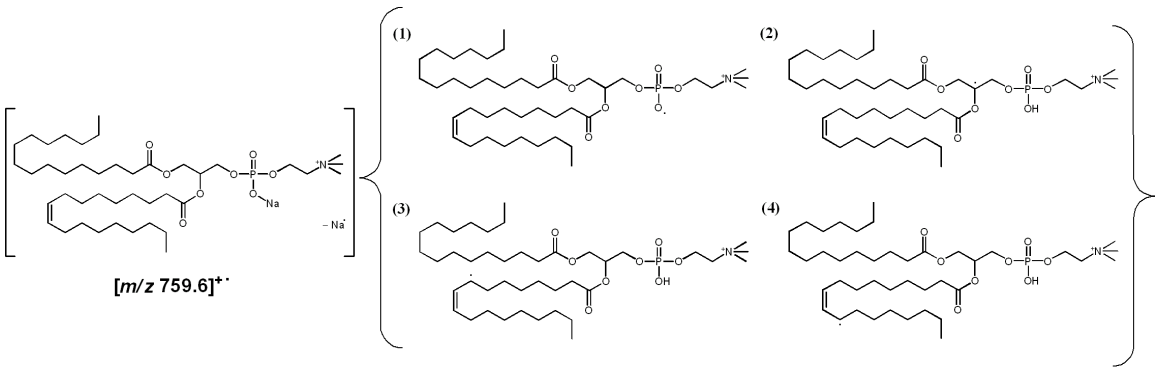

Scheme 5.1. Examples of possible isomeric structures of radical ion at *m/z* 759.6.

Different from their adducted parent ions, intermediates at *m/z* 759.6 produce almost indistinguishable fragmentation patterns at the MS^3level of fragmentation, regardless of whether the intermediate originates from the protonated, sodiated or potassiated forms of POPC (Figure 5.2b). The similarities in the CID spectra of the *m/z* 759.6 intermediate indicate that the intermediates are constitutionally similar radical cations. Whereas the adduct ions clearly affect the distribution of first-generation fragment ions in MAD (Figure 5.1), the isolated $[POPC]^{+\bullet}$ ions produced via MAD apparently have almost no memory of the original adducting species.

5.3.3 MAD-MS^3 CID of $[POPC+Na]^+$ vs. MAD of $[POPC+H]^+$

Figure 5.3a is a magnification of the MAD spectrum of sodiated POPC in Figure 5.2b and serves as an exemplar CID spectrum of $[POPC]^{+\bullet}$ (*m/z* 759.6). Figure 5.3b shows the He-MAD spectrum of $[POPC+H]^+$ (*m/z* 760.6), without CID. The two spectra are similar in that they both display fragmentation within the acyl chains, but distinct in that the relative abundance distribution of fragments is vastly different. The series of peaks labeled in black font from *m/z* 646.5 through 730.5 show clear 14 Da increments, and both acyl chains can contribute to these fragment ions. The double bond at the Δ9

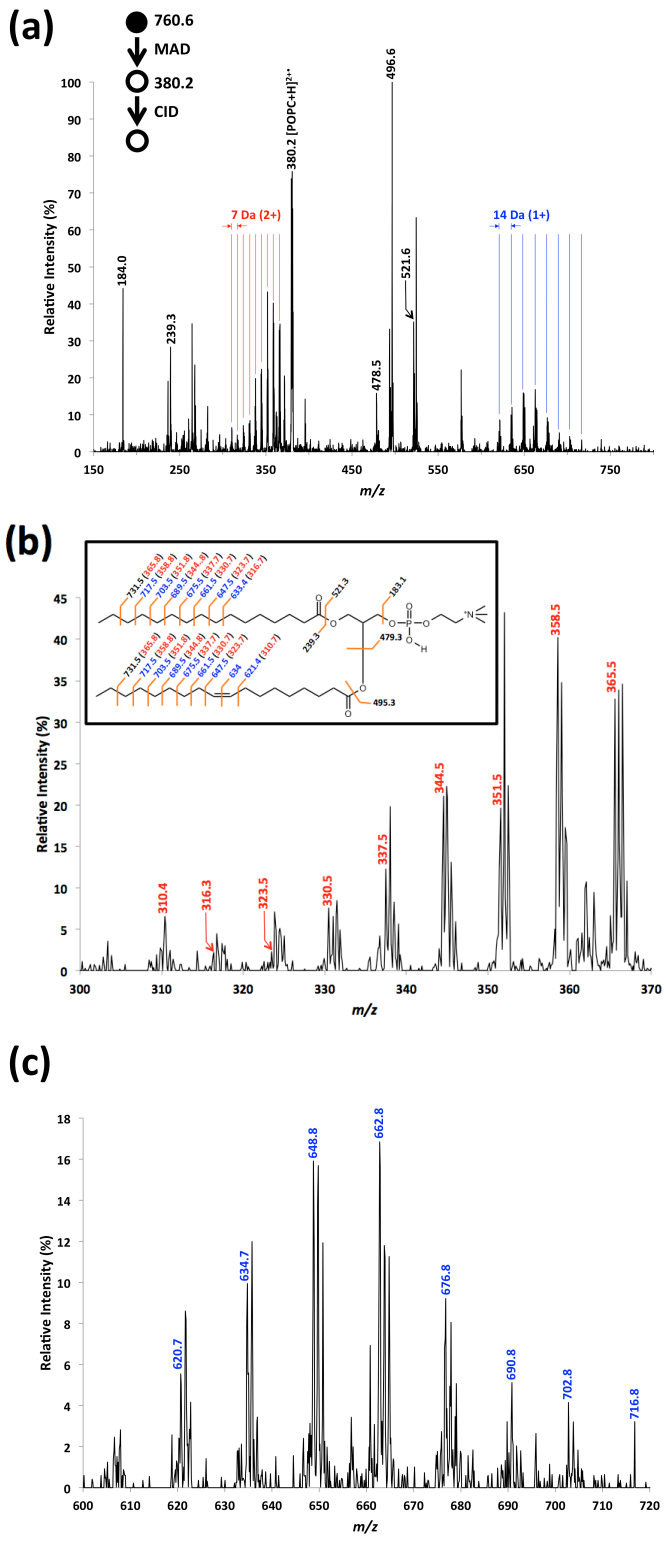

Figure 5.3. MS^3 CID spectrum of $[POPC+H]^{2+\bullet}$ derived from He-MAD of protonated POPC is shown in panel (a). The *m/z* ranges of interest are magnified and shown in panel (b) and (c).

position of the sn-2 acyl chain makes the acyl fragments differ in mass below *m/z* 646.5, so the fragments can be linked to each acyl chain. For example, the fragments labeled in blue font correspond to the losses from the saturated sn-1 chain, and the fragments labeled in green are for the unsaturated sn-2chain. This very pattern has also been observed in EIEIO spectra of phosphatidylcholines reported by Baba and coworkers [cite new EIEIO of lipids]. For the saturated sn-1 chain, the near complete fragmentation pattern was highly analogous to that of collisional activation of $[FAMEs]^{+\bullet}$ derived from EI [176]. The only difference lies in the lack of cleavage of the C4-C5 bond and the appearance of McLafferty rearrangement-type fragment at *m/z* 563.4. For the unsaturated sn-2 chain, alkylene moiety fragments at *m/z* 620.5 and 632.5 are characteristically spaced by 12 Da, while the rest of the acyl chain fragments exhibit a spacing of 14 Da. This diagnostic feature (the discrepancy in spacing between fragment derived from saturated and unsaturated moieties) serves an unambiguous identification of the double bond location, which has been long and widely utilized in elucidating unsaturation and branching sites in lipids and fatty acid derivatives [135, 166]. An interesting fragment ion pair at *m/z* 632.5 and 634.4 was observed, corresponding to 127 Da neutral loss of saturated $^{\bullet}C_9H_{19}$ and 125 Da neutral loss of unsaturated $^{\bullet}C_9H_{17}$) radicals respectively. The similar "doubled peak" pairs have been reported in the study using RDD for differentiation of lipid isomers, the formation of which has been rationalized via 1,4-hydrogen transfer, 1,6-elimination and β-scission [135, 166].

The MS^3 CID spectrum of $[POPC]^{+\bullet}$ is dominated by fragments of the sn-2 unsaturated chain, including peaks at *m/z* 477.4, 478.5, 550.5 and 606.6. The peak at *m/z* 550.5 is consistent with a 1,4-hydrogen shift and gamma cleavage relative to the sn-2

carbonyl group (Scheme 5.2). The peak at *m/z* 537.5 originated from McLafferty rearrangement of the proposed radical structure (2) in Scheme 5.1. The corresponding fragmentation pathway is shown in Scheme 5.3 and equation (4). The two similar products from the saturated acyl chain in the sn-1 position were observed as well (*m/z* 576.4 and *m/z* 563.4).

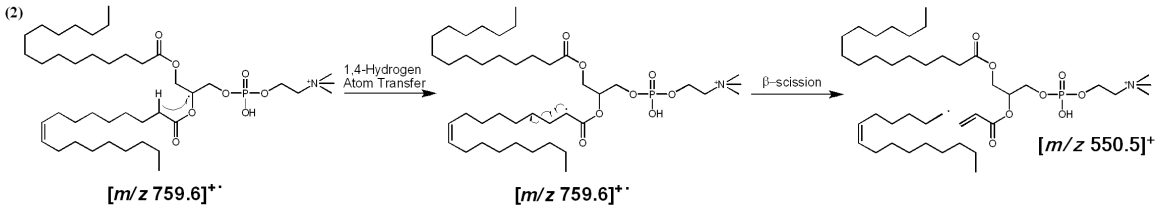

Scheme 5.2. Proposed fragmentation pathways for the formation of product ion at *m/z* 550.5.

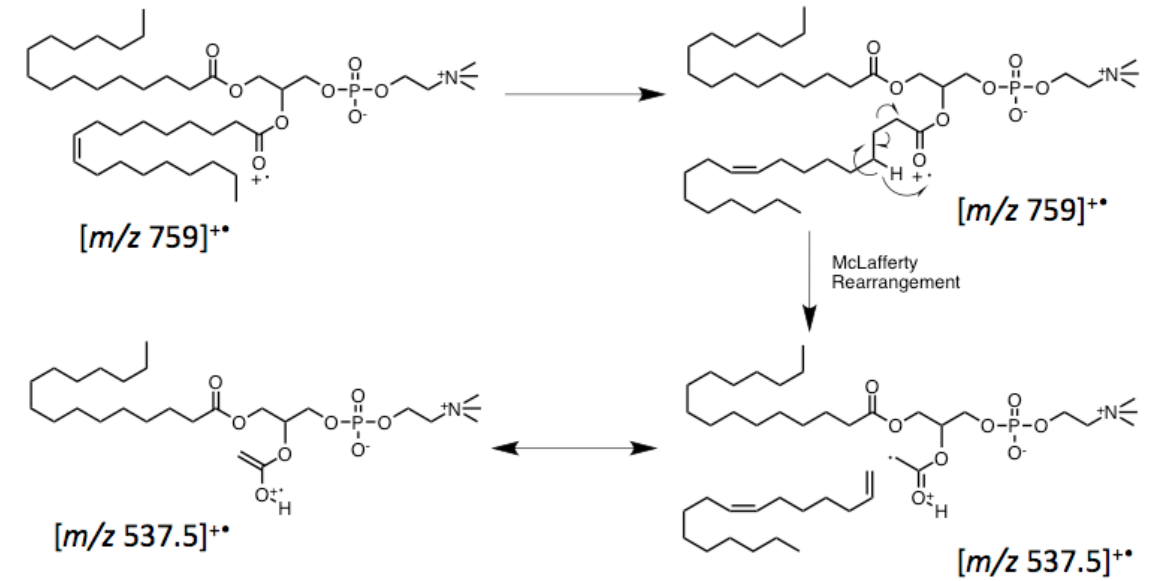

Scheme 5.3. Proposed fragmentation pathway for the formation of product ion at *m/z* 537.5.

$$[POPC^0 + Na^+] \xrightarrow{CTD} < POPC^{+\cdot} + e^- + Na^+ > \xrightarrow{CTD} POPC^{+\cdot} + Na^{\cdot} \quad (4)$$

In contrast to CID of the radical ion $[POPC]^{+\bullet}$, the He-MAD spectrum of $[POPC+H]^+$ shows dominant sn-1 and sn-2 glycerol backbone cleavages at *m/z* 496.5 and 521.4, which have been described elsewhere [169]. It is noteworthy that the MS^3 He-

MAD/CID spectrum in Figure 5.4a has superior signal-to-noise ratio than the MS^2 He-MAD spectrum in Figure 5.4b. The MS^3 He-MAD/CID spectrum selectively promotes radical-induced fragmentations over background noise and competing mechanisms/pathways.

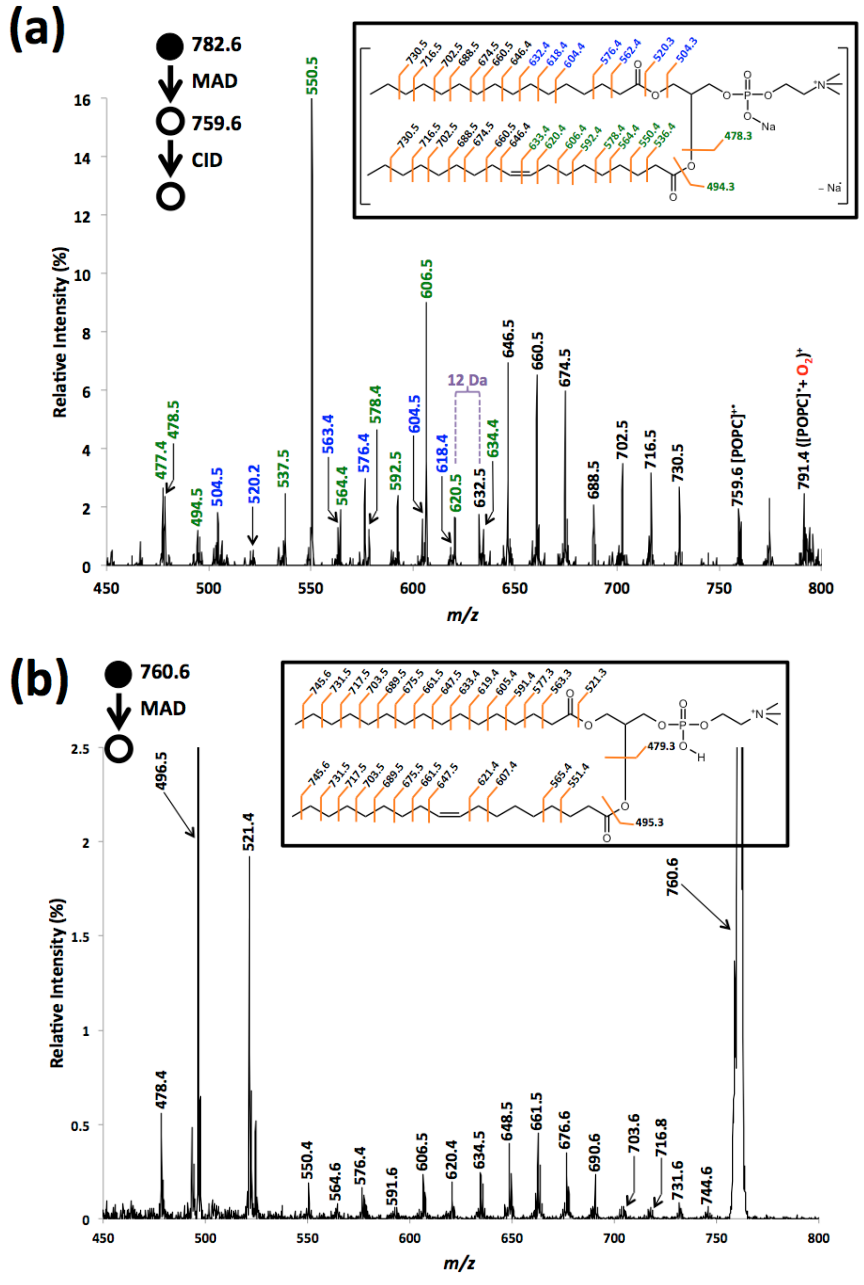

Figure 5.4. Magnified spectra of (a) MS^3 CID of radical cation at *m/z* 759.6 from He-MAD of sodiated form of POPC, (b) He-MAD of protonated form of POPC.

5.3.4 MAD-MS^3 CID of $[POPC+Na]^+$ vs. CID of $[POPC+H]^+$

Figure 5.5 compares a CID spectrum of the radical cation of POPC with a CID spectrum of even-electron $[POPC+H]^+$ cations at two different amplitudes. Using a CID amplitude of 0.35 V, the odd-electron $[POPC]^{+\bullet}$ precursor produced near-complete fragmentation of the lipid (as discussed in Figs 5.2 and 5.3). However, using the same CID amplitude of 0.35 V, the even electron $[POPC+H]^+$ precursor only produced two weak product ions: the loss of trimethylamine ($N(CH_3)_3$) and the loss of entire head group. Using a CID amplitude of 0.38 V (Fig 5.4c), the even-electron $[POPC+H]^+$ ion dissociated into more fragment ions with better efficiency, but with a significantly different distribution of product ions from the radical intermediate. When subjected to collisional activation, the odd-electron ion clearly has a significantly lower activation barrier than the even-electron precursor. Similar differences in collisional activation energies have been observed for the radical $[M+2H]^{+\bullet}$ precursors versus even-electron $[M+H]^+$ precursors of peptide ions [177].

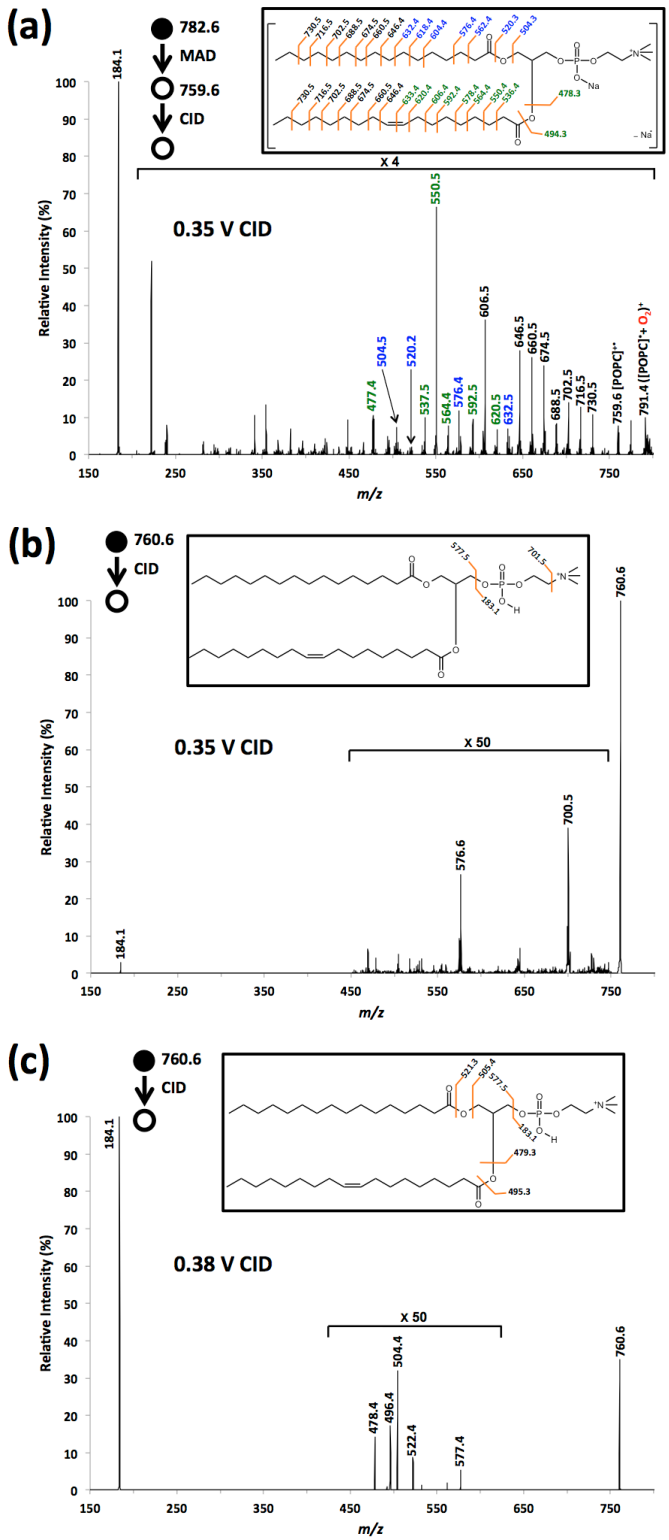

Figure 5.5. (a) MS^3 CID spectrum of the radical cation at *m/z* 759.6 from He-MAD of sodiated POPC ($[POPC+Na]^+$); (b) CID spectra of protonated form of POPC ($[POPC+H]^+$) with the same activation voltage (0.35 V)* as that in (a); (c) same as (b), but with higher activation voltage (0.38 V). *See experimental for details.

Figure 5.6 shows the magnified mass spectra of both MS^3 CID of $[POPC]^{+\bullet}$ and CID of $[POPC+H]^+$. When starting with even-electron precursor $[POPC+H]^+$ (Fig 5.6b), CID only produces even mass even electron fragments in this region. The commonly observed fragments at 478.4 and 496.4 are from sn-2 cleavages and the fragments at *m/z* 504.4 and 522.4 are from sn-1 cleavages. CID of the radical precursor $[POPC]^{+\bullet}$ provides similar cleavages around sn-1 and sn-2 positions, but with the presence of odd mass/radical fragments. In the case of potassiated and sodiated POPC, the more complicated spectra and poorer signal to noise ratios in the MS^3 spectrum makes conventional CID a superior tool for assessing the acyl chain lengths and degrees of unsaturation. However, the ability to first convert the protonated, sodiated and potassiated precursor ions to a generic radical molecular ion intermediate, then perform CID to fragment within the acyl chains provides a rather unique gas-phase ion manipulation tool for the structural interrogation of phospholipids.

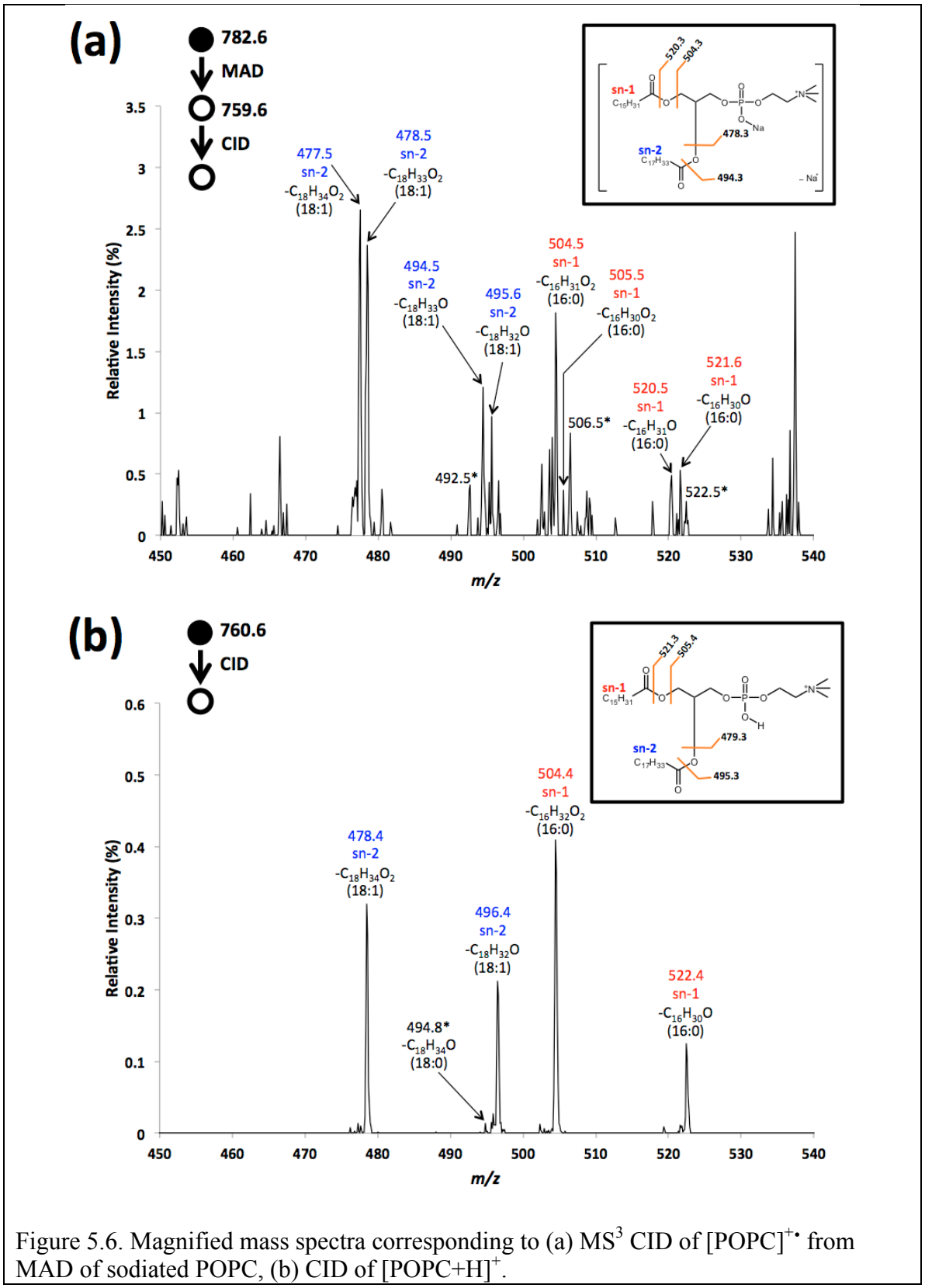

Figure 5.6. Magnified mass spectra corresponding to (a) MS^3 CID of $[POPC]^{+\bullet}$ from MAD of sodiated POPC, (b) CID of $[POPC+H]^+$.

CHAPTER 6: APPLICATION OF CHARGE TRANSFER DISSOCIATION (CTD) TO OTHER BIOANALYTICAL STUDIES

6.1 Charge Transfer Dissociation (CTD) of Lipids with Varying Head Groups

6.1.1 Introduction

Due to the critical biological relevance of phospholipids, enormous efforts have been put into the development and application of novel techniques and methodologies for obtaining their structural information (see Chapters 2 and 4). In addition to phospholipids, researchers have also investigated the structural analysis of lipids with other head groups, which have different biological and biochemical functions. Hsu and Turk showed that the lipid head group greatly affects CID fragmentation pattern in low-energy collision-induced dissociation experiments [36, 122]. McLuckey and coworkers made use of differential reactivity of phosphatidylcholine (PC) and phosphatidylethanolamine (PE) during a gas-phase ion/ion reaction to successfully separate the two lipid classes into distinct *m/z* ranges. The ability to manipulate the charge state of the lipid class according to their head group significantly improved the signal-to-noise (S/N) ratio for the detection of PCs and PEs [132]. Performance evaluation of charge transfer dissociation (CTD) on phosphocholine (PC) lipids was presented in Chapter 4, so this chapter is solely devoted to the investigation of CTD behavior of lipids with other head groups— phosphatidic acid (PA), phosphatidylserine (PS), phosphatidylglycerol (PG) and phosphatidylinositol (PI).

6.1.2 Experimental

The instrumentation and acquisition method were the same as detailed in Chapter 4.

All the lipids used in this experiment were purchased from Avanti Polar Lipids (Alabaster, AL). The involved lipids and their shorthand designations are as follows: L-α-phosphatidic acid (Egg, Chicken) (sodium salt)—PA, L-α-phosphatidylserine (Brain, Porcine) (sodium salt)—PS, L-α-phosphatidylglycerol (Egg, Chicken) (sodium salt)—PG, and L-α-phosphatidylinositol (Soy) (sodium salt)—PI. Lipid analytes were prepared at a concentration of ~60 μM in a solution of 49.5/49.5/1 (v/v/v) methanol/water/acetic acid or 49.5/49.5 (v/v) methanol/water with NaCl (final concentration aiming at ~1×10^{-3}mol/L) prior to positive electrospray ionization (ESI).

6.1.3 Results and Discussion

Figure 6.1 shows the structures of lipids that were subjected to CTD experiments in this section. To investigate the relationship between the adducting form of precursor ions and CTD fragmentation pattern, three adducting forms of PA solutions was prepared by adding acetic acid to protonate PA or sodium chloride to form the sodiated adduct.

The three adduct species studied were $[PA\text{-}Na+2H]^+$, $[PA+H]^+$, and $[PA+Na]^+$. After being directly infused into the Bruker mass spectrometer, the three adducting forms were mass-selected respectively, with each being exposed to collisional activation or Helium CTD. The corresponding MS/MS spectra are presented in Figure 6.2. CID of PA hardly produces any fragment ions, regardless of the charging adduct, except for a few cleavages solely on the glycerol backbone. For $[PA\text{-}Na+2H]^+$ and $[PA+H]^+$, CID broke the same C3-O bond, inducing an entire head group loss. For $[PA+Na]^+$, CID broke the C1-O and C2-O bonds, inducing the entire sn-1 and sn-2 acyl chain losses.

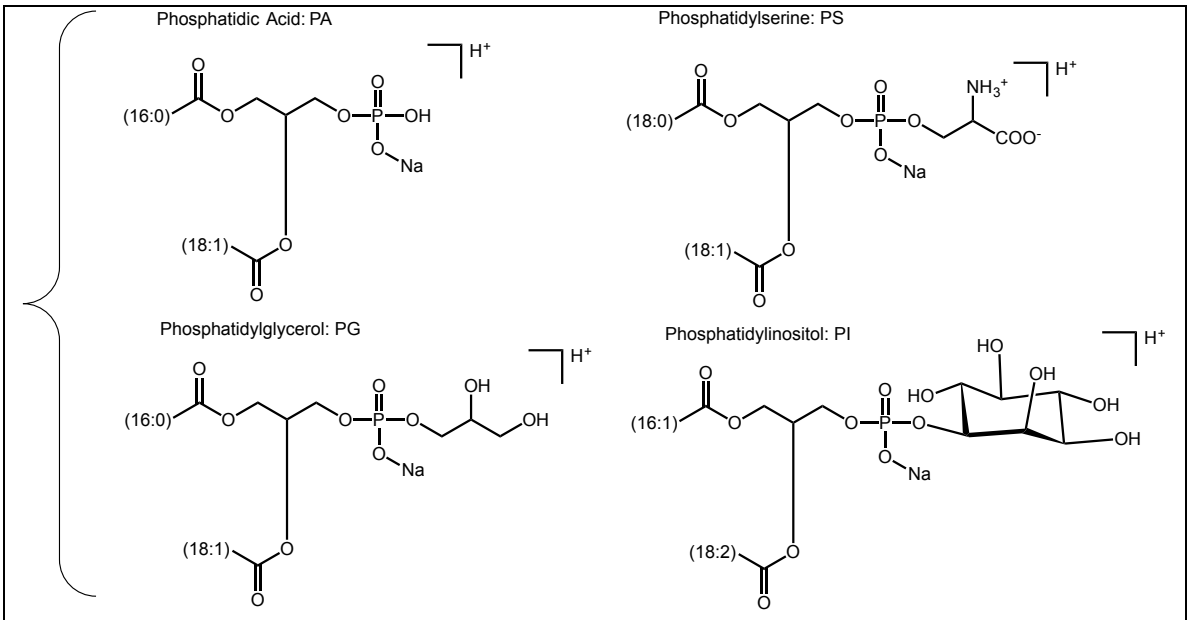

Figure 6.1. The structure of lipids involved in this study.

Different from the CID results, CTD produced a more enriched fragmentation pattern of the three adducting forms. CTD not only produced cleavages on the glycerol backbone, but also generated cleavages on the two acyl chains. The extent of acyl chain cleavage is dependent on the adducting form. Most cleavages were observed on $[PA+H]^+$, whereas fewer cleavages were observed for $[PA+Na]^+$. In addition to these fragment ions, a characteristic charge-increased product ion ($[PA+H]^{2+\bullet}$) was observed in the $[PA+H]^+$spectrum. This product originates from gas-phase oxidation, which was also observed in CTD of peptides (Chapter 2), CTD of bovine insulin (Chapter 3), and CTD of phosphocholine (PC) lipids (Chapter 4).

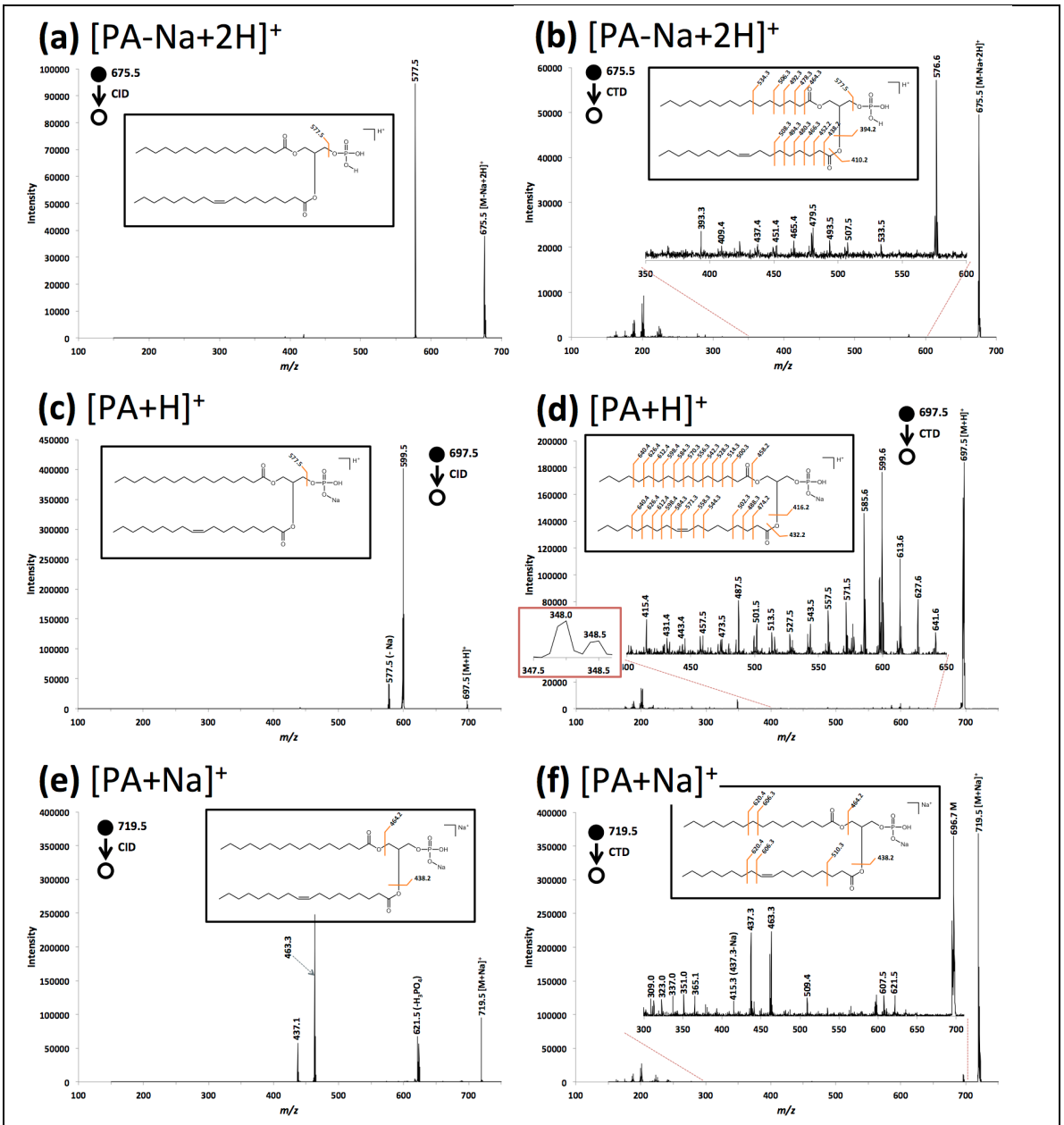

Figure 6.2. CID spectra of lipid PA: (a) $[PA\text{-}Na+2H]^+$, (c) $[PA+H]^+$, (e) $[PA+Na]^+$. CTD spectra of PA: (b) $[PA\text{-}Na+2H]^+$, (d) $PA+H]^+$, (f) $[PA+Na]^+$. The insets show possible fragment ions assuming no hydrogen rearrangements.

Given that the protonated-adducting form produced the most cleavages under CTD, the following CID/CTD examinations on PS, PG, and PI were all preformed on the protonated form of each lipid. The corresponding MS/MS spectra are shown in Figure 6.3, Figure 6.4, and Figure 6.5.

CID of $[PS+H]^+$ (Figure 6.3a) produced three cleavages around the lipid head group. The fragment ion at *m/z* 645.5 was accompanied by two fragment ions at *m/z* 627.5 (645.5-H_2O) and at *m/z* 605.5 (645.5-Na-H_2O). CTD of $[PS+H]^+$ (Figure 6.3b)

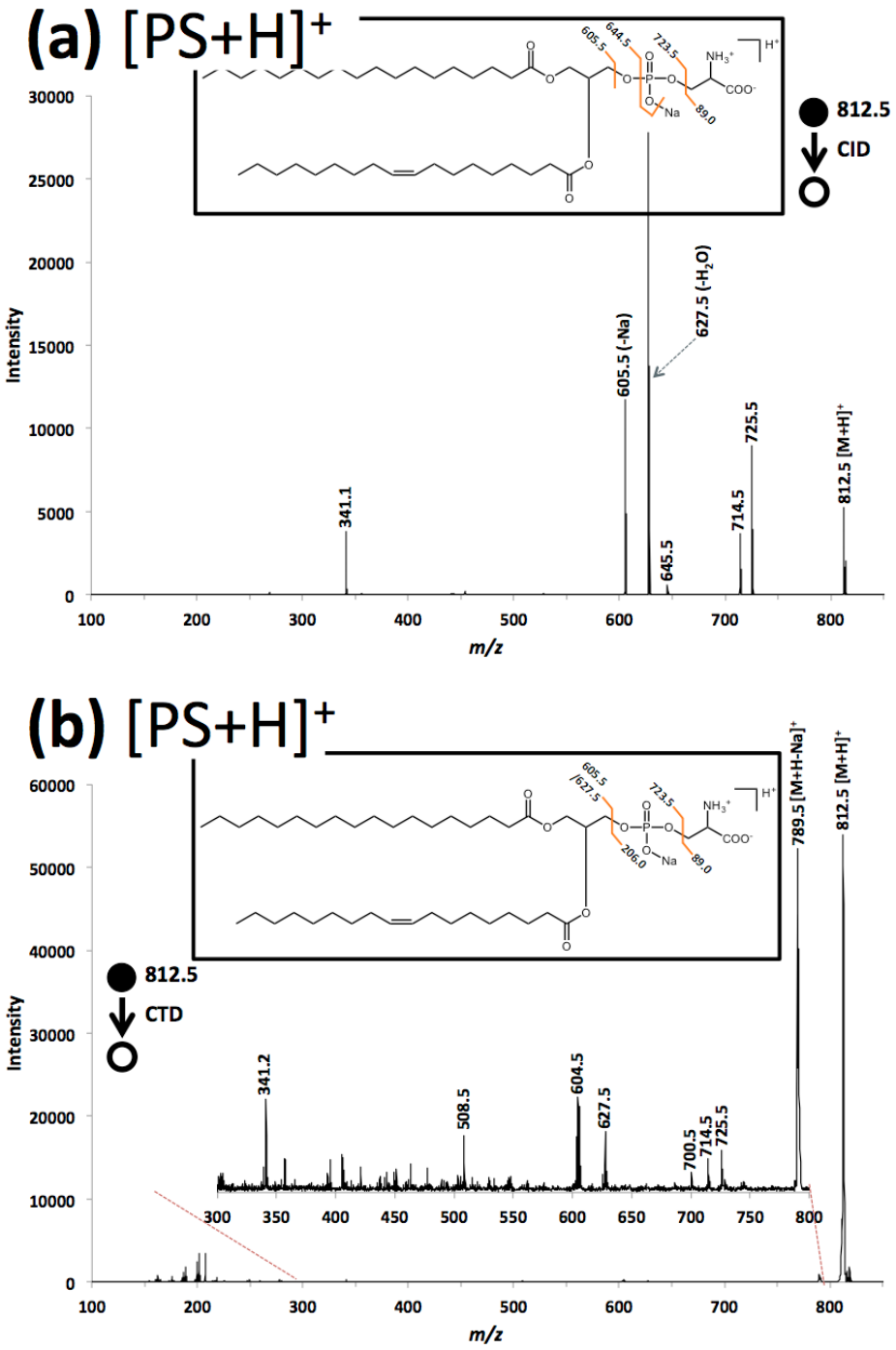

Figure 6.3. (a) CID spectrum of $[PS+H]^+$; (b) CTD spectrum of $[PS+H]^+$.

produced two cleavages around the lipid head group, which are analogous to the CID spectrum. The fragment ion pair at *m/z* 627.5 and at *m/z* 604.5 (627.5-Na) shows consistency with that observed in the CID spectrum.

CID of $[PG+H]^+$ (Figure 6.4a) produced two cleavages around the lipid head group. Similar to the CID spectrum of $[PS+H]^+$, a fragment ion set at *m/z* 617.6, *m/z* 599.6 (617.5-H_2O), and at *m/z* 577.6 (617.5-Na-H_2O) were also observed. CTD of $[PG+H]^+$ (Figure 6.4b) produced one cleavage on the glycerol backbone as well as several cleavages on the lipid acyl chains, which greatly differs from CTD spectrum of $[PS+H]^+$. Consistent with CTD spectrum of $[PA+Na]^+$, the gas-phase oxidation product ion at *m/z* 385.0 ($[PG+H]^{2+\bullet}$) was observed, which confirms the oxidative mechanism is occurring.

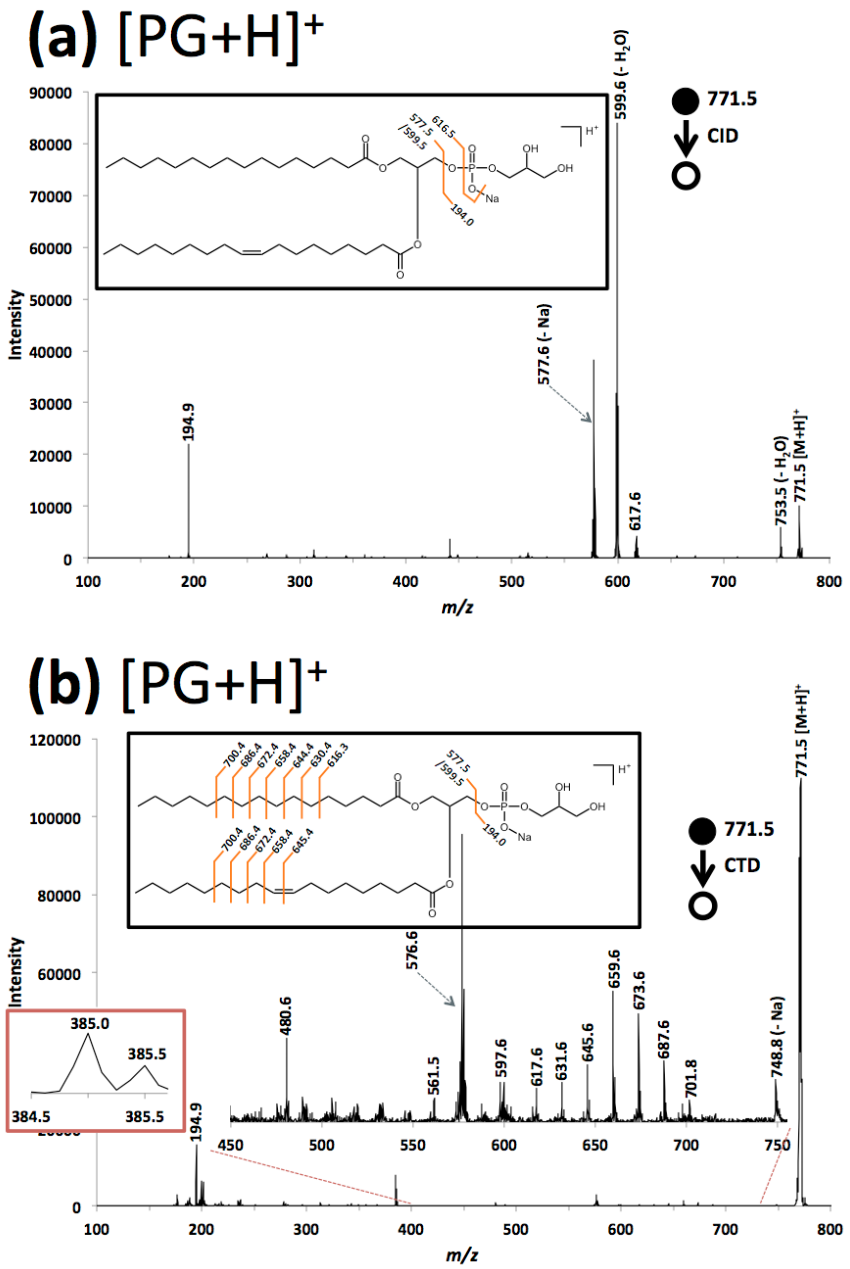

Figure 6.4. (a) CID spectrum of $[PG+H]^+$;(b) CTD spectrum of $[PG+H]^+$.

Analogous to CID results of $[PS+H]^+$ and $[PG+H]^+$, CID of $[PI+H]^+$ (Figure 6.5a) produced two cleavages around the lipid head group, along with a fragment ion set at *m/z* 615.6, *m/z* 597.6 (615.6-H_2O), and at *m/z* 575.6 (615.6-Na-H_2O). Similar to CTD of $[PG+H]^+$, CTD of $[PI+H]^+$ (Figure 6.5b) also produced one cleavage on the glycerol

backbone as well as a few cleavages on the lipid acyl chains. In agreement with CTD spectra of $[PA+Na]^+$ and $[PG+Na]^+$, the gas-phase oxidation product ion at *m/z* 429.0 ($[PI+H]^{2+\bullet}$) was also observed.

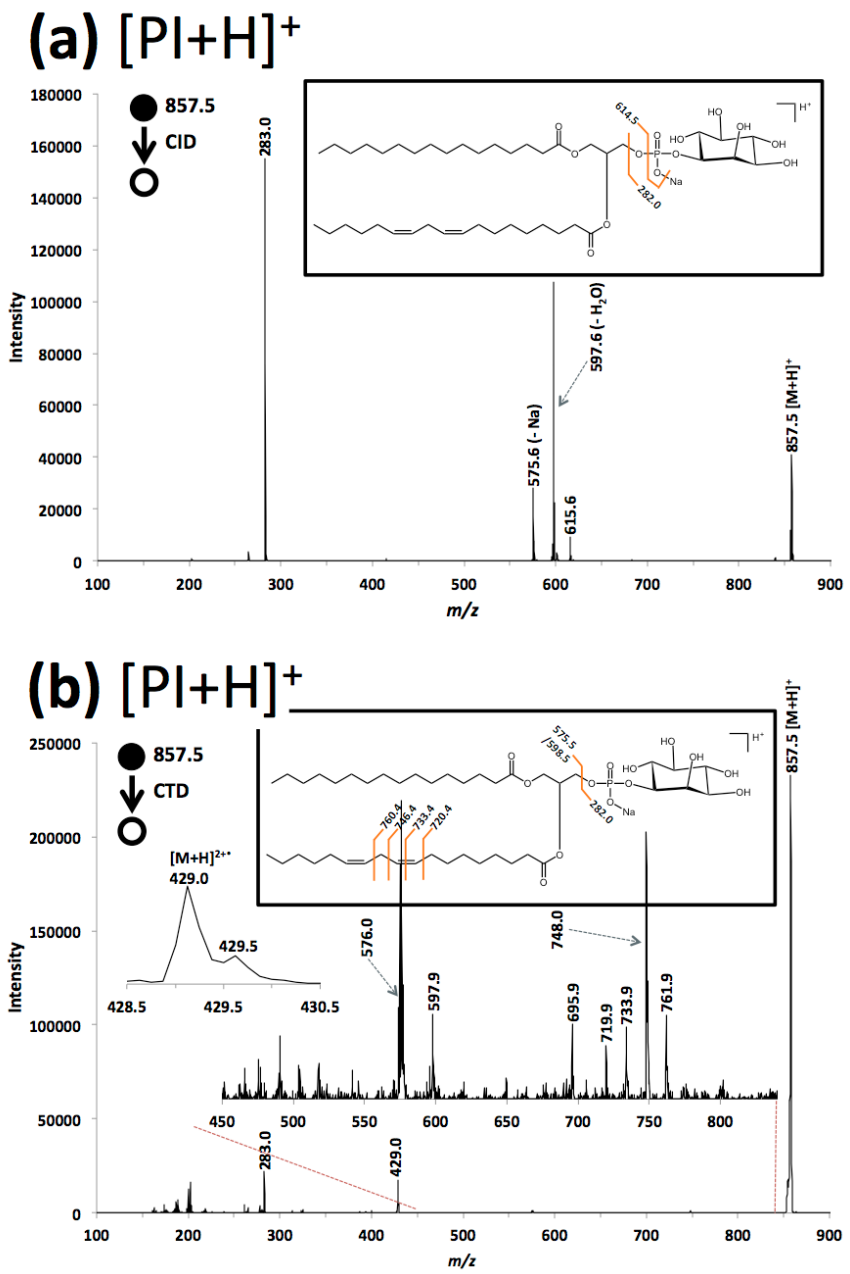

Figure 6.5. (a) CID spectrum of $[PI+H]^+$; (b) CTD spectrum of $[PI+H]^+$.

6.2 Charge Transfer Dissociation (CTD) of a Methylated Oligosaccharide

6.2.1 Introduction

One important aspect of oligosaccharides are that they comprise one of the most widespread post-translational modifications, including glycolipids, glycoproteins, etc. [52] Due to the critical biological relevance of oligosaccharides, researchers have developed a variety of strategies for their structural elucidation. Tandem mass spectrometry (MS/MS) is one of the fastest-developing techniques to fulfill this purpose.

As the most widely used MS/MS technique, low energy collision-induced dissociation (LE-CID) has been widely applied for characterization of oligosaccharides. LE-CID mainly produces between-ring cleavages, and its performance generally deteriorates with increasing oligomer size. Another drawback of LE-CID is the lack of cross-ring cleavages of oligosaccharides, which greatly limits the obtainable information regarding to branching pattern between the subunits [52]. LE-CID also tends to provide internal fragments, such as the loss of sugar residues form the reducing and non-reducing termini of the chain. LE-CID also results in abundant water losses and modification losses, such as methylated or sulfated groups.

To combat these issues with CID, photon-based and electron-based techniques have been investigated in detail. Using 193 nm ultraviolet photodissociation (UVPD), extensive between-ring and cross-ring cleavages are observed, along with double-cleavages, which provides valuable information for identification of oligosaccharides [52]. Electron detachment dissociation (EDD) produces abundant glycosidic and cross-ring cleavages, along with sufficient information for locating sites of sulfation [178].

Charge transfer dissociation (CTD) is a newly emerged MS/MS strategy, and has been successfully employed for the structural characterization of peptides and phospholipids. To assess its performance upon other biomolecules, an oligogalacturonan (DP5DM3) was subjected to a beam of helium cations. The resulting CTD spectra were discussed and compared with that of LE-CID and extreme ultraviolet photodissociation (XUVPD) in the following section [114].

6.2.2 Experimental

The XUVPD spectrum was collected by our collaborator, Dr. David Ropartz (INRA, UR1268 Biopolymers Interactions Assemblies, F-44316 Nantes, France). His group used a modified linear ion trap mass spectrometer (LTQ XL, Thermo Fisher), which was coupled with a synchrotron beamline at the SOLEIL synchrotron radiation facility in France. The LE-CID spectrum was also acquired on the same linear ion trap instrument. The experimental setup is detailed elsewhere [114].

The oligogalacturonan (DP5DM3) was provided by Dr. David Ropartz. A concentration of 10 μg/mL analyte solution was directly infused into the mass spectrometer, and all the resulting spectra were averaged for further analysis.

6.3.3 Results and Discussion

LE-CID mainly generated between-ring cleavages along the straight oligomer chain, most of which corresponds to fragments containing the reducing end of the oligosaccharide, as shown in the top panel of Figure 6.6. LE-CID only produced five cross-ring cleavages, three of which are $^{0,2}X$ fragment ions. Similar fragmentation pattern has been observed in CID results reported by Brodbelt et al. [52], Rogniaux et al. [179], etc. The lack of cross-ring fragmentation not only precludes the identification of sites of

post-translational modifications (PTMs), but also presents the potential limitation in elucidating the branching pattern of highly branched oligosaccharide samples in the future.

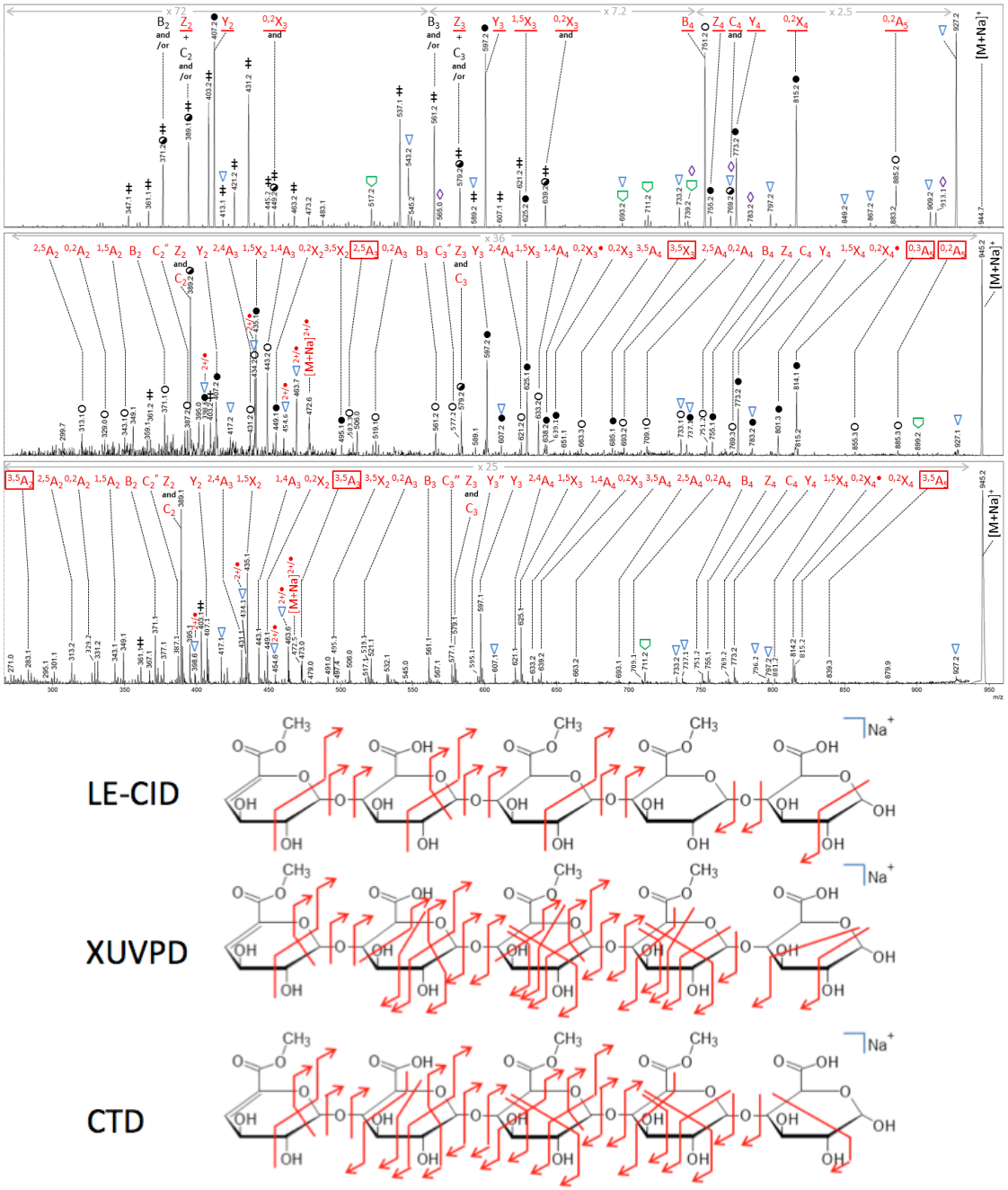

Figure 6.6. MS/MS spectra and fragment maps of (top) LE-CID, (middle) XUVPD, and (bottom) CTD upon $[DP5DM3+Na]^+$. Reproduced from reference [114] with permission.

The scenario is completely different when subjecting $[DP5DM3+Na]^+$ to extreme ultraviolet photon activation at 69 nm (photon energy = 18eV) or a beam of ~6 keV helium cations (electron affinity = 24.6 eV). In the second and third panels of Figure 6.6, XUVPD and CTD spectra greatly resemble each other, but significantly differ from that of LE-CID. Both techniques produced an enriched cross-ring fragmentation pattern, along with extensive between-ring fragmentation pattern. With this feature, XUVPD and CTD can provide more structural information for the unambiguous identification of oligosaccharides. Another highlight is the significant reduced number of dual-cleavages (i.e. double fragmentation) during XUVPD and CTD. LE-CID spectrum shows an abundant fragment ion at *m/z* 537.1, which may originate from the simultaneous cleavage of $^{0,2}A_4/Y_5$ or $^{0,2}A_5/Y_4$ (Figure 6.7). This ambiguity can be completely eliminated in XUVPD and CTD experiments.

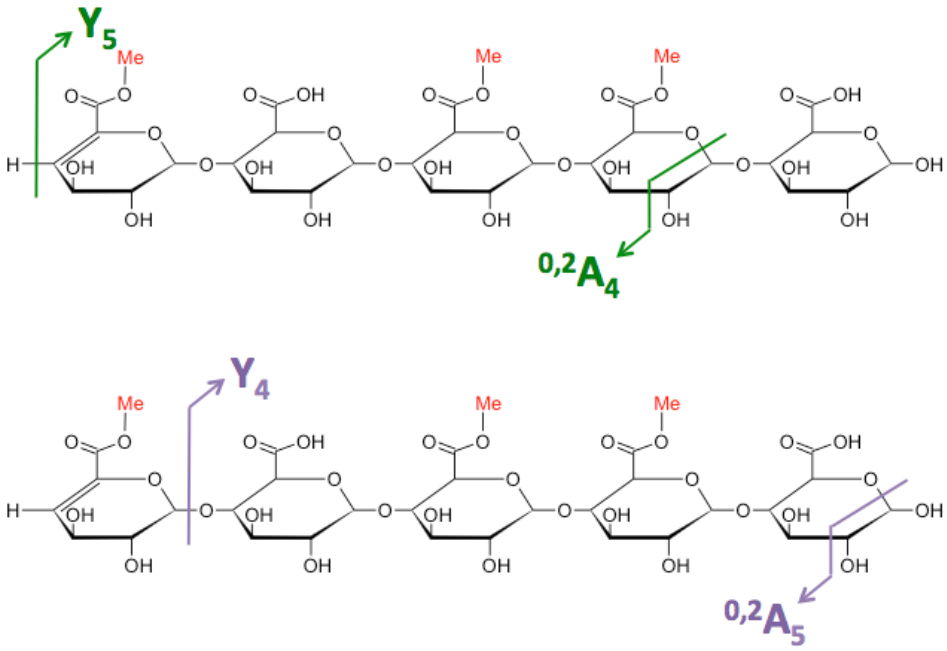

Figure 6.7. The possible dual-cleavages for the generation of *m/z* 537.1: $^{0,2}A_4/Y_5$ (top) and $^{0,2}A_5/Y_4$ (bottom).

The remarkable similarity between XUVPD and CTD not only lies in the analogous dissociation pattern, but also lies in that fact that they produced the same charge-increased product ion at *m/z* 472.6 ($[DP5DM3+Na]^{2+\bullet}$). The former could be explained by the fact that they both can impart > 18 eV energy into the oligosaccharide precursor. The latter indicates that they could adopt similar gas-phase oxidation channel.

6.3 Integration of Charge Transfer Dissociation (CTD) into an Hydrogen-Deuterium Exchange (HDX) Workflow

6.4.1 Introduction

Proteins are important biomolecules for every living organism, which perform numerous biological functions, such as DNA replication, molecular transportation and biocatalysis [180]. One critical factor that ensures proteins perform these functions properly is their biologically active conformations. Hydrogen deuterium exchange mass spectrometry (HDX-MS) is one of the important ongoing strategies for the examination of protein conformations [181].

As the most widely used tandem mass spectrometry (MS/MS) techniques, collision-induced dissociation (CID) has been included in several HDX-MS workflows and has achieved some positive results [182, 183]. However, due to its slow-heating nature, CID often facilitates hydrogen scrambling. When scrambling occurs, the measured deuterium uptake level is different from the "true" value, which hinders researchers from obtaining the original protein conformation. Electron transfer dissociation (ETD) [184] and electron capture dissociation (ECD) [185] are higher energy techniques that proceed through a "fast" process, both of which precede proton mobilization. Thus, they can yield the "true" deuterium uptake, and are not subjected to hydrogen scrambling.

Encouraged by the high-energy and fast ion activation in CTD of peptides, phospholipids and oligosaccharides, we incorporated CTD into an HDX-MS workflow. An ETD experiment was conducted in parallel to enable a side-by-side comparison with CTD in this workflow.

6.4.2 Experimental

Figure 6.8 shows the experimental setup for the HDX-MS workflow. Ubiquitin sample and related experimental supplies were provided via the collaboration with Dr. Gregory Donohoe and Dr. Stephen Valentine in the Department of Chemistry at West Virginia University (WVU, Morgantown, WV, USA). The sample preparation is described elsewhere [186].

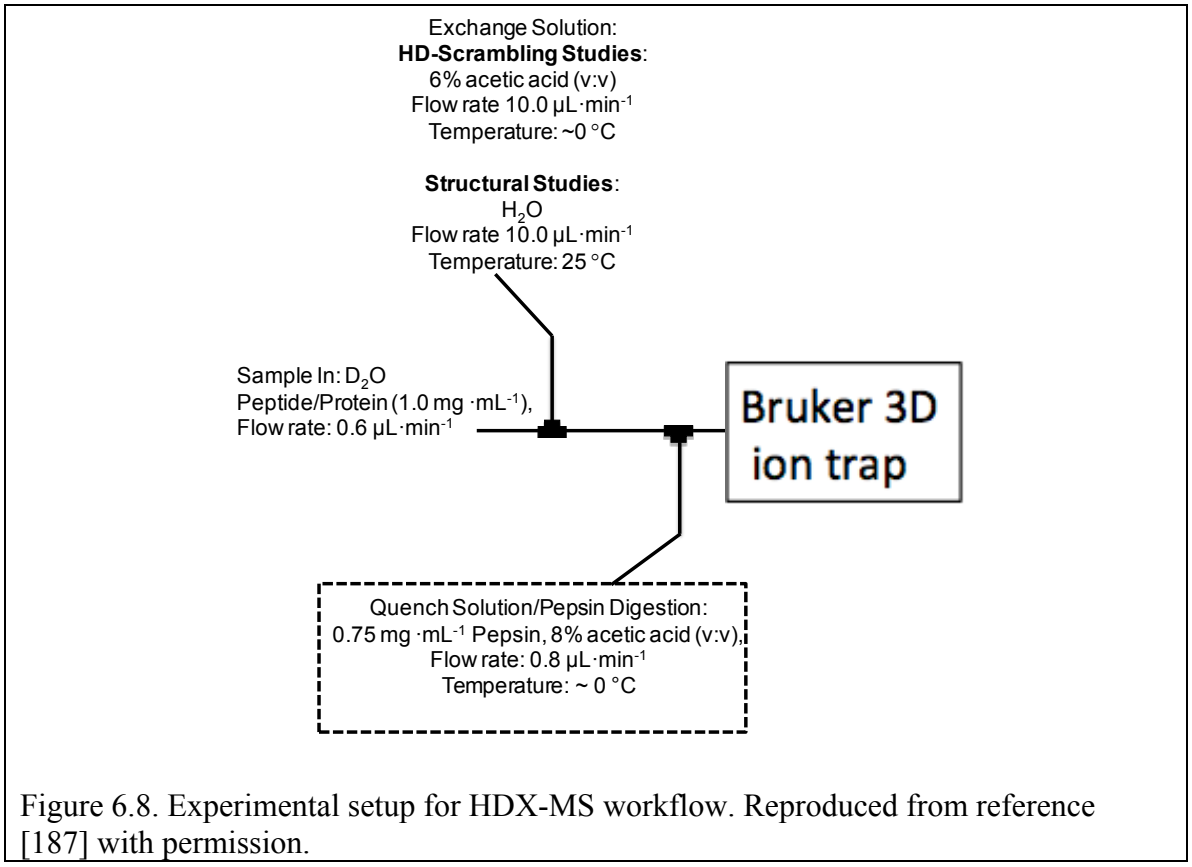

Figure 6.8. Experimental setup for HDX-MS workflow. Reproduced from reference [187] with permission.

CTD and ETD measurements were both performed using modified Bruker amaZon ETD mass spectrometer (Bruker Daltronics, Bremen, Germany), which has been detailed in Chapter 2. As an attempt to preserve the protein conformation, the temperature of ESI source and voltages on ion optics were carefully tailored according to reference [184].

6.4.3 Results and Discussion

The eluents from the microfluidic setup (Figure 6.8) were direct introduced into the modified Bruker mass spectrometer. The deuterium-labeled $[MQIFVKTLTGKTITL+3H]^{3+}$ ions were first mass-selected at the MS^2 level, then exposed to ETD-reagent anion or a beam of ~6 keV helium cations (CTD examination). The corresponding results from the two techniques were extracted and calculated using an in-house algorithm in the Valentine group, which establishes the extent of deuterium retention at each residue. The results are presented in a bar plot in Figure 6.9. The N-terminal region of ubiquitin consists of three regions: (1) a beta-strand (residues M_1-T_7); (2) unstructured region (L_8-G_{10}); (3) second beta-strand from (G_{10}-L_{15}).

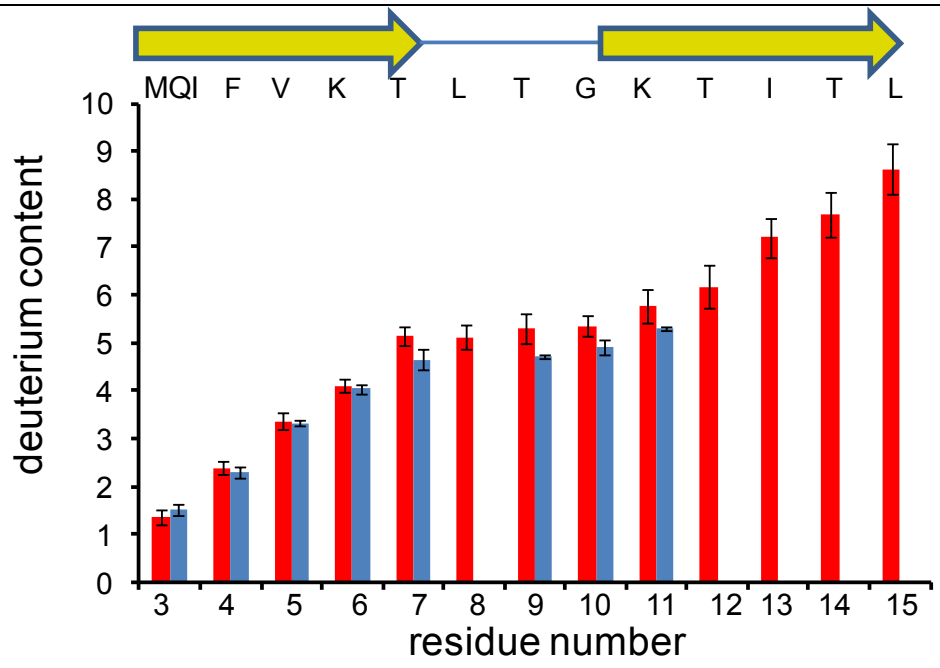

Figure 6.9. The total deuterium content level was plotted against per residue from ETD (red bars) and CTD (blue bars) of deuterium-labeled $[MQIFVKTLTGKTITL+3H]^{3+}$ ion (ubiquitin digest), respectively. Each n level was calculated from the c_{n-1} product ion. Reproduced from reference [187] with permission.

The ETD results (red bars) showed an excellent correspondence with the secondary structural confirmation of the MQIFVKTLTGKTITL sequence [183, 188]. As determined from the c ions, the deuterium retention started increasing from I_3-T_7, corresponding to the first beta-strand. Deuterium retention leveled off from L_8-G_{10}, corresponding to the unstructured region. Deuterium retention started increasing from K_{11}-L_{15}, corresponding to the second beta-strand.

The CTD results (blue bars) showed a deuterium retention trend that is highly analogous to the above ETD trend. As determined by the *c* ions, the deuterium retention level in CTD is slightly lower than that in ETD in general. CTD didn't produce any detectable deuterium retention (i.e. no *c*-ions) between at L_8 and from T_{12}-L_{15}. However, CTD did produce *a* and *x* ions in this region and we are currently investigating the use of *a* ions or *x* ions to calculated the deuterium uptake. Currently, for the *c*-ions, CTD exhibits deuterium retention ability that is comparable to the well-known ETD experiments. This strongly indicates that the potential utility of CTD in the HDX-MS workflow. If *a* and *x* ions are consistent with this result, CTD could offer the unique ability to fragment singly charged peptides in a fast process which mitigates hydrogen scrambling. Such a capability could open up the number and types of peptides that could be structurally characterized via H/D exchange.

6.4 Conclusions

CTD of PA, PS, PG and PI was carried out and described in this chapter. The CTD pattern is highly dependent on the adducting form of the precursor lipid. Compared with $[M-Na+2H]^+$ and $[M+Na]^+$, CTD of $[M+H]^+$ produced three times the amount of the fragment ions. With the same protonated lipid form, CTD of PA produced the most fragment ions—forming a near-complete fragmentation pattern, while CTD of PS produced the fewest and least abundant fragment ions. Compared with phosphocholine (PC) lipids in Chapter 4, CTD showed an inferior performance upon PA, PS, PG and PI. Nevertheless, CTD has exhibited a superior performance over CID in general, which presents the undeniable advantage of CTD in the MS/MS fragmentation tool kit.

DP5DM3 was also analyzed using LE-CID, XUVPD and CTD in this chapter. Compared with LE-CID, XUVPD and CTD induced an enhanced array of cross-ring cleavages, which offers more valuable information for the structural elucidation of oligosaccharides. The enriched cross-ring fragmentation makes XUVPD and CTD superior techniques over the traditional LE-CID. A significant limitation of XUVPD is the strong dependence on synchrotron beam facility. Given that CTD was carried out on a bench-top ion trap mass spectrometer modified with a fast ion source, CTD should see a more widespread utilization for glycan identification in the future.

CTD was also integrated in a microfluidic system, composed of HDX and pepsin digestion. CTD results showed remarkable similarity with that of ETD in maintaining the deuterium retention level for $[MQIFVKTLTGKTITL+3H]^{3+}$ ion. This capability greatly facilitates the mapping of the secondary structural elements in protein conformation. This potential, along with the relatively low-cost instrument platform, makes CTD a powerful

new adjunct to the existing HDX-MS techniques, and it should find broader applications regarding protein conformations, folding, dynamics, and interactions.

CHAPTER 7: CONCLUSIONS AND FUTURE WORK

Collision-induced dissociation (CID), electron transfer dissociation (ETD) and electron capture dissociation (ECD) are the most successfully commercialized ion activation techniques, the implementation of which has become a "standard configuration" for most mass spectrometry instrumentation on market. However, they all have certain deficiencies for real-life bioanalytical studies, and neither one is a 'silver bullet'.

This dissertation demonstrates that charge transfer dissociation (CTD) is capable of ionizing and fragmenting gas-phase biological ions in a manner that is highly beneficial for their structural elucidation. In this proof of concept study, we have demonstrated some of the first cation-cation reactions in the gas phase and demonstrate intriguing features for the investigation of peptides, proteins (insulin), lipids, and oligosaccharide structures. We also proved a one-step two-electron oxidation mechanism for 5+ and 6+ insulin, but reaction with oxygen at MS^4 level could not confirm the presence of one or two radicals on the doubly oxidized product ions.

For peptide analysis CTD is workable with 1+, 2+, and 3+ peptide precursors, with excellent performance for lower precursor charge states and slight performance decay for higher precursor charge states. CTD of peptides produces enriched amino acid side-chain losses that can complement peptide-sequencing information from backbone fragments. The type and the number of CTD fragment ions are dependent on the precursor charge states; i.e. *a/x* ions are more dominant from 1+ precursor ions and *c/z* ions become more as the charge state increases. These differences show that different mechanisms are dominant for different charge states. MS^3 CTD/CID experiments on

insulin produces enhanced structural information via the capability of cleaving disulfide linkages.

For lipid analysis, CTD produces extensive fragmentation along lipid acyl chains with varying length and degree of unsaturation. The adducting form of lipids (protonated versus sodiated) strongly influences the extent of CTD cleavages. CTD produces diagnostic fragment ion pairs that can yield information associated with C=C double bond positioning, and CTD shows significant fragment abundance change when examining lipids with acyl chains with C=C double bond geometry difference—cis versus trans—which could possibly be used to pinpoint stereochemistry information. Another benefit of CTD is the ease of implementation and cost-effective on both the saddle field ion source and mass spectrometric platform.

Despite the exciting achievements with CTD investigation, more work can be carried out in the future for the further development and evaluation of this technique. The first aspect is to enlarge the sample pool for CTD experiments. Most of the CTD results presented here were only conducted upon the samples from a narrow sample pool. For further CTD performance evaluation, more peptides, lipids, and oligosaccharides should be examined to validate the generality of the aforementioned fragmentation behaviors. For peptides, customized peptides, such as KAAAAXAAAAK (X represents one of the twenty amino acids) should be studied to achieve more mechanistic insight into CTD. For lipids, other lipid classes (cholesterol, free fatty acids, triglyceride, etc.) and other metal adducting forms (e.g. lithium, potassium and manganese) could be included in CTD experiments. For oligosaccharides, this bench-top CTD technique showed intriguing fragmentation pattern upon the linear pentamer. Given the promising CTD results,

oligosaccharides with different modifications (sulfation, acetylation, etc.) and branched structures should be included in the future CTD experiments.

Chapter 6 outlined some preliminary results of including CTD into an on-line HDX microfluidic system. CTD showed ETD-like suppression in hydrogen scrambling for the liquid phase HDX experiment. More protein molecule (other than ubiquitin) can be tested in such experiments. Some efforts can also be devoted to the integration of CTD into gas phase HDX workflows.

In another area of future work, the mass spectrometric platform (Bruker 3D ion trap) on which CTD is currently implemented possesses limited resolving power and mass accuracy, which greatly restrict the amount of obtainable structural information. A proper upgrade of the instrument platform to high-resolution mass spectrometers could remarkably facilitate the investigation of CTD. A Shimadzu IT-TOF, Thermo Scientific Orbitrap series or Waters Synapt G2 could be possible platforms for the implementation of CTD technique in the future. With improved resolving power and mass accuracy, CTD could be extended to the analysis of large proteins/glycans or possibly being included in top-down proteomic workflows. What's more, some of the said mass spectrometers offers extra functionalities, thus more sophisticated ion manipulations can be conducted in combination with CTD technique, which could be beneficial for furthering mechanistic studies of CTD or possibly leading to some more powerful "combined methods" for gas-phase ion activation.

Chapter 5 has presented some research work regarding MAD investigation. Since MAD has been studied in our group for more than 7 years, more biomolecule models have been examined with MAD than with CTD. Along with the previous publications

from Zubarev group and Berkout group, we have developed a better understanding of MAD than CTD. But there is still room for future investigation upon MAD. The future work on MAD could follow the aforesaid suggestions for CTD. One exception is that MAD showed great performance with peptide anions, following which more biomolecular anions (e.g. peptide and lipid anions) should be examined using MAD. Since MAD has not been tried on oligosaccharide sample, it should be a good idea to subject oligosaccharides to MAD fragmentation. Given the remarkable similarities observed in MAD and CTD spectra for the POPC sample (provided in Chapter 4), we have every reason to expect that MAD could produce mass spectra as informative as (or not worse than) CTD results for oligosaccharides.

REFERENCES

1. March, R.E.: An introduction to quadrupole ion trap mass spectrometry. J Mass Spectrom **32,** 351-369 (1997)

2. Gross, J.H., *Mass Spectrometry A Textbook* 2nd ed.; Springer Heidelberg Dordrecht London New York: 2011, 10.1007/978-3-642-10711-5.

3. Blanksby, S.J., Mitchell, T.W.: Advances in mass spectrometry for lipidomics. Annu Rev Anal Chem (Palo Alto Calif) **3,** 433-465 (2010)

4. Harris, F.M.: Mass spectrometry/mass spectrometry: Techniques and applications of tandem mass spectrometry Kenneth L. Busch, Gary L. Glish and Scott A. Mcluckey VCH Verlagsgesellschaft, Weinheim, Basel, Cambridge, New York, 1988. xii + 333p with 112 Figures and 10 Tables DM 154.00; £51.00 ISBN 0-89573-275-0. Rapid Commun Mass Sp **3,** i-i (1989)

5. Han, X.L., Gross, R.W.: Global analyses of cellular lipidomes directly from crude extracts of biological samples by ESI mass spectrometry: a bridge to lipidomics. Journal of Lipid Research **44,** 1071-1079 (2003)

6. Jackson, S.N., Woods, A.S.: Direct profiling of tissue lipids by MALDI-TOFMS. Journal of chromatography. B, Analytical technologies in the biomedical and life sciences **877,** 2822-2829 (2009)

7. Hsu, F.F., Turk, J.: Structural determination of sphingomyelin by tandem mass spectrometry with electrospray ionization. J Am Soc Mass Spectrom **11,** 437-449 (2000)

8. Johnson, R.S., Martin, S.A., Biemann, K., Stults, J.T., Watson, J.T.: Novel fragmentation process of peptides by collision-induced decomposition in a tandem mass spectrometer: differentiation of leucine and isoleucine. Anal Chem **59,** 2621-2625 (1987)

9. Sleno, L., Volmer, D.A.: Ion activation methods for tandem mass spectrometry. J Mass Spectrom **39,** 1091-1112 (2004)

10. Schlosser, A., Lehmann, W.D.: Special feature: Commentary - Five-membered ring formation in unimolecular reactions of peptides: a key structural element controlling low-energy collision-induced dissociation of peptides. J Mass Spectrom **35,** 1382-1390 (2000)

11. Wells, J.M., McLuckey, S.A.: Collision-induced dissociation (CID) of peptides and proteins. Method Enzymol **402,** 148-185 (2005)

12. Wysocki, V.H., Tsaprailis, G., Smith, L.L., Breci, L.A.: Special feature: Commentary - Mobile and localized protons: a framework for understanding peptide dissociation. J Mass Spectrom **35,** 1399-1406 (2000)

13. Zhou, M.W., Wysocki, V.H.: Surface Induced Dissociation: Dissecting Noncovalent Protein Complexes in the Gas phase. Accounts Chem Res **47,** 1010-1018 (2014)

14. Zubarev, R.A., Kelleher, N.L., McLafferty, F.W.: Electron capture dissociation of multiply charged protein cations. A nonergodic process. J Am Chem Soc **120,** 3265-3266 (1998)

15. Syka, J.E.P., Coon, J.J., Schroeder, M.J., Shabanowitz, J., Hunt, D.F.: Peptide and protein sequence analysis by electron transfer dissociation mass spectrometry. P Natl Acad Sci USA **101,** 9528-9533 (2004)

16. Zhurov, K.O., Fornelli, L., Wodrich, M.D., Laskay, U.A., Tsybin, Y.O.: Principles of electron capture and transfer dissociation mass spectrometry applied to peptide and protein structure analysis. Chem Soc Rev **42,** 5014-5030 (2013)

17. Liu, J., McLuckey, S.A.: Electron transfer dissociation: Effects of cation charge state on product partitioning in ion/ion electron transfer to multiply protonated polypeptides. Int J Mass Spectrom **330,** 174-181 (2012)

18. Nielsen, M.L., Budnik, B.A., Haselmann, K.F., Zubarev, R.A.: Tandem MALDI/El ionization for tandem Fourier transform ion cyclotron resonance mass spectrometry of polypeptides. Int J Mass Spectrom **226,** 181-187 (2003)

19. Fung, Y.M., Adams, C.M., Zubarev, R.A.: Electron ionization dissociation of singly and multiply charged peptides. J Am Chem Soc **131,** 9977-9985 (2009)

20. Brodbelt, J.S., Wilson, J.J.: Infrared Multiphoton Dissociation in Quadrupole Ion Traps. Mass Spectrom Rev **28,** 390-424 (2009)

21. Brodbelt, J.S.: Photodissociation mass spectrometry: new tools for characterization of biological molecules. Chem Soc Rev **43,** 2757-2783 (2014)

22. Ly, T., Julian, R.R.: Residue-specific radical-directed dissociation of whole proteins in the gas phase. J Am Chem Soc **130,** 351-358 (2008)

23. Kalcic, C.L., Gunaratne, T.C., Jonest, A.D., Dantus, M., Reid, G.E.: Femtosecond Laser-induced Ionization/Dissociation of Protonated Peptides. J Am Chem Soc **131,** 940-942 (2009)

24. Canon, F., Milosavljevic, A.R., Nahon, L., Giuliani, A.: Action spectroscopy of a protonated peptide in the ultraviolet range. Phys Chem Chem Phys **17,** 25725-25733 (2015)

25. Misharin, A.S., Silivra, O.A., Kjeldsen, F., Zubarev, R.A.: Dissociation of peptide ions by fast atom bombardment in a quadrupole ion trap. Rapid Commun Mass Spectrom **19,** 2163-2171 (2005)

26. Berkout, V.D.: Fragmentation of protonated peptide ions via interaction with metastable atoms. Anal Chem **78,** 3055-3061 (2006)

27. Berkout, V.D., Doroshenko, V.M.: Fragmentation of phosphorylated and singly charged peptide ions via interaction with metastable atoms. Int. J. Mass Spectrom. **278,** 150-157 (2008)

28. Berkout, V.D.: Fragmentation of singly protonated peptides via interaction with metastable rare gas atoms. Anal. Chem. **81,** 725-731 (2009)

29. Cook, S.L., Collin, O.L., Jackson, G.P.: Metastable atom-activated dissociation mass spectrometry: leucine/isoleucine differentiation and ring cleavage of proline residues. Journal of mass spectrometry : JMS **44,** 1211-1223 (2009)

30. Cook, S.L., Jackson, G.P.: Characterization of Tyrosine Nitration and Cysteine Nitrosylation Modifications by Metastable Atom-Activation Dissociation Mass Spectrometry. Journal of the American Society for Mass Spectrometry **22,** 221-232 (2011)

31. Cook, S.L., Jackson, G.P.: Metastable atom-activated dissociation mass spectrometry of phosphorylated and sulfonated peptides in negative ion mode. J. Am. Soc. Mass Spectrom. **22,** 1088-1099 (2011)

32. Cook, S.L., Zimmermann, C.M., Singer, D., Fedorova, M., Hoffmann, R., Jackson, G.P.: Comparison of CID, ETD and metastable atom-activated dissociation (MAD) of doubly and triply charged phosphorylated tau peptides. J Mass Spectrom **47,** 786-794 (2012)

33. Deimler, R.E., Razunguzwa, T.T., Reschke, B.R., Walsh, C.M., Powell, M.J., Jackson, G.P.: Direct analysis of drugs in forensic applications using laser ablation electrospray ionization-tandem mass spectrometry (LAESI-MS/MS). Anal. Methods **6,** 4810-4817 (2014)

34. Pulfer, M., Murphy, R.C.: Electrospray mass spectrometry of phospholipids. Mass Spectrom Rev **22,** 332-364 (2003)

35. Hsu, F.F., Turk, J.: Electrospray ionization/tandem quadrupole mass spectrometric studies on phosphatidylcholines: the fragmentation processes. J Am Soc Mass Spectrom **14,** 352-363 (2003)

36. Hsu, F.F., Turk, J.: Structural characterization of unsaturated glycerophospholipids by multiple-stage linear ion-trap mass spectrometry with electrospray ionization. J Am Soc Mass Spectrom **19,** 1681-1691 (2008)

37. Liang, X., Liu, J., LeBlanc, Y., Covey, T., Ptak, A.C., Brenna, J.T., McLuckey, S.A.: Electron transfer dissociation of doubly sodiated glycerophosphocholine lipids. J Am Soc Mass Spectrom **18,** 1783-1788 (2007)

38. Campbell, J.L., Baba, T.: Near-complete structural characterization of phosphatidylcholines using electron impact excitation of ions from organics. Anal Chem **87,** 5837-5845 (2015)

39. Jones, J.W., Thompson, C.J., Carter, C.L., Kane, M.A.: Electron-induced dissociation (EID) for structure characterization of glycerophosphatidylcholine: determination of double-bond positions and localization of acyl chains. J Mass Spectrom **50,** 1327-1339 (2015)

40. Zehethofer, N., Scior, T., Lindner, B.: Elucidation of the fragmentation pathways of different phosphatidylinositol phosphate species (PIPx) using IRMPD implemented on a FT-ICR MS. Anal Bioanal Chem **398,** 2843-2851 (2010)

41. Madsen, J.A., Cullen, T.W., Trent, M.S., Brodbelt, J.S.: IR and UV Photodissociation as Analytical Tools for Characterizing Lipid A Structures. Anal Chem **83,** 5107-5113 (2011)

42. Stutzman, J.R., Blanksby, S.J., McLuckey, S.A.: Gas-phase transformation of phosphatidylcholine cations to structurally informative anions via ion/ion chemistry. Anal Chem **85,** 3752-3757 (2013)

43. Thomas, M.C., Mitchell, T.W., Blanksby, S.J.: Ozonolysis of phospholipid double bonds during electrospray ionization: a new tool for structure determination. J. Am. Chem. Soc. **128,** 58-59 (2006)

44. Thomas, M.C., Mitchell, T.W., Harman, D.G., Deeley, J.M., Nealon, J.R., Blanksby, S.J.: Ozone-induced dissociation: elucidation of double bond position within mass-selected lipid ions. Anal Chem **80,** 303-311 (2008)

45. Budnik, B.A., Haselmann, K.F., Zubarev, R.A.: Electron detachment dissociation of peptide di-anions: an electron-hole recombination phenomenon. Chem Phys Lett **342,** 299-302 (2001)

46. Coon, J.J., Shabanowitz, J., Hunt, D.F., Syka, J.E.P.: Electron transfer dissociation of peptide anions. Journal of the American Society for Mass Spectrometry **16,** 880-882 (2005)

47. Yoo, H.J., Wang, N., Zhuang, S.Y., Song, H.T., Hakansson, K.: Negative-Ion Electron Capture Dissociation: Radical-Driven Fragmentation of Charge-Increased Gaseous Peptide Anions. J Am Chem Soc **133,** 16790-16793 (2011)

48. Chingin, K., Makarov, A., Denisov, E., Rebrov, O., Zubarev, R.A.: Fragmentation of Positively-Charged Biological Ions Activated with a Beam of High-Energy Cations. Anal Chem **86,** 372-379 (2014)

49. Hoffmann, W.D., Jackson, G.P.: Charge transfer dissociation (CTD) mass spectrometry of peptide cations using kiloelectronvolt helium cations. J Am Soc Mass Spectrom **25,** 1939-1943 (2014)

50. Budnik, B.A., Tsybin, Y.O., Hakansson, P., Zubarev, R.A.: Ionization energies of multiply protonated polypeptides obtained by tandem ionization in Fourier transform mass spectrometers. J Mass Spectrom **37,** 1141-1144 (2002)

51. Lee, H., An, H.J., Lerno, L.A., German, J.B., Lebrilla, C.B.: Rapid profiling of bovine and human milk gangliosides by matrix-assisted laser desorption/ionization Fourier transform ion cyclotron resonance mass spectrometry. Int J Mass Spectrom **305,** 138-150 (2011)

52. Ko, B.J., Brodbelt, J.S.: 193 nm Ultraviolet Photodissociation of Deprotonated Sialylated Oligosaccharides. Anal Chem **83,** 8192-8200 (2011)

53. Lopez-Clavijo, A.F., Duque-Daza, C.A., Creese, A.J., Cooper, H.J.: Electron capture dissociation mass spectrometry of phosphopeptides: Arginine and phosphoserine. Int J Mass Spectrom **390,** 63-70 (2015)

54. Voinov, V.G., Hoffman, P.D., Bennett, S.E., Beckman, J.S., Barofsky, D.F.: Electron Capture Dissociation of Sodium-Adducted Peptides on a Modified Quadrupole/Time-of-Flight Mass Spectrometer. Journal of the American Society for Mass Spectrometry **26,** 2096-2104 (2015)

55. Lu, J., Trnka, M.J., Roh, S.H., Robinson, P.J.J., Shiau, C., Fujimori, D.G., Chiu, W., Burlingame, A.L., Guan, S.H.: Improved Peak Detection and Deconvolution of Native Electrospray Mass Spectra from Large Protein Complexes. Journal of the American Society for Mass Spectrometry **26,** 2141-2151 (2015)

56. Flett, F.J., Walton, J.G.A., Mackay, C.L., Interthal, H.: Click Chemistry Generated Model DNA-Peptide Heteroconjugates as Tools for Mass Spectrometry. Anal Chem **87,** 9595-9599 (2015)

57. Kalcic, C.L., Reid, G.E., Lozovoy, V.V., Dantus, M.: Mechanism Elucidation for Nonstochastic Femtosecond Laser-Induced Ionization/Dissociation: From Amino Acids to Peptides. J Phys Chem A **116,** 2764-2774 (2012)

58. Cook, S.L., Collin, O.L., Jackson, G.P.: Metastable atom-activated dissociation mass spectrometry: leucine/isoleucine differentiation and ring cleavage of proline residues. J. Mass Spectrom. **44,** 1211-1223 (2009)

59. Cook, S.L., Jackson, G.P.: Metastable Atom-Activated Dissociation Mass Spectrometry of Phosphorylated and Sulfonated Peptides in Negative Ion Mode. J. Am. Soc. Mass Spectrom. **22,** 1088-1099 (2011)

60. Kjeldsen, F., Giessing, A.M.B., Ingrell, C.R., Jensen, O.N.: Peptide sequencing and characterization of post-translational modifications by enhanced ion-charging and liquid chromatography electron-transfer dissociation tandem mass spectrometry. Anal Chem **79,** 9243-9252 (2007)

61. Fung, Y.M.E., Adams, C.M., Zubarev, R.A.: Electron Ionization Dissociation of Singly and Multiply Charged Peptides. J Am Chem Soc **131,** 9977-9985 (2009)

62. Barbacci, D.C., Russell, D.H.: Sequence and side-chain specific photofragment (193 nm) ions from protonated substance P by matrix-assisted laser desorption ionization time-

of-flight mass spectrometry. Journal of the American Society for Mass Spectrometry **10,** 1038-1040 (1999)

63. Thompson, M.S., Cui, W., Reilly, J.P.: Factors That Impact the Vacuum Ultraviolet Photofragmentation of Peptide Ions. Journal of the American Society for Mass Spectrometry **18,** 1439-1452 (2007)

64. Misharin, A.S., Silivra, O.A., Kjeldsen, F., Zubarev, R.A.: Dissociation of peptide ions by fast atom bombardment in a quadrupole ion trap. Rapid Commun Mass Sp **19,** 2163-2171 (2005)

65. Hoffmann, W.D., Jackson, G.P.: Charge Transfer Dissociation (CTD) Mass Spectrometry of Peptide Cations Using Kiloelectronvolt Helium Cations. J. Am. Soc. Mass Spectrom. **25,** 1939-1943 (2014)

66. Pitteri, S.J., Chrisman, P.A., Hogan, J.M., McLuckey, S.A.: Electron transfer ion/ion reactions in a three-dimensional quadrupole ion trap: Reactions of doubly and triply protonated peptides with SO2 center dot-. Anal Chem **77,** 1831-1839 (2005)

67. Xia, Y., Chrisman, P.A., Pitteri, S.J., Erickson, D.E., McLuckey, S.A.: Ion/molecule reactions of cation radicals formed from protonated polypeptides via gas-phase ion/ion electron transfer. J Am Chem Soc **128,** 11792-11798 (2006)

68. Smith, S.A., Kalcic, C.L., Safran, K.A., Stemmer, P.M., Dantus, M., Reid, G.E.: Enhanced Characterization of Singly Protonated Phosphopeptide Ions by Femtosecond Laser-induced Ionization/Dissociation Tandem Mass Spectrometry (fs-LID-MS/MS). Journal of the American Society for Mass Spectrometry **21,** 2031-2040 (2010)

69. Li, P., Hoffmann, W.D., Jackson, G.P.: Multistage mass spectrometry of phospholipids using collision-induced dissociation (CID) and metastable atom-activated dissociation (MAD). Int J Mass Spectrom, doi.10.1016/j.ijms.2016.02.010 (2016)

70. Axelsson, J., Palmblad, M., Hakansson, K., Hakansson, P.: Electron capture dissociation of substance P using a commercially available Fourier transform ion cyclotron resonance mass spectrometer. Rapid Commun Mass Sp **13,** 474-477 (1999)

71. Leymarie, N., Costello, C.E., O'Connor, P.B.: Electron capture dissociation initiates a free radical reaction cascade. J Am Chem Soc **125,** 8949-8958 (2003)

72. Chalkley, R.J., Brinkworth, C.S., Burlingame, A.L.: Side-chain fragmentation of alkylated cysteine residues in electron capture dissociation mass spectrometry. Journal of the American Society for Mass Spectrometry **17,** 1271-1274 (2006)

73. Savitski, M.M., Nielsen, M.L., Zubarev, R.A.: Side-chain losses in electron capture dissociation to improve peptide identification. Anal Chem **79,** 2296-2302 (2007)

74. Falth, M., Savitski, M.M., Nielsen, M.L., Kjeldsen, F., Andren, P.E., Zubarev, R.A.: Analytical Utility of Small Neutral Losses from Reduced Species in Electron Capture Dissociation Studied Using SwedECD Database. Anal Chem **80,** 8089-8094 (2008)

75. Jensen, C.S., Wyer, J.A., Houmoller, J., Hvelplund, P., Nielsen, S.B.: Electron-capture induced dissociation of doubly charged dipeptides: on the neutral losses and N-C-alpha bond cleavages. Phys Chem Chem Phys **13,** 18373-18378 (2011)

76. Kaczorowska, M.A.: Electron capture dissociation and collision induced dissociation behavior of peptides containing methionine, selenomethionine and oxidized methionine. Int J Mass Spectrom **389,** 54-58 (2015)

77. Xia, Q.W., Lee, M.V., Rose, C.M., Marsh, A.J., Hubler, S.L., Wenger, C.D., Coon, J.J.: Characterization and Diagnostic Value of Amino Acid Side Chain Neutral Losses Following Electron-Transfer Dissociation. Journal of the American Society for Mass Spectrometry **22,** 255-264 (2011)

78. Laskin, J., Yang, Z.B., Ng, C.M.D., Chu, I.K.: Fragmentation of alpha-Radical Cations of Arginine-Containing Peptides. Journal of the American Society for Mass Spectrometry **21,** 511-521 (2010)

79. Cooper, H.J., Hudgins, R.R., Hakansson, K., Marshall, A.G.: Characterization of amino acid side chain losses in electron capture dissociation. Journal of the American Society for Mass Spectrometry **13,** 241-249 (2002)

80. Haselmann, K.F., Budnik, B.A., Kjeldsen, F., Polfer, N.C., Zubarev, R.A.: Can the (M center dot-X) region in electron capture dissociation provide reliable information on amino acid composition of polypeptides? Eur J Mass Spectrom **8,** 461-469 (2002)

81. Fung, Y.M.E., Chan, T.W.D.: Experimental and theoretical investigations of the loss of amino acid side chains in electron capture dissociation of model peptides. Journal of the American Society for Mass Spectrometry **16,** 1523-1535 (2005)

82. Curable fluoroelastomer compositions. http://www.google.com/patents/US8288482.

83. Flexible laminated fluoropolymer containing composites. http://www.google.com/patents/EP0202996A2?cl=en.

84. Hassan, I., Pinto, S., Weisbecker, C., Attygalle, A.B.: Competitive Deprotonation and Superoxide [O2 (-*)] Radical-Anion Adduct Formation Reactions of Carboxamides under Negative-Ion Atmospheric-Pressure Helium-Plasma Ionization (HePI) Conditions. J Am Soc Mass Spectrom **27,** 394-401 (2016)

85. Pshenichnyuk, S.A., Kukhto, A.V., Kukhto, I.N., Asfandiarov, N.L.: Resonance capture of electrons by electroactive organic molecules. Russ J. Phys. Chem. B **4,** 1014-1027 (2010)

86. Hunt, D.F., Harvey, T.M., Russell, J.W.: Oxygen as a reagent gas for the analysis of 2,3,7,8-tetrachlorodibenzo-p-dioxin by negative ion chemical ionization mass spectrometry. J. Chem. Soc. Chem. Commun., 10.1039/C39750000151 151-152 (1975)

87. Zhu, S.Y., Russ, H.A., Wang, X.J., Zhang, M.L., Ma, T.H., Xu, T., Tang, S.B., Hebrok, M., Ding, S.: Human pancreatic beta-like cells converted from fibroblasts. Nat Commun **7,** (2016)

88. Pulfer, M., Murphy, R.C.: Electrospray mass spectrometry of phospholipids. Mass Spectrom. Rev. **22,** 332-364 (2003)

89. Jones, M.D., Patterson, S.D., Lu, H.S.: Determination of disulfide bonds in highly bridged disulfide-linked peptides by matrix-assisted laser desorption/ionization mass spectrometry with postsource decay. Anal Chem **70,** 136-143 (1998)

90. Stephenson, J.L., Cargile, B.J., McLuckey, S.A.: Ion trap collisional activation of disulfide linkage intact and reduced multiply protonated polypeptides. Rapid Commun Mass Sp **13,** 2040-2048 (1999)

91. Mentinova, M., McLuckey, S.A.: Cleavage of multiple disulfide bonds in insulin via gold cationization and collision-induced dissociation. Int J Mass Spectrom **308,** 133-136 (2011)

92. Wells, J.M., Stephenson, J.L., McLuckey, S.A.: Charge dependence of protonated insulin decompositions. Int J Mass Spectrom **203,** A1-A9 (2000)

93. Chrisman, P.A., McLuckey, S.A.: Dissociations of disulfide-linked gaseous polypeptide/protein anions: Ion chemistry with implications for protein identification and characterization. J Proteome Res **1,** 549-557 (2002)

94. Zubarev, R.A., Kruger, N.A., Fridriksson, E.K., Lewis, M.A., Horn, D.M., Carpenter, B.K., McLafferty, F.W.: Electron capture dissociation of gaseous multiply-charged proteins is favored at disulfide bonds and other sites of high hydrogen atom affinity. J Am Chem Soc **121,** 2857-2862 (1999)

95. Kocher, T., Engstrom, A., Zubarev, R.A.: Fragmentation of peptides in MALDI in-source decay mediated by hydrogen radicals. Anal Chem **77,** 172-177 (2005)

96. Li, H.L., O'Connor, P.B.: Electron Capture Dissociation of Disulfide, Sulfur-Selenium, and Diselenide Bound Peptides. Journal of the American Society for Mass Spectrometry **23,** 2001-2010 (2012)

97. Gunawardena, H.P., Gorenstein, L., Erickson, D.E., Xia, Y., McLuckey, S.A.: Electron transfer dissociation of multiply protonated and fixed charge disulfide linked polypeptides. Int J Mass Spectrom **265,** 130-138 (2007)

98. Liu, J., Gunawardena, H.P., Huang, T.Y., McLuckey, S.A.: Charge-dependent dissociation of insulin cations via ion/ion electron transfer. Int J Mass Spectrom **276,** 160-170 (2008)

99. Chrisman, P.A., Pitteri, S.J., Hogan, J.M., McLuckey, S.A.: SO2- electron transfer ion/ion reactions with disulfide linked polypeptide ions. Journal of the American Society for Mass Spectrometry **16,** 1020-1030 (2005)

100. Cole, S.R., Ma, X.X., Zhang, X.R., Xia, Y.: Electron Transfer Dissociation (ETD) of Peptides Containing Intrachain Disulfide Bonds. Journal of the American Society for Mass Spectrometry **23,** 310-320 (2012)

101. Mentinova, M., Han, H.L., McLuckey, S.A.: Dissociation of disulfide-intact somatostatin ions: the roles of ion type and dissociation method. Rapid Commun Mass Sp **23,** 2647-2655 (2009)

102. Lioe, H., O'Hair, R.A.J.: Comparison of collision-induced dissociation and electron-induced dissociation of singly protonated aromatic amino acids, cystine and related simple peptides using a hybrid linear ion trap-FT-ICR mass spectrometer. Anal Bioanal Chem **389,** 1429-1437 (2007)

103. Kalli, A., Hakansson, K.: Preferential cleavage of S-S and C-S bonds in electron detachment dissociation and infrared multiphoton dissociation of disulfide-linked peptide anions. Int J Mass Spectrom **263,** 71-81 (2007)

104. Fung, Y.M.E., Kjeldsen, F., Silivra, O.A., Chan, T.W.D., Zubarev, R.A.: Facile disulfide bond cleavage in gaseous peptide and protein cations by ultraviolet photodissociation at 157 nm. Angew Chem Int Edit **44,** 6399-6403 (2005)

105. Agarwal, A., Diedrich, J.K., Julian, R.R.: Direct Elucidation of Disulfide Bond Partners Using Ultraviolet Photodissociation Mass Spectrometry. Anal Chem **83,** 6455-6458 (2011)

106. Stinson, C.A., Xia, Y.: Radical induced disulfide bond cleavage within peptides via ultraviolet irradiation of an electrospray plume. Analyst **138,** 2840-2846 (2013)

107. Soorkia, S., Dehon, C., Kumar, S.S., Pedrazzani, M., Frantzen, E., Lucas, B., Barat, M., Fayeton, J.A., Jouvet, C.: UV Photofragmentation Dynamics of Protonated Cystine: Disulfide Bond Rupture. J Phys Chem Lett **5,** 1110-1116 (2014)

108. Wongkongkathep, P., Li, H.L., Zhang, X., Loo, R.R.O., Julian, R.R., Loo, J.A.: Enhancing protein disulfide bond cleavage by UV excitation and electron capture dissociation for top-down mass spectrometry. Int J Mass Spectrom **390,** 137-145 (2015)

109. Ganisl, B., Breuker, K.: Does Electron Capture Dissociation Cleave Protein Disulfide Bonds? Chemstryopen **1,** 260-268 (2012)

110. Zhang, J., Loo, R.R.O., Loo, J.A.: Increasing fragmentation of disulfide-bonded proteins for top-down mass spectrometry by supercharging. Int J Mass Spectrom **377,** 546-556 (2015)

111. Misharin, A.S., Silivra, O.A., Kjeldsen, F., Zubarev, R.A.: Dissociation of peptide ions by fast atom bombardment in a quadrupole ion trap. Rapid Commun. Mass Spectrom. **19,** 2163-2171 (2005)

112. Berkout, V.D.: Fragmentation of protonated peptide ions via interaction with metastable atoms. Anal. Chem. **78,** 3055-3061 (2006)

113. Cook, S.L., Jackson, G.P.: Characterization of tyrosine nitration and cysteine nitrosylation modifications by metastable atom-activation dissociation mass spectrometry. J. Am. Soc. Mass Spectrom. **22,** 221-232 (2011)

114. Ropartz, D., Li, P.F., Fanuel, M., Giuliani, A., Rogniaux, H., Jackson, G.P.: Charge Transfer Dissociation of Complex Oligosaccharides: Comparison with Collision-Induced Dissociation and Extreme Ultraviolet Dissociative Photoionization. Journal of the American Society for Mass Spectrometry **27,** 1614-1619 (2016)

115. Li, P., Jackson, G.P.: Charge Transfer Dissociation (CTD) Mass Spectrometry of Peptide Cations: Study of Charge State Effects and Side-Chain Losses. J. Am. Soc. Mass Spectrom., 10.1007/s13361-016-1574-y 1-11 (2017)

116. Wysocki, V.H., Joyce, K.E., Jones, C.M., Beardsley, R.L.: Surface-induced dissociation of small molecules, peptides,and non-covalent protein complexes. J Am Soc Mass Spectr **19,** 190-208 (2008)

117. Li, P., Hoffmann, W.D., Jackson, G.P.: Multistage mass spectrometry of phospholipids using collision-induced dissociation (CID) and metastable atom-activated dissociation (MAD). Int J Mass Spectrom **403,** 1-7 (2016)

118. Op den Kamp, J.A.: Lipid asymmetry in membranes. Annu Rev Biochem **48,** 47-71 (1979)

119. Ramanadham, S., Bohrer, A., Gross, R.W., Turk, J.: Mass spectrometric characterization of arachidonate-containing plasmalogens in human pancreatic islets and in rat islet beta-cells and subcellular membranes. Biochemistry **32,** 13499-13509 (1993)

120. Al-Saad, K.A., Siems, W.F., Hill, H.H., Zabrouskov, V., Knowles, N.R.: Structural analysis of phosphatidylcholines by post-source decay matrix-assisted laser desorption/ionization time-of-flight mass spectrometry. J Am Soc Mass Spectrom **14,** 373-382 (2003)

121. Hsu, F.F., Turk, J.: Studies on phosphatidylglycerol with triple quadrupole tandem mass spectrometry with electrospray ionization: Fragmentation processes and structural characterization. Journal of the American Society for Mass Spectrometry **12,** 1036-1043 (2001)

122. Hsu, F.F., Turk, J.: Charge-remote and charge-driven fragmentation processes in diacyl glycerophosphoethanolamine upon low-energy collisional activation: a mechanistic proposal. J Am Soc Mass Spectrom **11,** 892-899 (2000)

123. Ho, Y.P., Huang, P.C.: A novel structural analysis of glycerophosphocholines as TFA/K(+) adducts by electrospray ionization ion trap tandem mass spectrometry. Rapid Commun Mass Spectrom **16,** 1582-1589 (2002)

124. Adams, J., Gross, M.L.: Charge-Remote Fragmentations of Closed-Shell Ions - a Thermolytic Analogy. J Am Chem Soc **111,** 435-440 (1989)

125. Adams, J.: Charge-Remote Fragmentations - Analytical Applications and Fundamental-Studies. Mass Spectrom Rev **9,** 141-186 (1990)

126. Ma, X., Xia, Y.: Pinpointing double bonds in lipids by Paterno-Buchi reactions and mass spectrometry. Angew Chem Int Ed Engl **53,** 2592-2596 (2014)

127. Thomas, M.C., Mitchell, T.W., Blanksby, S.J.: Ozonolysis of phospholipid double bonds during electrospray ionization: a new tool for structure determination. J Am Chem Soc **128,** 58-59 (2006)

128. Thomas, M.C., Mitchell, T.W., Harman, D.G., Deeley, J.M., Murphy, R.C., Blanksby, S.J.: Elucidation of double bond position in unsaturated lipids by ozone electrospray ionization mass spectrometry. Anal Chem **79,** 5013-5022 (2007)

129. Brown, S.H., Mitchell, T.W., Blanksby, S.J.: Analysis of unsaturated lipids by ozone-induced dissociation. Biochim Biophys Acta **1811,** 807-817 (2011)

130. Poad, B.L., Pham, H.T., Thomas, M.C., Nealon, J.R., Campbell, J.L., Mitchell, T.W., Blanksby, S.J.: Ozone-induced dissociation on a modified tandem linear ion-trap: observations of different reactivity for isomeric lipids. J Am Soc Mass Spectrom **21,** 1989-1999 (2010)

131. Pham, H.T., Maccarone, A.T., Campbell, J.L., Mitchell, T.W., Blanksby, S.J.: Ozone-induced dissociation of conjugated lipids reveals significant reaction rate enhancements and characteristic odd-electron product ions. J Am Soc Mass Spectrom **24,** 286-296 (2013)

132. Rojas-Betancourt, S., Stutzman, J.R., Londry, F.A., Blanksby, S.J., McLuckey, S.A.: Gas-Phase Chemical Separation of Phosphatidylcholine and Phosphatidylethanolamine Cations via Charge Inversion Ion/Ion Chemistry. Anal Chem **87,** 11255-11262 (2015)

133. Yoo, H.J., Hakansson, K.: Determination of double bond location in fatty acids by manganese adduction and electron induced dissociation. Anal Chem **82,** 6940-6946 (2010)

134. Pham, H.T., Ly, T., Trevitt, A.J., Mitchell, T.W., Blanksby, S.J.: Differentiation of complex lipid isomers by radical-directed dissociation mass spectrometry. Anal Chem **84,** 7525-7532 (2012)

135. Pham, H.T., Trevitt, A.J., Mitchell, T.W., Blanksby, S.J.: Rapid differentiation of isomeric lipids by photodissociation mass spectrometry of fatty acid derivatives. Rapid Commun Mass Spectrom **27,** 805-815 (2013)

136. Ropartz, D., Li, P., Fanuel, M., Giuliani, A., Rogniaux, H., Jackson, G.P.: Charge Transfer Dissociation of Complex Oligosaccharides: Comparison with Collision-Induced Dissociation and Extreme Ultraviolet Dissociative Photoionization. J Am Soc Mass Spectrom **27,** 1614-1619 (2016)

137. Cook, S.L., Collin, O.L., Jackson, G.P.: Metastable atom-activated dissociation mass spectrometry: leucine/isoleucine differentiation and ring cleavage of proline residues. J Mass Spectrom **44,** 1211-1223 (2009)

138. Klein, R.A.: Mass spectrometry of the phosphatidylcholines: dipalmitoyl, dioleoyl, and stearoyl-oleoyl glycerylphosphorylcholines. J Lipid Res **12,** 123-131 (1971)

139. Klein, R.A.: Mass spectrometry of the phosphatidylcholines: fragmentation processes for dioleoyl and stearoyl-oleoyl glycerylphosphorylcholine. J Lipid Res **12,** 628-634 (1971)

140. Castro-Perez, J., Roddy, T.P., Nibbering, N.M., Shah, V., McLaren, D.G., Previs, S., Attygalle, A.B., Herath, K., Chen, Z., Wang, S.P., Mitnaul, L., Hubbard, B.K., Vreeken, R.J., Johns, D.G., Hankemeier, T.: Localization of fatty acyl and double bond positions in phosphatidylcholines using a dual stage CID fragmentation coupled with ion mobility mass spectrometry. J Am Soc Mass Spectrom **22,** 1552-1567 (2011)

141. Deimler, R.E., Sander, M., Jackson, G.P.: Radical-Induced Fragmentation of Phospholipid Cations Using Metastable Atom-Activated Dissociation Mass Spectrometry (Mad-Ms). Int J Mass Spectrom **390,** 178-186 (2015)

142. Siska, P.E.: Molecular-beam studies of Penning ionization. Rev. Mod. Phys **65,** 337-412 (1993)

143. Maccarone, A.T., Duldig, J., Mitchell, T.W., Blanksby, S.J., Duchoslav, E., Campbell, J.L.: Characterization of acyl chain position in unsaturated phosphatidylcholines using differential mobility-mass spectrometry. J Lipid Res **55,** 1668-1677 (2014)

144. Wysocki, V.H., Ross, M.M.: Charge-Remote Fragmentation of Gas-Phase Ions - Mechanistic and Energetic Considerations in the Dissociation of Long-Chain Functionalized Alkanes and Alkenes. International Journal of Mass Spectrometry and Ion Processes **104,** 179-211 (1991)

145. Jensen, N.J., Tomer, K.B., Gross, M.L.: Gas-Phase Ion Decompositions Occurring Remote to a Charge Site. J Am Chem Soc **107,** 1863-1868 (1985)

146. Claeys, M., Nizigiyimana, L., VandenHeuvel, H., Derrick, P.J.: Mechanistic aspects of charge-remote fragmentation in saturated and mono-unsaturated fatty acid derivatives, evidence for homolytic cleavage. Rapid Commun Mass Sp **10,** 770-774 (1996)

147. Murphy, R.C., Harrison, K.A.: Fast atom bombardment mass spectrometry of phospholipids. Mass Spectrom Rev **13,** 57-75 (1994)

148. Dobson, G., Christie, W.W.: Mass spectrometry of fatty acid derivatives. Eur J Lipid Sci Tech **104,** 36-43 (2002)

149. Griffiths, W.J., Yang, Y., Lindgren, J.A., Sjovall, J.: Charge remote fragmentation of fatty acid anions in 400 eV collisions with xenon atoms. Rapid Commun Mass Sp **10,** 21-28 (1996)

150. Hejazi, L., Ebrahimi, D., Guilhaus, M., Hibbert, D.B.: Discrimination Among Geometrical Isomers of alpha-Linolenic Acid Methyl Ester Using Low Energy Electron Ionization Mass Spectrometry. Journal of the American Society for Mass Spectrometry **20,** 1272-1280 (2009)

151. Ann, Q.H., Adams, J.: Collision-Induced Decomposition of Sphingomyelins for Structural Elucidation. Method Enzymol **22,** 285-294 (1993)

152. Li, M., Zhou, Z., Nie, H., Bai, Y., Liu, H.: Recent advances of chromatography and mass spectrometry in lipidomics. Anal. Bioanal. Chem. **399,** 243-249 (2011)

153. Klein, R.A.: Mass spectrometry of phosphatidylcholines - dipalmitoyl, dioleoyl, and stearoyl-oleoyl glycerylphosphorylcholines. Journal of Lipid Research **12,** 123-& (1971)

154. Klein, R.A.: Mass spectrometry of phosphatidylcholines - fragmentation processes for dioleoyl and stearoyl-oleoyl glycerylphosphorylcholine. Journal of Lipid Research **12,** 628-& (1971)

155. Murphy, R.C., Harrison, K.A.: Fast-atom-bombardment mass-spectrometry of phospholipids. Mass Spectrom Rev **13,** 57-75 (1994)

156. Hsu, F.F., Turk, J.: Structural determination of sphingomyelin by tandem mass spectrometry with electrospray ionization. Journal of the American Society for Mass Spectrometry **11,** 437-449 (2000)

157. Hsu, F.F., Turk, J.: Electrospray ionization/tandem quadrupole mass spectrometric studies on phosphatidylcholines: The fragmentation processes. Journal of the American Society for Mass Spectrometry **14,** 352-363 (2003)

158. Hsu, F.F., Turk, J.: Structural characterization of unsaturated glycerophospholipids by multiple-stage linear ion-trap mass spectrometry with electrospray ionization. Journal of the American Society for Mass Spectrometry **19,** 1681-1691 (2008)

159. Ho, Y.P., Huang, P.C.: A novel structural analysis of glycerophosphocholines as TFA/K+ adducts by electrospray ionization ion trap tandem mass spectrometry. Rapid Commun Mass Sp **16,** 1582-1589 (2002)

160. Pham, H.T., Prendergast, M.B., Dunstan, C.W., Trevitt, A.J., Mitchell, T.W., Julian, R.R., Blanksby, S.J.: Dissociation of proton-bound complexes reveals geometry and arrangement of double bonds in unsaturated lipids. Int. J. Mass Spectrom., http://dx.doi.org/10.1016/j.ijms.2015.07.006 (2015)

161. Al-Saad, K.A., Siems, W.F., Hill, H.H., Zabrouskov, V., Knowles, N.R.: Structural analysis of phosphatidylcholines by post-source decay matrix-assisted laser desorption/ionization time-of-flight mass spectrometry. J. Am. Soc. Mass Spectrom. **14,** 373-382 (2003)

162. Pham, H.T., Maccarone, A.T., Campbell, J.L., Mitchell, T.W., Blanksby, S.J.: Ozone-induced dissociation of conjugated lipids reveals significant reaction rate enhancements and characteristic odd-electron product ions. J. Am. Soc. Mass Spectrom. **24,** 286-296 (2013)

163. Pham, H.T., Maccarone, A.T., Thomas, M.C., Campbell, J.L., Mitchell, T.W., Blanksby, S.J.: Structural characterization of glycerophospholipids by combinations of ozone- and collision-induced dissociation mass spectrometry: the next step towards "top-down" lipidomics. Analyst **139,** 204-214 (2014)

164. Madsen, J.A., Cullen, T.W., Trent, M.S., Brodbelt, J.S.: IR and UV photodissociation as analytical tools for characterizing lipid structures. Anal. Chem. **83,** 5107-5113 (2011)

165. Liang, X., Liu, J., LeBlanc, Y., Covey, T., Ptak, A.C., Brenna, J.T., McLuckey, S.A.: Electron transfer dissociation of doubly sodiated glycerophosphocholine lipids. J. Am. Soc. Mass Spectrom. **18,** 1783-1788 (2007)

166. Pham, H.T., Julian, R.R.: Radical delivery and fragmentation for structural analysis of glycerophospholipids. Int. J. Mass Spectrom. **370,** 58-65 (2014)

167. Berkout, V.D.: Fragmentation of protonated peptide ions via interaction with metastable atoms. Anal. Chem. **78,** 3055-3061 (2006)

168. Berkout, V.D., Doroshenko, V.M.: Fragmentation of phosphorylated and singly charged peptide ions via interaction with metastable atoms. Int. J. Mass Spectrom. **278,** 150-157 (2008)

169. Deimler, R.E., Sander, M., Jackson, G.P.: Radical-induced fragmentation of phospholipid cations using metastable atom-activated dissociation mass spectrometry

(MAD-MS). Int. J. Mass Spectrom, http://dx.doi.org/10.1016/j.ijms.2015.1008.1009 (2015)

170. Adams, J., Gross, M.L.: Charge-remote fragmentations of closed-shell ions - a thermolytic analogy. J. Am. Chem. Soc. **111,** 435-440 (1989)

171. Deterding, L.J., Gross, M.L.: Tandem mass spectrometry for identifying fatty-acid derivatives that undergo charge-remote fragmentations. Org. Mass Spectrom. **23,** 169-177 (1988)

172. Castro-Perez, J.M., Kamphorst, J., DeGroot, J., Lafeber, F., Goshawk, J., Yu, K., Shockcor, J.P., Vreeken, R.J., Hankemeier, T.: Comprehensive LC−MSE Lipidomic Analysis using a Shotgun Approach and Its Application to Biomarker Detection and Identification in Osteoarthritis Patients. Journal of Proteome Research **9,** 2377-2389 (2010)

173. Ruan, C., Huang, H., Rodgers, M.T.: A Simple Model for Metal Cation-Phosphate Interactions in Nucleic Acids in the Gas Phase: Alkali Metal Cations and Trimethyl Phosphate. J. Am. Soc. Mass Spectrom. **19,** 305-314 (2008)

174. Fales, B., Fujamade, N., Oomens, J., Rodgers, M.T.: Infrared Multiple Photon Dissociation Action Spectroscopy and Theoretical Studies of Triethyl Phosphate Complexes: Effects of Protonation and Sodium Cationization on Structure. J. Amer. Soc. Mass Spectrom. **22,** 1862-1871 (2011)

175. Xia, Y., Chrisman, P.A., Pitteri, S.J., Erickson, D.E., McLuckey, S.A.: Ion/molecule reactions of cation radicals formed from protonated polypeptides via gas-phase ion/ion electron transfer. J. Am. Chem. Soc. **128,** 11792-11798 (2006)

176. Ran-Ressler, R.R., Lawrence, P., Brenna, J.T.: Structural characterization of saturated branched chain fatty acid methyl esters by collisional dissociation of molecular ions generated by electron ionization. Journal of Lipid Research **53,** 195-203 (2012)

177. Swaney, D.L., McAlister, G.C., Wirtala, M., Schwartz, J.C., Syka, J.E., Coon, J.J.: Supplemental activation method for high-efficiency electron-transfer dissociation of doubly protonated peptide precursors. Anal Chem **79,** 477-485 (2007)

178. Leach, F.E., Xiao, Z.P., Laremore, T.N., Linhardt, R.J., Amster, I.J.: Electron detachment dissociation and infrared multiphoton dissociation of heparin tetrasaccharides. Int J Mass Spectrom **308,** 253-259 (2011)

179. Ropartz, D., Lemoine, J., Giuliani, A., Bittebiere, Y., Enjalbert, Q., Antoine, R., Dugourd, P., Ralet, M.C., Rogniaux, H.: Deciphering the structure of isomeric oligosaccharides in a complex mixture by tandem mass spectrometry: Photon activation with vacuum ultra-violet brings unique information and enables definitive structure assignment. Anal Chim Acta **807,** 84-95 (2014)

180. Konermann, L., Pan, J.X., Liu, Y.H.: Hydrogen exchange mass spectrometry for studying protein structure and dynamics. Chem Soc Rev **40,** 1224-1234 (2011)

181. Wales, T.E., Engen, J.R.: Hydrogen exchange mass spectrometry for the analysis of protein dynamics. Mass Spectrom Rev **25,** 158-170 (2006)

182. Abzalimov, R.R., Kaltashov, I.A.: Controlling Hydrogen Scrambling in Multiply Charged Protein Ions during Collisional Activation: Implications for Top-Down Hydrogen/Deuterium Exchange MS Utilizing Collisional Activation in the Gas Phase. Anal Chem **82,** 942-950 (2010)

183. Hoerner, J.K., Xiao, H., Kaltashov, I.A.: Structural and dynamic characteristics of a partially folded state of ubiquitin revealed by hydrogen exchange mass spectrometry. Biochemistry **44,** 11286-11294 (2005)

184. Zehl, M., Rand, K.D., Jensen, O.N., Jorgensen, T.J.D.: Electron Transfer Dissociation Facilitates the Measurement of Deuterium Incorporation into Selectively Labeled Peptides with Single Residue Resolution. J Am Chem Soc **130,** 17453-17459 (2008)

185. Rand, K.D., Adams, C.M., Zubarev, R.A., Jorgensen, T.J.D.: Electron capture dissociation proceeds with a low degree of intramolecular migration of peptide amide hydrogens. J Am Chem Soc **130,** 1341-1349 (2008)

186. Donohoe, G.C., Arndt, J.R., Valentine, S.J.: Online Deuterium Hydrogen Exchange and Protein Digestion Coupled with Ion Mobility Spectrometry and Tandem Mass Spectrometry. Anal Chem **87,** 5247-5254 (2015)

187. Dohohoe, G.C., Li, P., Jackson, G.P., Valentine, S.J.: Evaluation of charge transfer dissociation mass spectrometry (CTD-MS) for rapid, on-line hydrogen deuterium exchange experiments. Journal of The American Society for Mass Spectrometry, In preparation (2016)

188. Pan, J., Han, J., Borchers, C.H., Konermann, L.: Electron capture dissociation of electrosprayed protein ions for spatially resolved hydrogen exchange measurements. J Am Chem Soc **130,** 11574-+ (2008)

189. Xia, Y., Han, H., McLuckey, S.A.: Activation of intact electron-transfer products of polypeptides and proteins in cation transmission mode ion/ion reactions. Anal Chem **80,** 1111-1117 (2008)

190. Horn, D.M., Ge, Y., McLafferty, F.W.: Activated ion electron capture dissociation for mass spectral sequencing of larger (42 kDa) proteins. Anal Chem **72,** 4778-4784 (2000)

191. Ledvina, A.R., McAlister, G.C., Gardner, M.W., Smith, S.I., Madsen, J.A., Schwartz, J.C., Stafford, G.C., Syka, J.E.P., Brodbelt, J.S., Coon, J.J.: Infrared

Photoactivation Reduces Peptide Folding and Hydrogen-Atom Migration following ETD Tandem Mass Spectrometry. Angew Chem Int Edit **48,** 8526-8528 (2009)

192. Pitteri, S.J., Chrisman, P.A., McLuckey, S.A.: Electron-transfer ion/ion reactions of doubly protonated peptides: Effect of elevated bath gas temperature. Anal Chem **77,** 5662-5669 (2005)